EXAMINING THE INFLUENCE OF METEOROLOGICAL EVENTS ON PLANKTON DYNAMICS IN A COASTAL ECOSYSTEM (LUNENBURG BAY, CANADA)

by

Arnaud Laurent

Submitted in partial fulfillment of the requirements
for the degree of Doctor of Philosophy

at

Dalhousie University
Halifax, Nova Scotia
May 2011

DALHOUSIE UNIVERSITY

DEPARTMENT OF OCEANOGRAPHY

The undersigned hereby certify that they have read and recommend to the Faculty of Graduate Studies for acceptance a thesis entitled "EXAMINING THE INFLUENCE OF METEOROLOGICAL EVENTS ON PLANKTON DYNAMICS IN A COASTAL ECOSYSTEM (LUNENBURG BAY, CANADA)" by Arnaud Laurent in partial fulfillment of the requirements for the degree of Doctor of Philosophy.

Dated: May 11, 2011

External Examiner: _____

Research Supervisors: _____

_____

Examining Committee: _____

_____

_____

DALHOUSIE UNIVERSITY

DATE: May 11, 2011

AUTHOR: Arnaud Laurent

TITLE: EXAMINING THE INFLUENCE OF METEOROLOGICAL EVENTS ON PLANKTON DYNAMICS IN A COASTAL ECOSYSTEM (LUNENBURG BAY, CANADA)

DEPARTMENT OR SCHOOL: Department of Oceanography

DEGREE: PhD CONVOCATION: October YEAR: 2011

Permission is herewith granted to Dalhousie University to circulate and to have copied for non-commercial purposes, at its discretion, the above title upon the request of individuals or institutions. I understand that my thesis will be electronically available to the public.

Signature of Author

To those who wonder what, why and how.

Table of Contents

List of Tables

List of Figures

Abstract

Pelagic ecosystems are inherently complex in coastal inlets where they are controlled by physical processes and influenced by biogeochemical and foodweb interactions. Meteorological events are important drivers of this ecological variability. This thesis investigates their effect on the plankton dynamics of Lunenburg Bay, an inlet on the Atlantic coast of Nova Scotia (Canada). In this region, meteorological events are dominated by upwelling in summer, which are a dominant source of flushing and nutrient variability for the inlets. Despite these events, which induce phytoplankton blooms in other regions, the concentration of phytoplankton as chlorophyll remains relatively low throughout the summer in Lunenburg Bay. To reveal the underlying processes limiting the development of phytoplankton biomass, and therefore to improve our understanding of the factors regulating plankton dynamics in this inlet, the objectives of this thesis are to determine the main drivers of variability in phytoplankton biomass and plankton community structure, and to identify the factors limiting the development of phytoplankton biomass in Lunenburg Bay. For that, I use a dataset collected at a coastal observatory located in Lunenburg Bay that covers the years 2003–2006, complemented by a series of transects carried out in summer 2006. The dataset covers physical, chemical and biological properties of the bay, including plankton taxonomy. Two types of physical-biological coupled models are developed: a low-resolution box model of Lunenburg Bay with steady-state wind forcing, and a high-resolution nested model of Lunenburg Bay using the Regional Ocean Modelling System (ROMS) to hindcast a series of upwelling events in 2006. The results reveal that four factors regulate the phytoplankton response to upwelling events in Lunenburg Bay, namely (1) the duration of an upwelling event, (2) the low nitrate concentration in source waters, (3) the flushing rate of the inlet (hence transport), and (4) the bathymetry along the inshore-offshore axis of the bay. In addition, (5) the occurrence of upwelling and (6) the inshore-offshore gradient of increasing depth influence the structure of respectively phytoplankton and zooplankton communities, indicating a dissimilarity in the processes structuring plankton communities in the lower food web. A conceptual model is then developed to describe the role of transport and nitrate concentration in source waters in controlling plankton dynamics in an inlet.

List of Abbreviations and Symbols Used

a_ϕ	Light absorption coefficient for phytoplankton	m^{-1}
α	Initial slope of instantaneous growth rate vs light curve	d^{-1} $(W\ m^{-2})^{-1}$
AUV	Autonomous Underwater Vehicle	
AZMP	Atlantic Zone Monitoring Program	
BB	Bedford Basin	
β	Assimilation efficiency	
CDOM	Chromophoric Dissolved Organic Matter	
Chl	Chlorophyll	$mg\ m^{-3}$
$\Delta\widehat{\text{Chl}}$	Chlorophyll anomalies	$mg\ m^{-3}$
ΔChl	Observed change in chlorophyll biomass	$mg\ m^{-3}$
$(\text{Chl})_{a_\phi}$	Chlorophyll biomass from optical data	$mg\ m^{-3}$
C:N	Redfield carbon to nitrogen ratio	$mol\ mol^{-1}$
CTD	Conductivity, Temperature, Depth	
D	Detritus	$mmolN\ m^{-3}$
DIN	Dissolved inorganic nitrogen	
E	Photosynthetically available radiation	$W\ m^{-2}$
E_0	Sea surface photosynthetically available radiation	$W\ m^{-2}$
E_{top}	Photosynthetically available radiation at top of layer	$W\ m^{-2}$
$E_{\text{NO}_3^-}$	Efficiency of nitrate trapping	%
EOF	Empirical Orthogonal Functions	
f	Coriolis parameter	s^{-1}
F^*	Dimensionless specific transport	
F_T	Flushing time	d
F_R	Flushing rate	d^{-1}
g_P	Zooplankton grazing on phytoplankton	d^{-1}
g_Z	Zooplankton death rate	d^{-1}
GOOS	Global Ocean Observing System	
ICOM	Integrated Coastal and Ocean Management	
IOC	Intergovernmental Oceanographic Commission	

ISS-LB	Inner Scotian Shelf - Lunenburg Bay model grid	
I_Z	Maximum ingestion rate	d^{-1}
K_d	Light attenuation coefficient	m^{-1}
k_P	Phytoplankton grazing half saturation	mmolN m^{-3}
k_Z	Zooplankton grazing half saturation	mmolN m^{-3}
k_N	Nutrient half saturation	mmolN m^{-3}
L	Internal Rossby radius	km
λ	Remineralization rate	d^{-1}
LB	Lunenburg Bay	
LOICZ	Land-Ocean Interactions in the Coastal Zone	
μ	Phytoplankton growth rate	d^{-1}
μ_{max}	Maximum phytoplankton growth rate	d^{-1}
$\mu(E,T)$	Light and temperature limited growth rate	d^{-1}
MB	Mahone Bay	
MEPS-Bay	Marine Environmental Prediction System for Lunenburg Bay	
MODIS	Moderate Resolution Imaging Spectroradiometer	
MPDATA	Multidimensional Positive Definite Advection Transport Algorithm	
MSC	Meteorological Service of Canada	
N	Nutrient	mmolN m^{-3}
NAO	North Atlantic Oscillation	
NCEP	National Center for Environmental Prediction	
NENA	North East North America model grid	
NMDS	Non Metric Dimensional Scaling	
NO_3^-	Nitrate + nitrite	mmol m^{-3}
NS	Nova Scotia	
$\widehat{NO_3^-}$	Nitrate estimated from density	mmol m^{-3}
$(\widehat{NO_3^-})_b$	Bottom nitrate estimated from density	mmol m^{-3}
OS	Offshore Station	
P	Phytoplankton	mmolN m^{-3}
PON	Particulate Organic Nitrogen	
P:T	Production:Transport ratio	

$\overline{Q}_{adv}$	Tidally averaged advective flux	$m^3\ s^{-1}$
Q^h_{adv}	Horizontal advective flux	$m^3\ s^{-1}$
Q^v_{adv}	Vertical advective flux	$m^3\ s^{-1}$
Q^h_{diff}	Horizontal diffusive flux	$m^3\ s^{-1}$
Q^v_{diff}	Vertical diffusive flux	$m^3\ s^{-1}$
R	Rossby radius of deformation	m
r	Respiration rate	d^{-1}
ρ	Water density	$kg\ m^3$
r_{adv}	Advective exchange rate	d^{-1}
RB	Rose Bay	
r_{diff}	Diffusive exchange rate	d^{-1}
RNT	ROMS Numerical Toolbox	
ROMS	Regional Ocean Modelling System	
ρ_s	Surface water density	$kg\ m^3$
ρ_b	Bottom water density	$kg\ m^3$
S	Salinity	
S^*	Dimensionless nutrient availability	
S2	Station 2	
SD	Standard deviation	
SMB	Saint Margarets Bay	
SS	Scotian Shelf	
SSS	Sea Surface Salinity	
SST	Sea Surface Temperature	
SVD	Singular Value Decomposition	
T	Temperature	°C
τ_a	Alongshore wind stress	$N\ m^{-2}$
τ_c	Crossshore wind stress	$N\ m^{-2}$
τ_x	u-component of wind stress on model grid	$N\ m^{-2}$
θ	Carbon to chlorophyll ratio	$g\ g^{-1}$
θ_s	Surface vertical stretching parameter	
θ_b	Bottom vertical stretching parameter	
TNO3	Horizontal transport of nitrate	$mmol\ s^{-1}$
TDIN	Horizontal transport of DIN	$mmol\ s^{-1}$

TNO3	Horizontal transport of phytoplankton	mmolN s^{-1}
T_{cline}	Width of surface or bottom stretching boundary	m
U_C	Cross-shore current	m s^{-1}
U_x	Cross-shore wind speed	m s^{-1}
U_y	Along-shore wind speed	m s^{-1}
w_P	Phytoplankon sinking velocity	m d^{-1}
w_D	Detritus sinking velocity	m d^{-1}
X_y^*	Dimensionless accumulation of variable y	
ξ	Zooplankton mortality going to Nutrients	
Z	Zooplankton	mmolN m^{-3}

Acknowledgements

A PhD—as research in general—is not a solitary work but rather a collective project which requires guidance, collaboration and support. Without those, I wouldn't have been able to carry out this research, and many people need to be acknowledged for that.

For the guidance and the financial support I would like to thank my supervisors Alain Vézina and John Cullen. The content of this thesis is in large part the result of discussions, comments, criticisms or insights from them. I would also like to thank the members of my committee Charles Hannah, Mike Dowd and Marlon Lewis for sharing their ideas and criticisms. I acknowledge their patience and their help to improve my english writing (a.k.a. butchering) skills. They all helped me, one way or the other, '*to grow into a scientist*' (*Hannah*, 2011). I would also like to thank my external examiner Peter Franks for taking the time to read my thesis and for his insightful comments.

The fieldwork and the data analysis wouldn't have been possible without the support from the Lunenburg Project team, in particular Stéphane Kirschoff, Adam Comeau, Richard Davis, Cathy Ryan, Cheryl Rafuse, Chris Jones, Diego Ibarra, Dave Bowen and the numerous summer students that participated to the sampling. I would also like to thank the present and former members of the plankton lab and the MEMG group for their help and support during this journey, as well as Chris Taggart and Hal Ritchie for their assistance during the fieldwork.

The modelling work was carried out in collaboration with Mike Dowd (Box model), Jinyu Sheng, Li Zhai (CANDIE) and Katja Fennel (ROMS) who I thank for their help during the design of the models and for providing their model results. I particularly thank Katja Fennel for her comments on the thesis and the help during the learning of ROMS, with support from Diego Ibarra and Moritz Lehmann. The ROMS modelling was carried out with the support of the Atlantic Computational Excellence Network (ACEnet).

A final—and special—thank goes to Natasha, my family and my friends for cheering me up during this marathon.

Financial support was provided by the NSERC, the U.S. Office of Naval Research and the Canadian Foundation for Climate and Atmospheric Sciences (CFCAS).

Chapter 1

General Introduction

This thesis investigates the effects of local and remote meteorological forcing on the plankton communities of a nearshore tidal system located on the Atlantic coast of Nova Scotia, Canada. Data collection, data analysis and modelling experiments are carried out to describe and explain the observed variability in plankton biomass and community structure during the summer. The following sections discuss the general principles of plankton variability and its environmental control in nearshore tidal systems that are relevant to the present research. This discussion leads to the development of a set of hypotheses that establish a framework for this study.

1.1 Preliminary Considerations

1.1.1 The Global Context

Phytoplankton can be compared to primary producers in terrestrial systems (e.g., *Margalef*, 1997). They are the foundation of the marine food web and a key biological element of the earth system. Terrestrial and marine primary producers contribute roughly equally to the global primary production of the biosphere (*Longhurst et al.*, 1995; *Field et al.*, 1998). However, phytoplankton represent only 0.2% of the photosynthetically active carbon biomass in the biosphere (*Field et al.*, 1998) and have consequently a much faster turnover time (2–6 days, *Behrenfeld and Falkowski*, 1997). Fast growth is balanced by consumption by herbivores, which induces a rapid cycling of biogeochemical elements in the surface ocean. Consequently, marine phytoplankton are a major component of the

global carbon cycle (*Falkowski et al.*, 1998, 2000) and contribute significantly to biogeochemical cycles in the ocean (*Arrigo*, 2005).

Within the ocean system, continental margins have a significant role in the marine biogeochemical cycles of carbon and nitrogen (*Walsh*, 1991), although this role is still poorly understood (*Siefert and Plattner*, 2004; *Liu et al.*, 2010). Continental margins represent a modest 7% of the total surface area of the global ocean but, being at the confluence of the terrestrial, oceanic and atmospheric biogeochemical systems, are regions of high biogeochemical activity, amongst the most active of the biosphere (*Gattuso et al.*, 1998). In these areas, the interactions between topography, oceanic circulation, coastal wind regimes and tides result in a set of very diverse coastal biomes in comparison to the open ocean (*Longhurst*, 1998). It is therefore not surprising that the coastal ocean represents 29% of the annual net primary production in the global ocean (*Ducklow and McCallister*, 2005), accounts for 40% of the carbon sequestration in marine sediments (*Muller-Karger et al.*, 2005) and is a significant component of the carbon and nutrient cycling of the biosphere (*Liu et al.*, 2010).

As a consequence, coastal areas are a valuable biome for ecosystem services (*Costanza et al.*, 1997), supporting a large amount of the human population and activities which in turn modify these systems over a range of spatial and temporal scales. Continental margins are greatly affected by human activities (*Walsh*, 1988; *Chen*, 2010; *Talaue-McManus*, 2010). Given the particularities of these areas, the effect of perturbations on the supply of nutrients to primary producers may be amplified (*Muller-Karger et al.*, 2005). This anthropogenic pressure and the fact that most of the continental margins are undersampled with respect to the carbon cycle (*Hales et al.*, 2008), led to the recent development of international research programs on the coastal zone (e.g., LOICZ, *Kremer et al.*, 2004). Such programs aim to study the anthropogenic impacts on ecosystems and biogeochemical cycles of the coastal ocean. Studies are however difficult to carry out because of the complex physical interactions characteristic of the coastal areas and their strong influence on marine ecosystems (*Denman and Powell*, 1984).

The importance of physical processes for phytoplankton lies in their requirement for both light for photosynthesis, and nutrients for survival and growth. The spatial separation between light (at the surface) and nutrients (increasing below the pycnocline) limits primary production in the ocean (*Yentsch*, 1981). Consequently, phytoplankton are highly dependent on physical processes to generate their optimum supporting environment, notably to maximize light and nutrient conditions (optimal stability window, *Gargett and Marra*, 2002). Phytoplankton dynamics are thus strongly coupled with physical processes in the surface ocean (e.g., *Legendre and Demers*, 1984; *Dickey*, 1991). Synoptic meteorological events are particularly important in this interplay (e.g., *Kiørboe and Nielsen*, 1990; *Marra et al*., 1990).

1.1.2 General Characteristics of Continental Margins

The origin and fate of organic matter in the ocean is estimated with the f ratio, the ratio between new—i.e., from sources of nitrogen external to the euphotic zone (e.g., from the injection of deep nutrients)—and total (new + regenerated) phytoplankton production (*Eppley and Peterson*, 1979). The f ratio, hence new production, is higher in the continental margins in comparison to the open ocean (*Walsh*, 1991). However, this characteristic is not spatially uniform and large variations occur. Continental margins are typically referred to as either 'exporting' or 'recycling' (*Chen et al*., 2003), which relates to their f ratio. This terminology was recently updated and continental margins reclassified as slope-dominated and shelf-dominated margins for clarity (*Jahnke*, 2010). The distinction between the two categories is important for the biogeochemistry of continental margins.

Slope-dominated continental margins usually have narrow continental shelves with short water residence time and high nutrient inputs at the shelf break, in particular from wind driven coastal upwelling, which sustain high rates of primary production and export of organic matter to the open ocean. In these systems, located notably along the western coast of the Americas and Africa, nutrient fluxes from benthic regeneration are generally limited and new production, supported by nutrient transport from the deep sea, dominates.

Shelf-dominated continental margins are relatively wide and shallow with longer water residence time which allows for an efficient use of nutrients and their recycling through benthic-pelagic coupling. In these environments, which can be found along the western boundary of ocean basins and in particular along the northeast coast of North America, most of the production is recycled locally with limited export of organic material; in these systems, recycled production then dominates. This is the case of the Scotian Shelf, off Nova Scotia's Atlantic coast (Canada), where 80% of phytoplankton production has been attributed to recycled nitrogen (*Fournier et al.*, 1977), although this value has been challenged recently (*Petrie and Yeats*, 2000). Denitrification in the sediments can be a significant process for the nitrogen cycle and an important factor limiting primary production (*Fennel et al.*, 2006). In the Mid-Atlantic Bight for instance, 90% of the nitrogen entering the system is lost through this process, resulting in a net sink of nitrogen (ibid).

In coastal embayments, where the variability arises in part from processes occurring on the shelf, nitrate concentration in source waters (i.e., the distribution of nitrate on the shelf), hence the biogeochemistry of the continental margin can have an essential influence on biological processes well inshore.

1.1.3 Ekman Transport at the Coast

At the ocean surface, wind stress is the main source of turbulent kinetic energy. It generates small and large scale circulation patterns and controls vertical mixing, which sets the conditions necessary for primary production through the trade-off between light and nutrient supply (*Yentsch*, 1981). The frictional drag of the wind and its interaction with the Earth's rotation induces Ekman transport in the surface ocean (*Ekman*, 1905). In the northern (southern) hemisphere, this process moves the momentum transferred from the wind to the water increasingly to the right (left) as depth increases, generating a net transport at 90° to the right (left) of the wind over the Ekman layer. Detailed explanations of Ekman transport are found in theoretical analysis (*Pond and Pickard*, 1983) and from in-situ observations and modelling of the Ekman spiral (*Price et al.*, 1987; *Wijffels et al.*, 1994; *Chereskin*, 1995). An important deviation from the classical Ekman model can result from the diurnal and seasonal surface stratification typical of mid-latitudes in summer, which induce a surface-trapped Ekman layer of reduced thickness oriented more in

the downwind direction (*Price and Sundermeyer*, 1999). At the coast, the offshore transport of the Ekman layer is compensated with the upwelling of generally cooler, saltier and nutrient-rich deeper waters; simultaneously, the resulting cross-shore surface pressure gradient induces a downwind surface alongshore current. A brief description and discussion of the Ekman phenomenon is given in Appendix A.

Ekman transport is essential to nutrient dynamics in the surface ocean. At the global scale, Ekman transport has a prominent role in biogeochemical processes because it creates upwelling in divergence zones and downwelling in convergence zones, hence controlling the supply of nutrients to the upper ocean (*Sarmiento and Gruber*, 2006). Along the coast, offshore Ekman transport generates the upwelling of deep water to the surface, leading to the input of nutrients to the euphotic layer where it stimulates primary production. This phenomenon is well documented along eastern boundary regions (e.g., *Wooster et al*., 1976; *Boje and Tomczak*, 1978; *Richards*, 1981, and references therein) where it is the dominant process for the supply of nutrients to the surface of the coastal ocean. Upwelling is often a seasonal process due to the seasonality of atmospheric forcing, but variability can also occur on the time-scale of several days, associated with the periodicity of atmospheric depressions (*Andrews and Hutchings*, 1980). The alternation of upwelling/relaxation cycles associated with this periodicity is typical of upwelling environments and is an important process for the local accumulation of phytoplankton biomass along the coast (*Maclsaac et al*., 1985; *Dugdale and Wilkerson*, 1989). Because of their dependency on atmospheric processes, coastal upwellings are susceptible to the variation in atmospheric forcing resulting from climate change (*Bakun*, 1990; *Snyder et al*., 2003; *Wang et al*., 2010). Changing atmospheric conditions due to global warming, may therefore have a significant effect on coastal and nearshore phytoplankton production and on the coastal food web (*Barth et al*., 2007; *Bakun et al*., 2010).

Similarly, episodic coastal upwelling generated by the prevailing seasonal wind conditions or by storm events can develop along the western boundary of ocean basins. This type of upwelling event is biologically less important than in the eastern boundary upwelling regions (*Mann and Lazier*, 1992) and has therefore received less attention. This is the case of the northeast coast of North America, a shelf-dominated continental margin. In this region, the development of coastal upwelling conditions has a significant effect

locally. For instance on the Scotian Shelf, upwelling events contribute to the transport of nutrients onto the shelf at the shelf break (*Petrie et al*., 1987) and are associated with the onset of annual phytoplankton blooms (*Greenan et al*., 2004). On the New Jersey Shelf, upwelling events contribute to the variability in phytoplankton biomass and phytoplankton community structure and favour the development of hypoxia along the coast due to the local accumulation of particulate organic matter (*Glenn et al*., 2004).

Upwelling-favourable winds periodically relax or reverse in coastal upwelling systems, resulting in the onshore movement of water and the development of downwelling conditions along the coast and nearshore. As opposed to upwelling, downwelling or relaxation events are not associated with the supply of nutrients to the euphotic zone, but rather with a deepening of the pycnocline nearshore. Consequently, these events don't stimulate primary production. Rather, they promote cross-shelf transport and the retention of surface water nearshore, which can be an important process controlling larval transport (*Miller and Emlet*, 1997; *Shanks and Brink*, 2005) and phytoplankton community structure (*Moline et al*., 2004), especially when associated with preceding upwelling conditions (upwelling–downwelling sequence). In this case, episodic downwelling conditions can promote the retention of primary production (*Tilstone et al*., 2000) or lead to the development of harmful algal blooms in the nearshore area (*Tilstone et al*., 1994; *Figueiras and Rios*, 1993).

1.2 Biophysical Interactions in Nearshore Pelagic Environments

1.2.1 Overview

Biological–physical interactions are particularly important in temperate bays in summer when nutrients are limiting in the euphotic layer. During this period, the background phytoplankton populations can be described as in a *quasi–equilibrium* (*Evans and Parslow*, 1985; see *Cloern*, 1996), where primary production and phytoplankton losses through mortality and transport compensate each other. Physical variability in the environment is then essential for phytoplankton communities because it creates episodic sources of nutrients that generate transient departures from this equilibrium (*Cloern*, 1996). In turn, this

variability determines the structure of phytoplankton communities (*Margalef*, 1978a) and therefore ultimately controls the amount of energy transferred to higher trophic levels.

Among these physical processes, reviewed by *Cloern* (1996), two are dominant contributors to the coupling between inlets and their adjacent coastal ocean, therefore regulating the transport of nutrients and particulate organic matter (plankton, detritus) across the bay–ocean interface: tides and Ekman transport at the coast.

Tides are a dominant, most predictable physical process controlling nearshore circulation. At the diurnal and semi-diurnal frequencies, the tidal circulation determines exchanges locally as well as between the inlet and the coastal ocean. These exchanges, and the effect of tides on pelagic-benthic coupling through a stratification-destratification process, influence the spatial patterns of phytoplankton biomass (*Lucas et al.*, 1999b), phytoplankton communities (*Cloern and Dufford*, 2005) and the rates of pelagic ecosystem process (e.g., primary production, grazing) along the inshore-offshore axis of the inlet (*Dowd*, 2003). Changes in zooplankton species composition can occur along this axis in association with the change in habitat related to the variation in transport patterns (*Jouffre et al.*, 1991). However, tidal exchanges are restricted to the tidal excursion distance, which is often limited to a small fraction of the length of the inlet (*Geyer and Signell*, 1992).

At the subtidal frequency, Ekman transport at the coast promotes exchanges at the land-sea interface. Coastal upwelling is a particularly significant process because it promotes the flushing of bays and estuaries (*Heath*, 1973; *Duxbury*, 1979) and contributes to their seasonal variability in nutrient concentration (*Platt et al.*, 1972), phytoplankton biomass (e.g. *Bode and Varela*, 1998; *Hickey and Banas*, 2003) and phytoplankton community structure (see Section 1.2.2 below). Alongshore transport of phytoplankton blooms (e.g., *Franks and Anderson*, 1992a,b) also interacts with Ekman transport at the coast (*Figueiras et al.*, 2006). Despite this positive relationship between Ekman transport and phytoplankton biomass, uncoupling between primary and secondary production nearshore have been reported in coastal upwelling systems (*Peterson et al.*, 1988). Overall at the subtidal timescale, upwelling-induced coupling between bays, estuaries and the adjacent inner shelf has a significant effect on nearshore biological processes and can be the dominant source of biological variability in systems where nutrient sources are limited.

1.2.2 Nova Scotian Inlets Versus Eastern Boundary Systems

Along the Atlantic coast of Nova Scotia, the prevailing wind orientation in summer—associated with the position of the Bermuda High—and the orientation of the coast (*Smith and Schwing*, 1991) leads to the development of upwelling conditions on the Scotian Shelf (*Hachey*, 1937; *Petrie et al*., 1987). It induces the flushing of coastal inlets (*Heath*, 1973), which influences the local supply of nutrients (*Platt et al*., 1972), as well as the transport and physiology of phytoplankton populations (*Côté and Platt*, 1983). The variability of inshore pelagic systems in this region is tightly coupled with the wind-induced exchanges at the inlet-shelf interface and therefore inshore biological systems are dominated by remote (i.e., occurring on the shelf) rather than local processes (*Lewis and Platt*, 1982).

Overall, we understand the dominant source of phytoplankton variability in the inlets along the Nova Scotian Atlantic coast. However, despite the series of seminal studies mentioned above, the processes of biophysical coupling at the inlet-shelf interface remain unclear and the specific processes controlling the spatial and temporal variability of inshore plankton populations remain to be analyzed. Understanding these processes is essential to apprehend inshore plankton dynamics and biogeochemistry, and subsequently to improve the understanding of biogeochemical cycling in the coastal zone (*Siefert and Plattner*, 2004). These processes have been investigated in the better documented eastern boundary inlets, where upwelling events are seasonal and their biological effect generally important. For instance in the Galician rias (northwest Spain), which are located at the northern boundary of the productive Northwest African upwelling system (*Joint et al*., 2001), relationships between alongshore wind events (upwelling, downwelling), phytoplankton biomass and phytoplankton community composition were demonstrated (*Fraga et al*., 1988; *Figueiras and Rios*, 1993; *Tilstone et al*., 1994, 2000; *Bode and Varela*, 1998; *Figueiras et al*., 2006). As in typical coastal upwelling areas (e.g., *Estrada and Blasco*, 1985), diatoms are favoured during upwelling conditions and dinoflagellates during upwelling relaxation and downwelling conditions.

In the rias, the intensity of upwelling events (*Figueiras and Rios*, 1993), as well as preceding stratification conditions (*Álvarez-Salgado et al*., 1996b) are important factors influencing the phytoplankton during the events. Weak upwelling induces stratification

and the retention of nutrients (nutrient trap) and phytoplankton due to the local accumulation of nutrients and their utilization by the phytoplankton (*Álvarez-Salgado et al*., 1996b; *Piedracoba et al*., 2008a). On the contrary, strong upwelling leads to a rapid flushing of the inlets that promotes the export of primary production to the shelf area (*Álvarez-Salgado et al*., 1996b; *Crespo et al*., 2006). This export of diatom species is considered to benefit higher trophic levels on the shelf (*Tilstone et al*., 2000). The subsequent retention during the relaxation phase benefits inshore secondary producers (*Figueiras et al*., 2002), as evidenced by the location of an intense shellfish mariculture in the rias (*Blanton et al*., 1987). Altogether, in the rias, atmospheric forcing controls the seasonal variability in phytoplankton production and community structure during the summer and fall. The biological response of the rias to the upwelling events is nonetheless complex. It depends on meteorological conditions, but also on morphometry (*Tilstone et al*., 1994) and local or remote hydrographic conditions (*Bode and Varela*, 1998; *Prego et al*., 2007), resulting in high variability in response.

Similar investigations need to be carried out along the Atlantic coast of Nova Scotia, to fully appreciate the importance of coastal upwelling events occurring on the Scotian Shelf for the pelagic ecosystem of coastal inlets. However, Spanish rias differ significantly from Nova Scotian inlets given the atmospheric forcing, the buoyancy-driven circulation and the biochemical processes occurring on their adjacent coastal ocean (i.e., slope- versus shelf-dominated continental margins). The contrast is even greater when Nova Scotian inlets are compared with the inlets along the west coast of North America (Oregon, California), which are located on upwelling systems where nitrate concentration typically reach 10 mmol m^{-3} at the surface during the upwelling season (*Hickey and Banas*, 2003), reflecting the slope-dominated shelf system.

The coastal ocean is the main source of nitrate for most inlets along the Atlantic coast of Nova Scotia (*Strain and Yeats*, 1999). However, nitrate is depleted in the euphotic layer of the Scotian Shelf in summer (*Petrie et al*., 1999) and therefore, nitrate concentration is typically low in the inlets during this period. For example, preliminary observations from a nearshore coastal observatory located in Lunenburg Bay (Marine Environmental Prediction System Lunenburg Bay, hereafter MEPS-Bay, see Section 1.6) indicate an average nitrate concentration of 0.3 ± 0.4 mmol m^{-3} SD (n = 715) between June and

August (weekly samples from the observing system dataset, i.e., *Cullen et al*., 2008). In this system, the subtidal variability in hydrography is dominated by the occurrence of alongshore wind events such as upwelling or downwelling (*Zhai et al*., 2007). Upwelling events are particularly important because they are a source of nitrate in summer (e.g., *Platt et al*., 1972). Phytoplankton blooms are a typical response to such an episodic nitrate injection, as observed in the eastern boundary inlets (e.g., *Hickey and Banas*, 2003; *Álvarez-Salgado et al*., 2010). However, large variations in chlorophyll biomass have not been observed at the observatory in summer, where the average chlorophyll biomass is low (1.1 ± 0.6 mg m^{-3} SD, $n = 690$). These observations indicate an apparent discrepancy between a dominant process controlling the hydrography of the bay (upwelling), which should induce phytoplankton blooms, and the low chlorophyll biomass measured at the observatory. Several factors can lead to this apparent discrepancy: (1) an inappropriate sampling frequency to observe the phytoplankton response to the upwelling events (water samples are collected weekly), (2) the occurrence of processes limiting the delivery of nitrate, or (3) the occurrence of processes limiting the development and/or accumulation of phytoplankton.

This information suggests two directions of research necessary to improve the understanding of summer plankton dynamics and their relationship with atmospheric forcing in Nova Scotian inlets: first, diagnose the variability of nutrients and plankton in summer, principally in relation to meteorological events; and then investigate the processes controlling and limiting this variability.

1.3 Observing, Hindcasting and Forecasting Coastal Ecosystems

Understanding the variability within coastal marine ecosystems and its underlying biological-physical processes requires the capability to separate the signals resulting from intrinsic ecosystem processes from the specific effects of physical forcing (*Rothschild*, 2005). Coupled biogeochemical-physical numerical models provide a tool to examine—with testable hypotheses—the specific processes underlying a set of observations (*Franks*, 1995). These tools are commonly used to study plankton dynamics in aquatic systems (*Franks*, 1995, 2002). They provide the means to quantify and ultimately to forecast

the effects of specific physical processes on nearshore plankton ecosystems (*Fennel and Neumann*, 2004; *Oschlies*, 2006). The objective is often best realized by using a hierarchy of models (*Griffies*, 2004), which reduce the spatial and structural resolution to an optimum level of complexity that best describes the key processes of interest (*Håkanson*, 1995; *Fulton et al*., 2003).

The so-called "box models" are on the low end of this spectrum. In the case of biogeochemical-physical coupled models, they have a coarse spatial resolution that reduces the hydrodynamics to its most important spatial patterns allowing to focus on the biogeochemical processes under consideration. In bays for example, the system can be reduced to several boxes in the horizontal and one or two in the vertical depending on the dominant hydrography (i.e. stratified or mixed water column). This type of model has been used successfully to describe some key aspects of coastal pelagic processes, with respect to mariculture (*Raillard and Ménesguen*, 1994; *Dowd*, 1997, 2005), eutrophication (*Chapelle et al*., 1994; *Bujan et al*., 2000; *Guillaud et al*., 2000), benthic-pelagic coupling (*Le Pape et al*., 1999), nutrient cycling (*Murray and Parslow*, 1999) and harmful algal blooms (*Yamamoto and Okai*, 2000; *Yamamoto et al*., 2002). It was also used extensively to describe the patterns and time-scales of circulation and hydrography in Spanish rias (*Rosón et al*., 1997; *Álvarez-Salgado et al*., 2000; *Pardo et al*., 2001; *Gilcoto et al*., 2001, 2007), as well as to investigate biological-physical interactions during periods of upwelling conditions (*Álvarez-Salgado et al*., 1996a,b; *Tilstone et al*., 2000; *Piedracoba et al*., 2008b).

Given their coarse resolution, box models underestimate the local variance, acting as a low pass filter. Moreover, spatial or temporal averaging used in box models can induce errors resulting from simplifying assumptions (*Webster et al*., 2000). Fine-grid, fully explicit biological-physical models provide the potential for better resolved results (temporally and spatially) over a wide range of time and space scales (*Ménesguen et al*., 2007). The Regional Ocean Modelling System (ROMS, http://www.myroms.org)(*Shchepetkin and McWilliams*, 1998, 2003, 2005; *Haidvogel et al*., 2008) is arguably the state-of-the-art of these ocean models; regardless, it is an open-source development and widely used. It is particularly suited for coastal and nearshore applications including biogeochemistry or ecosystem dynamics and can be used for both the hindcast or forecast of biological processes in the coastal ocean.

In-situ observations are necessary to force and constrain ocean models, as well as to verify their results. This motivated the development of coastal ocean observing systems in the last decade for observing, hindcasting and forecasting coastal physical and biological processes. This was the aim of the MEPS-Bay coastal observatory (http://www.cmep.ca, *Cullen et al*., 2008) located in Lunenburg Bay on the Atlantic coast of Nova Scotia (see Section 1.6). The observatory has provided a framework for the study of nearshore bio-physical ocean dynamics, using Lunenburg Bay as a test case. Recent hydrodynamic studies have emphasized the role of meteorological events in structuring the physical variability of Lunenburg Bay and neighbouring systems during the summer and fall (*Wang et al*., 2007; *Zhai et al*., 2007, 2008b; *Sheng et al*., 2009). The observatory dataset, complemented by specific sampling, provides the opportunity to investigate a series of hypotheses on the effects of meteorological events on the plankton dynamics and biogeochemistry of Lunenburg Bay (see Section 1.5 below).

1.4 Research Objectives

The influence of summer meteorological events on nutrient dynamics and on phytoplankton production and variability has been established in several Nova Scotian inlets (*Platt et al*., 1972; *Lewis and Platt*, 1982; *Côté and Platt*, 1983). However, the specific mechanisms that control these dynamics, or that influence the structure of nearshore plankton communities, are still unresolved for these systems. The preliminary observations of a discrepancy between the occurrence of upwelling events and the relatively low phytoplankton concentration and variability inside Lunenburg Bay during summer suggests limiting processes, associated with local ecosystem processes (primary production, grazing), biological transport at the bay-shelf interface (patterns and intensity) or processes controlling plankton and nutrient concentrations on the shelf. Resolving the importance of these influences is important locally, but also with regards to the general understanding of biological dynamics in western boundary inlets. It is also important to understand the possible consequences of expected changes in global climate, such as changes in the frequency of storm and coastal upwelling events that will influence the coastal and nearshore pelagic ecosystems (*Snyder et al*., 2003; *Diffenbaugh et al*., 2004; *Harley et al*.,

2006). Characterizing the current processes structuring plankton communities nearshore and their response to transient meteorological events is therefore essential to anticipate the response of these communities to global warming. Therefore, in order to improve the understanding of the processes controlling plankton dynamics in Lunenburg Bay, this thesis has two objectives:

(1) ***to determine the main drivers of variability in phytoplankton biomass and plankton community structure; and***

(2) ***to identify the factors limiting the development of phytoplankton biomass.***

1.5 Hypotheses

Specific hypotheses have been developed to reach the two objectives. They are focused on Lunenburg Bay where the research will be conducted. The hypotheses include alternate hypotheses, which are not mutually exclusive but rather can represent multiple interacting processes. The hypotheses are described below.

1.5.1 Variability in Phytoplankton Biomass

Hypothesis 1.0: The variations in phytoplankton biomass in summer are independent of meteorological events.

Alternate hypothesis:

(1.1) The effects of meteorological events account for significant amounts of variability in phytoplankton biomass in summer.

1.5.2 Upwelling Effect on Phytoplankton Biomass

Hypothesis 2.0: The input of nutrient-rich inner shelf waters during upwelling events leads to significant increases in primary production and phytoplankton biomass inside Lunenburg Bay.

Alternate hypotheses:

(2.1) Phytoplankton biomass has no detectable response to upwelling events inside Lunenburg Bay.

(2.2) Low nitrate concentration in the source waters limits the magnitude of variability in phytoplankton biomass in Lunenburg Bay.

(2.3) The short duration of upwelling events limits the development of phytoplankton biomass in Lunenburg Bay because it limits the periods for which nitrate is available to primary producers.

(2.4) The bathymetry constrains the exchanges between inshore areas and the shelf, limiting the nitrate available for primary production in shallow inshore areas.

1.5.3 Role of Transport in Limiting Phytoplankton Niomass

Hypothesis 3.0: The rapid flushing of Lunenburg Bay limits the magnitude of variability in phytoplankton biomass to that observed on the inner Scotian Shelf.

1.5.4 Seasonal Variability in Plankton Communities

Hypothesis 4.0: Dominant phytoplankton groups (diatom or dinoflagellate) are determined by the occurrence of upwelling events.

Hypothesis 5.0: The taxonomic structure of zooplankton communities is determined by the occurrence of upwelling events.

Alternate hypothesis:

(5.1) Zooplankton communities are structured spatially along a depth gradient representing a change in habitat between the inshore and offshore areas of the bay.

1.6 Research Framework

The study takes place in Lunenburg Bay, the site of the MEPS-Bay coastal observatory for the period 2002–2007. Lunenburg Bay has a 40 km^2 surface area, with a mean depth of about 15 m, increasing to 40 m towards the southwest where the bay connects with the

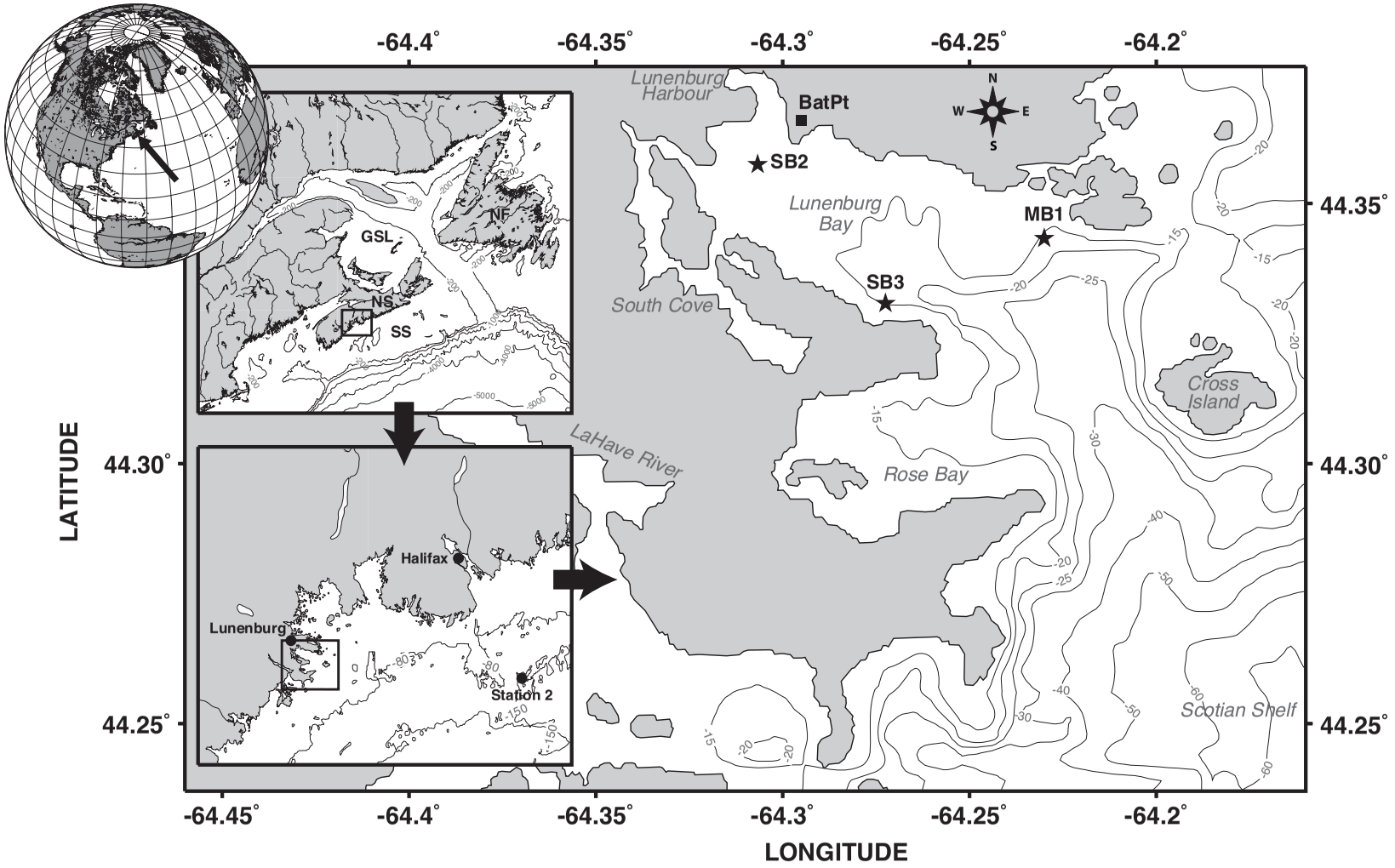

Figure 1.1: Map of the study site. Upper left: Location of Nova Scotia on the Northwest Atlantic and Atlantic coast of Canada, including Newfoundland (NL), the Gulf of Saint-Lawrence (GSL), the Scotian Shelf (SS) and Nova Scotia (NS). Lower left: Inner Scotian Shelf and location of Station 2, Lunenburg and Halifax. The Bedford Basin, discussed in the text, is located in the northwest of Halifax. Main panel: MEPS-Bay coastal observatory (main locations), including the location of the three moorings (★) and the meteorological station Battery Point (BatPt, ■). The bathymetry was provided by Doug Mercer and Jinyu Sheng.

Scotian Shelf (Figure 1.1). The circulation in the bay is dominated by the semi-diurnal tide (M2) and is sensitive to meteorological events and wind direction (*Sheng and Wang*, 2004; *Zhai et al*., 2007, 2008b), which are recurrent phenomena in summer and fall.

The MEPS-Bay coastal observatory was a state-of-the-art nearshore network of three moorings and other sensors that provided high-frequency observations (hydrography, optical properties, meteorological data), complemented by weekly in situ measurements to collect variables that were not measured automatically (nutrients, chlorophyll, plankton composition). Research components of the MEPS-Bay project focused on multiple aspects of the bay oceanographic processes such as tidal and wind–driven circulation (*Zhai et al*., 2008b; *Sheng et al*., 2009), wave-induced circulation (*Mulligan et al*., 2008), biological variability (*Huot et al*., 2007), as well as atmospheric processes, to improve weather prediction models. The MEPS-Bay project developed a multi-component modelling tool using real-time data to study and to reach a forecast capability of coastal marine conditions (*Cullen et al*., 2008). The current work has taken place within this project and uses the data collected at the observatory during its six years of operation, with an emphasis on the year 2006 when specific data were collected for this work.

1.7 Outline of the Thesis

The thesis is divided into six chapters. The first chapter (Chapter 1) is the introduction of the project. The next three chapters (Chapter 2–4) each investigate specific components of the influence of meteorological events on the dynamics of nearshore plankton populations, using a different set of techniques and analysis. Chapter 5 discusses some insights gained during the study on the MEPS-Bay coastal observatory. Chapter 6 is a synthesis of the results and a generalization of the processes examined in Chapters 2 to 4, followed by the conclusions of the thesis. Chapters 2 to 4, which will be the subjects of specific publications, are summarized below.

Chapter 2 addresses the first objective of the thesis (i.e., drivers of variability) and lays out several explanatory factors for the observed phytoplankton dynamics in Lunenburg Bay. The chapter evaluates if and how upwelling-favourable summer meteorological

events influence the dynamics of inshore planktonic communities in a Nova Scotian inlet. The study combines weekly transects conducted between June and August 2006 in Lunenburg Bay, with biophysical data collected by the MEPS-Bay coastal observatory. The dataset covers physical, chemical and biological properties of the bay, including plankton taxonomy. Results from the analysis of the dataset show the succession of upwelling events during summer 2006 in Lunenburg Bay and reveal two types of meteorological events with contrasting effects on inshore plankton communities in summer. It demonstrates the effects of sustained upwelling events on (1) the structure of phytoplankton communities and (2) the phytoplankton biomass, which is estimated and predicted from density measurements collected at the observatory. The chapter also reveals a strong spatial structuring of zooplankton communities inside Lunenburg Bay that appears to be decoupled from the occurrence of upwelling events.

Chapter 3 addresses the second objective of the thesis (i.e., limiting factors) in steady state (or pseudo steady state) conditions using two levels of analysis. First, the influence of wind-driven circulation on nearshore biogeochemical processes is assessed with a spatially-explicit box model developed to simulate planktonic ecosystem processes under tidal, downwelling and upwelling circulation regimes in Lunenburg Bay. Model results indicate that wind driven circulation affects plankton dynamics along an inshore-offshore axis, but the effects are small and depend on the wind regime. Overall, the analysis establishes that in Lunenburg Bay, wind-induced accelerated flushing controls the dynamics of nutrients and limits the accumulation of plankton biomass. Second, a spatially-averaged sensitivity analysis is carried out with the ecosystem model to explore the role of flushing rate and nutrient concentrations in source waters in a more general context. This analysis results in a dimensionless framework (S^* vs. F^*) that explains the magnitude of plankton and nutrient concentrations in an inlet given the scaled nutrient concentration available at the inlet-coastal ocean interface (S^*) and flushing rate (F^*).

Chapter 4 addresses both objectives of the thesis, although more specifically the second objective (i.e., limiting factors), by exploring the factors controlling the spatial and temporal variability of phytoplankton biomass in Lunenburg Bay. A biophysical ocean model (ROMS) is used to simulate the sequence of summer upwelling events observed in 2006 (Chapter 2). The results demonstrate that the dynamics of inshore phytoplankton

biomass are controlled by three factors during this period of upwelling: (1) the intermittent and short duration of upwelling conditions that limits the retention of nitrate for subsequent use by primary producers, (2) the rapid transport and the outwelling of phytoplankton from the bay that limits the accumulation of phytoplankton in the bay and (3) the nitrate concentration in upwelled water that limits—in association with the nearshore bathymetry—the development of phytoplankton biomass during the relaxation phase of the upwelling.

Chapter 2

Influence of Summer Wind Events on Phytoplankton Biomass and Planktonic Community Structure in Lunenburg Bay, Canada

2.1 Introduction

In the coastal upwelling systems on the eastern boundary of major ocean basins, phytoplankton variability is associated with the spatial and temporal variations in hydrography and nutrient concentrations (*Boje and Tomczak*, 1978; *Richards*, 1981). This determines phytoplankton biomass (*Small and Menzies*, 1981) and a sequence of phytoplankton assemblages, often dominated by diatoms (*Margalef*, 1978b; *Estrada and Blasco*, 1985). This variability extends to adjacent coastal inlets where the enhanced coupling with the coastal ocean during periods of upwelling generates flushing (*Duxbury*, 1979). This is an important process for inshore biological systems since it concurrently promotes the exchange of biota and nutrients between inlets and the inner shelf (*Hickey and Banas*, 2003; *Piedracoba et al*., 2008a,b). This contributes to local nutrient cycling (*Álvarez-Salgado et al*., 1996a,b) and influences the development and transport of phytoplankton blooms (*Roegner and Shanks*, 2001; *Roegner et al*., 2002), including harmful blooms (*Fraga et al*., 1988; *Figueiras et al*., 2006). Furthermore, it promotes changes in phytoplankton composition (*Garrison*, 1979; *Figueiras and Rios*, 1993) and stimulates local and remote secondary production (*Tilstone et al*., 2000). In the eastern boundary regions, wind-induced coastal upwelling has a significant influence on the biology of inlets (*Hickey and Banas*, 2003; *Álvarez-Salgado et al*., 2010).

Although of lower intensity, similar dynamics occur in summer on the Scotian Shelf along the Atlantic coast of Nova Scotia, Canada (*Hachey*, 1937; *Petrie et al*., 1987; *Andrade*, 1991). These events contribute to the flushing (*Heath*, 1973) and to the variability in nutrient concentration of Nova Scotian inlets (*Platt et al*., 1972). Upwelling-induced changes in phytoplankton physiology and species composition have previously been observed at a subsurface sampling station located in a small semi-enclosed eutrophic estuarine basin (Bedford Basin, see Figure 1.1 in Chapter 1) connected to the Scotian Shelf (*Côté and Platt*, 1983). The transport of deeper dark-adapted shelf phytoplankton populations (*Ceratium longipes*) was associated with the upwelling event. The study of *Côté and Platt* (1983) has been an important step towards understanding the relationship between meteorological events and phytoplankton dynamics in Nova Scotian inlets and has placed emphasis on the difficulty to predict the short-term variations in the rate of phytoplankton production in this type of environment due to the high-frequency variability induced by atmospheric events. However, this predictability was not assessed nor was the spatial variability in biochemical and hydrographic conditions (horizontal and vertical) resolved in this study. Therefore, the mechanisms of biochemical-physical coupling between inlets and the coastal ocean, as well as the relationship between upwelling-induced nutrient inputs, phytoplankton biomass and plankton assemblages, remain unclear.

In order to resolve these mechanisms, it is then important to diagnose the spatial and temporal impacts of upwelling events on nearshore plankton communities, especially in oligotrophic inlets since the Scotian Shelf is their dominant source of nitrate (*Strain and Yeats*, 1999), a major limiting nutrient in marine systems (*Dugdale and Goering*, 1967; *Ryther and Dunstan*, 1971; *Parsons et al*., 1984). This is critical to understand the dynamics of inshore biological systems along the Atlantic coast of Nova Scotia, and ultimately to enable their prediction, a prerequisite to the management of coastal environments.

Recently, at the coastal observatory located in Lunenburg Bay (Figure 2.1), an oligotrophic inlet on the Atlantic shore of Nova Scotia, investigations on the succession of upwelling and downwelling conditions during summer and fall 2003 have demonstrated the importance of atmospheric events in driving the local subtidal circulation and hydrography (*Zhai et al*., 2008b). The study revealed a meteorological control over high-frequency salinity and temperature variations dominated by the alongshore component of the wind

stress, especially around the head of the bay (*Zhai et al*., 2007). The biological responses to upwelling have not been studied in Lunenburg Bay however, nor in similar systems in the area, despite the need to expand the findings from *Côté and Platt* (1983). Such responses may be limited given the small nitrate (0.3 ± 0.4 mmol m^{-3} SD, $n = 715$) and chlorophyll (1.1 ± 0.6 mg m^{-3} SD, $n = 690$) concentrations observed inside the bay in summer (observing system dataset, i.e. *Cullen et al*. 2008).

The objective of this chapter is to evaluate if and how upwelling events influence the dynamics of plankton communities in Lunenburg Bay. It is hypothesized that upwelling events are the main driver of plankton variability inside Lunenburg Bay in summer because they result in the input of nitrate from the inner shelf, which (1) induces a significant increase in the phytoplankton biomass in Lunenburg Bay (> 5 mgChl m^{-3}, as typically observed in the spanish rias, *Tilstone et al*., 2000; *Cermeño et al*., 2006), (2) determines the group of species dominating phytoplankton and zooplankton communities and (3) regulates the spatial patterns in plankton biomass and community structure along the inshore-offshore axis of the bay (see Section 1.5).

To achieve this objective, a study was conducted at the coastal observatory in Lunenburg Bay from May 31 to August 15, 2006. During this time, sustained periods of upwelling favourable northeastward winds were selected for analysis. In order to address the timescale issue and therefore to better understand the dynamics of the meteorological forcing resulting in the development of coastal upwelling conditions, an additional adaptive sampling campaign was conducted during a high-frequency storm event (roughly 1 day duration) characterized by upwelling favourable northeastward wind conditions.

2.2 Materials & Methods

2.2.1 Study Site

The study takes place in Lunenburg Bay (Figure 2.1), a 5x8 km inlet that was the site of the MEPS-Bay observatory between 2002 and 2007 (http://www.cmep.ca, *Cullen et al*., 2008).

2.2.2 Observatory Dataset

2.2.2.1 Meteorological Data

Wind speed and direction were recorded hourly at the Battery Point meteorological station (BatPt, Figure 2.1); wind speed was decomposed into cross-shore (U_x, 150°) and along-shore (U_y, 60°) components to compute wind stress using the bulk formula from *Large and Pond* (1981).

2.2.2.2 Chlorophyll Time Series

High frequency time series of estimated chlorophyll biomass were collected at the buoys. The series are data products from the observing system and are computed from measurements of the apparent optical properties collected at the moorings, using the inverse model developed by *Huot et al*. (2007). Details on the data collection and the methodology are available in *Huot et al*. (2007). Phytoplankton absorption time series from the model (a_ϕ at 490 nm; m^{-1}) were subsequently transformed into chlorophyll biomass (mg m^{-3}) using an algorithm developed with 2004 water samples ($n = 132,\ r^2 = 0.575,\ p < 0.01$). The semi-continuous data were subsequently median-averaged for each day.

2.2.2.3 Hydrographic Conditions

Water column physical characteristics (temperature, salinity) were recorded at the mooring station SB3 (mid-bay station, Figure 2.1), with a frequency of 1 or 2 h^{-1}. Surface (1 m, except in 2003: 3 m) and bottom (9 m) sensors were used to infer changes in physical conditions of the water column in relation to upwelling events. Temperature and salinity data were not available from the bottom sensor after August 3 (day 215). Finally, conditions on the inner Scotian Shelf during the sustained and storm-induced upwelling events were assessed using MODIS Sea Surface Temperature measurements (SST; °C), post-processed to fill in for missing pixels (C. Jones, pers comm 2007).

2.2.3 Sampling Campaigns

Weekly sampling campaigns were conducted along a cross-shore transect line from May 31 to August 15, 2006 (13 transects), as part of the routine sampling at the observatory

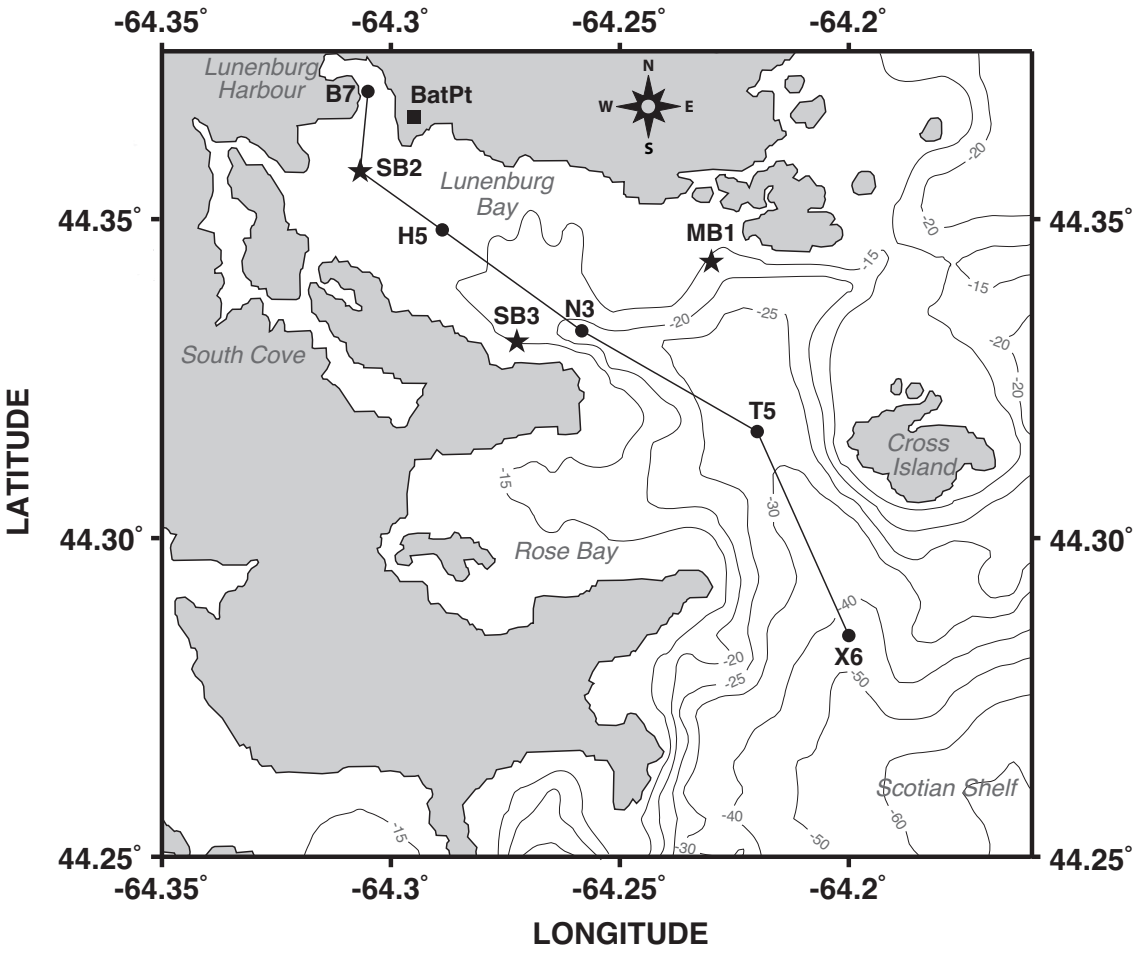

Figure 2.1: Map of Lunenburg Bay and the MEPS-Bay coastal observatory (main locations). ★ Location of the moorings. ● Extra stations sampled in 2006. The black line indicates the transect location. ■ Battery Point meteorological station (BatPt). Doug Mercier and Jinyu Sheng generated the bathymetry data.

(see Figure 2.1). CTD and fluorescence profiles were carried out at each station with the Free-falling Optical Profiler (Satlantic Inc.) whereas water samples were collected with a Niskin bottle at four depths representative of the water column. Chlorophyll biomass was measured using the Welschmeyer fluorometric method (*Welschmeyer*, 1994) with samples collected on GF/F filters. Fluorescence profiles were calibrated for each sampling date by fitting the in-situ chlorophyll measurements (mg m^{-3}) from the water samples collected at all stations on that date to their corresponding fluorescence (volts) measured with the optical profiler (linear fit, $n \sim 26$ on each date). Nitrate concentration (nitrate + nitrite, hereafter referred as NO_3^-) was measured with an automated nutrient analyzer following the technique described by *Grasshoff et al*. (1999).

Integrated water column samples were collected weekly as part of the routine sampling at the mooring stations MB1 (0–13 m, entrance of the bay) and SB2 (0–10 m, inshore) with a PVC pipe and then sub-sampled and preserved into 250 ml bottles (1% paraformaldehyde). Phytoplankton species larger than 10 μm were identified and enumerated using the filter-transfer-freeze technique (*Hewes and Holm-Hansen*, 1983; *Cembella and Rafuse*, 2010). Phytoplankton was sampled during most of the enhanced sampling campaigns, except on day 191 at MB1 and days 150 and 179 at SB2.

Vertical net tows (253 μm mesh size) were carried out at SB2, N3 and X6 along the transect line (Figure 2.1). Samples were stored in 500 ml bottles with a 4% buffered formaldehyde solution and zooplankton species were subsequently identified following the Atlantic Zonal Monitoring Program (AZMP) sampling protocol (*Mitchell et al*., 2002).

A three-days intensive sampling campaign along the same transect line was carried out following a storm event over the period August 8 to 10, 2006 (days 220–222, see Section 2.3.1). The same dataset was collected (including in-situ nitrate and chlorophyll), twice a day during daylight (ebb and flood tide transects), except for phytoplankton taxonomy that were not collected. Therefore, phytoplankton community composition cannot be analyzed during this event. Altogether, a total of six transects were carried out over the three days (water samples were not collected at the mooring stations SB3 and MB1). Adverse weather conditions prevented sampling at the outer deep end station during some of the transects.

2.2.4 Data processing and Analysis

2.2.4.1 Nitrate-Density Relationship

The water samples and CTD profiles were used to calculate a nitrate-density relationship (Figure 2.2) by matching nitrate concentrations in the water samples (NO_3^-; mmol m^{-3}) to the density measured with the CTD profiler (ρ; kg m^{-3}). The relationship indicates that nitrate estimated from density ($\widehat{NO_3^-}$; mmol m^{-3}) is $\widehat{NO_3^-} = 2.763\,\rho - 2830.565$ when $\rho > 1024.43$ kg m^{-3} ($n = 69, r^2 = 0.66, p < 0.01$) and otherwise $\widehat{NO_3^-} = 0.22 \pm 0.15$ SD ($n = 297$). Mid-water samples (4–25 m, $n = 16$) from days 187 and 191 were excluded from the relationship due to apparent nitrate utilization during the upwelling events. This nearshore relationship differs from the relationship observed at Station 2 (see location in Figure 1.1) on the Scotian Shelf (AZMP data, *Therriault et al*., 1998, see Chapter 4). Deep nitrate concentrations are higher at lower density in Lunenburg Bay (lower cut-off value, see Figure 2.2). A shallower euphotic zone (*Zentara and Kamykowski*, 1977), a higher grazing control nearshore (*Minas et al*., 1986) or different water masses could explain this difference.

This relationship does not account for the increase in nitrate at low density due to a terrestrial source of nitrate from surface runoff. The absence of river in Lunenburg Bay, the low nitrate concentration in the water samples inside the bay, in particular at the surface and the lack of relationship with nitrate at low density (Figure 2.2) indicate that runoff is not a significant source of nitrate in Lunenburg Bay. Some nitrate may however originate from a local source such as sewage from the Lunenburg Harbour. Given the data collected in 2006, in particular at station B7 (Lunenburg Harbour), this source of nitrate appear to be negligible in comparison to the oceanic source of nitrate. The assumption of the absence of a terrestrial source of nitrate is therefore valid for Lunenburg Bay.

The nitrate-density relationship is used to generate proxies for a nitrate concentration time series at the mooring station SB3 using the CTD sensors and for water column profiles of nitrate concentration at the transect stations using the CTD profiler. At the SB3 mooring station, the deep nitrate time series stops after day 215 due to the lack of CTD data. The 1024.43 kg m^{-3} cut-off value from the nitrate-density relationship, hereafter referred as the reference isopycnal, will be used as a proxy for the nitracline.

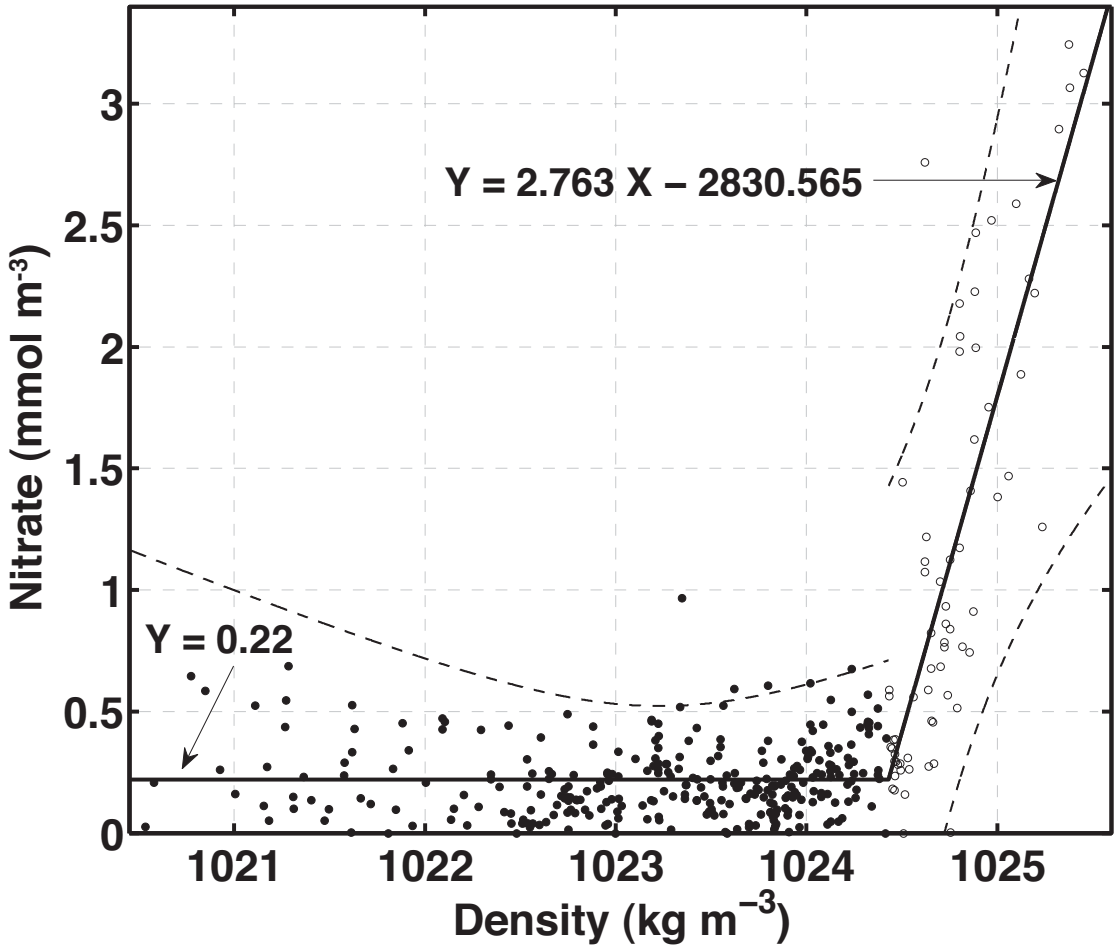

Figure 2.2: Nitrate vs. density relationship using in-situ data collected from May 31 to August 15, 2006. The cut-off value is 1024.43 kg m^{-3}; below that, no relationship is found and the mean value 0.22 mmol m^{-3} is used; above it, the relationship is represented by a linear fit. Dashed lines represent the upper and lower 95% prediction limits for both curves.

2.2.4.2 *Upwelling Effect on Chlorophyll Biomass*

The local contributions of short-term accumulation of phytoplankton biomass to the change in nitrate concentration and chlorophyll biomass during an upwelling event was assessed by calculating chlorophyll anomalies (see *Yentsch*, 1974) in the upper 20 m (estimated depth to the 1% light level) at each station between days 179 and 187 (hereafter referred as the $\widehat{\text{Chl}}$ analysis). Chlorophyll anomalies ($\Delta\widehat{\text{Chl}}$, mg m^{-3}) are estimated from the difference between the change in concentration of nitrate expected from the change in density over days 179 to 187 and the measured change in nitrate (i.e., change in nitrate due to source water, minus uptake) multiplied by a typical ratio of chlorophyll to nitrogen (Eq. 2.1). Chlorophyll anomalies are then compared with the observed change in chlorophyll biomass (ΔChl, mg m^{-3}) over the same period (Eq. 2.2). The following relationships were used:

$$\Delta\widehat{\text{Chl}} = \left(\left[\widehat{\text{NO}_3^-}\Big|_{\sigma_t}^{187} - \widehat{\text{NO}_3^-}\Big|_{\sigma_t}^{179} \right] - \left[\text{NO}_3^-\Big|_{\text{obs}}^{187} - \text{NO}_3^-\Big|_{\text{obs}}^{179} \right] \right) \cdot \frac{12}{\theta} \cdot \text{C:N} \tag{2.1}$$

$$\Delta\text{Chl} = \left(\text{Chl}\Big|_{\text{obs}}^{187} - \text{Chl}\Big|_{\text{obs}}^{179} \right) \tag{2.2}$$

where θ is the carbon to chlorophyll ratio (50 gC $gChl^{-1}$), C:N is the Redfield carbon to nitrogen ratio of 6.625 molC $molN^{-1}$ and 12 is the atomic weight of carbon (g mol^{-1}). The vertical bar on the right of each variable indicates the day number (top) and the type of variable (bottom)(obs: observed, σ_t: inferred from density).

Nitrate concentration in the absence of local net primary production ($\widehat{\text{NO}_3^-}$; mmol m^{-3}) was estimated from density using the CTD profiles (Section 2.2.4.1), observed chlorophyll biomass (Chl; mg m^{-3}) was determined from the fluorescence profiles (Section 2.2.3), and observed nitrate concentration (NO_3^-; mmol m^{-3}) was determined from water samples. All values were averaged over the upper 20 m at each station.

2.2.4.3 *Phytoplankton Biomass Prediction Model*

In order to determine if the magnitude and variability of phytoplankton biomass can be accounted for by hydrography and upwelled nutrients, a phytoplankton biomass prediction model is developed at the mooring station SB3 (mid-bay) using a relationship between

chlorophyll biomass estimated from the optical data ($(\mathrm{Chl})_{a_\phi}$; mg m^{-3}) and three explanatory variables: water density at the surface (ρ_s; kg m^{-3}), water density near the bottom (ρ_b; kg m^{-3}) and estimated bottom nitrate ($(\widehat{\mathrm{NO_3^-}})_b$; mmol m^{-3}). Water density both at surface and bottom was selected to represent the hydrographic conditions in Lunenburg Bay, which reflect a range of dynamic processes including mixing, stratification, upwelling (onset, relaxation) or downwelling. Bottom nitrate (estimated from density) was selected to account for the change in phytoplankton biomass resulting from the input of nitrate during upwelling events. It is important to include this predictor independently of density since nitrate concentration is not linearly related to density but rather depends on a density threshold that represents the nitracline (bilinear relationship, Figure 2.2).

The relationship is determined using a multiple linear regression model formulated as follows:

$$\mathrm{Chl}(t) = a \cdot \rho_b(t) + b \cdot \rho_s(t) + c \cdot (\widehat{\mathrm{NO_3^-}})_b(t - \Delta t) + d + \varepsilon(t) \tag{2.3}$$

where a and b (mgChl kg^{-1}), c (mgChl mmolN^{-1}) and d (mgChl m^{-3}) are the model coefficients, $\varepsilon(t)$ represents the model residuals (uncorrelated to the other terms) and Δt is a time lag introduced to account for the time between the onset of the upwelling and the subsequent increase in phytoplankton biomass. Δt was chosen to maximize the fit of the linear regression to the dataset through an incremental procedure. The multiple linear regression coefficients are also estimated using standardized variables in order to retrieve standardized coefficients (beta coefficients), which are an indication of the contribution of each predictor to the model.

In the study, the multiple regression model is estimated with the first half of the dataset (days 150–189) and the rest of the dataset used to predict chlorophyll biomass. To test its overall ability to predict chlorophyll biomass, the model is also used for prediction (period June-August) for all the years covered by the observing system (2003–2006, required data not available for 2002 and 2007). In 2006, the lack of bottom salinity and temperature data at SB3 after day 215 prevents the prediction of chlorophyll biomass after that date.

2.2.4.4 Multivariate Analysis of Plankton Community Structure

Changes in plankton community structure between sites were assessed with the Bray-Curtis dissimilarity index (*Bray and Curtis*, 1957) which was used as an input for Non Metric Multidimensional Scaling (NMDSp for phytoplankton and NMDSz for zooplankton). This statistical method, which maximizes the correlations between community dissimilarity and ordination distance, is used to visualize the similarities and dissimilarities in community composition in a multi-dimensional space (*Legendre and Legendre*, 1998). The analysis was carried out using the statistical program R with the vegan package (*Dixon*, 2003).

2.3 Results

2.3.1 Wind Events Selected for the Study

Typical of the summer, the dominant winds were oriented northeastward during the study (i.e., positive alongshore wind stress in Figure 2.3A). Two distinct types of alongshore upwelling favourable wind events (i.e. wind oriented 60°, see *Petrie et al*., 1987) were analyzed during the study: sustained and storm-induced upwelling events.

A sustained upwelling is defined as a prolonged period of synoptic intermittent northeastward winds ($\geqslant$ 4 day), typical for the development of offshore Ekman transport along the coast of Nova Scotia. A minimum threshold of 0.1 N m^{-2} for the maximum (positive) alongshore wind stress is used to discriminate these events. In early summer 2006, two successive periods of sustained upwelling, June 28–July 3 (day 179–184, hereafter Sustained 1) and July 9–July 12 (day 190–193, hereafter Sustained 2), were selected using these criteria (Figure 2.3). The average alongshore wind stress during the overall time interval including the two events (June 28–July 12) is 0.03 N m^{-2}, which coincides with the value reported by *Petrie et al*. (1987) over 31 days during a time period of sustained upwelling in July 1984.

A storm-induced upwelling event is defined as a short period of strong northeastward

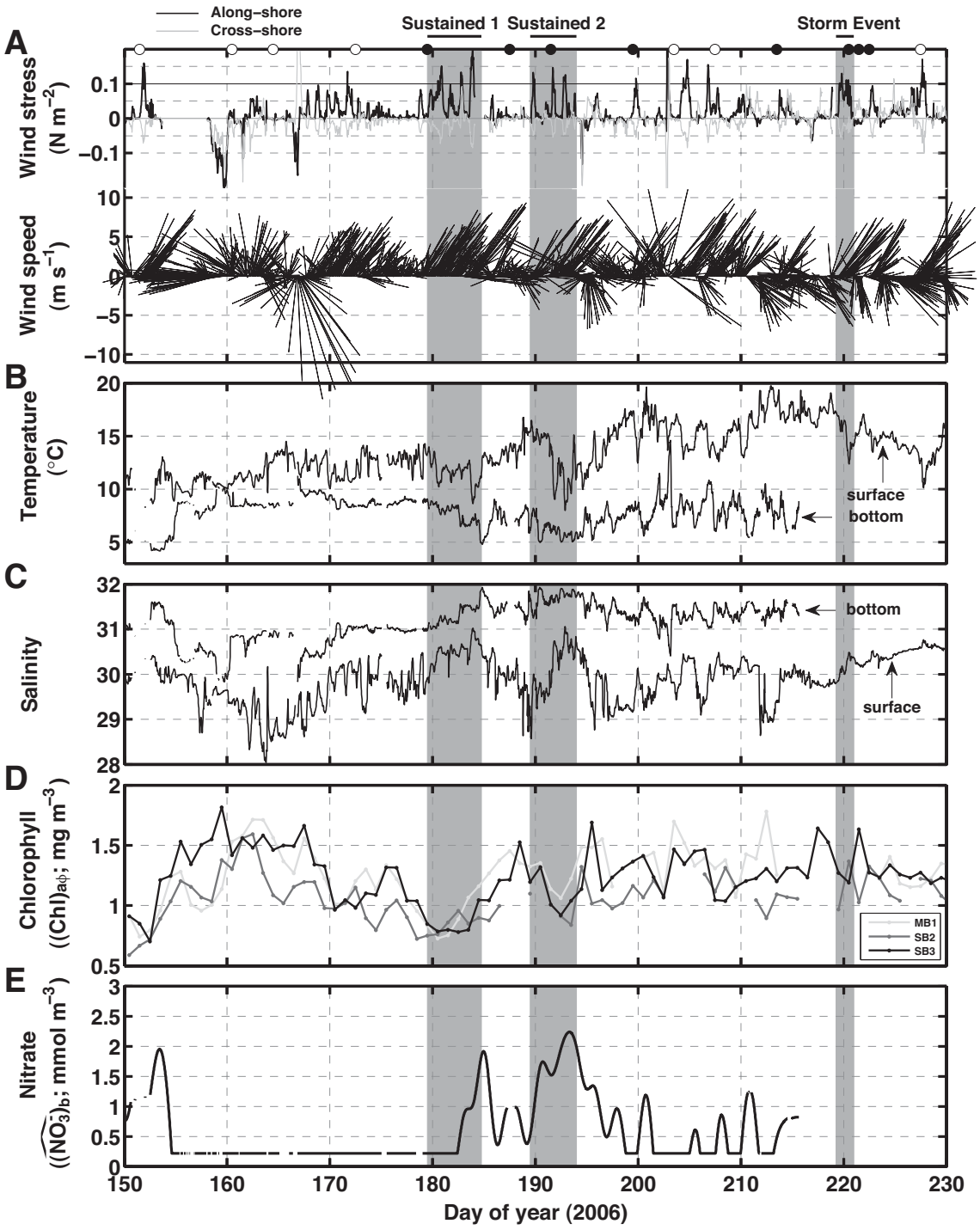

Figure 2.3: Time series from the observatory for the period May 30 - August 18, 2006. A. Wind stress and wind speed vectors from BatPt station. Top circles indicate the dates of the transects and filled circles the transects presented in the analysis. The black thin line is the cut-off wind stress (0.1 N m^{-2}) for selecting sustained upwelling periods. Shaded areas indicate the meteorological events selected for analysis (see Section 2.3.1). B-C. Temperature and salinity from the SB3 mooring surface (1 m) and bottom (9 m) sensors. D. Daily estimates of chlorophyll concentration at the three moorings (see Section 2.2.2.2). E. Proxy for bottom nitrate (9 m) at SB3 (see Section 2.2.4.1 and more details in Figure 2.7B).

winds (~1 day duration) generated by the transit of a storm. The timescale differs significantly from a sustained upwelling. The same minimum threshold of 0.1 N m^{-2} for the maximum (positive) alongshore wind stress is used to select such an event. A storm-induced upwelling event (hereafter Storm Event, Figure 2.3) was detected in mid-summer 2006 using localized weather forecast. An intensive adaptive sampling was conducted following the Storm Event (see Section 2.2.3 for details).

2.3.2 Variability Associated with Sustained Upwelling

The development of the first sustained upwelling event (Sustained 1) is observed on the SST images of the inner Scotian Shelf (Figure 2.4). Coastal bands of cold water appear during the event, reaching a maximum area on day 184 (July 3) with surface water down to 8°C outside Lunenburg Bay. Inside the bay, a peak of 1025.3 kg m^{-3} bottom density is recorded (T = 4.8°C, S = 31.9, Figure 2.3 & 2.5), which corresponds to water found at a maximum of 33 m depth on the Scotian Shelf in July (1999–2005 Station 2 data, *Therriault et al*., 1998). A coastal band of cold water is also observed on the SST images at the end of the second sustained upwelling event (sustained 2) (limited spatial coverage, Figure 2.4), with a similar increase in density inside Lunenburg Bay.

The biological effects inside Lunenburg Bay appear on the enhanced sampling transects (Figure 2.5). Chlorophyll biomass is low prior to Sustained 1 event during a period of weak wind conditions (Figure 2.3 & 2.5). Low chlorophyll biomass is also characteristic of the onset of the event, an indication of the transport inshore of phytoplankton-poor deep water from the shelf. The event then leads to an increase in chlorophyll biomass, mainly in the deep area around the entrance of the bay (stations N3, T5 and X6) where the maximum in-situ chlorophyll biomass occurs at 11 m at station T5 (4.5 mg m^{-3}). A comparison with the pre-upwelling transect reveals an upward movement of the reference isopycnal from 21 m to 7 m, indicating the shoaling of the nitracline and consequently the input of nitrate in the photic layer during the event. Deep and subsurface nitrate samples collected during the two dates confirm this process (Figure 2.6A). Similar hydrographic conditions are found on day 191 during Sustained 2 event, associated with a decrease in chlorophyll biomass (Figure 2.3 & 2.5), followed on day 199 by stratified conditions with a deepening of the reference isopycnal, the consequence of upwelling relaxation. Thin

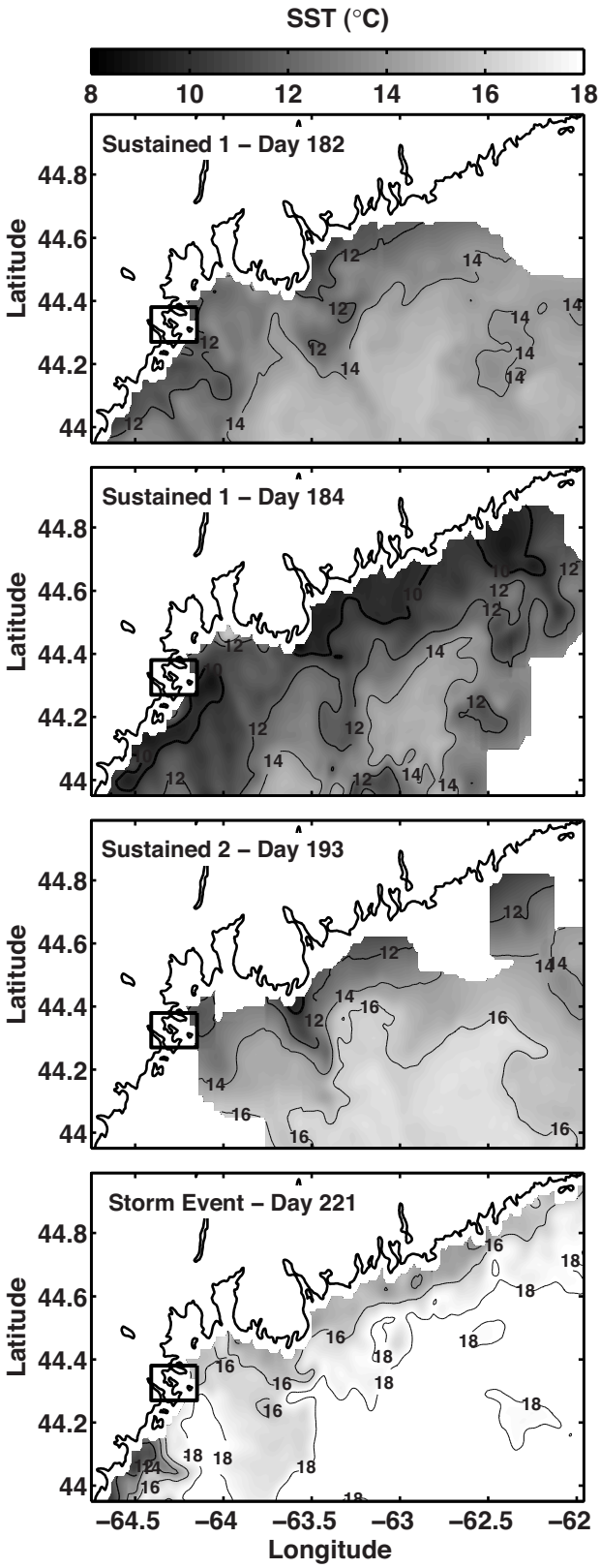

Figure 2.4: Sea surface temperature of the inner Scotian Shelf from MODIS in 2006 during (top to bottom) Sustained 1 event (days 182 and 184), Sustained 2 event (day 193) and after the Storm Event (day 221). The black box represents the location of LB.

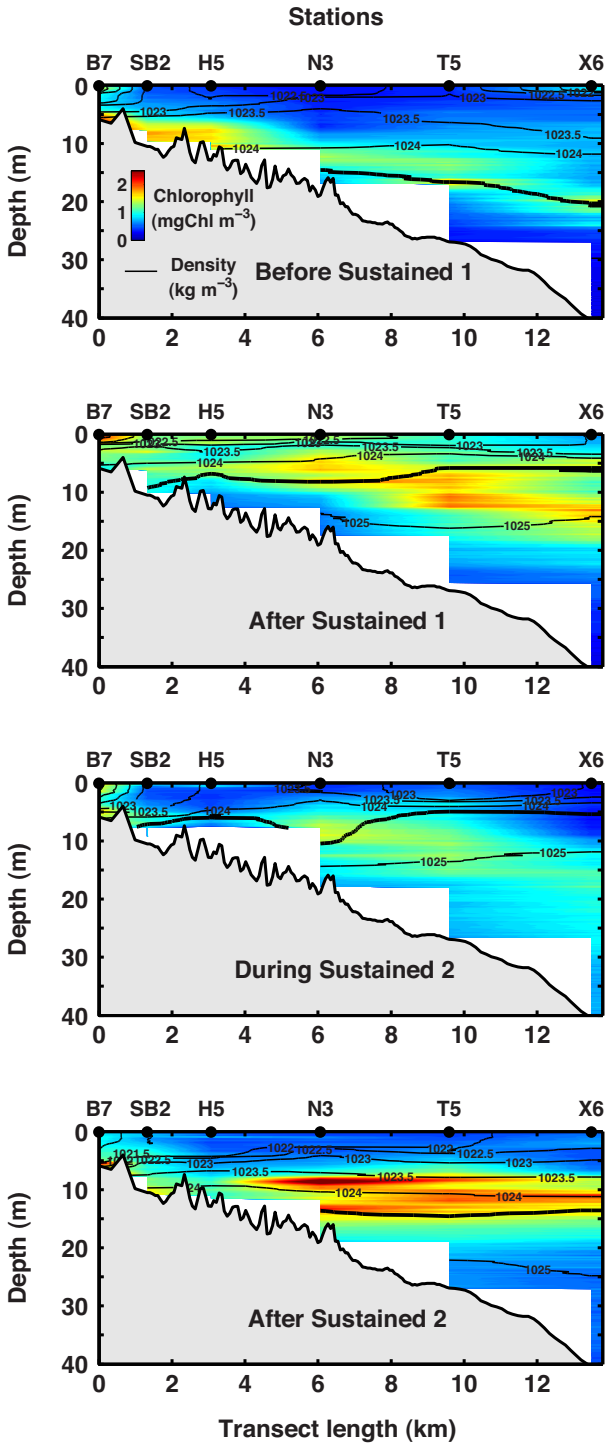

Figure 2.5: Transects of chlorophyll (colour-scale) and density (contours) in Lunenburg Bay for (top/bottom) June 28 (day 179), July 6 (day 187), July 10 (day 191) and July 18, 2006 (day 199). The thick black line indicates the reference isopycnal (1024.43 kg m^{-3}). The location of the stations are described in Figure 2.1. Each station corresponds to a vertical profile of chlorophyll (from fluorescence) and density. The profiles are then interpolated between stations. The bathymetry along the transect is represented by the gray area.

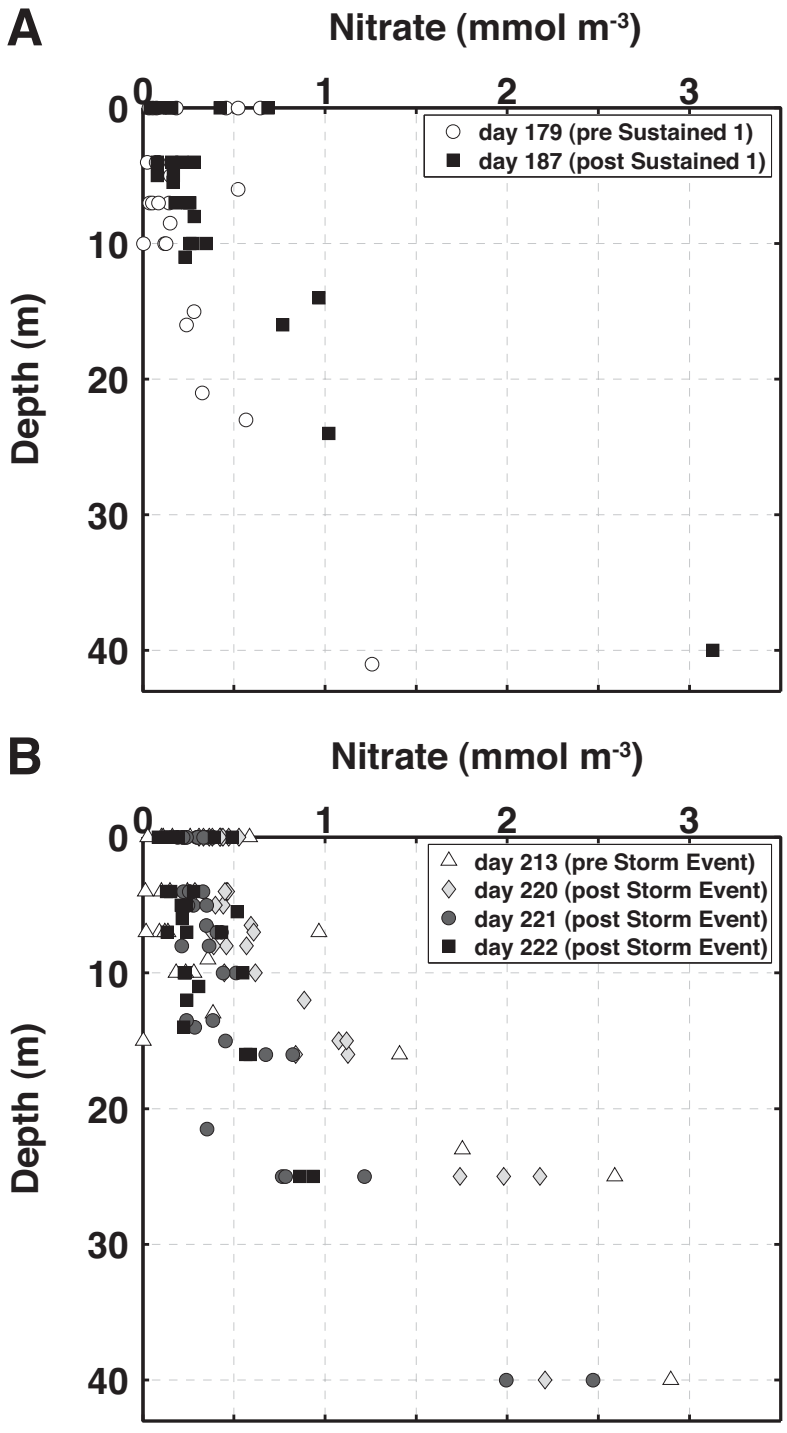

Figure 2.6: Nitrate data collected before/after Sustained 1 event (A) and before/after the Storm Event (B). The data include all stations along the transect. The data collected below 10 m correspond to the stations N3, T5 and X6 in the deep outer side of the transect (see Figure 2.1).

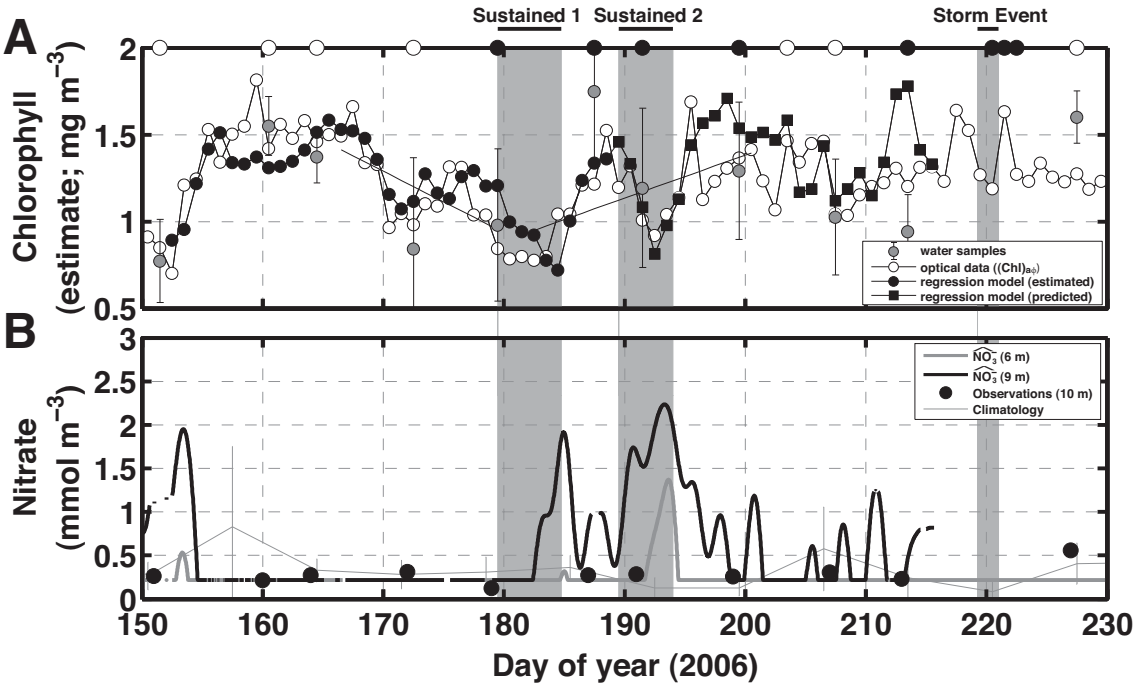

Figure 2.7: Time series of chlorophyll and nitrate from the mooring station SB3. A. Daily-averaged chlorophyll estimated from observed optical properties with the inverse optical model (white circles, *Huot et al.*, 2007), and estimated and predicted from the regression model based on density and the nitrate proxy (black circles: regression estimates for days 152–188 and black squares: predictions for days 189–215, see Section 2.2.4.3). The grey circles are the water-column averaged chlorophyll concentration from the water samples (collected at 0, 4, 7 and 10 m; no samples on days 213 and 220–222). The standard deviation is indicated (n = 4). The black straight lines are linear fits to the optical data for the periods before (days 166–179; slope: a = –0.035 mgChl m^{-3} d^{-1}, n = 15) and during and after (days 180–200; slope: a = 0.025 mgChl m^{-3} d^{-1}, n = 21) Sustained 1 event. B. Nitrate time series at 6 m (thick gray line) and 9 m (thick black line) estimated from density with the nitrate-density relationship (Figure 2.2). The thin gray line is the weekly climatology of bottom nitrate (2002–2006) calculated from samples collected at 10 m. Error bars represent the standard deviations (n = 2–5). Black dots represent bottom nitrate data (10 m) collected at SB3 during the study. Shaded areas indicate the selected meteorological events and the circles at the top of the figure indicate the sampling dates (see Figure 2.3).

layers of phytoplankton were detected at this date on the deep end side (Figure 2.5) with a maximum biomass at 12 m at station X6 in the water samples (2.8 mg m^{-3}) and at 9 m at station N3 in the fluorescence profiles (3.0 mg m^{-3}).

The estimated nitrate time series at SB3 (mid-bay) indicates an increase of nitrate concentration to about 2 mmol m^{-3} during Sustained 1 and Sustained 2 events (Figure 2.7B). This is significant compared to the low-nitrate background concentration observed throughout the summer on the climatology, and confirms that sustained upwelling events are a source of nitrate to Lunenburg Bay. On the time series, some discrepancy occurs between observed and estimated nitrate concentration during Sustained 2 event (Figure 2.7B), which suggests the utilization of nitrate for primary production during the sustained upwelling events, not taken into account by the nitrate proxy.

This process is evaluated with the $\widehat{\text{Chl}}$ analysis during Sustained 1 event, when pre and post-event transects are available (Figure 2.8). The comparison between the chlorophyll anomalies calculated from density and the observed variation in chlorophyll during the event indicates a good agreement at stations N3, T5 and X6, which are located in the deep end side near the entrance or outside of Lunenburg Bay. This agreement indicates an increase in chlorophyll biomass due to local primary production in this area, induced by the input of upwelled nitrate inside Lunenburg Bay during Sustained 1 event. At the inshore stations (B7, SB2 and H5), chlorophyll anomalies are small, indicating a weak or no expected effect of the event on the local accumulation of chlorophyll biomass. The disagreement with the observed chlorophyll biomass at SB2 suggests other processes of phytoplankton accumulation at this station.

To summarize, the two sustained upwelling events were a source of nitrate from the inner Scotian Shelf to Lunenburg Bay and resulted in enhanced phytoplankton biomass in the deep end side of the bay. These changes in chlorophyll concentration were relatively small compared to the variability in other well studied upwelling systems (*Hickey and Banas*, 2003; *Álvarez-Salgado et al*., 2010), however; lower than the $>$ 5 mgChl m^{-3} typically observed in the spanish rias and used as a threshold to validate our hypothesis.

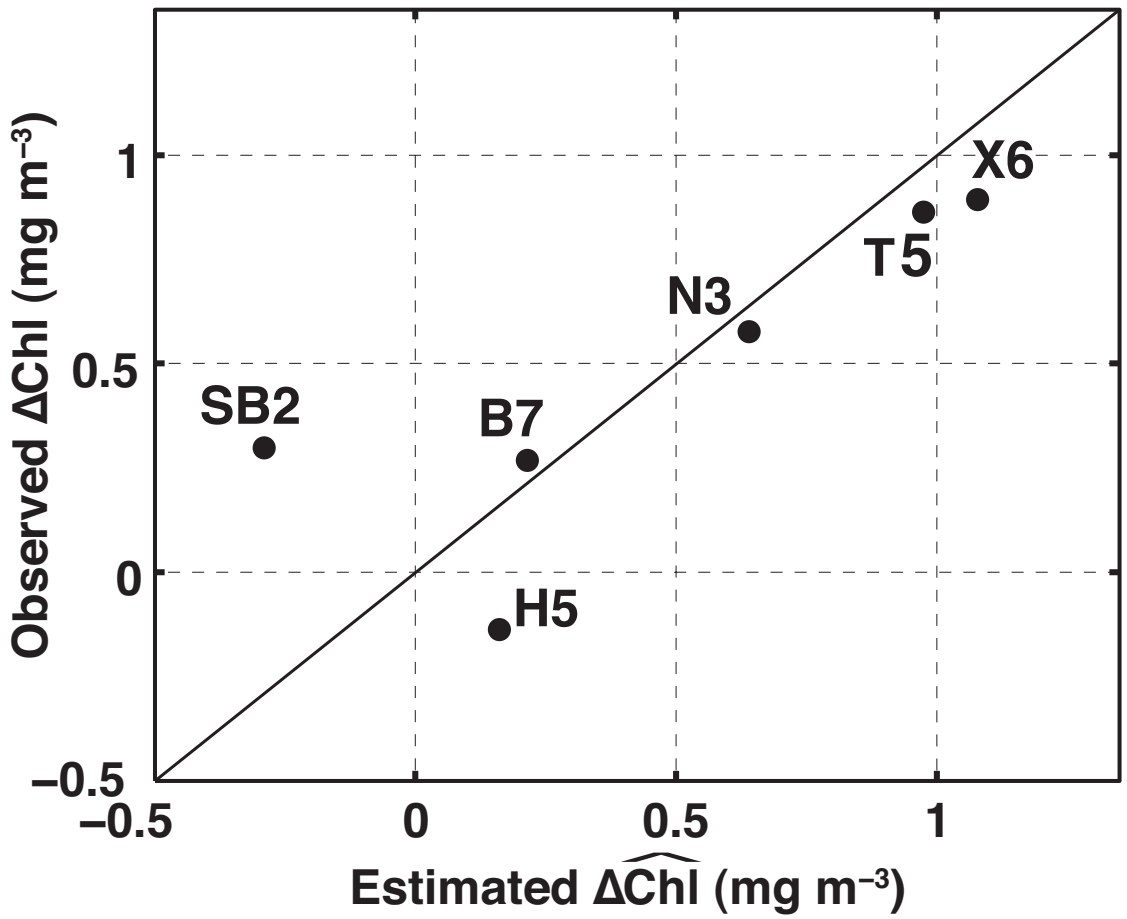

Figure 2.8: Estimated change in chlorophyll biomass due to nitrate utilization by phytoplankton ($\Delta\widehat{\text{Chl}}$); calculated from observed nitrate concentration compared to that expected from the nitrate-density relationship, versus observed change in chlorophyll biomass (ΔChl) in the upper 20 m at each station along the transect between June 28 (day 179, before Sustain 1 event) and July 6, 2006 (day 187, after Sustain 1 event). The black line indicates the 1:1 relationship. A detailed explanation of the analysis is provided in Section 2.2.4.2.

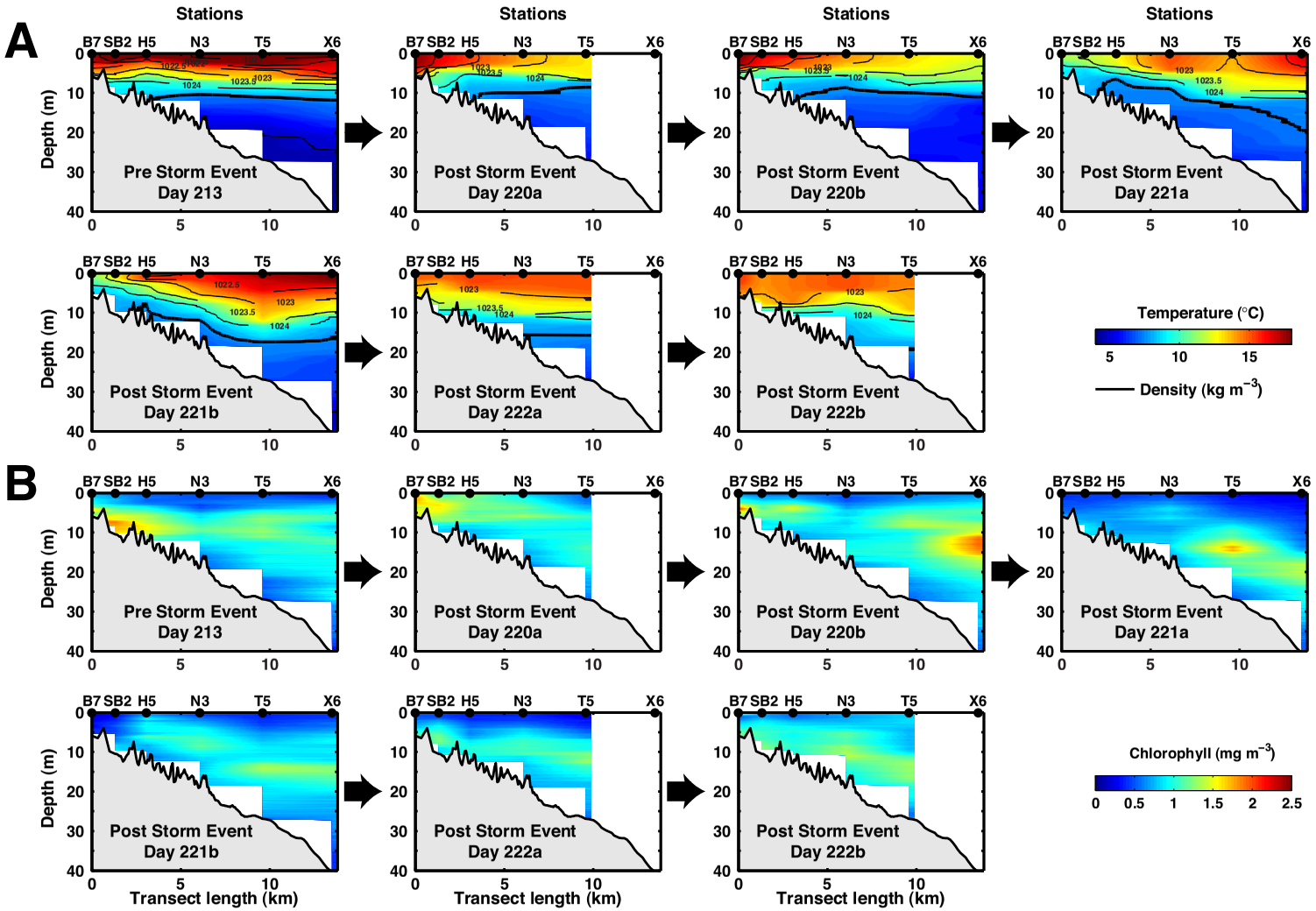

Figure 2.9: Transects of A. temperature (colour-scale) and density (contours) and B. chlorophyll estimated from fluorescence in Lunenburg Bay before and after the Storm Event. Transects are ordered by day (from August 1 to 10, 2006, left/right, top/bottom). Subscripts a and b correspond respectively to ebb and flood tide transects (morning/afternoon). The contour plots are similar to the one described in Figure 2.5.

2.3.3 Variability Associated with Storm-Induced Upwelling

Conditions on the inner Scotian Shelf after the Storm Event (day 221, second day of the intensive adaptive sampling) indicate warm surface temperatures, about 15°C at the coast, which corresponds to the surface water temperature concurrently observed in Lunenburg Bay (Figure 2.3B,C & 2.9A). Pre-event conditions are available a week before the storm (day 213), indicating stratified conditions throughout Lunenburg Bay (Figure 2.9A). Immediately following the Storm Event (day 220), estuarine conditions are observed inshore. Local storm-induced surface circulation combined with heavy rainfall during the storm can explain this pattern. A tilt in the isopycnals appears along the transect line the next day (day 221). The reference isopycnal propagates inshore to mid-depth where shallower isopycnals reach the surface and deepen shelfward (from 10 to 20 m at X6). Stratified conditions are observed the third day (day 222) throughout the bay indicating the relaxation of the event. This high-frequency variability can be explained by the wind-induced local movement of surface water towards the mouth and then the head of the bay, which results in the local inclination of subsurface isopycnals and leads to the transient upwelling of local shallow subsurface waters at the inshore locations SB2 and B7. This local process can be contrasted with the sustained upwelling events that result in the shoaling of deep isopycnals on the inner shelf which translate to Lunenburg Bay. On the contrary, deepening of subsurface isopycnals shelfward during the Storm Event resulted in lower nitrate concentration in the surface layer (deeper nitracline, Figure 2.6B), whereas inshore, the upwelling of local shallow water with low nitrate concentrations (< 0.5 mmol m^{-3}, day 221 on Figure 2.6B) did not influence nitrate concentration in the surface layer. This rapid decrease in nitrate concentration in the upper 20 m did not result in a subsequent increase in chlorophyll biomass (Figure 2.6 & 2.9). This suggests an advective process rather than nitrate utilization by primary producers.

The maximum chlorophyll values following the event (2–3 mg m^{-3}) were found in the surface samples at the inner stations (B7 and SB2) during the first day of sampling reflecting either previous local production, transport, or resuspension of benthic diatoms by mixing during the Storm Event (Figure 2.9B). Similar observations were made during the sustained upwelling events (i.e., mismatch between measured and estimated ΔChl, Figure 2.8), as well as after a downwelling event (day 159, data not included) indicating an

analogous local effect inshore. A subsurface peak of chlorophyll is also present at X6 the day following the storm. The rest of the samples indicate low chlorophyll concentrations in the bay (1 mg m^{-3}).

To summarize, the storm-induced upwelling event, despite the strong northeastward wind conditions, was not a source of nitrate to Lunenburg Bay and did not induce a local phytoplankton response.

2.3.4 Drivers of Variability in Phytoplankton Biomass

The results denote that during the time period investigated, the dominant variability in phytoplankton biomass arises around the period of sustained upwelling. Two periods representing a month-long time interval can be isolated in the time series (Figure 2.3 & 2.7A). Before the two sustained upwelling events, a long period of low nitrate concentration (proxy times series, Figure 2.7B) corresponds to an overall decline in phytoplankton biomass over the two-week period preceding Sustained 1 event (June 15–28, Figure 2.7A). This is followed by a three-week period of increasing phytoplankton biomass (June 29–July 19) associated with the input of nitrate from the shelf during the period of sustained upwelling.

The phytoplankton biomass prediction model is used to determine the contribution of hydrographic conditions to the variability in phytoplankton, including the nitrate input associated with upwelling conditions. The multiple regression for Eq. 2.3 yields a prediction model with the form:

$$\mathrm{Chl}(t) = -0.256 \cdot \rho_b(t) - 0.309 \cdot \rho_s(t) + 0.210 \cdot (\widehat{\mathrm{NO}_3^-})_b(t - 2.75) + 579.792 \quad (2.4)$$

A summary of the regression model statistics is presented in Table 2.1. A significant part of the variability in chlorophyll biomass is explained by the model (days 152–188, $R^2 = 0.64$), which has also some predictive skill, in particular during Sustained 2 event. The second part of the 2006 dataset (days 189–215) indicates however that the prediction skill of the model is limited for that time period ($R^2 = 0.26$). Considering the whole 2003–2006 period, the model demonstrates the ability to predict chlorophyll biomass in the bay ($R^2 = 0.49$, see Figure 2.10). This ability is relatively similar in 2004 ($R^2 = 0.48$)

Table 2.1: Summary of statistics for the phytoplankton biomass prediction model (Regression model, i.e. Eq. 2.4, left) and for the prediction from the model for each year and for the entire 2003–2006 period (Predictive skill). In 2006, the regression model is estimated from the dataset for the days 152 to 188 and the prediction is calculated for the days 189 to 215. R^2 is the coefficient of determination, F is the F-statistic, n is the number of observations and p indicates the level of significance.

	Regression model	Predictive skill				
	(estimate)	2003	2004	2005	2006	All years
R^2	0.64	0.14	0.48	0.40	0.26	0.49
F	62.4	13.5	80.6	10.0	0.26	244.1
n	37	88	90	17	27	259
p	< 0.01	< 0.01	< 0.01	< 0.01	< 0.01	< 0.01

and in 2005 ($R^2 = 0.40$), but not in 2003 when the model yields poor predictive skills ($R^2 = 0.14$). Optical estimates of chlorophyll biomass are significantly lower in 2003 compared to the other years ($t = -13.6, n = 305, p < 0.01$), which could explain the poor predictive skills during that year. The poor fit in 2003 may also indicate a different regime during that year, which the regression fails to represent.

Overall, about half of the variability observed in optically estimated phytoplankton biomass at SB3 is associated with the changes in water column density and the time lag for the phytoplankton response to changes in nitrate inferred from bottom sea water density (Table 2.1). The sign of the model coefficients reveals that phytoplankton biomass is negatively correlated with bottom and surface density (a, b respectively), suggesting a negative effect of the onset phase of sustained upwelling events on phytoplankton biomass whereas the effect is positive during the relaxation phase of the events. The same patterns were revealed in an empirical orthogonal functions analysis of the SB2 (inshore) and SB3 (mid-bay) mooring dataset over the same time range (see Appendix B).

As expected, the lagged nitrate term (c) has a positive effect on phytoplankton biomass in the prediction model, indicating the positive response of phytoplankton biomass to the

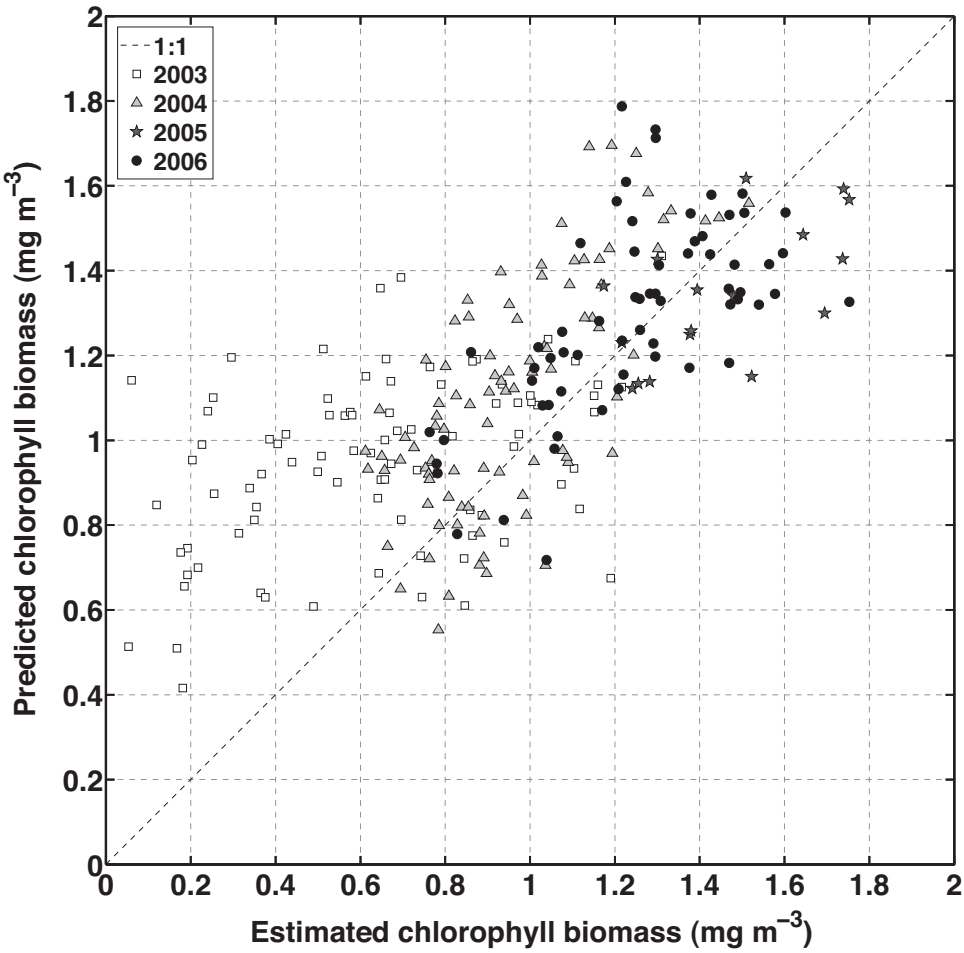

Figure 2.10: Comparison between chlorophyll biomass at station SB3, estimated from observed optical data with the inverse optical model (*Huot et al*., 2007), and predicted primarily from density measurements using the phytoplankton biomass prediction model during the period June-August from 2003 to 2006.

input of nitrate during sustained upwelling events. The time lag found in the analysis (Δt = 2.75 days) is an indication of the time scale of this response and corresponds to a typical growth rate for phytoplankton (0.4 d^{-1}). The regression model is therefore able to estimate the growth rate of phytoplankton during the periods of upwelling events in Lunenburg Bay.

The prediction skill of the model for the period 2004–2006 indicates that the underlying processes in the regression model are recurrent drivers of phytoplankton variability during the summer in Lunenburg Bay. The standardized regression coefficients for Eq. 2.3, respectively $a = -0.42$ (bottom density); $b = -0.55$ (surface density); and $c = 0.36$ (lagged

Table 2.2: Summary of plankton species composition in 2006. N is the total abundance of phytoplankton (×1000, ind m^{-3}) and zooplankton (×1000, ind m^{-2}), S is the total species number and H' is the Shannon diversity index. Phytoplankton < 10 μm were not enumerated. The percentage of diatoms (Diat), dinoflagellates (Dino) and copepods is indicated for each sample as well as the two dominant species and their relative occurrence. The species are: Diatom species: ske: *Skeletonema* spp., chs: *Chaetoceros* (small), stu: *Striatella unicata*, pen: pennate diatoms, pse: *Pseudo-nitzschia delicatissima*, nil: *Nitzschia longissima*, par: *Paralia*, rhi: *Rhizosolenia*. Dinoflagellate species: cel: *Ceratium longipes*, hen: *Heterocapsa niei*. Zooplankton species: ois: *Oithona similis*, tel: *Temora longicornis*, con: copepoda nauplii, acc: *Acartia clausi*, pol: polychaeta, bil: bivalvia larvae, evs: *Evadne* sp, pse: *Pseudocalanus* sp, fri: *Fritillaria* sp.

A. PHYTOPLANKTON

	N		S		H'		% Diat/Dino		Main species		% Total	
Day	SB2	MB1	SB2	MB1	SB2	MB1	SB2	MB1	SB2	MB1	SB2	MB1
151	–	8.85	–	7	–	0.52	–	90/10	–	*ske,hen*	–	90,4
160	103.15	84.13	22	8	0.44	0.30	98/2	99/1	*ske,chs*	*ske,stu*	92,2	94,2
164	53.07	60.41	20	10	1.00	0.29	95/4	97/2	*ske,chs*	*ske,cel*	77,9	95,1
172	2.85	2.97	13	10	1.94	1.85	27/69	55/42	*cel,stu*	*ske,cel*	48,14	34,30
179	–	0.79	–	8	–	2.35	–	34/61	–	*ske,stu*	–	28,22
187	35.33	20.11	26	25	2.43	2.46	88/12	71/25	*pen,chs*	*chs,nil*	23,14	29,13
191	23.55	–	22	–	1.93	–	85/14	–	*ske,chs*	–	43,13	–
199	66.68	216.58	24	25	0.74	1.16	90/10	98/2	*ske,psd*	*ske,psd*	86,3	70,12
207	23.77	35.31	25	17	1.98	1.52	85/15	91/6	*ske,psd*	*par,ske*	42,17	43,31
213	14.68	73.31	18	21	1.52	0.87	71/28	98/2	*ske,hen*	*ske,chs*	61,15	70,25
227	305.72	64.52	20	7	0.76	0.63	99/1	100/0	*ske,chs*	*ske,rhi*	80,11	83,11

B. ZOOPLANKTON

	N			S			% Copepod			Main species			% Total		
Day	SB2	N3	X6	SB2	N3	X6	SB2	N3	X6	SB2	N3	X6	SB2	N3	X6
151	269	–	246	19	–	23	88	–	85	*con,acc*	–	*ois,tel*	21,20	–	28,21
160	192	–	–	12	–	–	75	–	–	*con,pol*	–	–	48,22	–	–
164	501	324	653	19	23	18	69	88	91	*acc,pol*	*ois,con*	*ois,pse*	28,26	37,21	34,22
172	213	677	470	19	24	21	71	77	73	*ois,pol*	*ois,tel*	*ois,bil*	29,15	21,20	31,18
179	180	458	426	23	20	22	68	78	56	*con,acc*	*tel,ois*	*ois,bil*	13,12	30,12	29,19
187	48	131	198	17	23	21	86	76	74	*con,acc*	*con,acc*	*ois,pse*	38,18	20,14	20,19
191	260	642	889	21	20	28	78	81	71	*con,acc*	*con,acc*	*ois,tel*	27,23	20,20	24,18
199	265	490	266	19	22	27	78	72	81	*acc,con*	*acc,con*	*ois,pse*	35,13	21,20	25,14
203	296	453	340	20	20	25	67	73	79	*acc,con*	*acc,ois*	*ois,tel*	21,11	21,14	26,18
207	361	–	370	22	24	29	75	–	44	*acc,ois*	–	*par,ois*	18,13	–	36,18
213	237	337	233	18	25	26	75	69	60	*ois,acc*	*tel,evs*	*ois,evs*	19,16	17,14	28,15
220.35	358	517	–	21	23	–	60	72	–	*acc,bil*	*tel,ois*	–	19,16	26,15	–
220.65	427	274	47	17	19	25	81	61	71	*acc,con*	*tel,fri*	*ois,con*	41,12	31,13	36,11
221.35	523	504	105	19	24	18	82	77	75	*acc,ois*	*tel,acc*	*ois,con*	41,12	25,14	30,20
221.65	526	531	134	19	21	22	73	77	79	*acc,bil*	*tel,acc*	*ois,con*	39,16	26,14	38,15
222.35	539	405	–	19	22	–	85	62	–	*acc,tel*	*tel,ois*	–	46,16	16,15	–
222.65	304	685	–	20	21	–	88	69	–	*acc,con*	*tel,acc*	–	44,11	23,15	–
227	609	761	102	18	25	22	79	81	69	*acc,tel*	*tel,acc*	*ois,con*	49,7	30,12	25,23

bottom nitrate), indicate a larger contribution of surface density to the relationship. This dissimilarity between the contribution of surface and bottom density suggests that surface density stratification also contributes to the variability of phytoplankton biomass at SB3. The remainder of the variability, which is not accounted for by the three predictors in the phytoplankton biomass model, can result from uncertainties in the optical model (see *Huot et al*., 2007) that induce a mismatch with the predictions and an error in the regression model, and from other processes not included in the regression model, that contribute to the control of phytoplankton biomass in Lunenburg Bay during the summer.

2.3.5 Effects on Plankton Assemblages

2.3.5.1 Phytoplankton

A total of 69 phytoplankton taxa ($> 10\,\mu$m) were identified during the study, among which most species were diatoms and dinoflagellates. Phytoplankton abundance (ind m^{-3}) was dominated by the coastal and opportunistic diatom *Skeletonema* spp. in 2006 (Table 2.2A), except for the period preceding and during Sustained 1 and Sustained 2 events. On the date preceding Sustained 1 event (day 179), *Skeletonema* spp. is absent from the phytoplankton assemblage. This date corresponds to the end of the 2–3 week time period without nitrate input from the Scotian Shelf and the concurrent decline in phytoplankton biomass (see Section 2.3.4). The decrease in phytoplankton abundance over the same period, and its seasonal minimum observed inside Lunenburg Bay on day 179, corroborate the decline observed in phytoplankton biomass.

The multivariate analysis presented in Figure 2.11 ($r^2 = 0.94, stress = 0.243$) segregates the scores of the species weighted average (i.e., centroid of the species on the NMDS axes) along the first dimension of the NMDSp into two distinct groups representing diatoms and dinoflagellates ($p < 0.01, n = 37$, see Table 2.3). Therefore along this dimension, temporal changes of the sample scores (i.e. location of a community at particular time and location in the multidimensional space) represent a shift in the phytoplankton community structure (dinoflagellates/diatoms). This shift is also associated with a change in phytoplankton abundance since dinoflagellates dominate the community when phytoplankton abundance is low, whereas diatoms (predominantly *Skeletonema* spp.) dominate

Table 2.3: Spearman rank correlations of environmental and temporal variables with the NMDS sample scores of phytoplankton ($n = 19$) and zooplankton ($n = 47$), as well as phytoplankton group types (diatom, dinoflagellate, flagellate) with the phytoplankton species scores ($n = 37$) along the two dimensions of the NMDSp and NMDSz; bold values indicate a significant correlation with $^{*}p < 0.05$ and $^{**}p < 0.01$.

	Phytoplankton		Zooplankton	
Variables	NMDSp 1	NMDSp 2	NMDSz 1	NMDSz 2
Day of year	0.14	**−0.49***	−0.18	0.14
Algal group	**−0.80****	−0.19	–	–
Temperature (surface)	−0.24	−0.40	0.02	−0.25
Temperature (bottom)	0.17	0.24	−0.08	0.02
Salinity (surface)	0.05	−0.45	−0.19	0.23
Salinity (bottom)	−0.12	**−0.52***	−0.20	0.21
Density (surface)	0.18	−0.17	−0.14	0.28
Density (bottom)	−0.23	−0.40	−0.03	0.11
Stratification index	−0.30	−0.08	0.06	−0.15
Depth	−0.15	−0.08	**0.90****	0.04
Distance to shore	0.15	0.08	**0.90****	0.03

the community during periods of high phytoplankton abundance (see Table 2.2A). These two dominant phytoplankton groups are similar throughout the summer 2006 at the mooring stations SB2 and MB1 where the data were collected. Among the two stations, SB2 is located at the head of Lunenburg Bay, whereas MB1 is near the entrance (Figure 2.1), suggesting that phytoplankton assemblages were similar throughout Lunenburg Bay during the period investigated. More spatially resolved data are necessary to support this pattern however. The rest of the analysis focuses on the patterns in phytoplankton community structure observed at MB1.

The temporal patterns of the sample scores along the first dimension of the NMDSp (Figure 2.11A), indicate that at MB1 the phytoplankton shifts towards a dinoflagellate dominated assemblage prior to Sustained 1 event (days 172 and 179). This period corresponds to the decline in phytoplankton biomass and abundance during the period without nitrate input from the Scotian Shelf (Section 2.3.4). Sustained 1 event leads to a rapid shift towards a mixed assemblage dominated by diatoms, but where dinoflagellates reach their

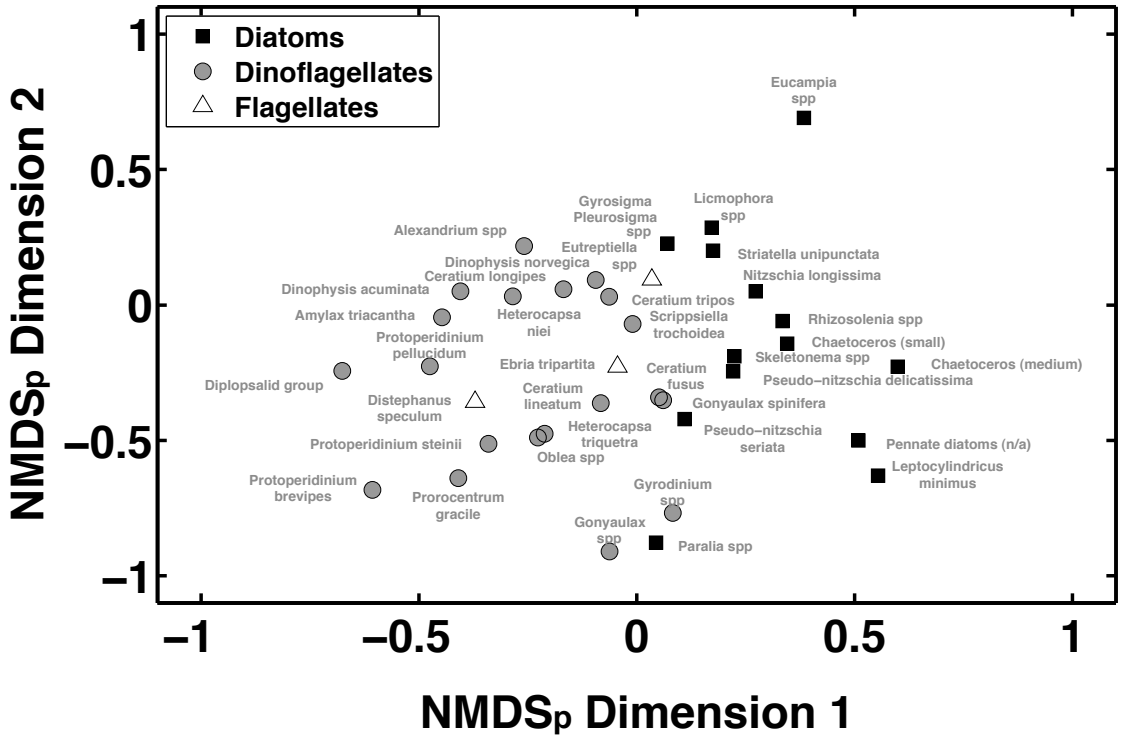

Figure 2.11: Species weighted average scores along the two dimensions of the NMDSp analysis. The name of each species is indicated for each symbol. Rare and low abundance species are not represented on the figure.

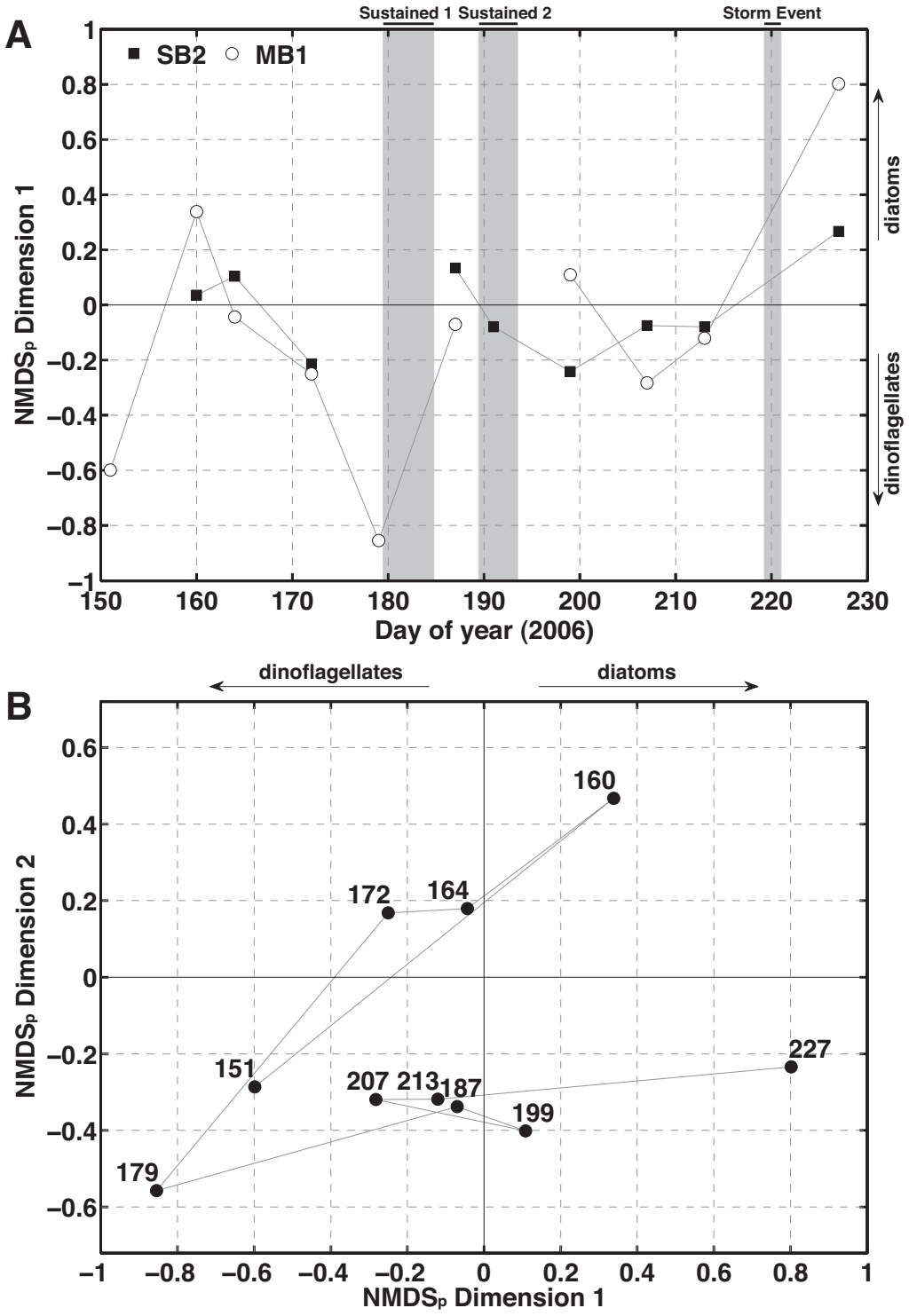

Figure 2.12: Changes in phytoplankton community composition as represented by sample scores along the dimensions of the NMDSp. A. Time series of the sample scores along the first dimension at stations SB2 (■) and MB1 (○). Shaded areas represent the sustained and storm-induced wind events. B. Sample scores (labelled by day number) along the two dimensions for station MB1. Variations along Dimension 1 represent changes in the dominant group of species (see Figure 2.11 & Table 2.3).

seasonal maximum in abundance. At that time, dinoflagellate species are dominated by *Ceratium longipes*, typical of deep phytoplankton populations on the Scotian Shelf. This is an indication of the inshore transport of phytoplankton species during the upwelling event (cf *Côté and Platt*, 1983). This response to Sustained 1 event corresponds to a 3-fold increase in the number of species that reaches a seasonal maximum (Table 2.2A). A mixed phytoplankton assemblage largely dominated by the diatom *Skeletonema* spp. is present after Sustained 2 event (day 199) when phytoplankton abundance reaches a seasonal maximum at the mooring station MB1 (Table 2.2A). The increase in phytoplankton abundance during this relaxation phase is more pronounced at MB1, which reveals a spatial pattern of phytoplankton abundance resulting from the relaxation of the upwelling conditions. This agrees with the observations of chlorophyll biomass (Section 2.3.2). The variations of the sample scores are not as clear along the second axis (Figure 2.11B), but suggest temporal patterns of phytoplankton assemblages that are not related to the occurrence of the sustained upwelling events.

Given the short time-scale of the storm-induced upwelling event, the low nitrate concentrations and low chlorophyll biomass observed throughout the event (Section 2.3.3), neither changes in phytoplankton community structure nor in abundance were expected during this event. Nevertheless, since phytoplankton taxonomy data were not available during the event, the short-term variability in phytoplankton species composition associated with the storm-induced upwelling event cannot be examined.

2.3.5.2 Zooplankton

The dominant species recorded in the zooplankton samples are listed in Table 2.2B. On average, copepods represent 75% of the total zooplankton abundance, the dominant species being the small copepods *Acartia clausi*, *Oithona similis*, *Temora longicornis*, as well as *Pseudocalanus* sp. (Table 2.2B). In contrast to the temporal patterns observed in the phytoplankton, the multivariate analysis reveals that zooplankton sample scores along the first dimension of the NMDSz ($r^2 = 0.96, stress = 0.190$, Figure 2.13) are significantly grouped by sampling location along an inshore-offshore gradient of increasing depth ($p < 0.01, n = 47$, see Table 2.3). This correlation is statistically significant and appears to be the only correlation with the environmental and temporal variables tested in

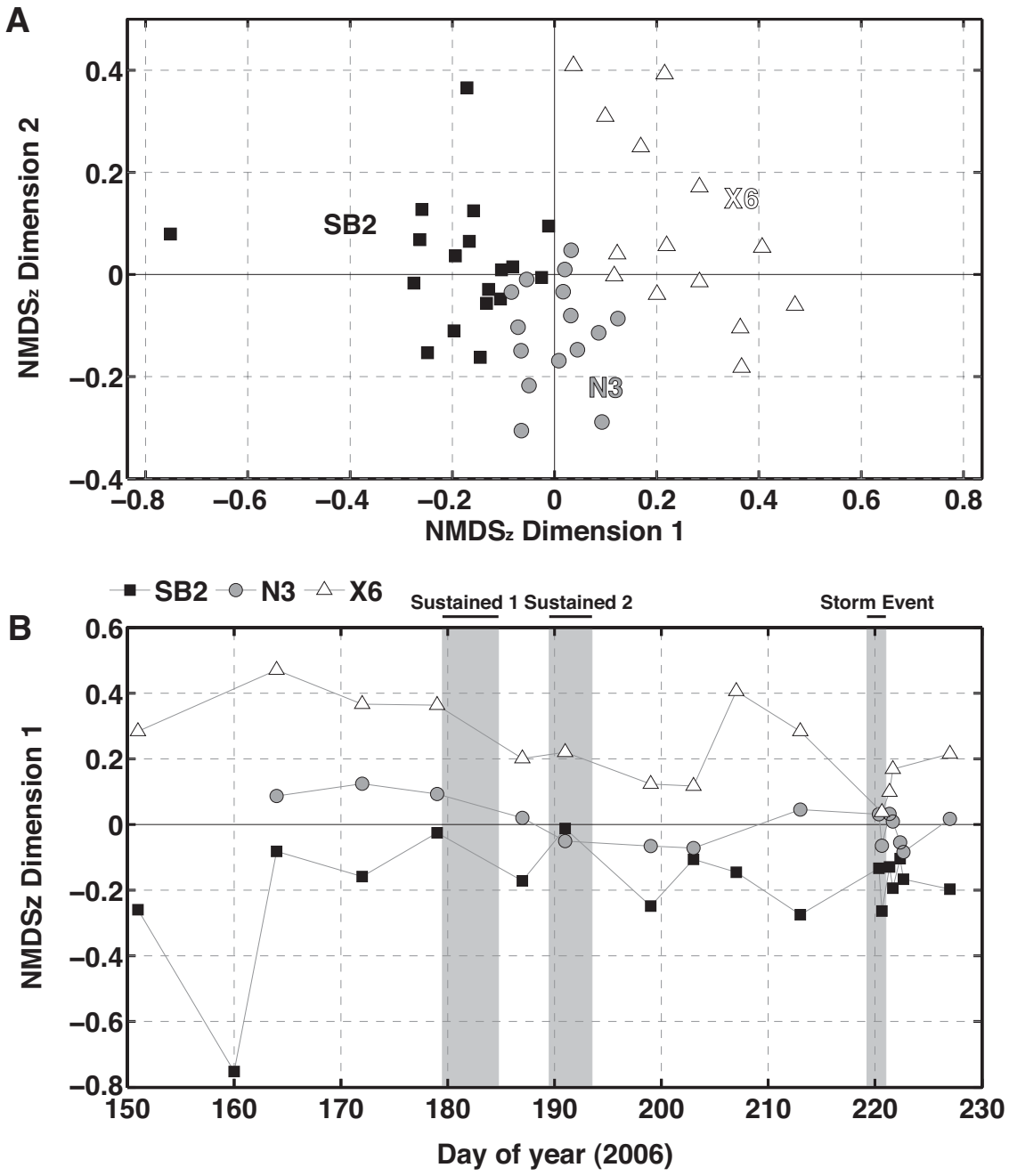

Figure 2.13: Changes in zooplankton community composition as represented by sample scores along the dimensions of the NMDSz analysis. The samples are grouped by station. A. Scatter plot of the sample scores along the two dimensions of the NMDSz. B. Time series of sample scores along the first dimension of the NMDSz. Shaded areas represent the sustained and storm-induced wind events.

Table 2.4: Main species in the zooplankton samples and their scores on the two dimensions of the NMDS*z*. The species are ordered from their position along the first dimension of the NMDS*z* (NMDS*z* 1).

Species/taxon	NMDS*z* 1	NMDS*z* 2
Harpacticoida	–1.07	–0.02
Podon sp.	–0.42	0.32
Eurytemora herdmani	–0.38	0.00
Acartia clausi	–0.33	–0.13
Bryozoans	–0.16	–0.07
Acartia sp. (copepodite)	–0.12	–0.01
Podon leuckartii	–0.09	–0.15
Paracalanus sp.	–0.09	–0.41
Polychaetes (larvae)	–0.08	–0.01
Euphausiids (calyptopsis)	–0.06	0.35
Copepods (nauplii)	–0.05	0.01
Centropages typicus	–0.04	–0.62
Gastropods (larvae)	–0.04	–0.03
Copepods (copepodite)	–0.02	–0.03
Evadne sp.	–0.01	0.04
Temora longicornis	–0.01	–0.02
Acartia longiremis	0.00	–0.04
Oithona similis	0.00	0.03
Bivalves (larvae)	0.00	–0.01
Limacina helicina	0.04	–0.08
Centropages sp. (copepodite)	0.06	0.06
Oithona sp.	0.06	–0.02
Pseudocalanus sp.	0.09	0.02
Obelia sp.	0.14	–0.25
Euphausiids (nauplii)	0.16	0.43
Calanus finmarchicus	0.19	0.03
Echinoderms (larvae)	0.26	–0.20
Mysidacaea (larvae)	0.30	0.16
Oithona atlantica	0.31	0.06
Limacina sp.	0.32	0.22
Euphausiids (egg)	0.38	0.75
Metridia lucens	0.50	–0.08
Cnidarians	0.62	0.26
Metridia longa	0.63	0.40
Aglantha digitale	0.66	–0.13
Parasagitta sp.	0.93	–0.10

the analysis for the two axes of NMDS*z*. The second dimension of the NMDS*z* also contributes to discriminate the groups and despite some overlapping along the first dimension, the groups remain distinct throughout the study (Figure 2.13A). High frequency variability appears within each group during the intensive adaptive sampling (Storm Event), when the sampling frequency is higher, which illustrates the importance of high-frequency data collection. Despite this variability the overall spatial patterns remain, which confirms the pattern observed during the weekly sampling.

Along this inshore-offshore gradient of increasing depth, at the inshore mooring station SB2, the zooplankton community is dominated by the nearshore copepod *Acartia clausi*, whereas offshore at X6, the abundant and ubiquitous copepod species *Oithona* spp., in particular *Oithona similis*, are dominant. Station N3 is at an intermediate position along the spatial gradient and a mix of SB2 and X6 communities occurs (Figure 2.13, Table 2.2B & 2.4). Zooplankton abundance at the three locations varies throughout the summer (Table 2.2B). However, it is related to the occurrence of neither sustained nor storm-induced upwelling events, apart from a lower abundance following Sustained 1 event, which do not influence the spatial variability in community structure. There is therefore no evidence of a temporal structure in the zooplankton assemblages, which are decoupled from the occurrence of the northeastward wind events (Figure 2.13B). Opposing the temporal patterns in phytoplankton community structure, zooplankton communities are therefore structured spatially by a depth-distance gradient representing a change in habitat.

2.4 Discussion

Despite the occurrence of coastal upwelling over the inner Scotian Shelf in summer (*Petrie et al*., 1987) and the resulting effects on the hydrography and nutrient variability in adjacent inlets (*Platt et al*., 1972; *Heath*, 1973), the biological effects of upwelling conditions on the lower pelagic food web and the productivity of an oligotrophic inlet has not previously been investigated, either in this region or in similar inlets across the northeast coast of North America where similar nearshore conditions occur (e.g. *Clemente-Colón*

and Yan, 1999). The observations made in Lunenburg Bay in summer 2006, and the predictions covering the time period 2003–2006, are therefore important for the region and confirm the effect of atmospheric forcing in driving the variability of nitrate and phytoplankton in Nova Scotian inlets, as demonstrated by previous studies (*Platt et al*., 1972; *Lewis and Platt*, 1982; *Côté and Platt*, 1983). Adding on these studies, this work demonstrates that sustained upwelling events have a significant influence on the variability of phytoplankton biomass inside Lunenburg Bay, which has been associated with and predicted from the changes in water density and the input of nitrate from the Scotian Shelf. It reveals that at the seasonal scale, sustained upwelling events play a role in determining the mean state of productivity in this type of oligotrophic system. At shorter time scales, the study indicates that these events influence phytoplankton assemblages and regulate the spatial patterns of phytoplankton biomass inside Lunenburg Bay.

2.4.1 Biological Variability Associated with Upwelling Events

In early summer 2006, the development of coastal upwelling conditions associated with two successive periods of sustained upwelling was typical of nearshore areas in coastal upwelling systems. Sustained northeastward winds induced the development of coastal upwelling conditions that resulted in the intrusion of the nitracline in the euphotic layer inside Lunenburg Bay, inducing a transient increase in nitrate concentration. Given the otherwise low background nitrate concentrations in the bay, this is a prominent process for the local nitrate dynamics in summer. This result verifies the hypothesis of an input of nitrate from the inner Scotian Shelf into Lunenburg Bay during periods of sustained upwelling.

These events influenced the temporal patterns of phytoplankton biomass in two ways in 2006. First, the onset phase of the upwelling was characterized by low phytoplankton biomass, indicating the Ekman transport of phytoplankton-poor waters into the bay. This was represented by the occurrence of the dinoflagellate *Ceratium longipes*, as previously observed in a neighbouring inlet (*Côté and Platt*, 1983). In general, this process contributes to the seasonal variability in phytoplankton biomass and productivity (*Brown and Hutchings*, 1985; *Crespo et al*., 2006). In Lunenburg Bay, it contributed to the seasonal dynamics in phytoplankton biomass during 2006. The negative contributions of

density to chlorophyll biomass in the phytoplankton biomass prediction model confirm that it is a general process influencing the local phytoplankton biomass. Despite this process, and the relatively short duration of each pulse of upwelling, the shoaling of the nitracline inside the bay stimulated the local accumulation of phytoplankton during the sustained upwelling events in 2006. The peak in phytoplankton (abundance and biomass) was reached during the relaxation phase of the upwelling, with a two-fold increase in chlorophyll biomass. This was confirmed by the phytoplankton biomass prediction model (Section 2.3.4). The relaxation phase of the upwelling, as seen in other systems (e.g., *Fraga et al*., 1988; *Tilstone et al*., 2000), is therefore important for the development of phytoplankton biomass in Lunenburg Bay.

Spatial variability is associated with the sustained upwelling events and appears on the longitudinal axis of the bay. Along this axis, nitrate concentrations are enhanced towards the mouth and the outside of the bay where upwelling source water originates. During the upwelling relaxation phase, it promotes the development of a phytoplankton gradient (abundance and biomass increasing outward) along the same axis of enhanced coupling with the inner shelf (Figure 2.8). It confirms that sustained upwelling events regulate the spatial patterns of phytoplankton biomass (and abundance) in Lunenburg Bay. Such a horizontal gradient is inherent to upwelling systems and can be related to circulation and bathymetry patterns (*Álvarez-Salgado et al*., 1996b), but also to the intensity of the events (*Tilstone et al*., 1994). Variations in residence time along this axis of increasing coupling with the inner shelf may influence this gradient. This aspect will be investigated in Chapter 3.

The extended time period without nitrate input from the shelf in 2006, the concurrent decrease in phytoplankton biomass and abundance and their subsequent increase during the upwelling pulses suggest that sustained upwelling events have a positive effect on the overall productivity of Lunenburg Bay in summer. This is supported by the nitrate term in the prediction model that increases the magnitude of chlorophyll biomass in the relationship. It is then suggested that the periodic nitrate inputs driven by sustained upwelling events, enhance the mean state of productivity inside Lunenburg Bay in summer.

Despite the significant effects of sustained upwelling events on the spatial and temporal

patterns of phytoplankton biomass, the magnitude of phytoplankton variability is rather small and therefore sustained upwelling events do not induce the large increase in phytoplankton biomass hypothesized (chlorophyll biomass > 5 mg m^{-3}). This contrasts with other inlets in the vicinity of major upwelling regions (*Hickey and Banas*, 2003; *Álvarez-Salgado et al*., 2010). However, the chlorophyll anomalies in the $\widehat{\text{Chl}}$ analysis (i.e., nitrate proxy vs. observed variation in chlorophyll, Figure 2.8) and the phytoplankton biomass prediction model (Section 2.3.4) revealed that the magnitude of the phytoplankton response in Lunenburg Bay corresponds to the magnitude of nitrate variations induced by the upwelling event. Both of these analyses were based exclusively on density and its relationship with nitrate to estimate or predict chlorophyll biomass. This dependency on the nitrate-density relationship emphasizes the importance of nitrate distribution on the Scotian Shelf for the biological dynamics in Lunenburg Bay. It suggests a limitation in the magnitude of the inshore phytoplankton biomass response to the sustained upwelling events resulting from low nitrate concentrations in upwelling source waters.

Overall, the sequences of sustained upwelling in 2006 and the relationship between density and phytoplankton variability reveal the role of wind-induced coastal upwelling events in controlling the short-term temporal variability of phytoplankton during the summer in Lunenburg Bay (i.e. period > 1 day). These dynamics support the concept of a dominant control by wind-induced offshore processes over inshore biological systems in the region (*Lewis and Platt*, 1982). The analysis of a storm-induced upwelling event has demonstrated that the effects of upwelling events depend on the characteristic time-scale of the wind forcing, which controls the development of coastal upwelling conditions on the Scotian Shelf (*Petrie et al*., 1987). The Storm Event was characterized by a dynamic response of Lunenburg Bay to the wind forcing, without the shoaling and the propagation of the nitracline into Lunenburg Bay. Rather, it resulted in the upwelling of local, nitrate depleted, subsurface shallow waters at the head of the bay that did not influence local primary production.

2.4.2 Implications for Plankton Communities

The upwelling induced inshore-offshore gradient revealed for phytoplankton biomass and abundance during the periods of sustained upwelling, is not apparent in the phytoplankton assemblages, despite some spatial variability in the dominant species. Therefore, sustained upwelling events do not appear to regulate the spatial patterns of community structure in phytoplankton assemblages. The temporal variability in phytoplankton biomass and abundance induced by the upwelling events is nonetheless associated with a modification in the structure of the phytoplankton community inside Lunenburg Bay. The phytoplankton community was generally dominated by diatoms in summer 2006, as often seen in inlets (*Cloern and Dufford*, 2005; *Varela et al*., 2008). Weak wind conditions and a prolonged period of low nitrate concentration in early summer promoted a structural shift in the phytoplankton community with the development of a dinoflagellate-dominated phytoplankton assemblage, interrupting the dominance over the phytoplankton community by diatoms. The sequence of sustained upwelling events promoted a subsequent shift in the phytoplankton community with the development of a mixed phytoplankton assemblage dominated numerically by diatom species. This period was characterized by an increase in the number of co-existing phytoplankton species in the bay, which is promoted by transport and habitat heterogeneity in open coastal ecosystems (*Cloern and Dufford*, 2005). At the seasonal scale, shifts in phytoplankton community structure inside Lunenburg Bay are therefore associated with meteorological conditions. Accordingly, sustained upwelling events do not control directly the variability in phytoplankton community structure, but by modifying the local hydrography and periodically the nutrient conditions, influence the local succession of phytoplankton assemblages. Pre-existing conditions and thus the frequency of these events are then important factors for the effects of upwelling events on phytoplankton assemblages (*Tilstone et al*., 1994; *Marañon and Fernández*, 1995). Similar temporal patterns are observed in other upwelling areas, where the occurrence of upwelling pulses interrupts the seasonal succession of phytoplankton communities nearshore (*Garrison*, 1979).

The composition of the plankton community is tied to the structure of the food web and has therefore a key role in the transfer of energy to higher trophic levels (*Legendre and Le Fèvre*, 1989; *Kiørboe*, 1991; *Cullen et al*., 2002). In Lunenburg Bay the changes

in zooplankton community were not associated with the occurrence of either sustained or storm-induced upwelling events in 2006; hence it did not follow the structural change in the phytoplankton assemblage. Instead, the zooplankton community is structured along an inshore-offshore gradient of increasing water depth that represents a change in habitat. Inshore, zooplankton assemblages are dominated by the neritic copepod *Acartia* spp., characteristic of inlets (*Paranjape and Conover*, 1973; *Sullivan and McManus*, 1986; *Ueda*, 1991), whereas outside in the deep water region, the small ubiquitous copepod *Oithona* spp. dominates.

The contrast between the spatial structure in zooplankton assemblages and the temporal shift in phytoplankton community structure associated with upwelling suggests different processes controlling the phytoplankton and zooplankton communities and implies that top-down spatial structuring of phytoplankton communities did not dominate during the study. The short duration of upwelling pulses and the low phytoplankton biomass in the bay can explain the lack of response in the zooplankton community. However, food level is not necessarily a structuring mechanism for inshore zooplankton communities (*Kimmerer*, 1993). Hydrodynamic patterns (*Jouffre et al*., 1991), reduced habitat diversity due to shallow depth (*Kimmerer*, 1991) or size selective predation (*Kimmerer*, 1991, 1993) are important structuring mechanisms inshore. Also, the depth-habitat gradient in Lunenburg Bay may be a selective pressure for species with restricted migratory behaviour such as *Acartia* spp. (*Tiselius*, 1998), since migration behaviour interacts with water depth (*Bollens and Frost*, 1989). Diel vertical migrations are primarily a predator avoidance mechanism, not directly related to resource distribution when the food level is sufficient (*Zaret and Suffern*, 1976; *Ohman*, 1990; *Pearre*, 2003). The role of these factors in structuring zooplankton communities in Lunenburg Bay cannot be addressed in this study. Specific investigations should be conducted to identify which of these mechanisms controls the spatial structure of zooplankton communities observed in Lunenburg Bay.

2.5 Summary and Conclusions

The present work revealed the dominance of bottom-up processes controlling the magnitude and variability of phytoplankton biomass in Lunenburg Bay, which are associated with the development of coastal upwelling conditions on the inner Scotian Shelf during sustained periods of northeastward wind. Sustained upwelling events represent an intermittent source of nitrate to Lunenburg Bay in summer. They result in enhanced phytoplankton biomass towards the interface between the bay and the inner Scotian Shelf where upwelling source waters originate. The magnitude of this variability is limited in comparison to other upwelling systems where the upwelling source waters are richer in nutrients, but given the low background level of phytoplankton this intermittent source of nitrate is important for the mean state of productivity of the bay. The duration of northeastward wind events and consequently the type of meteorological forcing, represented by the sustained and storm-induced upwelling events, is important because only the former type is associated with the input of nitrate into the bay. Given the broad-scale development of upwelling conditions along the Atlantic shore of Nova Scotia and their effect on nearshore hydrography, similar processes may control phytoplankton dynamics in other inlets along the Atlantic coast of Nova Scotia.

The study also revealed that shifts in phytoplankton community structure are determined by meteorological conditions and are influenced by the occurrence of sustained upwelling events, but they do not propagate to higher trophic levels. Rather, zooplankton communities are organized along an inshore-offshore axis following a depth-habitat gradient. This implies the presence of a spatial component in the local foodweb structure, but also that top-down spatial structuring of phytoplankton communities does not dominate in this system. Functions describing ecosystem interactions in current ocean models do not have a spatial component reflecting consistent differences between nearshore and shelf plankton. More complex ecosystem models including size specific grazing or migrating/non migrating behaviour may provide a more accurate representation of spatially dynamic processes in a nearshore ecosystem (e.g., *Morozov and Arashkevich*, 2010). It is also recommended to collect higher frequency data on plankton assemblages to infer plankton species variability at the time-scale of upwelling events, and in particular the effect of advective processes on plankton distributions. The tools to collect such data

are still in development but are becoming available as technology for coastal observatories progresses and metrics for phytoplankton communities and techniques for in situ zooplankton species identification are being developed (*Wiebe and Benfield*, 2003; *Babin et al*., 2005, 2008).

Finally, the development of a phytoplankton biomass prediction model and its use for prediction at a multiannual time scale has demonstrated some predictability of phytoplankton biomass in Lunenburg Bay based on water density and the nitrate-density relationship. The model captures about half of the variability in summer phytoplankton biomass in Lunenburg Bay and represents a simple tool that can be used to assess the variability in phytoplankton biomass in other oligotrophic inlets of the region. In combination with other tools accounting for unresolved regulating processes, the model could be useful to predict this variability.

Chapter 3

Summer Plankton Dynamics Under Different Wind Regimes in Lunenburg Bay, Canada: A Box Model Experiment

3.1 Introduction

The coastal ocean constitutes a highly dynamic system with tight coupling between physical and biogeochemical processes, influencing phytoplankton growth and food web processes, which ultimately determine coastal ecosystem dynamics over a multitude of scales (*Denman and Powell*, 1984). In temperate inlets (bays, fjords), wind-driven circulation from local and remote meteorological forcing is an important source of physical variability at a subtidal frequency (*Weisberg*, 1976; *Kjerfve et al*., 1978; *Carter et al*., 1979). The development of upwelling and downwelling events is particularly important because it enhances the coupling between inlets and their adjacent inner shelf (*Dyer*, 1973, 1979; *Garvine*, 1985; *Wong and Valle-Levinson*, 2002), otherwise controlled by tides but limited to the scale of the tidal excursion (*Geyer and Signell*, 1992). Upwelling generates the flushing of bays and estuaries (*Heath*, 1973; *Duxbury*, 1979) with nutrient-rich subsurface waters (*Platt et al*., 1972), whereas downwelling conditions promote the shoreward transport and the retention of nutrient-depleted—but sometimes phytoplankton rich—surface waters nearshore (*Álvarez-Salgado et al*., 1996a). This can be a mechanism of phytoplankton biomass accumulation, particularly when following periods of upwelling conditions (*Crespo et al*., 2006).

In Lunenburg bay, the subtidal variability in circulation and hydrography is generated by the wind forcing in summer and fall (*Sheng and Wang*, 2004; *Wang et al*., 2007; *Zhai*

et al., 2007; *Yang and Sheng*, 2008), which enhances the hydrodynamic connectivity with the inner Scotian Shelf (*Sheng et al*., 2009). During this period, the variations in temperature and salinity inside the bay are induced by the occurrence of upwelling and downwelling events (*Zhai et al*., 2007). Concerning the upwelling, their development is associated with the seasonal synoptic wind field in summer (*Smith and Schwing*, 1991), which affects concurrently the hydrography of the Scotian Shelf (*Hachey*, 1937; *Petrie et al*., 1987; *Andrade*, 1991) and the local inlets (*Heath*, 1973). It influences inshore nitrate concentration, phytoplankton biomass, as well as phytoplankton species composition (*Platt et al*., 1972; *Côté and Platt*, 1983, see Chapter 2). Downwelling conditions on the other hand, which are associated with summer and fall storm events, were found to affect the patterns of circulation in Lunenburg Bay and to generate the coupling with the inner Scotian Shelf and the adjacent inlets (*Zhai et al*., 2008a; *Sheng et al*., 2009).

Despite the occurrence of upwelling and downwelling conditions, the magnitude of phytoplankton variability recorded in Lunenburg Bay is relatively modest throughout the summer (average chlorophyll is 1.1 ± 0.6 mg m^{-3} SD, $n = 690$, observing system dataset, i.e. *Cullen et al*. 2008). This can be contrasted with other inlets in different coastal areas where large variations in chlorophyll biomass (> 5 mgChl m^{-3}) are associated with upwelling, and even downwelling conditions during the summer and fall (*Roegner et al*., 2002; *Prego et al*., 2007; *Brown and Ozretich*, 2009). Several controlling processes can be suggested to explain the limited biological variability observed in Lunenburg Bay: the top-down control of inshore phytoplankton by grazing; the bottom-up control of inshore phytoplankton due to moderate inputs of nitrate from the Scotian Shelf during periods of upwelling; and the control of inshore phytoplankton by horizontal transport (and therefore the flushing rate of Lunenburg Bay).

Early work has been carried out on bivalves in the South Cove, a semi-enclosed shallow site connected to Lunenburg Bay (*Grant et al*., 1993, 1995; *Hatcher et al*., 1994; *Dowd*, 1997). However, no aquaculture occurs in the bay and a substantial grazing pressure from bivalves, as emphasized for other systems (*Cloern*, 1982; *Dowd*, 2005; *Banas et al*., 2007), is unlikely. Zooplankton grazing is more likely, although a decoupling between phytoplankton and zooplankton response to upwelling events has been reported in Chapter 2 and therefore the top-down spatial structuring of phytoplankton communities

does not seem to dominate in the bay. On the contrary, the results from Chapter 2 support the hypothesis of a biological system limited by nitrate concentration in upwelling source waters. Also, the transport patterns and the accelerated flushing rate associated with local and remote meteorological forcing, which were not investigated in Chapter 2, may control the local accumulation of phytoplankton biomass, as observed elsewhere (*Tilstone et al.*, 2000). It seems thus probable that in Lunenburg Bay the local accumulation of phytoplankton biomass during the summer is controlled by:

(1) the intensity of the flushing (associated with the wind forcing); and

(2) the low nitrate concentration in source waters (on the Scotian Shelf).

The present study will investigate the two hypotheses in order to identify which key process determines the variability in phytoplankton biomass in Lunenburg Bay under the dominant summer hydrodynamic conditions, i.e. when circulation is forced by tides and alongshore winds. For that, a coupled physical-biogeochemical box model is developed for Lunenburg Bay that simulates planktonic ecosystem processes under three experimental meteorological regimes: no wind (M2 tides only), downwelling wind and upwelling wind regimes. Results from the three regimes are compared and discussed, and a series of sensitivity studies conducted to build a a conceptual model describing phytoplankton variability in Lunenburg Bay and other comparable inlets, considering flushing and nitrate concentration in source waters.

3.2 Materials & Methods

3.2.1 Study Site

Lunenburg Bay is a 40 km^2 inlet with a mean depth of about 15 m, increasing to a maximum of 40 m on its eastern side where the Rose Bay-Lunenburg Bay system (hereafter referred to as Lunenburg Bay) connects with the Scotian Shelf (Figure 3.1A,B). Recent studies have pointed out the influence of the semi-diurnal tide (M2) and of meteorological events and wind direction on the local circulation and hydrography (*Sheng and Wang*, 2004; *Zhai et al.*, 2008a). The MEPS-Bay coastal observatory, operated in Lunenburg

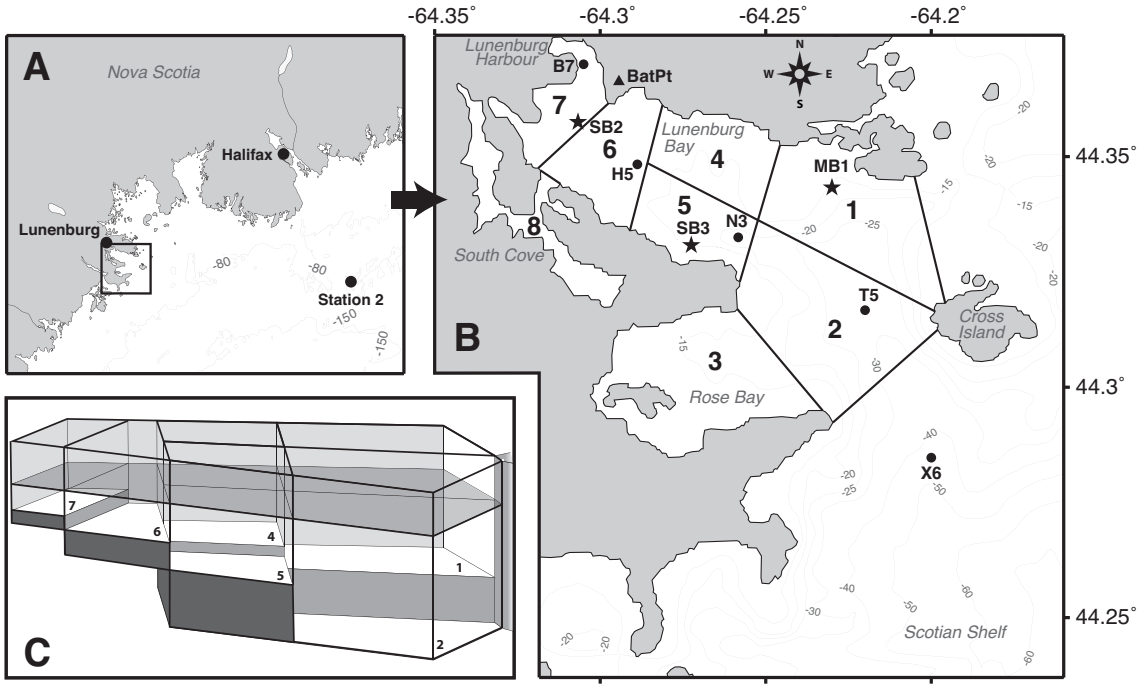

Figure 3.1: Map of the box model. A. Location of Lunenburg Bay on the Atlantic coast of Nova Scotia and bathymetry of the inner Scotian Shelf. B. Map of Lunenburg Bay, the MEPS-Bay coastal observatory (main locations) and the boundaries of the box model. ★ Location of the moorings. ● Extra stations sampled during the sampling campaigns in 2006. ▲ Battery Point meteorological station (BatPt). The black lines indicate the boundaries of the box model, each box being represented by its number (1-8). C. Diagram representing a northward view of the three dimensional structure of the box model. The box number is given in the bottom right end side of each box. The southern boxes 3 (Rose Bay) and 8 South Cove are not represented for clarity. The bathymetry data were generated by Doug Mercer and Jinyu Sheng

Bay between 2002 and 2007, resulted in the development of a multi-component modelling tool with forecast capability for coastal marine conditions (*Cullen et al*., 2008). The circulation component of the model is used to simulate the wind-driven circulation during the study. Data from the observatory corresponding to the simulated wind regimes were used to compare the model results with observations.

3.2.2 Circulation Model

The circulation in Lunenburg Bay is modelled with a nested-grid ocean circulation model (*Sheng and Wang*, 2004; *Zhai et al*., 2008a). The model was developed from the free-surface version of the CANDIE circulation model (*Lu et al*., 2001; *Sheng and Wang*, 2004) using a finite difference formulation of the primitive equation with 24 z-levels in the vertical and about 200 m horizontal grid resolution (*Zhai et al*., 2008a). This model was used in a recent series of hydrodynamic studies of Lunenburg Bay (*Yang and Sheng*, 2008; *Zhai et al*., 2008a,b; *Sheng et al*., 2009). In the present study, the baroclinic version of the model has been initialized with horizontally uniform and vertically stratified temperature and salinity.

For this study, three experiments have been carried out with the circulation model to simulate the circulation in Lunenburg Bay forced by the M2 tides only (tidal regime), the M2 tides and northeastward wind (0.1 Pa, upwelling regime) and the M2 tides and southwestward wind (0.1 Pa, downwelling regime). The circulation model is run for 10 days for each experiment with output every 10 minutes. The last tidal cycle of the simulation is then used to calculate times series of exchange rates in a box model (see Appendix C.1 & C.2).

3.2.3 Box Model

The model divides the bay into 8 boxes (Figure 3.1). Their locations were chosen to represent the areas with comparable bathymetry, the main circulation patterns and to include the various observing stations. The lateral division of the bay is important given the three circulation patterns compared in this study. Four zones are enclosed in the box model: South Cove (box 8) is a semi-enclosed shallow area connected to Lunenburg Bay

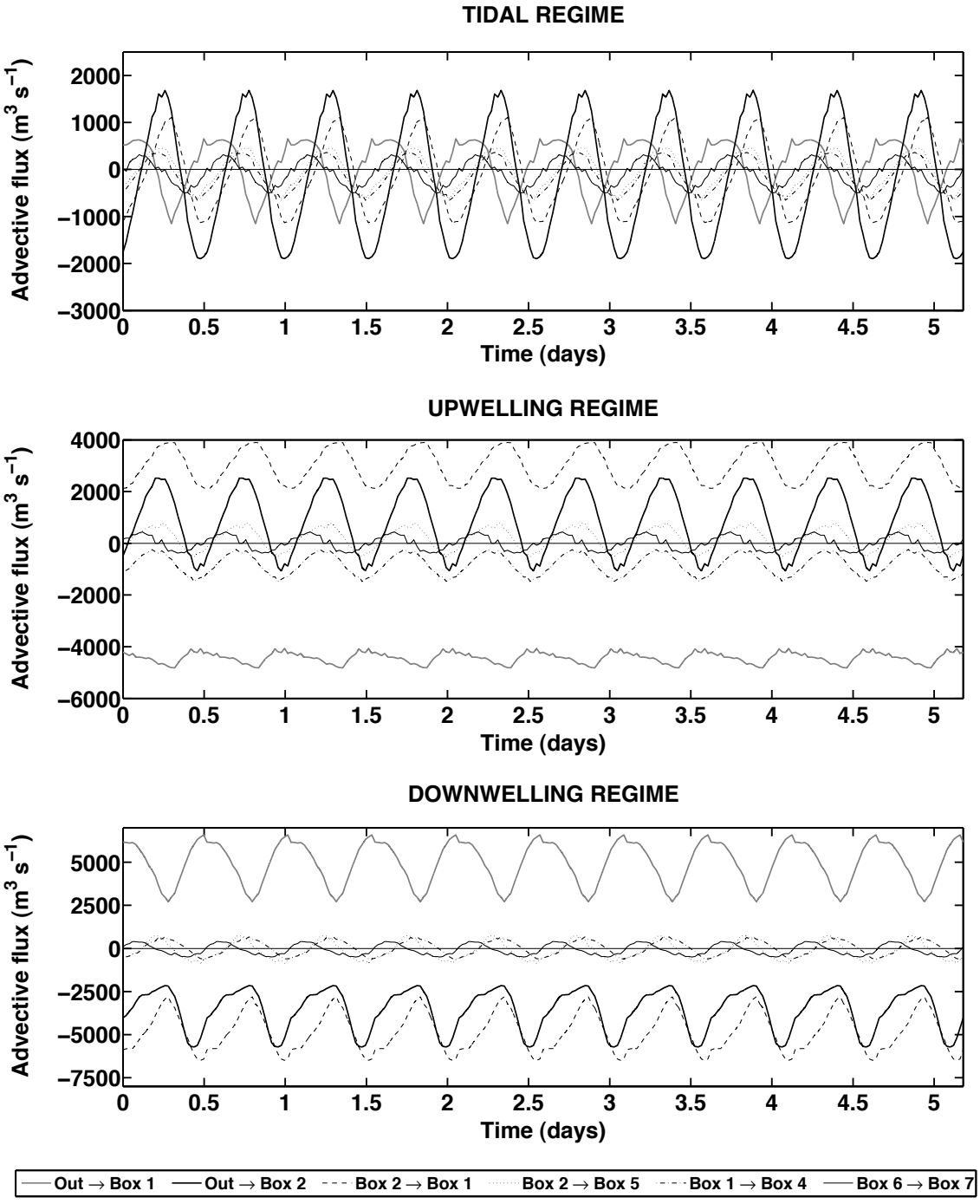

Figure 3.2: Time series of the advective fluxes in the surface layer of the box model across six of the boundaries, for each circulation regime. Each flux represents the volume of water crossing the entire area of a boundary per unit time. The legend indicates the direction of a positive advective flux. The negative values indicate an opposite direction.

(box 4–7 and part of box 1) through a tidal jet. Rose Bay (box 3) is a small inlet isolated from the main Lunenburg Bay with extended shallow areas. The mouth of Lunenburg Bay (box 1 and 2) is a deeper area that connects to the Scotian Shelf along the northern and southeastern sides of Cross Island. Each box has the same vertical structure, divided vertically into a 5 m deep upper layer and a lower layer extending down to the bottom (Figure 3.1C). The depth of the surface layer was chosen to represent the average depth of the pycnocline in summer (CTD profiles, data not included).

The box model boundaries are aligned with the grid of the circulation model and the nearest grid points used for the calculation of horizontal and vertical exchanges between boxes (see computation in Appendix C.1 & C.2). The tidal cycle of advection and diffusion rates at the box model boundaries has been applied to create a time series of boundary fluxes for each circulation regime. An example of advective fluxes time series in the upper layer of the box model is given in Figure 3.2. Tidally-averaged advective transports are calculated from these times series, by averaging advection values over the entire tidal cycle for each boundary in the box model (horizontal and vertical, see Figure 3.3).

The flushing time (F_T; d) of a given box is defined as the e-folding flushing time-scale of the box. It is calculated from the exponential decay of a tracer (X; mmol m^{-3}) with time (t; d), given the volumetric flow rate ($\overline{Q}_{adv}$; m^3 d^{-1}) and the volume of the box (V; m^3), using the following formulation (e.g., *Monsen et al.*, 2002):

$$X(t) = X(0) \cdot \exp\left(-\frac{\overline{Q}_{adv}}{V} \cdot t\right) , \tag{3.1}$$

where $F_T = V/\overline{Q}_{adv}$. The volumetric flow rate ($\overline{Q}_{adv}$) corresponds to the sum of the outgoing tidally averaged advective transports across the boundaries of the box as presented in Figure 3.3 (outgoing arrows only). The flushing rate (F_R; d^{-1}) is the inverse of F_T.

3.2.4 Ecosystem Model

3.2.4.1 Model Formulation

A biological model is coupled to the transport framework to simulate the nitrogen cycle in the water column. The model represents a *PZND*-type ecosystem of the lower trophic

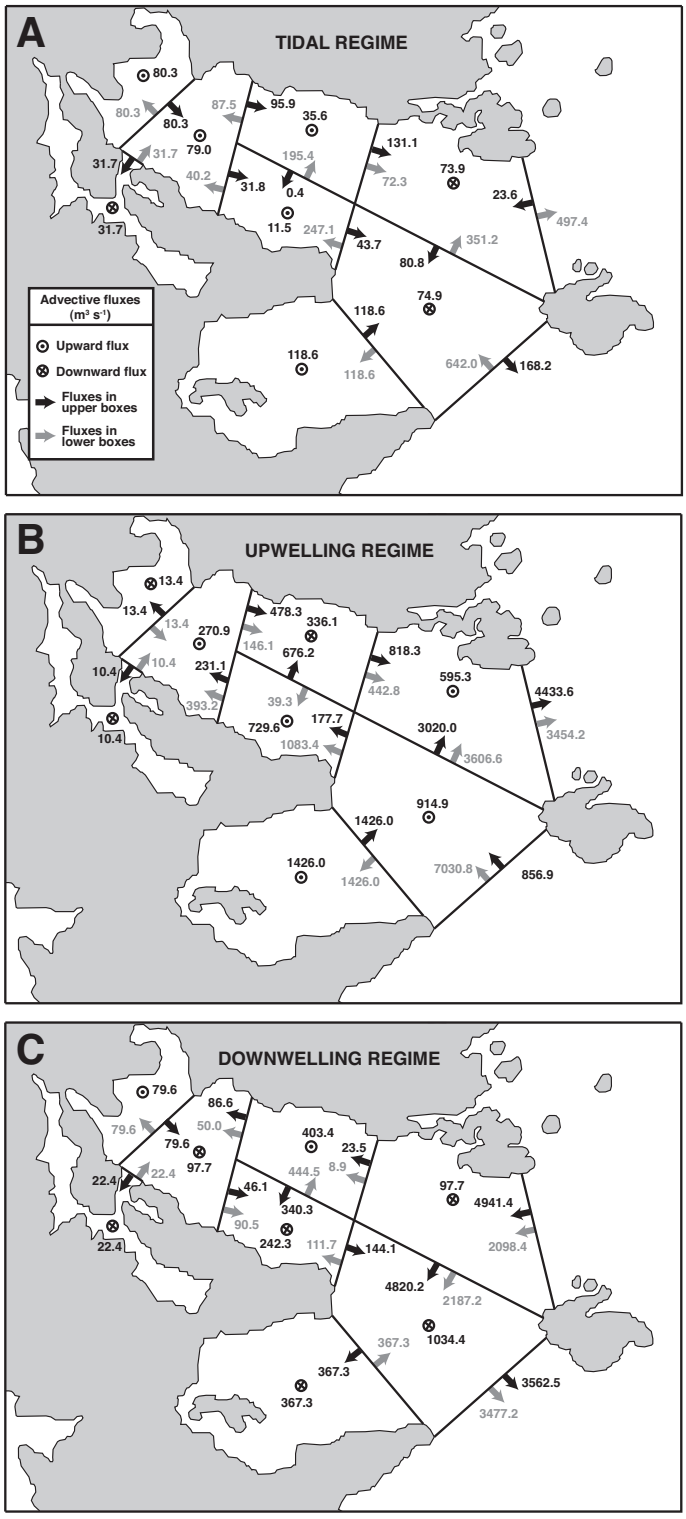

Figure 3.3: Tidally-averaged advective fluxes across each boundary of the box model (m^3 s^{-1}) are presented for the A. tidal, B. upwelling and C. downwelling circulation regimes. Each flux represents the average volume of water crossing the entire area of a boundary per unit time. The arrows indicate the direction of the flux.

levels with units of mmolN m^{-3}. The model includes phytoplankton (P), zooplankton (Z), nutrients (N) and detrital particulate organic matter (D). A schematic of the ecosystem model is given in Figure 3.4. The rate of change of ecosystem variables resulting from biological processes (mmolN m^{-3} d^{-1}) are formulated as follows:

$$\frac{dP}{dt} = \mu P - rP - g_P Z - S_P \tag{3.2}$$

$$\frac{dZ}{dt} = \beta g_P Z - g_Z Z \tag{3.3}$$

$$\frac{dN}{dt} = -\mu P + rP + \xi g_Z Z + \lambda D \tag{3.4}$$

$$\frac{dD}{dt} = -\lambda D + (1-\beta) g_P Z + (1-\xi) g_Z Z - S_D \tag{3.5}$$

The parameter values used in the model have been selected from the literature (Table 3.1). The definition and value of each parameter is given in Table 3.1 and the formulation for biological processes are discussed below.

Phytoplankton growth rate (μ; d^{-1}) is limited simultaneously by nutrient uptake $h(N)$ and light $f(E)$ such as:

$$\mu = \mu_{max}(T) \cdot h(N) \cdot f(E) \ , \tag{3.6}$$

where $\mu_{max}(T)$ (d^{-1}) is the maximum growth rate of phytoplankton which depends on the temperature (T; °C) following the formulation of *Eppley* (1972):

$$\mu_{max}(T) = \ln(2) \cdot 0.851 \cdot 1.066^T \tag{3.7}$$

The nutrient uptake limitation follows a Michaelis-Menten functional form:

$$h(N) = \frac{N}{k_N + N} \ , \tag{3.8}$$

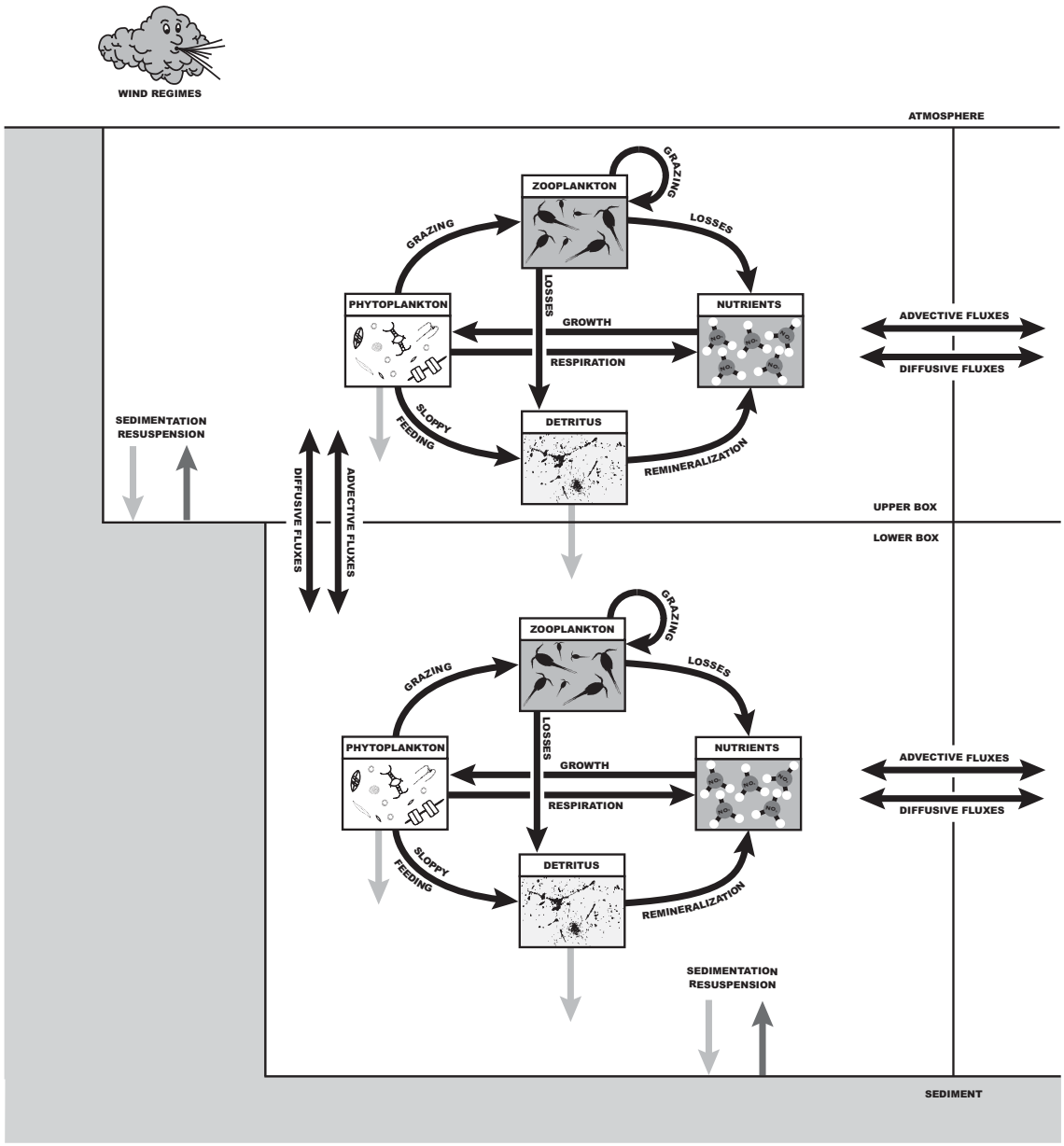

Figure 3.4: Diagram representing the ecosystem processes within the box model framework. Dark arrows represent the ecosystem processes. Light grey arrows represent sedimentation on the phytoplankton and detritus variables. Dark grey arrows represent the resuspension of the same variables

where k_N (mmolN m^{-3}) is the nutrient uptake half-saturation concentration. The photosynthetically available radiation at the sea surface (E_0; W m^{-2}) follows a daily cycle according to the classical astronomical formula (*Brock*, 1981) for the latitude of Lunenburg Bay (44.34°N) at mid-summer (day 210) and is attenuated with water depth according to the Lambert-Beer law using an attenuation coefficient for all constituents of seawater (K_d; m^{-1}). The average light in a box (E; W m^{-2}) is calculated for each layer as:

$$E = E_{top} \cdot \frac{1 - e^{-K_d\, z}}{K_d\, z} \,, \tag{3.9}$$

where E_{top} (W m^{-2}) is the photosynthetically available radiation at the top of the layer (E_0 for the surface box) and z (m) is the thickness of the layer. The light limitation function for phytoplankton growth depends on an exponential formulation of the instantaneous growth rate vs. light curve (similar to the photosynthesis-light formulation in *Webb et al.*, 1974; *McBride*, 1992), such as:

$$f(E) = 1 \; - \; \exp(-\frac{\alpha E}{\mu_{max}(T)}) \,, \tag{3.10}$$

where α (d^{-1} (W m^{-2})$^{-1}$) is the initial slope of the instantaneous growth rate vs. light curve. The zooplankton grazing on phytoplankton (g_P; d^{-1}) and the zooplankton death rate (g_Z; d^{-1}) are represented by a sigmoidal functional form (Holling Type III):

$$g_X = I_X \, \frac{X^2}{k_X^2 \; + \; X^2} \,, \tag{3.11}$$

where X stands for either phytoplankton or zooplankton and their concentration, I_X (d^{-1}) is the maximum ingestion rate and k_X (mmolN m^{-3}) the half saturation constant for grazing. This commonly used functional form allows a saturating response at high prey concentration and a refuge from grazing at low concentration, which is important for the stability of the model (see *Gentleman et al.*, 2003 for a discussion on functional types) and is a realistic representation of grazing in natural zooplankton populations (*Steele and Henderson*, 1981; *Morozov and Arashkevich*, 2008; *Morozov*, 2010). The choice of grazing and zooplankton mortality terms is important for the behaviour of the ecosystem (e.g., *Franks et al.*, 1986; *Franks*, 2002).

Phytoplankton and detritus sedimentation (S_X; mmolN m^{-3} d^{-1}) in the upper and lower layers is formulated such as:

$$S_X = w_X \left(\frac{X}{z} - \frac{X_{up}}{z_{up}} \right) , \tag{3.12}$$

where X stands for either phytoplankton or detritus and their concentration, z_{up} is the thickness of the box above, and w_X (m d^{-1}) is the sinking velocity of phytoplankton or detritus. X_{up}/z_{up} is equal to zero in the surface layer. The model has a reflective boundary. Therefore, when phytoplankton or detritus sink to the bottom they are immediately resuspended. Due to the bathymetry of the bay, some parts of the upper boxes reach the bottom. Those are treated as sediment areas, where sinking material is reflected (i.e. resuspension). In the rest of the boxes, sedimenting materials go to the lower layer.

The rate of change of ecosystem variables resulting from physical processes is then formulated as follows:

$$\frac{dX(k)}{dt} = \sum_{i=1}^{n} \left(r_{adv}(i) \cdot X_0(i) + r_{diff}(i) \cdot (X_{\text{OUT}}(i) - X(k)) \right) , \tag{3.13}$$

where $X(k)$ represents the concentration of the ecosystem state variable in box k, $X_{\text{OUT}}(i)$ is the concentration in the box adjacent to open boundary i and $X_0(i)$ is the concentration in the box upstream the advective flow for boundary i ($X(k)$ or $X_{\text{OUT}}(i)$). The calculation of the advective and diffusive exchange rates (r_{adv}, r_{diff}) is detailed in Appendix C.1 & C.2. The system of equations is integrated in time using an implicit ordinary differential equations solver in Matlab. The spatially averaged results of the biological model presented in Section 3.3 are calculated over the last 20 tidal cycles of the model output for the outer bay (OUT, box 1 and 2), the mid-bay (MID, box 4 and 5) and the inner bay (IN, box 6, 7 and 8).

3.2.4.2 Boundary Conditions

Boundary conditions are set at the outer boundaries (i.e., open boundaries) of box 1 (northeast) and box 2 (southeast) which are in contact with the coastal ocean (Figure 3.1). There are four open boundaries in total: upper and lower open boundaries of box 1, and upper

Table 3.1: Parameters used in the ecosystem model.

State variable	Parameter name	Value	Range	Units	Definition	Source value (range)
Phytoplankton	$\mu_{max}(T)$	1.63	0.81 – 2.12	d^{-1}	Maximum growth rate at temperature T	1
	α	0.025	±75%	d^{-1} $(W\ m^{-2})^{-1}$	Initial slope of growth vs. light curve	2
	r	0.0359	0.002 – 0.1	d^{-1}	Respiration rate	3 (3)
	w_P	1	0.32 – 1.69	$m\ d^{-1}$	Sinking velocity	4 (5)
Zooplankton	β	0.6	0.325 – 0.921	-	Assimilation efficiency	6 (7)
	I_Z,I_P	1	0.63 – 1.48	d^{-1}	Maximum ingestion rate	8 (9)
	k_P,k_Z	1	0.5 – 1.2	$mmolN\ m^{-3}$	Grazing half saturation	10 (10)
Nutrients	ξ	0.25	±50%	-	Zooplankton mortality going to N	11 (-)
	k_N	0.5	0.009 – 1.319	$mmolN\ m^{-3}$	Nutrient half saturation	8 (12)
Detritus	λ	0.1	0.01 – 0.2	d^{-1}	Remineralization rate	13 (13)
	w_D	1	0 – 10	$m\ d^{-1}$	Sinking velocity	14 (15)
Others	T	15.9	5 – 20	°C	Water temperature	16 (-)
	E	0 – 433	-	$W\ m^{-2}$	Surface Irradiance	17 (-)
	K_d	0.1	0.04 – 0.25	m^{-1}	Light attenuation coefficient	-

Sources are: 1: *Eppley et al.* (1979), 2: *Oschlies and Garçon* (1999), 3: *Geider and Osborne* (1989), 4: *Bienfang and Harrison* (1984), 5: *Bienfang* (1981), 6: *Fenchel* (1982), 7: *Conover* (1966), 8:*Evans and Parslow* (1985), 9: *Paffenhöfer and Harris* (1976), 10: *Fasham et al.* (1990), 11: *Murray* (2001), 12: *Harrison et al.* (1996), 13: *Kiørboe* (2001), 14: *Bienfang* (1980), 15: *Denman and Peña* (1999), 16: *Dowd* (1997), 17: *Brock* (1981)

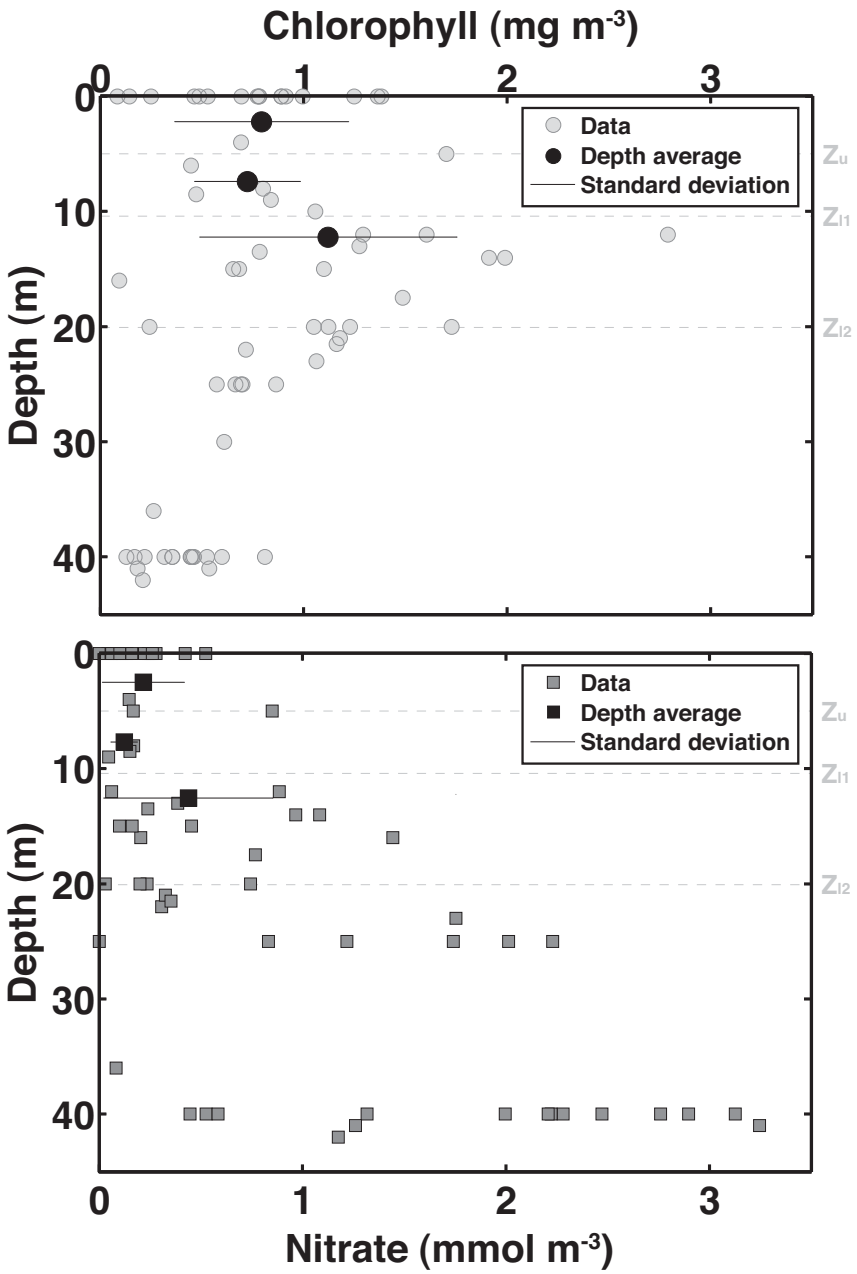

Figure 3.5: Set of data collected at station X6 in 2005 and 2006 used to compute boundary conditions for phytoplankton (upper panel) and nutrient (lower panel) at the open boundaries of box 1 and box 2. Z_u indicates the depth of the upper layer whereas Z_{l1} and Z_{l2} indicate the depth of the lower layers at the open boundary of boxes 1 and box 2 respectively. Black dots (chlorophyll) and black squares (nitrate) represent the mean values for (top to bottom) the upper open boundaries, and box 1 and box 2 lower open boundaries. Black lines indicate the standard deviations.

Table 3.2: Boundary conditions at the upper and lower open boundaries of box 1 and box 2 and initial values in each box (upper and lower layers), for each state variables in the ecosystem model. Values are indicated for the standard run (upper half) and for the sensitivity analyses (lower half). Values are expressed in mmolN m^{-3}. Percentages refer to deviation from the standard run.

Type	Location	P	N	Z	D
		Standard run			
Initial values	all boxes	0.599	0.217	0.212	1.488
Boundary conditions	upper box 1 & 2	0.599	0.217	0.212	1.488
	lower box 1	0.546	0.123	0.212	1.488
	lower box 2	0.846	0.439	0.212	1.488
		Sensitivity to parameterization			
Boundary conditions	box 1 & 2	±75%	±75%	±75%	±75%
		Ecosystem response to flushing rate and boundary nutrients			
Initial values	-	0.664	0.260	0.212	1.488
Boundary conditions	-	0.664	0–4	0.212	1.488

and lower open boundaries of box 2. The boundary conditions are set constant in time for the state variables (Table 3.2). It is therefore assumed that nutrients are never depleted at the open boundaries of the box model. For zooplankton and detritus, a single value is used for all four open boundaries (Table 3.2). The value is estimated from data collected at Station 2 (Figure 3.1A) and from local time series retrieved in the BIOCHEM database (*Gregory and Narayanan*, 2003). Zooplankton biomass (mmolN m^{-3}) is calculated from wet weight using the empirical relationship of *Banse* (1962). Detritus (mmolN m^{-3}) is retrieved from the particulate organic nitrogen (PON) data available in the database. It is assumed that all PON is detritus. For phytoplankton and nutrients, boundary conditions vary in space. At the upper open boundaries (box 1 and 2), the boundary conditions are set with the same value (Table 3.2), whereas at the lower open boundaries the value differs in box 1 and box 2 due to the difference in average depth (shallow for box 1 and deep for box 2). These boundary conditions are calculated using values from a set of data collected in 2005 and 2006 at station X6 outside the model domain which are averaged over the depth range of each boundary: 0–5 m in the upper layer and 5 m to bottom in the lower layer (Z_{l1} = 10.4 m and Z_{l2} = 19.9 m for box 1 and box 2 respectively) (Figure 3.5).

Given the biological and physical constraint in the model, the ecosystem response to the three circulation regimes represents the quasi-equilibrium cycle that the system would reach under a stable forcing (e.g. *Evans and Parslow*, 1985). Although this differs significantly from a natural system under a dynamic forcing, this experimental design enables one to study and compare the specific effect of circulation patterns and to explore the processes that influence the accumulation of phytoplankton biomass inshore.

3.2.5 Sensitivity Studies

3.2.5.1 Model Parameterization

An analysis of sensitivity to model parameterization is carried out for each circulation regime. The sensitivity of the model results to the variation in parameter values and boundary conditions are investigated using the Plackett-Burman technique (*Plackett and Burman*, 1946; *Beres and Hawkins*, 2001). This method enables the test of an extensive set of parameters using a limited number of scenarios (about twice the number of parameters tested). The implementation of this sensitivity analysis is described in *Beres and*

Hawkins (2001). In this analysis, a set of 17 parameters is used which gives a Plackett-Burman table of 40 scenarios. The model is therefore run 40 times for each circulation regime, changing the value of each parameter simultaneously to its maximum or minimum value (see Table 3.1) according to the Plackett-Burman scenario. The results of the analysis are displayed using a sensitivity index calculated as follows (*Jørgensen and Bendoricchio*, 2001):

$$\mathrm{SENS}_X = \frac{\Delta X}{X} \Big/ \frac{\Delta p}{p} \ , \tag{3.14}$$

where X is a state variable and ΔX the change in the state variable X due to the variation Δp in the parameter p.

3.2.5.2 Ecosystem Response to Flushing Rate and Boundary Nutrients

To determine the combined effect of flushing rate and nutrient concentration in source waters (i.e., open boundary conditions) on the ecosystem, a series of steady state sensitivity studies is carried out considering the entire model domain (i.e., sum of all boxes). In this configuration, everything remains the same (i.e., Section 3.2.4) except for (1) transport and (2) nutrient boundary condition, which are the two variables of interest. The initial and boundary conditions for phytoplankton and initial conditions for nutrients are changed slightly from the standard run due to the spatial averaging. They are set to the average boundary conditions in box 1 and box 2 of the standard run (Table 3.2).

Transport is reduced to the exchange rate between the bay and the inner shelf. This exchange is specified by a constant volumetric flow rate (i.e., $\overline{Q}_{adv}$, see Eq. 3.1) that represents the tidally averaged advective flux across the outer boundaries of the model (i.e., mean inflow equals mean outflow). In the case of the three wind regimes, it corresponds to 665.6 $m^3\ s^{-1}$ for the tidal regime, 7887.8 $m^3\ s^{-1}$ for the upwelling regime, and 7039.7 $m^3\ s^{-1}$ for the downwelling regime (Figure 3.3). The transport rate is varied over a large range of values to account for all types of circulation regimes, including the tidal, upwelling and downwelling regimes described in Section 3.2.2. The corresponding flushing rates are calculated using Eq. 3.1 (Section 3.2.3). For each transport rate, nutrient boundary condition is varied over a realistic range of values (0–4 mmol m^{-3}) to account for various types of nutrient concentration in source waters. For each combination of transport and nutrient,

the model is run for 40 days to let the ecosystem model reach a steady state solution.

Flushing rate, boundary nutrient concentration and ecosystem variables are scaled to the appropriate biological scaling factors in order to present a non-dimensional solution of the sensitivity analysis (e.g., *O'Brien and Wroblewski*, 1973; *Wroblewski et al*., 1975; *Lewis et al*., 1984). The dimensionless variables are:

$$F^* = \frac{F_{\mathrm{R}}}{\mu(E,T)} \tag{3.15}$$

$$S^* = \frac{N_{\mathrm{OUT}}}{k_N} \tag{3.16}$$

$$X_i^* = \frac{X_{i\mathrm{IN}}}{X_{i\mathrm{OUT}}} \tag{3.17}$$

In this dimensionless framework, the flushing rate (F_{R}; d^{-1}) is scaled by the light and temperature limited growth rate ($\mu(E,T)$; d^{-1}) to represent the specific transport relevant to primary producers (F^*); a small value of F^* indicates a system where internal dynamics dominate, whereas a large value indicates a system where transport dominates. The boundary nutrient concentration (N_{OUT}; mmol m^{-3}) is scaled to the half saturation for nutrient uptake (k_N; mmol m^{-3}) to represent the nutrient concentration available to primary production in source waters (S^*); a small value of S^* indicates a lack of nutrient, whereas a large value indicates the availability of nutrient in source waters. For each state variable X_i ($i = P, Z, N, D$), the concentration inside the bay ($X_{i\mathrm{IN}}$), which is the model solution, is scaled by its boundary concentration ($X_{i\mathrm{OUT}}$) to represent the internal accumulation (or loss) of a state variable with respect to its concentration at the boundary (X_i^*). When $X_i^* > 1$ there is an accumulation, whereas when $X_i^* < 1$ there is a loss of the state variable in the inlet.

3.2.6 Data Collection

The data used for comparison with the model results were collected in 2006 at the five stations in Lunenburg Bay and three moorings indicated in Figure 3.1B. The dataset and the sampling campaigns are discussed in Chapter 2. Three dates have been chosen amongst the sampling dates, corresponding to tidal, upwelling or downwelling regimes depending

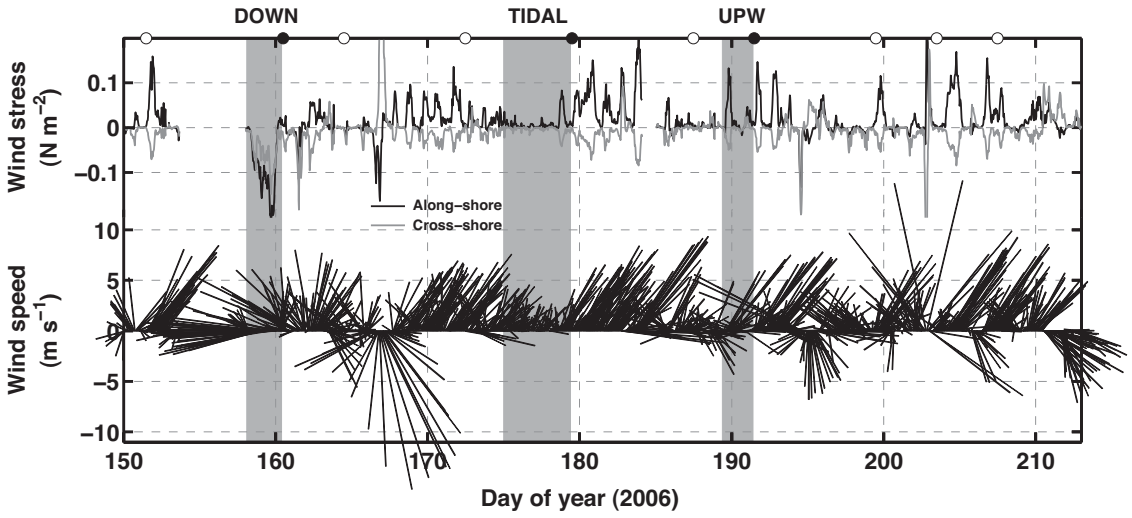

Figure 3.6: Wind stress and wind speed vectors from Battery Point meteorological station. Wind stress is calculated using the bulk formula from *Large and Pond* (1981). Positive cross-shore values indicate southeastward wind (i.e., oriented offshore) and positive along-shore values indicate northeastward wind (i.e., oriented along-shore). Circles indicate the dates of data collection available. Filled circles correspond to the sampling dates selected to compare with model results. The type of wind regime is indicated on the top of the figure (DOWN: downwelling, UPW: upwelling) and shaded areas indicate the period of interest prior to the data collection.

on the wind direction and intensity prior to the data collection (Figure 3.6). Each category of data was subsequently used to compare with the circulation regimes: the downwelling sampling date follows a period of strong downwelling wind, the date selected for the tidal case follow a week of weak wind and the upwelling date is included during the development of upwelling conditions in Lunenburg Bay (see Chapter 2 for details). The data, which include usually 4 samples per station (4 depths), are depth- and station-averaged (if more than one station per area) to retrieve a mean value for the inner (IN), middle (MID) and outer (OUT) areas (see Section 3.3.2).

3.3 Results

3.3.1 Residual Circulation Patterns

The tidally averaged circulation patterns are presented in Figure 3.3. In the tidal regime, fluxes have a general inward direction (toward the head of the bay) in the bottom layer and an outward direction (toward the mouth of the bay) in the upper layer, an indication of shear in the tidal transport. A sub-circulation is also apparent, with water entering along the southern side of Lunenburg Bay, through the deep layer of the southeast box 2 and leaving along the northern side through the northeast box 1. Tidal residual vertical fluxes are oriented upward in most of the model domain except for the open boundary boxes 1 and 2.

The influence of the wind regimes is important on the residual circulation for both the patterns and the magnitude of the water fluxes which are increased by an order of magnitude at the interface between the bay and the inner shelf (outer boundaries). The flushing time of the bay is therefore greatly reduced with the wind forcing, in the outer bay for the downwelling regime and throughout the bay for the upwelling regime (Figure 3.7). Circulation patterns are also modified. In the upwelling case, water enters Lunenburg Bay through the southeast box 2, mainly in the deep layer, and leaves through the northeast box 1. Fluxes in the upper and lower layers are in general unidirectional in this configuration, with fluxes inward (entering the bay) on the southern side of Lunenburg Bay and outward (leaving the bay) on the northern side. All the fluxes are enhanced (except in the inshore box 7 and 8), including vertical fluxes which are mainly oriented upward. On the contrary, the pattern of residual circulation under the downwelling regime indicates an inflow through the northeast box 1 (mostly in the surface layer) and an outflow through the southeast box 2, with inward fluxes along the northern side of the bay and a recirculation in the mid-bay. The recirculation increases the flushing time in the middle of the bay and limits the exchanges between the inner bay and the open boundaries.

The wind-driven circulation patterns are especially important at the outside boundaries where nutrient and phytoplankton concentrations are different in the lower layer of the outer box 1 and box 2 due to varying mean depth. Also, most of the water entering the bay under the wind circulation regimes leaves directly on the other side of Cross Island, which

has implications for biological transport (see section 3.3.2.3). The wind-driven patterns of circulation at the bay-inner shelf interface, and hence the biological conditions in this area, are therefore critical to the delivery and export of nutrients and plankton to/from Lunenburg Bay.

3.3.2 Biological Dynamics

The magnitude of the biological response to wind circulation regimes is rather small (Figure 3.7 & 3.8), especially in comparison to the changes in circulation associated with the wind regimes (magnitude and direction). The boundary conditions are fixed in the model and therefore the variations in state variables result from changes in the circulation at the boundary and in the bay and not from changes in boundary conditions. The upwelling induced increase in nutrient resulting from the shoaling of the nutricline (as observed in Chapter 2) is therefore not modelled, which explains the small increase in nitrate concentration near the open boundary under the upwelling regime. The comparison between the circulation experiments reveals nonetheless interesting patterns; the biological response to the wind-induced circulations varies in space and magnitude. The results under the three circulation regimes and the underlying patterns are discussed below.

3.3.2.1 Spatial Patterns

Nutrient concentrations are low and spatially homogeneous throughout the bay when circulation is forced by tides only (Table 3.2). Phytoplankton biomass decreases in the inshore area, opposing the zooplankton concentration, which increases in the middle and inner areas. The model state variables have a weak response to the wind-induced circulation. Nutrient concentrations remain low throughout Lunenburg Bay with the exception of a small increase near the open boundary under the upwelling regime. The spatial patterns of zooplankton are maintained under the wind regimes but with reduced biomass. The results concerning the detritus are not presented on Figure 3.7 for clarity. However the time series presented in Figure 3.8 indicates detritus concentrations similar to boundary conditions under a tidal regime and a small decrease under the wind regimes. The decrease is maximal in the case of the downwelling. The main response to wind-induced circulation occurs in the phytoplankton for which the two wind regimes have an opposing effect. A

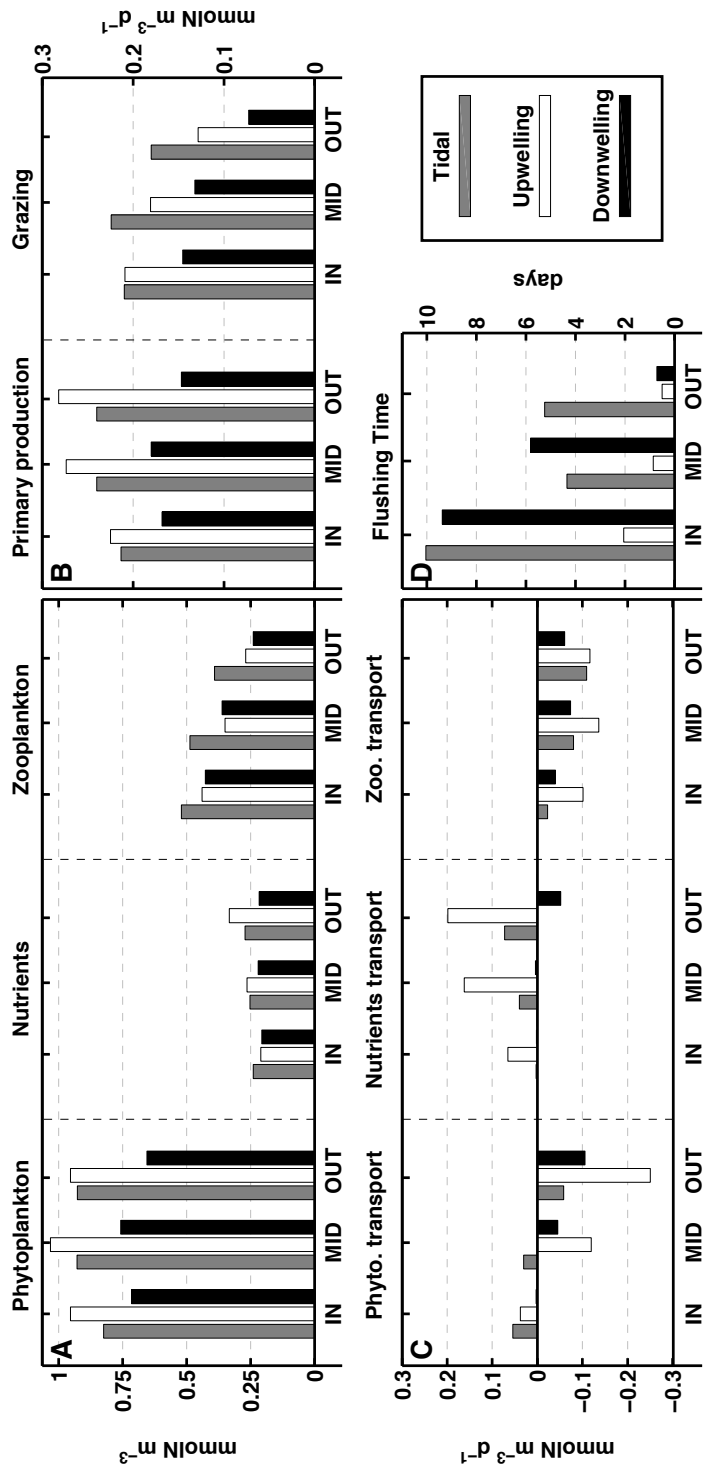

Figure 3.7: Summary of model results under the three circulation regimes in each area of the bay for A. the state variables, B. the ecosystem processes, C. the net biological transports and D. the flushing time. Results are an average from the upper and lower layers.

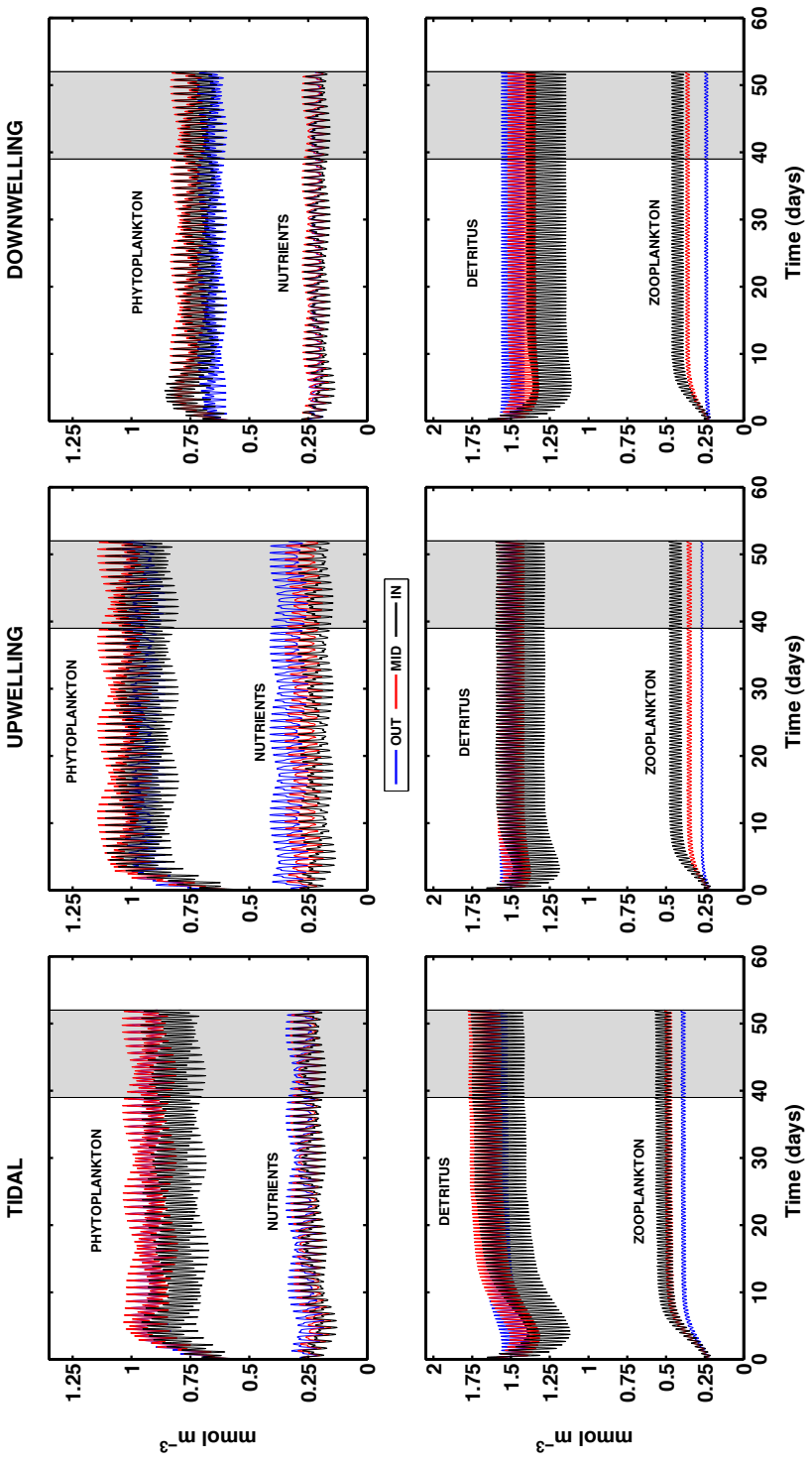

Figure 3.8: Spatially-averaged state variable time series for each circulation regime (left to right) in the upper and lower layers of the outer bay (OUT, Box 1 & 2), the mid-bay (MID, Box 4 & 5) and the inner bay (IN, Box 6, 7 & 8) boxes. The shaded areas correspond to the period used for the calculation of the averages displayed in Figure 3.7 & 3.9.

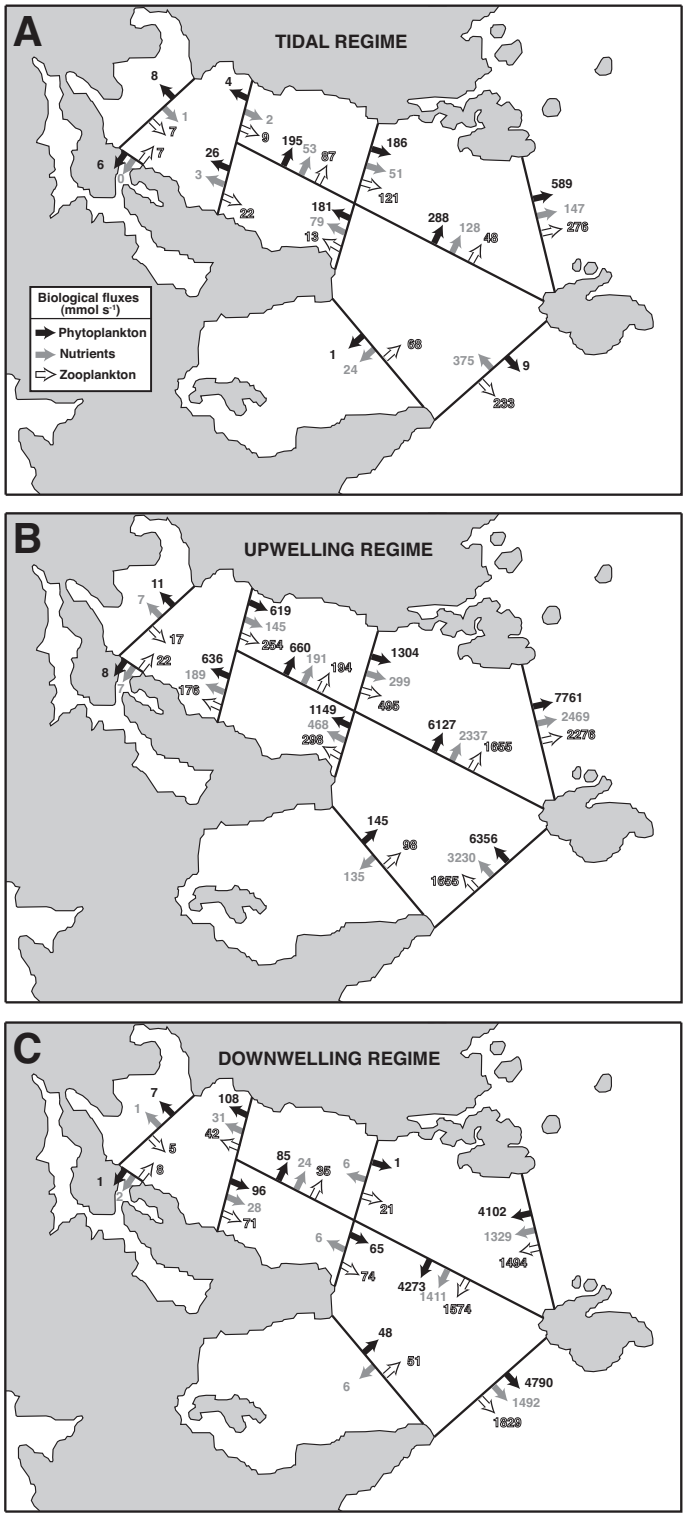

Figure 3.9: Tidally averaged transport of nutrient, phytoplankton and zooplankton across each horizontal boundary of the box model (mmol s^{-1}) under the A. tidal, B. upwelling and C. downwelling circulation regimes. Each arrow represents the sum of the transports in the upper and lower layers.

downwelling circulation induces a decrease of phytoplankton biomass throughout the bay (matching the decline in the other state variables) whereas an upwelling circulation leads to a moderate increase in phytoplankton biomass inward, with a maximum at mid-bay (Figure 3.7A).

3.3.2.2 Ecosystem Processes

When circulation is forced by tides, nutrient limitation constrains phytoplankton growth at the same level throughout the bay (Figure 3.7B). This constraint is somewhat released at the open boundaries under the upwelling regime, leading to a higher rate of primary production that partly explains the observed spatial pattern in phytoplankton biomass. Despite enhanced primary production and higher phytoplankton biomass, grazing decreases in the bay under the upwelling circulation regime due to the decrease in zooplankton biomass, except inshore where grazing is sustained at its tidal regime level. Conversely, the downwelling regime induces a significant decrease in primary production and grazing everywhere in Lunenburg Bay in comparison to the other circulation regimes. Overall, it leads to a reduction of all biological processes throughout the bay.

3.3.2.3 Biological Fluxes

The patterns and magnitude of biological transports are critical to explain the model results. Transport is accelerated in the outer bay (downwelling) and the whole bay (upwelling) under the wind regimes in comparison to the tidal case (Figure 3.7D). Fast transport, relative to the rate of biological processes such as primary production or grazing, imposes a strong constraint over the development of internal biological dynamics inside Lunenburg Bay.

Under a tidal regime, the prolonged flushing time leads to the decrease in nutrient transport shoreward, away from the source of nutrient (Figure 3.7C). Simultaneously, it favours the development of zooplankton biomass inshore, which explains the decrease in phytoplankton biomass in the inshore area. A characteristic of the model is the export of zooplankton from the model domain (Figures 3.7C & 3.9A). All transports are negative indicating that local zooplankton production is exported. This occurs in all circulation

regimes. Some phytoplankton is exported as well from the outer bay, balancing the input of nutrients from the southeastern boundary in the tidal regime.

The wind regimes result in very different biological transports. With a downwelling circulation the net biological transports are reduced (Figure 3.7C). Transports are however large across the open boundaries and between the outer box 1 and box 2, due to the enhanced water fluxes and plankton concentrations are reduced to their boundary conditions in this area. In this configuration, water enters Lunenburg Bay through the shallow northeastern boundary (box 1) where deep nutrient concentrations are low and leave through the southeastern boundary (box 2, Figure 3.3C). A similar amount of nutrients enters and leaves the bay (Figure 3.9C), resulting in little net transport of nutrients or net increase in phytoplankton inside the bay (Figure 3.7C).

Conversely, upwelling circulation results in enhanced biological transport. Nutrient transport increases significantly, in particular in the outer and mid bay (Figure 3.7C). The transport rate of nutrients entering Lunenburg Bay from the outside is 2.4 times higher under the upwelling in comparison to the downwelling circulation (Figure 3.9B). In this configuration, the main boundary flow is into the deep layer of the southeast box 2 (Figure 3.3B), which results in higher nitrate input into the bay due to higher deep nutrient concentration at this location. The negative net transport of phytoplankton under the upwelling circulation indicates the export of phytoplankton produced in the bay (Figure 3.7C). It explains the discrepancy between the observed rates of primary production and the limited increase in phytoplankton biomass. The amount of phytoplankton produced in the outer part of the bay is compensated by an export of similar magnitude through the northeastern boundary (box 1) and therefore phytoplankton biomass does not accumulate in the bay. The overall effect of the upwelling circulation on the different areas of Lunenburg Bay is therefore the result of a balance between transport and production: in the outer part, production is balanced by transport and there is no net increase in local phytoplankton biomass; in the mid-bay primary production exceeds phytoplankton transport (export) which allows for a moderate increase in phytoplankton biomass; in the inner bay primary production is lower but compensated by a shoreward transport of phytoplankton that also results in a moderate increase of phytoplankton biomass.

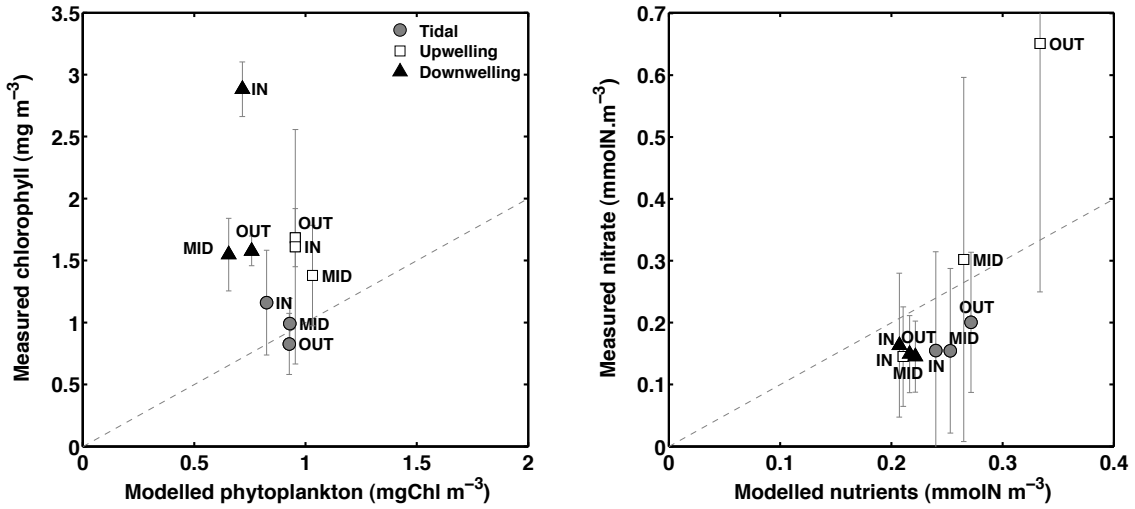

Figure 3.10: Comparison between model results (phytoplankton, nutrient) and observations (chlorophyll, nitrate) for each wind regime. The grey bars indicate the standard deviations in the observations and the dashed line represents the 1:1 relationship.

3.3.3 Comparison with Observations

The results from the experiments cannot be compared with specific observations since constant boundary conditions or sustained wind circulation are idealistic conditions, far from the dynamic conditions encountered in a coastal system. Nonetheless, contrasting modelled and measured data can help to interpret the modelling results and gain insight into the processes controlling biological variability in Lunenburg Bay. This comparison is not meant to assess the model performance with a quantitative measure of skill.

The comparison indicates that observed and modelled phytoplankton biomass compare well for the tidal circulation case, but the model underestimates the observations in the case of the wind-induced circulations (Figure 3.10). For the upwelling circulation, the discrepancy between modelled nutrients and observed nitrate suggests that the underestimation in phytoplankton biomass is likely the result of the fixed nutrient boundary conditions in the model. For the downwelling circulation the discrepancy between modelled phytoplankton and measured chlorophyll cannot be explained by a difference between modelled nutrients and measured nitrate which fall within the same range. This discrepancy is especially large in the inner part of the bay.

The variability and the magnitude of phytoplankton biomass measured in Lunenburg Bay is very low compared to other inlets adjacent to upwelling systems (see Chapter 2). The model captures the dominant processes regulating this variability. However, the model is unable to simulate the processes inducing phytoplankton variability inshore under downwelling conditions. Steady state boundary conditions for phytoplankton are probably not a reasonable assumption during a downwelling event.

3.3.4 Sensitivity Studies

3.3.4.1 Model Parameterization

The sensitivity analysis to the variation in boundary conditions and parameter values (Figure 3.11) reveals three general patterns:

(1) the model is more sensitive to these variations under a tidal circulation regime;

(2) nutrients (i.e., nitrate) is the most sensitive state variable in the model; and

(3) sensitivity is higher in the inner bay.

This is in agreement with the results discussed so far. The flushing time is longer when the circulation is forced by tides only and the inner bay is less influenced by transport than the boundaries of the model domain. This leads to the development of ecosystem interactions that influence the concentration of the local state variables, resulting in a higher sensitivity to parameter changes. In addition, nutrient concentrations are low in all wind configurations. It is then not surprising to find that they are sensitive to parameters that control their uptake through primary production, and their production through recycling such as grazing, mortality or remineralization.

A noticeable result of the sensitivity analysis is that modelled phytoplankton and nutrients are sensitive to parameters related to phytoplankton grazing and zooplankton mortality, with a sensitivity increasing inward where zooplankton biomass is higher, whereas phytoplankton biomass is not sensitive to the variation in growth parameters. These sensitivity patterns can be related to the low background level of nutrients throughout the bay which limits the effects of growth processes on phytoplankton biomass. Nutrient

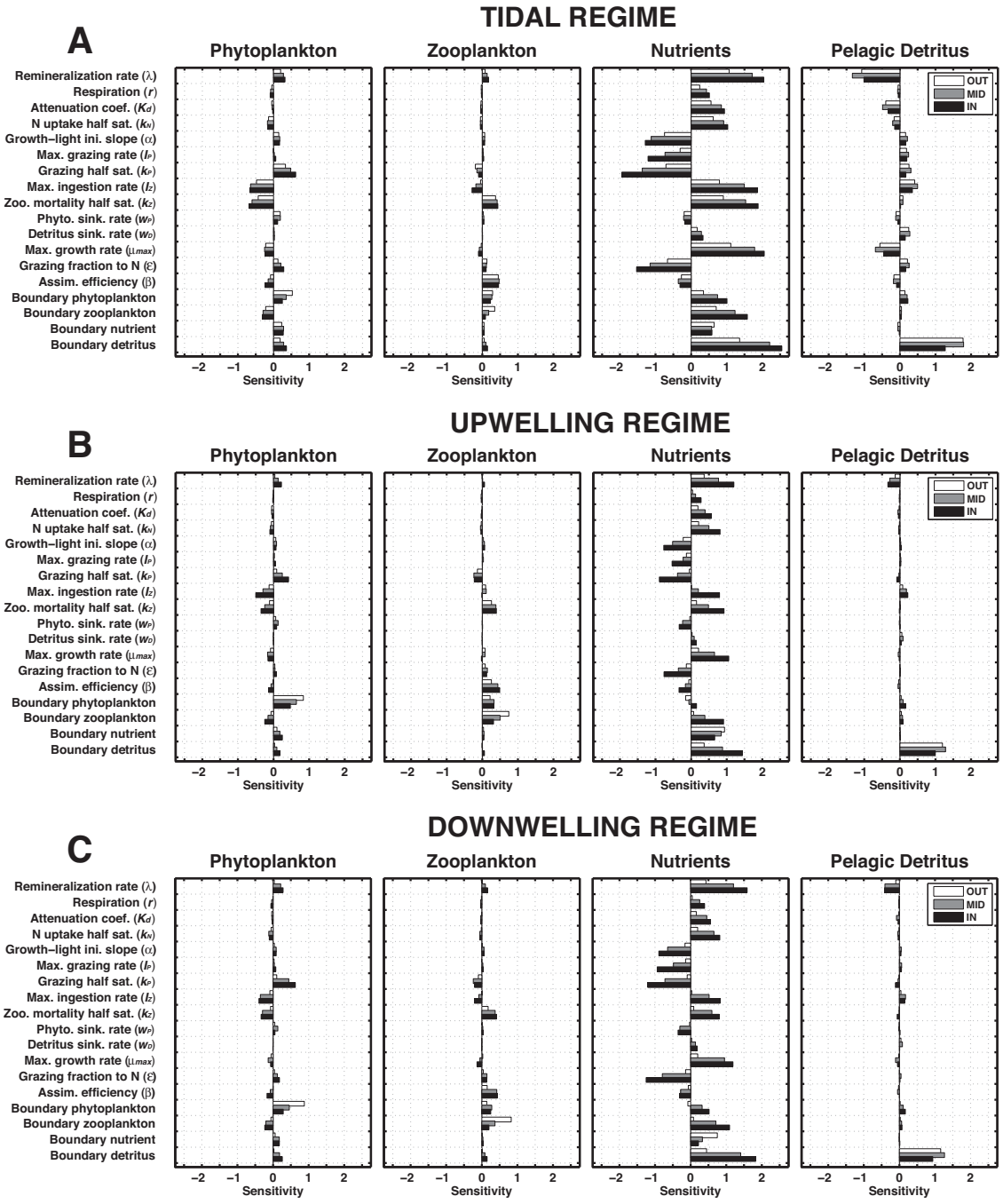

Figure 3.11: Results from the sensitivity analysis in the inner (white), middle (grey) and outer (black) parts of Lunenburg Bay for the A. tidal, B. upwelling and C. downwelling circulation regimes. The x-axis represents the sensitivity of the model results to a specific parameter/boundary condition, specified on the left hand side of the figure, using a sensitivity ratio (see Section 3.2 for the methodology).

concentrations are also sensitive to zooplankton, nutrients and detritus boundary conditions suggesting the importance of nutrients sources in the model, either from the open boundaries (i.e., to the processes occurring on the shelf), or from recycling. Zooplankton concentration is however not very sensitive to parameterization, except to boundary conditions under wind-induced circulations. Finally, pelagic detritus is only sensitive to its boundary conditions, except under a tidal regime, when remineralization and maximum growth rate become more important. Overall, sensitivity patterns are relatively similar for each circulation regime but the magnitude decreases under wind-induced circulations.

3.3.4.2 Ecosystem Response to Flushing Rate and Remote Nutrients

In ocean-dominated inlets, the delivery of nutrients depends on the concentration of nutrients at the open boundaries of the inlet (i.e., in source waters) and on the transport rate at the inlet-ocean interface. The combination of the two processes has then a key role in the dynamics of inshore ecosystems. This role is described for inshore plankton, nutrient and detritus concentrations with the non-dimensional solution of the sensitivity analysis (Figure 3.12). Because of the scaled variables, this analysis can be used to describe the dynamics of inlets more generally. It is thus not limited to Lunenburg Bay and can help to synthesize the results from the box model and to discuss them in a larger context. The analysis is designed to represent ocean-dominated inlets (e.g., Lunenburg Bay). Therefore, the relationship between nitrate availability in source waters (S^*) and specific transport (F^*) represents the effects of the inlet-ocean coupling on the internal dynamics of an inlet (i.e., on X_P^*, X_Z^*, X_N^* or X_D^*, see Section 3.2.5.2). However, this analysis is not limited to these systems. The main assumption of the analysis is that nutrient delivery and flushing are coupled, which is similar to a chemostat system; the plankton dynamics described hereafter can then be generalized to systems approaching these conditions, such as a section of a river, a lake, the river-inlet coupling in systems dominated by runoff, or the mixed layer in the surface ocean.

Overall, five types of dynamics emerge from the analysis (hereafter the S^* vs. F^* framework) that result from particular dynamical range of S^* and F^*. Each type has been delineated on Figure 3.12D:

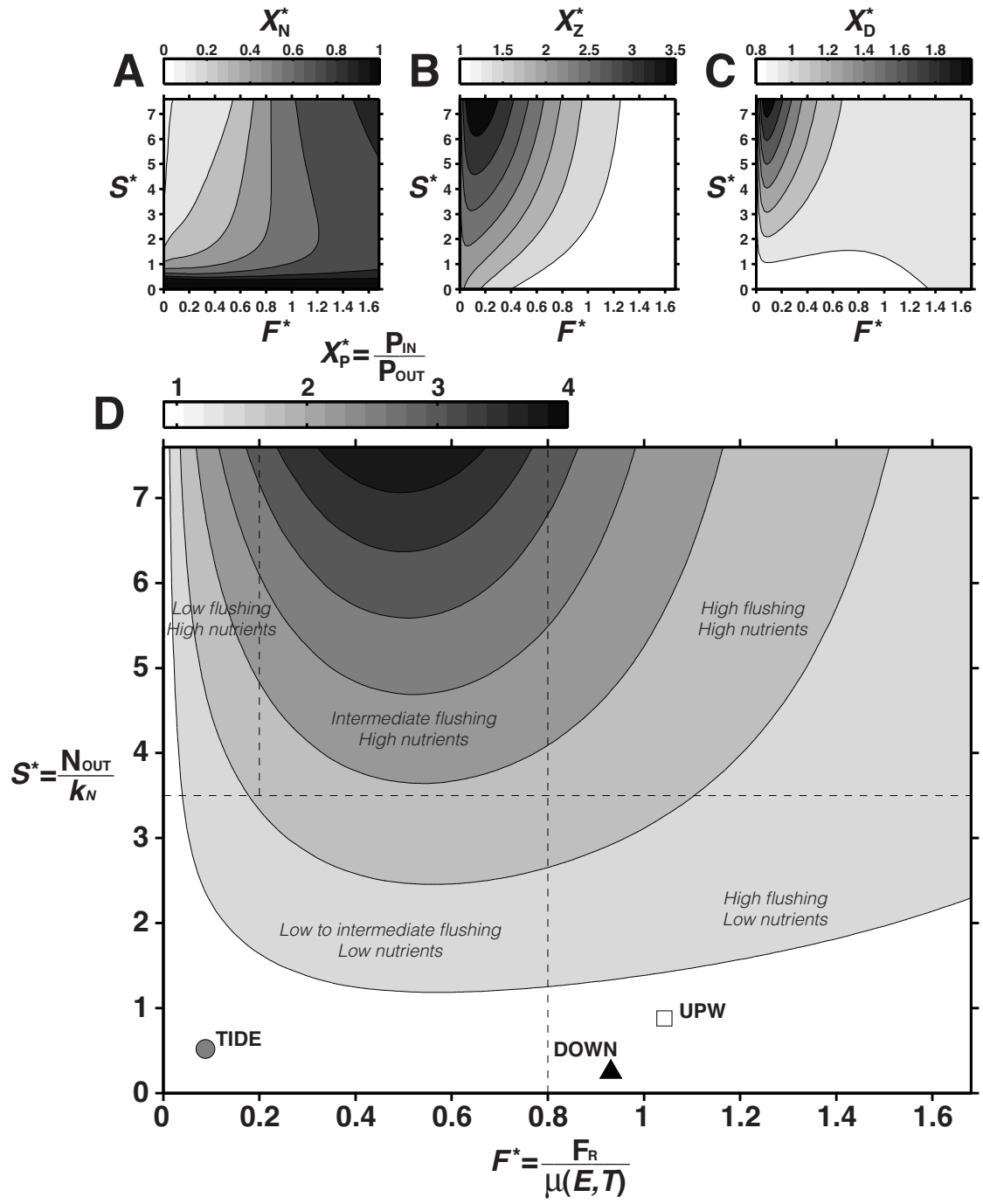

Figure 3.12: Effect of flushing (F^*) and nutrient boundary conditions (S^*) on the relative concentration of A. nutrient (X^*_N), B. zooplankton (X^*_Z), C. detritus (X^*_D) and D. phytoplankton (X^*_P) inside an inlet. The relative concentration (X^*) is the ratio between concentrations inside the inlet (X_{IN}; mmol m^{-3}) and at the boundary (X_{OUT}; mmol m^{-3}). Flushing (F^*) is the ratio between the flushing rate (F_R; d^{-1}) and the light (E; W m^{-2}) and temperature (T; °C) limited growth rate of phytoplankton ($\mu(E,T)$; d^{-1}). Nutrient boundary conditions (S^*) is the ratio between nitrate concentration at the boundary (N_{OUT}; mmol m^{-3}) and the half-saturation constant for nutrient uptake by phytoplankton (k_N; mmol m^{-3}). The three wind regimes are represented on the figure (TIDE: tidal, UPW: upwelling and DOWN: downwelling) and five zones of specific dynamics are suggested (details in text).

(1) *Low to intermediate flushing-Low nutrients in source waters*, where phytoplankton biomass is low due to nutrient limitation;

(2) *Low flushing-High nutrients in source waters*, where internal biological processes dominate and phytoplankton biomass is limited by both nutrients and grazing;

(3) *High flushing-Low nutrients in source waters*, where primary production is limited by nutrients and the concentration of biological variables dominated by transport;

(4) *High flushing-High nutrients in source waters*, where phytoplankton export prevails and the concentration of the other biological variables dominated by transport; and

(5) *Intermediate flushing-High nutrients in source waters*, where phytoplankton accumulates inshore.

These dynamics can be explained by the relative time scale between nutrient delivery into the inlet, biological processes (i.e., growth vs. loss processes) and transport of biological variables (plankton and detritus). When F^* is small (low specific transport), the time scale of nutrient utilization by primary producers is rapid in comparison to the transport time scale (which sets the rate of nutrient delivery into the inlet) and therefore inshore nutrient concentration is limited, even when a significant concentration is available offshore (Figure 3.12A). The accumulation of phytoplankton is then limited by the availability of nutrients (Figure 3.12D). At $F^* < 0.2$, the time scale of phytoplankton loss to grazers is short in comparison to growth (because nitrate delivery is limited) and transport. Secondary producers accumulate ($X_Z^* > 1$, Figure 3.12B) and control the accumulation of phytoplankton (Figure 3.12D). Detritus, the production of which is dominated by secondary producers, accumulates similarly ($X_D^* > 1$, Figure 3.12C). At large F^* (rapid specific transport), the time scale of transport is short in comparison to the biological time scales and therefore phytoplankton biomass is controlled by transport (Figure 3.12D).

Despite the simplifications, the analysis reveals the existence of an optimum 'window' for the accumulation of phytoplankton biomass inside an inlet ($X_P^* \gg 1$) at intermediate transport time scales ($0.2 < F^* < 0.8$) when boundary nutrient is sufficient ($S^* > 3.5$) (Figure 3.12D). Within this range, the balance between the rates of nutrient delivery, losses to secondary producers and phytoplankton export, is optimal for the local accumulation of phytoplankton. The specific values of nutrient concentration in source waters

and flushing rate at which these dynamics occur depend on phytoplankton physiology, represented by the scaling factors $\mu(E,T)$ and k_N. These values depend on the underlying taxonomic and environmental conditions (e.g., phytoplankton species, light fields, temperature, nutrient status), which can vary over various time scales in a natural environment.

The location of the Lunenburg Bay circulation regimes on the S^* vs. F^* framework (Figure 3.12D) reflects the limitations previously described for each regime. The tidal regime is located in the low flushing-low nutrients region where nutrient limitation is important and secondary production develops. Increasing the boundary nutrient concentration (or lowering k_N, e.g., smaller phytoplankton cell size) would induce a shift towards a system dominated by internal biological dynamics where secondary production is important but the phytoplankton biomass limited. The upwelling and downwelling regimes are both in the high flushing-low nutrients region where transport dominates the biological system. Nutrient limitation is particularly important under the downwelling regime. The position of the upwelling regime on the figure indicates that at higher nutrient concentration in source waters than the one tested with the box model, the local accumulation of phytoplankton biomass would be limited by export. Overall, the analysis shows that dynamics in Lunenburg Bay are limited by low nutrient concentration in source waters.

3.4 Discussion

Fluctuations in the local and remote wind forcing have a substantial role in nearshore areas because they control the local circulation and the flushing of inlets, promoting the coupling with the coastal ocean (*Garvine*, 1985). In Lunenburg Bay, this coupling has a dominant role in the variability of nitrate and phytoplankton in summer (Chapter 2). To assess the underlying factors associated with this coupling, two levels of analysis were presented, which demonstrate that wind induced accelerated flushing and low nitrate concentration in source waters are important factors controlling phytoplankton biomass in Lunenburg Bay. The spatially explicit Box model analysis has revealed a significant effect of wind-induced circulation on nutrient transport and on the rate of ecosystem processes in Lunenburg Bay, but also on the rapid transport of phytoplankton which limits its accumulation in the bay, whereas a spatial pattern of zooplankton appeared with reduced

flushing under a tidal circulation. The spatially-averaged sensitivity analysis provides a generalization of these results on a dimensionless framework, which represents a conceptual model of the interaction between nitrate availability in source waters and specific transport (S^* vs. F^*). This interaction determines the accumulation of phytoplankton biomass (and other biological properties) inside an inlet. The role of the two processes is discussed in the context of Lunenburg Bay and then generalized based on the dimensionless framework.

3.4.1 Factors Controlling Phytoplankton Biomass in Lunenburg Bay

The three meteorological forcing regimes (tidal, upwelling and downwelling) generate contrasting circulation patterns in Lunenburg Bay (Figure 3.3). They have distinct effects on nutrient transport and local ecosystem processes, but result in a limited change in local concentrations. The S^* vs. F^* framework provides an explanation to this narrow range of concentrations.

When circulation is controlled by the semi-diurnal tide, the flushing time of the bay (estimated to 15 days) is significantly greater than the biological time scales, hence biological processes dominate. The delivery of nutrient from the shelf is limited due to both the low concentration on the Scotian Shelf and the limited flow at the bay-ocean interface (Figure 3.3). In this configuration (low flushing, low nutrient), the S^* vs. F^* framework indicates that in an inlet the local accumulation of phytoplankton biomass is limited but also that the long flushing time allows for the development of secondary producers, which accumulate in the bay (Figure 3.12). This accumulation occurs along the inshore-offshore axis of increasing coupling between Lunenburg Bay and the Scotian Shelf, zooplankton reaching a maximum biomass at the head of the bay (Figure 3.7A). This spatial pattern is characteristic of semi-enclosed inlets, where water circulation has a dominant role in structuring plankton spatial variability along the longitudinal axis (*Jouffre et al*., 1991; *Dowd*, 2003). At the mouth of the inlet, inner shelf conditions are prevalent due to the increased intensity of transport, whereas inshore, reduced transport allows for a control by grazers over phytoplankton biomass (*Dowd*, 2003), resulting in the local accumulation of zooplankton (*Pinel-Alloul*, 1995). Spatial variability is then characteristic of the tidal circulation.

The wind regimes induce the accelerated flushing of the bay, which imposes a hydrodynamic control over the biological system due to the rapid transport in comparison to the biological time scales (Figure 3.7). Despite this control, specific differences have arisen from the comparison between the upwelling and the downwelling circulations. Under both regimes, the biophysical coupling is accelerated at the interface between Lunenburg Bay and the inner shelf. In this area, the rapid transverse flow (north-south axis) is controlled by the intensity and the orientation of the wind (*Yang and Sheng*, 2008), water entering in the southeastern (northeastern) side and leaving through the northeastern (southeastern) side of Lunenburg Bay in the upwelling (downwelling) wind regime (Figure 3.3B,C). This change in the orientation of the flow at the inlet-ocean interface has a significant effect on local biological processes because it influences the delivery of nutrient into the bay (Figure 3.7C). Under persistent southeastward winds (downwelling), residual nutrient fluxes are negligible due to the lack of nutrient in source waters (surface). Plankton dynamics inside Lunenburg Bay are reduced and the phytoplankton limited to the biomass occurring in source waters. The mismatch observed in the model-data comparison suggests however that other processes are regulating phytoplankton variability under this wind regime. Shoreward transport of phytoplankton during period of downwelling is a mechanism of phytoplankton accumulation inshore (*Crespo et al*., 2006). This process is not represented in the box model which uses steady state boundary conditions; hence the effect of allochtonous phytoplankton transport into Lunenburg Bay during periods of downwelling cannot be investigated.

When the bay circulation is driven by northeastward winds (upwelling), enhanced deep nutrient fluxes promote local primary production. Because of the wind-induced accelerated flushing of the bay, the local phytoplankton production is exported to the inner Scotian Shelf (Figure 3.7C). The wind induced accelerated flushing of upwelling and downwelling conditions is represented by a shift toward the right-hand side of the S^* vs. F^* framework (Figure 3.12) where biological dynamics are limited by both rapid transport and low nutrient concentrations. It confirms the role of accelerated flushing and shows the dominant limiting effect of the low average nutrient concentration on the biological system of Lunenburg Bay. The summer-averaged nitrate concentration used in the box model analysis is representative of tidal and downwelling-driven circulations but underestimates the concentration observed during a sustained upwelling event (i.e.

2 mmolN m^{-3} inside the bay, see Chapter 2). Nonetheless, the S^* vs. F^* framework indicates that the rapid flushing characteristic of the upwelling circulation limits phytoplankton biomass in Lunenburg Bay at a more representative nutrient concentration (Figure 3.12D).

In Lunenburg Bay, the hypothesis of a limitation of summer phytoplankton biomass by the intensity of wind-induced flushing and by the low nitrate concentration in the source waters is therefore well supported. The interaction between the two processes explains the observed phytoplankton biomass over a range of wind-induced circulations. The distinct dynamics under the three meteorological regimes demonstrates that the concept of source waters, which relates to the origin of the water entering the bay, hence associated to specific patterns of circulation—e.g., deep shelf water for an upwelling, surface water for a downwelling—is more accurate than boundary conditions and the ordinate of the S^* vs. F^* framework (i.e., S^*) should refer to this definition.

3.4.2 Generalization of Results Based on S^* vs. F^*

The relationship between growth, loss and transport time scales governs phytoplankton dynamics in aquatic systems (*Lucas et al.*, 2009). In coastal inlets, biological dynamics are also determined by the balance between the processes occurring locally in the inlet and the processes occuring in the adjacent coastal ocean (shelf biogeochemistry, physical processes), which are related through local and coastal transport (*Dowd*, 2005). The S^* vs. F^* framework demonstrates the importance of the balance between local and remote processes and attempts to explain the general ecosystem dynamics of an inlet based on offshore nutrient concentration and transport.

The importance of transport patterns and intensity was established for Lunenburg Bay throughout this study (Figure 3.7C). The role of nutrients in source waters was illustrated by the transport patterns in the wind regimes. Although the variations in plankton biomass and nutrient concentration were small, the study has illustrated the effect of the interaction between nutrient in source waters and transport on plankton dynamics in Lunenburg Bay (Figure 3.7). Because of the scaled variables in S^* vs. F^*, the dynamics in Lunenburg Bay can be compared to other inlets. For instance, a fundamental

difference between Lunenburg Bay or other inlets located on the Atlantic coast of Nova Scotia and the inlets located on the west coast of North America or the west coast of the Iberian Peninsula arises from the nitrate concentrations available on their adjacent shelves (i.e., shelf-dominated vs. slope-dominated continental margins, see Chapter 1). It can be significant on the west coast during the upwelling season (*Hickey and Banas*, 2003; *Álvarez-Salgado et al*., 2010), which influences nitrate concentration in the inlets source waters (*Hutchings et al*., 1995). For example, on the Northwest coast of North America, upwelling-induced transport provides high concentration of nitrate to the coastal inlets (e.g., 10–30 mmol m^{-3} in Yaquina Bay, *Brown and Ozretich*, 2009), which is an order of magnitude higher than the estimated value in Lunenburg Bay (see Chapter 2). At this level of nitrate in source waters, an inlet is located at the top (and beyond) of the of the S^* axis (ordinate) on the S^* vs. F^* framework (i.e., $S^* > 6.6$, assuming $k_N = 1.5$ mmol m^{-3}) where plankton dynamics are controlled by the flushing time scale rather than the availability in nutrient. Similar dynamics are found in the rias on the west coast of the Iberian Peninsula where nitrate concentration in source waters are in the range 5–9 mmol m^{-3} (i.e., $3.3 < S^* < 6$, assuming $k_N = 1.5$ mmol m^{-3}) depending on the intensity of the upwelling (*Álvarez-Salgado et al*., 1996a). In these systems, weak upwelling conditions favour the retention of nutrients and the accumulation of primary producers in the inlet (*Álvarez-Salgado et al*., 1996b; *Piedracoba et al*., 2008a), whereas strong upwelling is associated with rapid flushing, which promotes the export of primary production to the shelf (*Álvarez-Salgado et al*., 1996b; *Crespo et al*., 2006). Although the value of F^* remains to be calculated for these inlets, these dynamics agree qualitatively with the dynamics described by the framework. In comparison, Nova Scotian inlets and similar ocean-dominated systems along the western boundaries of ocean basins are located on the lower part of the framework where nutrients in source waters is a dominant limiting factor for the local development of phytoplankton biomass, as seen in Lunenburg Bay.

The S^* vs. F^* framework also reveals the combined effect of transport and nutrient concentration in source waters on growth (phytoplankton) and loss (zooplankton) processes in the ecosystem and therefore gives an insight on the structure of the plankton ecosystem as a function of nutrient and transport. At rapid and intermediate flushing, transport or growth processes dominate and therefore bottom-up factors regulate the ecosystem. However, when the time-scale of transport is long and a significant population of grazers

is present in an inlet, trophic interactions become a dominant factor regulating phytoplankton biomass (*Alpine and Cloern*, 1992). The S^* vs. F^* framework predicts the threshold value for specific transport (F^*)—dependent on the nutrient source (S^*)—at which the change in ecosystem structure occur. Below this value, higher trophic levels are expected to have a more important role on the regulation of the ecosystem. This was suggested for Lunenburg Bay with the box model experiment that indicated an increasing sensitivity of phytoplankton biomass to grazing parameters at low flushing rate (tidal circulation).

Nutrient dynamics of shelf systems and reduced or accelerated flushing associated with meteorological conditions are therefore dominant factors controlling the biological dynamics of coastal inlets. The S^* vs. F^* framework is an effective, first order assessment tool that can be used to describe these dynamics given a limited set of data.

3.4.3 Limitations

Several limitations to the use of the S^* vs. F^* framework need to be noted. Boundary forcing associated with meteorological events is generally a dynamical process. For instance, wind-induced upwelling events are often a succession of particular conditions with specific effects on the ecosystem. The delivery of nitrate (onset phase) and the development of a phytoplankton bloom (relaxation phase) can be dissociated in time, but both are essential to the local accumulation of phytoplankton (e.g., *Edwards et al*., 1996; *Tilstone et al*., 2000). This temporal variability is absent of the framework, which represents steady state conditions.

Another limitation of the framework is that it assumes the coupling between nutrient input and flushing. This can represent both ocean and river dominated systems but only if the dominant source of flushing for the inlet represents the dominant source of nutrient. The framework therefore does not take into account internal sources of nutrient (sewage discharge, benthic regeneration). Similarly, the framework does not take into account benthic filter feeders or shellfish aquaculture which can influence or even control the magnitude of phytoplankton accumulation in an inlet (*Cloern*, 1982; *Cloern*, 1996). This is the case in Yaquina Bay (*Brown and Ozretich*, 2009) and in the Spanish rias (*Figueiras et al*., 2002). Hence, the effect of internal processes will need to be assessed in further

development of the S^* vs. F^* framework. This can be carried out as sensitivity studies of the framework to ecosystem structure (e.g. including benthic grazers), ecosystem parameter values and internal sources of nutrients. These sensitivity studies will provide further insights into the role of local processes in comparison to the offshore processes highlighted in this study.

3.5 Summary and Conclusions

Two factors were hypothesized to control the accumulation of phytoplankton biomass in Lunenburg Bay: the intensity of wind-induced flushing and the low nutrient concentration in source waters. The analysis has validated both hypotheses by demonstrating that both factors are essential to explain the dynamics observed in Lunenburg Bay. Under the dominant meteorological conditions in summer, they limit the variability of phytoplankton biomass inside the bay. Nutrient concentration on the Scotian Shelf appears to be a dominant factor controlling phytoplankton in Lunenburg Bay under the three meteorological regimes, in particular when the circulation is driven by southwestward winds (downwelling) and/or the semi-diurnal tide. Despite this limitation, enhanced biological dynamics (transport and production) were revealed under a circulation driven by northeastward winds (upwelling). Under these conditions, the accelerated flushing limits the accumulation of local production and therefore becomes a dominant factor controlling the biological system.

The S^* vs. F^* framework (scaled external nutrient concentration vs. flushing rate) has enabled the extension of these findings to other systems. This framework represents a conceptual model of plankton dynamics in coastal inlets. Several limitations to both the framework and the box model results have been discussed. The present work should therefore be extended to more realistic dynamic conditions, in particular during summer episodes of upwelling when the succession of onset and relaxation phases can have a significant effect on the development of local phytoplankton biomass. This aspect will be considered in the following chapter (Chapter 4). Future work should also evaluate the framework with data from various inlets with different shelf dynamics such as Nova Scotian and west coast inlets, for which flushing rates were not available.

Chapter 4

Investigating the Factors Controlling Phytoplankton Dynamics in a Coastal Embayment During Summer Upwelling Events

4.1 Introduction

The role of transport—and its interaction with source nutrients—in the regulation of phytoplankton biomass in Lunenburg Bay was explored in the previous chapter (Chapter 3). In this inlet, rapid transport during meteorological events and low nitrate concentration available on the Scotian Shelf, can explain the apparent discrepancy between the occurrence of upwelling events, and the rather small levels of phytoplankton biomass observed in summer. The dominant factors regulating phytoplankton variability are therefore identified for this system. However, the processes modulating their effect during an upwelling event remain unknown. This information is essential, first to comprehend the mechanisms underlying the observations made in 2006 in Lunenburg Bay (Chapter 2), and then to achieve a comprehensive understanding of the controls exerted on nearshore phytoplankton populations along the Atlantic coast of Nova Scotia in summer. The steady-state assumption for nutrient and phytoplankton boundary conditions, and the spatial and temporal averaging applied with the box modelling experiments did not allow for the investigation of these processes.

Several processes modulate the effect of transport during an upwelling event. The intensity and duration of upwelling pulses are associated with the synoptic wind forcing.

The inshore biological response to an upwelling event depends on both processes. A weak upwelling favours the development of a phytoplankton bloom inshore whereas a strong upwelling induces the rapid flushing of the system (*Álvarez-Salgado et al*., 1996b; *Piedracoba et al*., 2008a). The duration of an upwelling is important since short events limit productivity due to the low concentration of phytoplankton biomass in upwelled waters (*Brown and Field*, 1986). Both the intensity and the duration of an upwelling event determine the efficiency of an inlet to trap the upwelled nitrate (*Álvarez-Salgado et al*., 1996b; *Piedracoba et al*., 2008a) and to accumulate or export phytoplankton (*Álvarez-Salgado et al*., 1996b; *Tilstone et al*., 2000; *Crespo et al*., 2006). Bathymetry modulates the effect of transport locally.

The delivery of upwelled nitrate is modulated through transport and therefore depends on the intensity of the upwelling and its duration (e.g., sustained vs. storm-induced upwelling, Chapter 2). However, upwelled nitrate concentration also depends on the vertical distribution of nitrate on the Scotian Shelf (i.e., nitracline depth) which is a characteristic of the continental margin (i.e., shelf-dominated, *Jahnke*, 2010). A second factor modulating the delivery of upwelled nitrate to Lunenburg Bay is suggested hereafter. An inshore-offshore increase in the phytoplankton response to the Sustained 1 upwelling event—along a bathymetry gradient of increasing depth—was observed in the 2006 dataset (Figure 2.8). To explain this pattern, it is proposed that shallow depth in the inshore areas limits the delivery of upwelled nitrate to the inshore areas of Lunenburg Bay in comparison to the deep outer area. Shallow depth is not a limiting factor in eastern boundary inlets since surface nitrate concentration on the inner shelf is usually elevated (e.g., *Brown and Ozretich*, 2009). However, given the limited nitrate concentration in upwelling source waters, this factor may be important for Nova Scotian inlets.

The objective of this chapter is to examine how these processes modulate the effects of transport and nitrate concentration available to primary producers on the dynamics of phytoplankton biomass in Lunenburg Bay during an upwelling event. For transport, it is hypothesized that (1) the short duration of an upwelling event and (2) the rapid transport limit the development of phytoplankton biomass due to the short period of time for which nitrate is available to primary producers. For nitrate, it is hypothesized that during an upwelling event, (3) the low nitrate concentration in upwelling source waters and

(4) the inshore bathymetry patterns limit the development of phytoplankton biomass due to the low nitrate concentration available to primary producers.

The method we choose to evaluate these hypotheses is to develop a high resolution three dimensional hydrodynamic-biological coupled model of Lunenburg Bay and the inner Scotian Shelf that simulates the 2006 period of sustained upwelling events analyzed in Chapter 2. The fine resolution modelling framework was selected for several reasons. We discussed the limitations and the need to upscale the box model framework used in Chapter 3 in order to examine the processes modulating the effects of transport and nitrate during an upwelling event. In a recent numerical study, *Zhai et al*. (2008b) demonstrated the importance of baroclinic dynamics and realistic bottom topography to resolve the circulation in Lunenburg Bay and the surrounding nearshore areas. In general, high resolution 3D model are recommended to investigate processes finely resolved spatially (*Ménesguen et al*., 2007). This type of model better represents the spatial structures and is able to simulate the inshore-offshore continuum. These characteristics are necessary to investigate the bathymetry hypothesis. Including the inner Scotian Shelf in the modelling framework is also necessary to model the development of coastal upwelling events on the Scotian Shelf and the resulting biophysical coupling between Lunenburg Bay and the inner Scotian Shelf. This extension of the spatial domain enables the comparison of the phytoplankton response to upwelling in Lunenburg Bay and the neighbouring areas.

4.2 Methods

4.2.1 Study Site

This work is mainly carried out in Lunenburg Bay. However, the modelling framework also includes the inner Scotian Shelf and the neighbouring inlets Rose Bay, Mahone Bay and Saint Margarets Bay (Figure 4.1). Lunenburg Bay is connected to Rose Bay on its southeastern side and to Mahone Bay on its shallow northeastern side (connected further north to Saint Margarets Bay). The MEPS-Bay coastal observatory (*Cullen et al*., 2008) was located in Lunenburg Bay between 2002 and 2007. The data used in this study have been collected at the observatory, except for the sea surface temperature (SST) on the

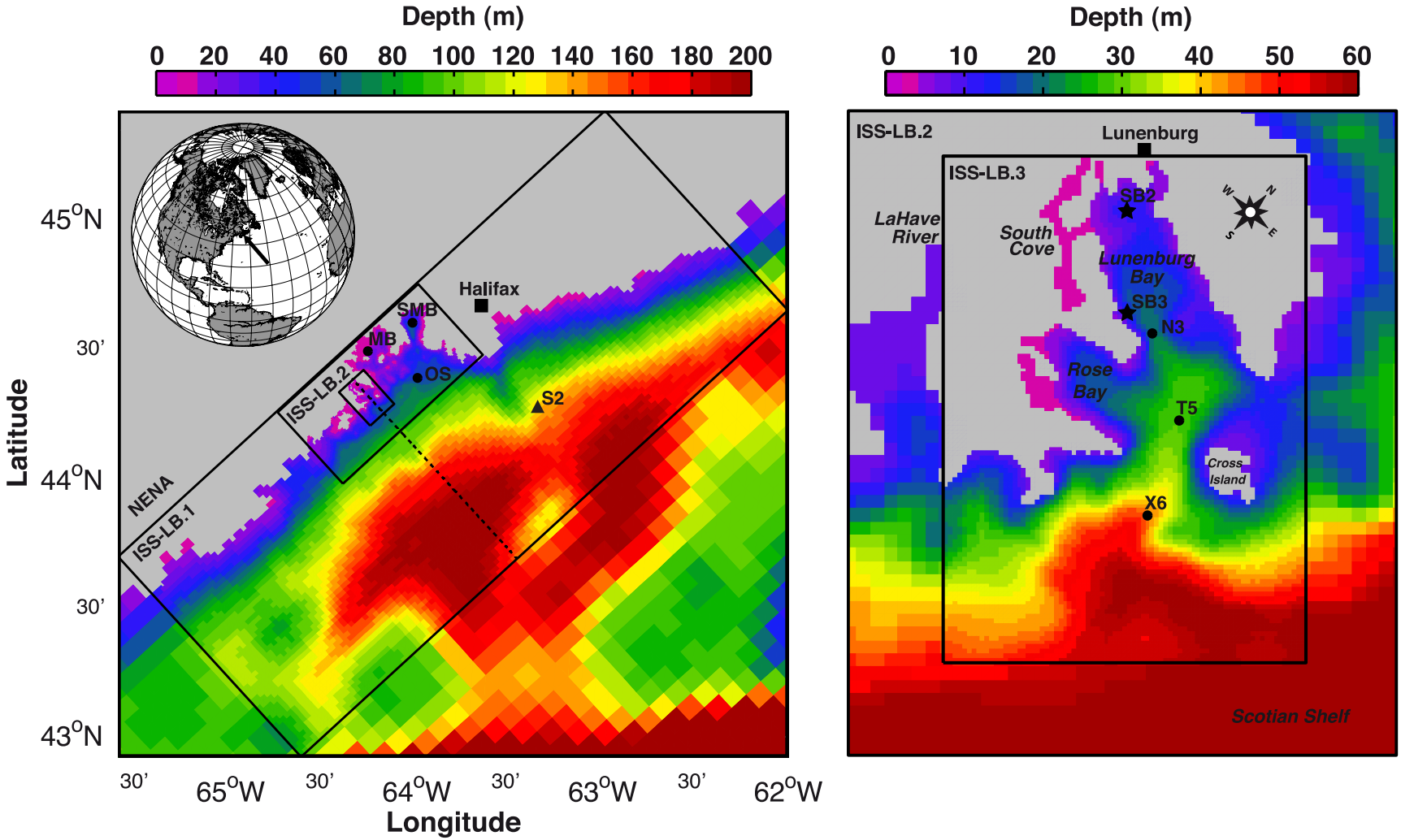

Figure 4.1: Map of the study site and model grids. Left panel: Bathymetry and boundaries of the three nested grids. The bathymetry from the NENA grid is plotted outside the model domains. Also plotted: the location of station 2 (S2, ▲), the three extra locations used in the analysis (●) and the location of the cross-shore transect (---). Right panel: Bathymetry of the high resolution model grid, including Lunenburg Bay, Rose Bay and the locations of the MEPS-Bay moorings (★) and extra stations sampled in 2006 (●).

Scotian Shelf which was collected from satellite imagery (MODIS). The methodology and the dataset are described in Chapter 2.

4.2.2 Model Description

The upwelling simulation is carried out with the Regional Ocean Modelling System (ROMS, http://www.myroms.org). ROMS is a free-surface primitive equations ocean model with Boussinesq and hydrostatic approximations. The terrain following (or sigma) vertical coordinates system stretches according to the bathymetry and the free surface, which allows for a continuous representation of the bathymetry and a variable vertical resolution, including a higher resolution in the euphotic and bottom layers. A detailed description of the model can be found in *Shchepetkin and McWilliams* (1998, 2003, 2005) and in *Haidvogel et al*. (2008). The model is implemented for the inner Scotian Shelf area (ISS), including Saint Margarets Bay, Mahone Bay, Rose Bay and Lunenburg Bay with a series of nested grids with increasing resolution.

4.2.2.1 Spatial Discretization and Nesting Procedure

The model is set up with four nested computational domains (grid name and horizontal grid resolution provided in parenthesis): the Northeast North American shelf domain (NENA, 8 km), which is used to provide initial and boundary conditions, and the three ISS-LB domains (Figure 4.1) including a large coarse resolution domain of the inner Scotian Shelf (ISS-LB.1, 2 km), the outer Lunenburg Bay domain (ISS-LB.2, 500 m) and a high resolution domain representing Lunenburg Bay, Rose Bay and the deep area connecting the two inlets (ISS-LB.3, 170 m). The grids are constructed with the SeaGrid Orthogonal Grid Maker For Matlab (http://woodshole.er.usgs.gov/operations/modeling/seagrid). The bathymetry data used for the ISS-LB domains are interpolated from local data generated by D. Mercer and J. Sheng and from the NENA grid bathymetry data. A maximum slope parameter $r = 0.2$ is used for bathymetry smoothing in order to limit pressure gradient errors (*Beckmann and Haidvogel*, 1993). The number of vertical layers are N = 30 in the two outer model grids and N = 20 in the high resolution ISS-LB.3 grid. The vertical grid resolution is determined using stretch parameters (*Song and Haidvogel*, 1994), which are the same for all ISS-LB domains, such that $\theta_s = 5$ (surface stretching

parameter), $\theta_b = 0.4$ (bottom stretching parameter) and $T_{cline} = 50$ m (width of stretching layer).

Each grid provides boundary conditions to its child grid (next finest) through a one-way offline nesting procedure. The output from the NENA model (*Fennel et al.*, 2008) is used to provide open boundary conditions for ISS-LB.1 including physical and biological tracers, momentum and sea surface elevation. Physical and biological boundary conditions for the two small grids (ISS-LB.2 and ISS-LB.3) are computed from the results of their parent grid (next largest). The frequency of the time series used for boundary conditions of the ISS-LB grids is 1 h^{-1} for all variables except for the biological variables in ISS-LB.1 where the frequency is 1 d^{-1}. The nesting procedure and the post processing of the model results are carried out using ROMSTOOLS (*Penven et al.*, 2008) and the ROMS Numerical Toolbox for Matlab (RNT, http://www.o3d.org/RNT/). For each ISS-LB grid, boundary sea-surface elevation and barotropic velocity are prescribed using respectively *Chapman* (1985) and *Flather* (1976) radiation conditions at the boundaries to allow for the radiation of tides and gravity waves. Baroclinic velocity and tracers radiation are prescribed at the boundaries using a Dirichlet radiation condition (clamped), which performed best after testing the several techniques available for radiation condition in ROMS.

4.2.2.2 Circulation Model

The circulation model uses the default advection schemes: a third-order upstream-biased (*Shchepetkin and McWilliams*, 1998) and a fourth-order centered for the horizontal and vertical advection of momentum respectively. A third-order upstream advection scheme is used for turbulent kinetic energy fields (*Shchepetkin and McWilliams*, 2005). As in NENA, the advection of tracers is formulated with the recursive MPDATA 3D advection scheme (*Smolarkiewicz and Margolin*, 1998), which reduces inaccuracies in the advection of biological tracers. In addition, the model uses the parabolic splines density Jacobian pressure gradient algorithm (*Shchepetkin and McWilliams*, 2003).

Vertical mixing is set using the Mellor-Yamada level 2.5 closure scheme (*Mellor and Yamada*, 1982; *Galperin et al.*, 1988) with the Kantha and Clayson stability function (*Kantha and Clayson*, 1994). The velocity dependent Smagorinsky scheme (*Smagorinsky*,

1963) is used to parametrize horizontal subgrid processes for momentum. Finally, the bottom stress is approximated with a quadratic bottom friction formulation and a stress coefficient set to $3 \cdot 10^{-3}$ (see *Haidvogel and Beckmann*, 1999).

4.2.2.3 Biogeochemical Model

The circulation model is coupled to the biogeochemical model developed by *Fennel et al.* (2006). The model is a modification of the commonly used Fasham model (*Fasham et al.*, 1990). The model divides the pelagic nitrogen cycle into seven compartments (Figure 4.2) representing phytoplankton, chlorophyll (CHL) that acclimates to light and nutrient conditions (*Geider et al.*, 1996, 1997), zooplankton, dissolved inorganic nitrogen (DIN)—split into nitrate (NO3) and ammonium (NH4) to represent respectively 'new' and 'regenerated' production (*Dugdale and Goering*, 1967; *Eppley and Peterson*, 1979)—as well as a small detritus pool (particles size < 10 μm) that receives losses from phytoplankton and zooplankton and a large detritus pool that represents aggregates of phytoplankton and small detritus. The aggregation rate is related to the square of particle abundance to account for increase particle encounter at high abundance. The nitrification rate is light dependent and inhibited at high light intensity. A description of the model formulations is presented in Appendix D with the value of each parameter used during the simulation.

The model was developed for the study of biogeochemistry of coastal systems and therefore includes a sediment component with a denitrification pathway. The sediment is modelled as a bottom boundary condition where deposited organic matter (phytoplankton and detritus) undergo instant mineralization through both aerobic and anaerobic pathways, assuming that a constant fraction of organic matter is mineralized through denitrification (lost from the nutrient pool). The remaining fraction is returned to the overlying water column as ammonia. The formulation of sediment processes is given in Appendix D.

The model parameters for ecosystem processes are the same for the four domains. More details on the model and the rationale for the choice of formulations are available in *Fennel et al.* (2006). The analysis of the simulation focuses on the nitrate and phytoplankton components of the ecosystem.

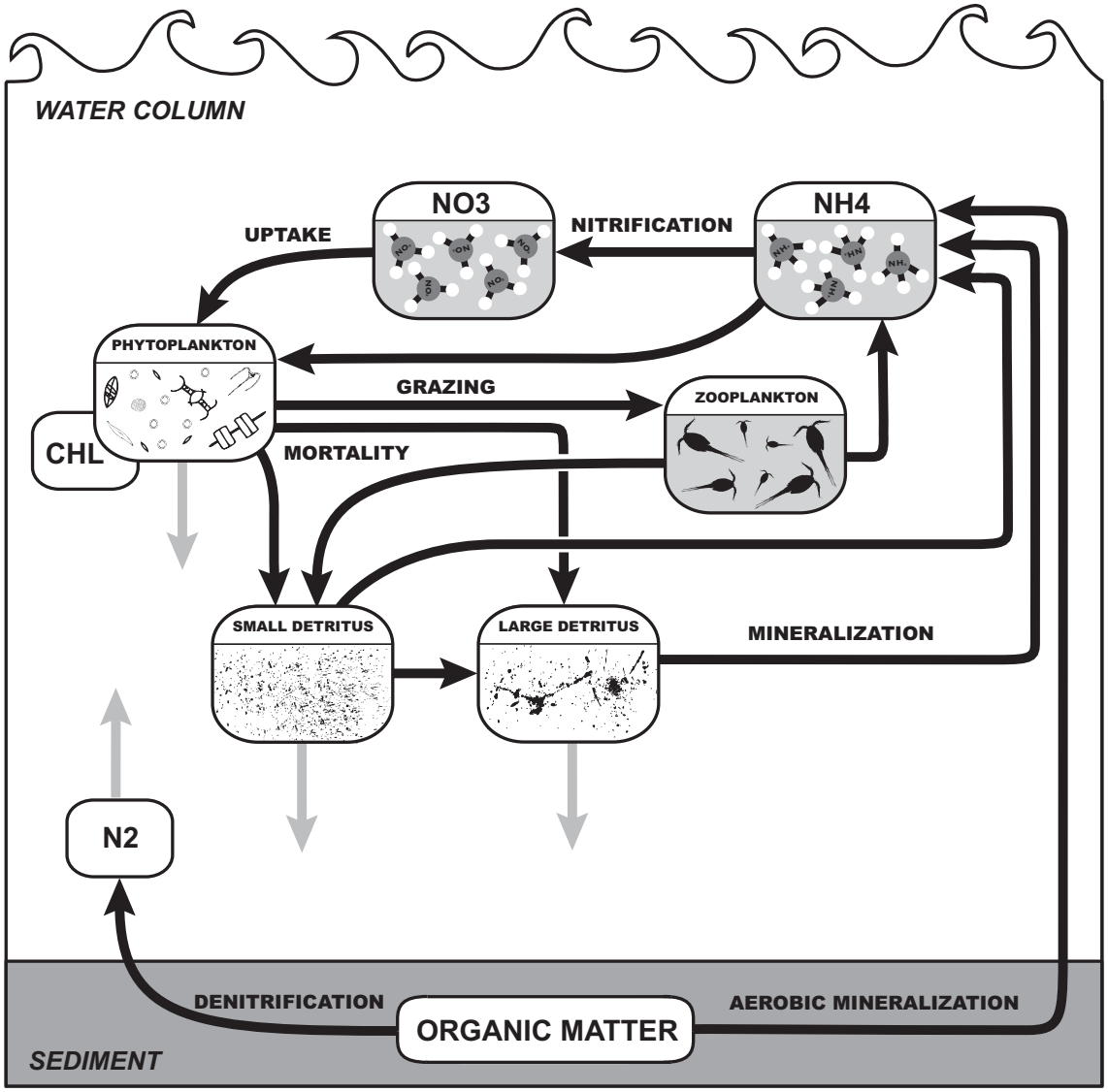

Figure 4.2: Schematic of the ecosystem model (redrawn from *Fennel et al*., 2006). Dark arrows indicate ecosystem processes and downward grey arrows the sinking of tracers. The upward grey arrow indicates the loss of molecular nitrogen (N2)—the end-product of denitrification—from the nutrient pool. The sediment layer represents an instant mineralization or denitrification of sedimenting particulate organic matter into the water column.

4.2.2.4 Initialization and Boundary Conditions

Boundary and initial conditions for physical tracers, momentum and sea surface height in the larger ISS-LB.1 domain are set from the output of the NENA model. Biological tracers are set up similarly, except for nitrate which is not initialized from NENA but prescribed using a nitrate-density relationship constructed with nitrate and density data collected on the Scotian Shelf along the Halifax Line (1999-2005, see *Petrie*, 2004), such that:

$$\widehat{NO_3^-} = \begin{cases} 8.444\,\rho - 8658.498 & \text{if } \rho > 1025.5 \\ 0.316 & \text{otherwise,} \end{cases} \tag{4.1}$$

where ρ (kg m^{-3}) is the water density and $\widehat{NO_3^-}$ (mmol m^{-3}) the nitrate estimated from density (Figure 4.3D). Data with values greater than 3 standard deviations from the regression estimate were considered outliers and excluded from each relationship. The modification of the nitrate field is imposed to represent accurately the vertical distribution of nitrate along the coast, which is essential to this study. It also enables to vary the nitracline depth on the Scotian Shelf (see sensitivity analysis, Section 4.2.3.2). The model is run for a month prior to the simulation to spin up the biological variables.

4.2.2.5 Atmospheric Forcing

Surface forcing is imposed on the circulation model for each domain using the NCEP reanalysis dataset (*Kalnay et al.*, 1996), which is also used for NENA. The dataset includes mean daily wind speed, short-wave and long-wave radiation, air temperature, air pressure, air relative humidity, rainfall, as well as sensible, latent and net heat flux. The dataset is interpolated from the NENA domain to each ISS-LB grid. The time series of wind stress used for the simulation is given in Figure 4.4 (mid ISS-LB.1 grid). The model configuration allows for net sea surface heat and freshwater flux corrections in ISS-LB.2 and ISS-LB.3 domains based on sea surface temperature and salinity observations at the mid-bay station SB3 (see time series in Figure 2.3B,C).

The NCEP wind forcing time series can be divided into five periods (Figure 4.4). (1) A period of moderate wind at the beginning of the simulation (day 175–178). (2) A period of strong northeastward winds (day 179–186) that corresponds to sustain 1 event in

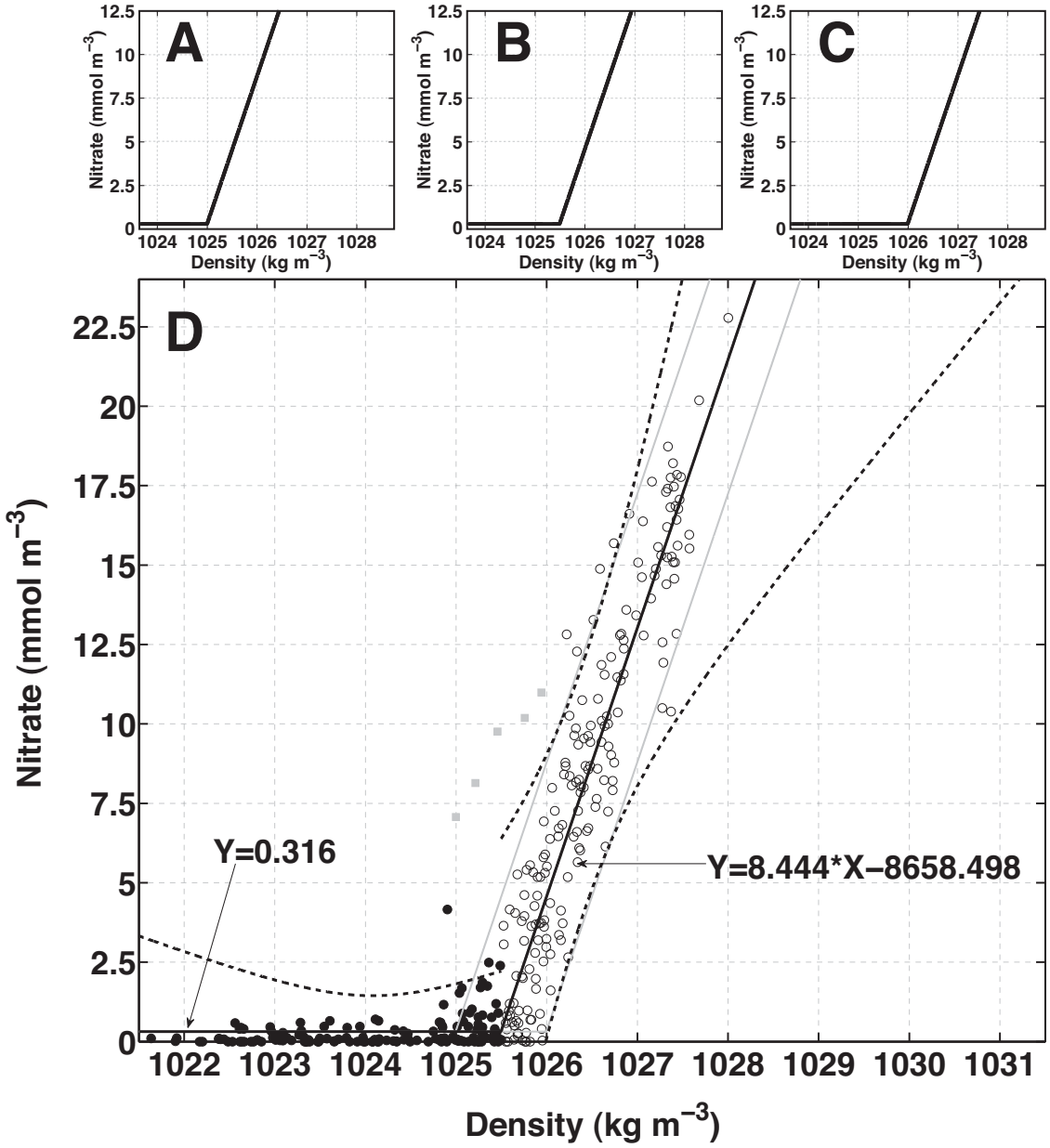

Figure 4.3: Nitrate vs. density relationship. A-C Relationships used for the simulation runs S^+, S^0 and S^- respectively (see Section 4.2.3.2). D. Main relationship (Black line, same as panel B) derived from CTD profiles and water samples collected on the Scotian Shelf along the Halifax Line in June and July for the period 1999–2005. The cut-off value between the two lines is 1025.5 kg m^{-3}. Below that, no relationship is found and the mean value 0.316 mmol m^{-3} is used. Above it, the relationship is represented by a linear fit to the data (open circles). Dashed lines represent the upper and lower 95% prediction limits for both curves. Filled circles indicate data below the cut-off density whereas open circles are above. Grey squares are outliers discarded for the computation (> ±3 SD). The grey lines represent the relationships used in the sensitivity model runs S^+ and S^- (same as panel A & C) with a cut-off density of ±0.5 kg m^{-3} relative to the original fit.

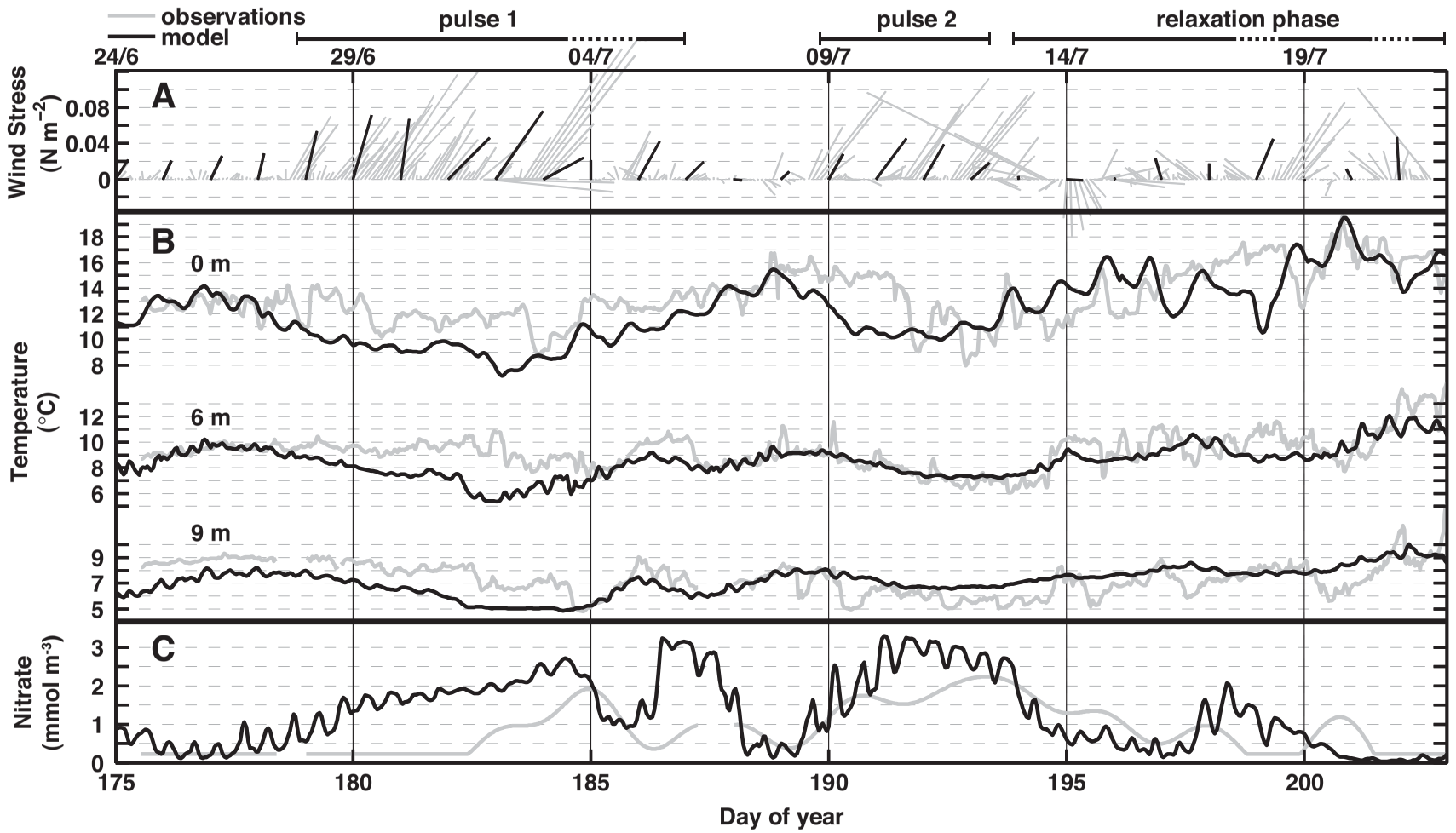

Figure 4.4: Observed (grey) and modelled (black) atmospheric and water column conditions during the simulation in Lunenburg Bay. A. Bi-hourly wind stress recorded at the onshore meteorological station Battery Point (near B7) and daily wind stress from NCEP. B. Observed and modelled temperature time series at the SB3 mooring location at 0, 6 and 9 meters. C. Bottom nitrate time series at the SB3 mooring location from the model (black) and from a proxy constructed from observed density (grey, see Chapter 2). Pulse 1, pulse 2 and the relaxation phase following pulse 2 are indicated at the top of the figure.

Chapter 2, extended to include the period of increased wind intensity on day 186. This is referred to as pulse 1; this period includes a day of moderate wind on day 185. (3) A period of low wind (day 187–189), which corresponds to the relaxation of sustain 1 event in Chapter 2 (shorter in the simulation). (4) A period of moderate to strong northeastward winds (day 190–193) that corresponds to sustain 2 event in Chapter 2 and is referred to as pulse 2. (5) A period of low winds (day 194–203) at the end of the simulation, referred to as the relaxation phase. This period is interrupted by strong wind conditions on days 199 and 202. The analysis is focused on the main periods of upwelling: pulse 1, pulse 2 and the relaxation phase after the two sustained upwelling events.

4.2.3 Simulation

4.2.3.1 Standard Run

The model simulates the whole time-period of sustained upwelling events that occurred in early summer 2006 (see Chapter 2). The simulation is carried out for the duration of the events from June 24 to July 22, which includes the two periods of sustained upwelling as well as the pre- and post-upwelling time periods. The model is forced by daily mean atmospheric variables and therefore is not designed to hindcast rigorously the high-frequency variability in hydrographic conditions observed at the MEPS-Bay coastal observatory during the time period of the simulation.

The analysis of the simulation results focuses particularly on the ISS-LB.3 domain to assess the biological response to the upwelling in Lunenburg Bay. Particular locations have been selected for the analysis (Figure 4.1). The mooring stations SB2 (inshore) and SB3 (mid-bay) enable the comparison of model results with time series from the observing system. SB2 is also used as the inshore location of a transect line across the Lunenburg Bay-Rose Bay domain (see Chapter 2), which also includes the stations N3 (mid-bay), T5 (deep-end side) and X6 (outside). The Lunenburg Bay-Rose Bay domain is referred to as Lunenburg Bay hereafter. Three other stations from the ISS-LB.2 model domain are used: MB (shallow) that represents Mahone Bay, SMB (deep) that represents Saint Margarets Bay and OS that represents the deep outer part of this coastal area (Figure 4.1). Several zones and boundaries have also been defined inside Lunenburg Bay (ISS-LB.3 domain) to

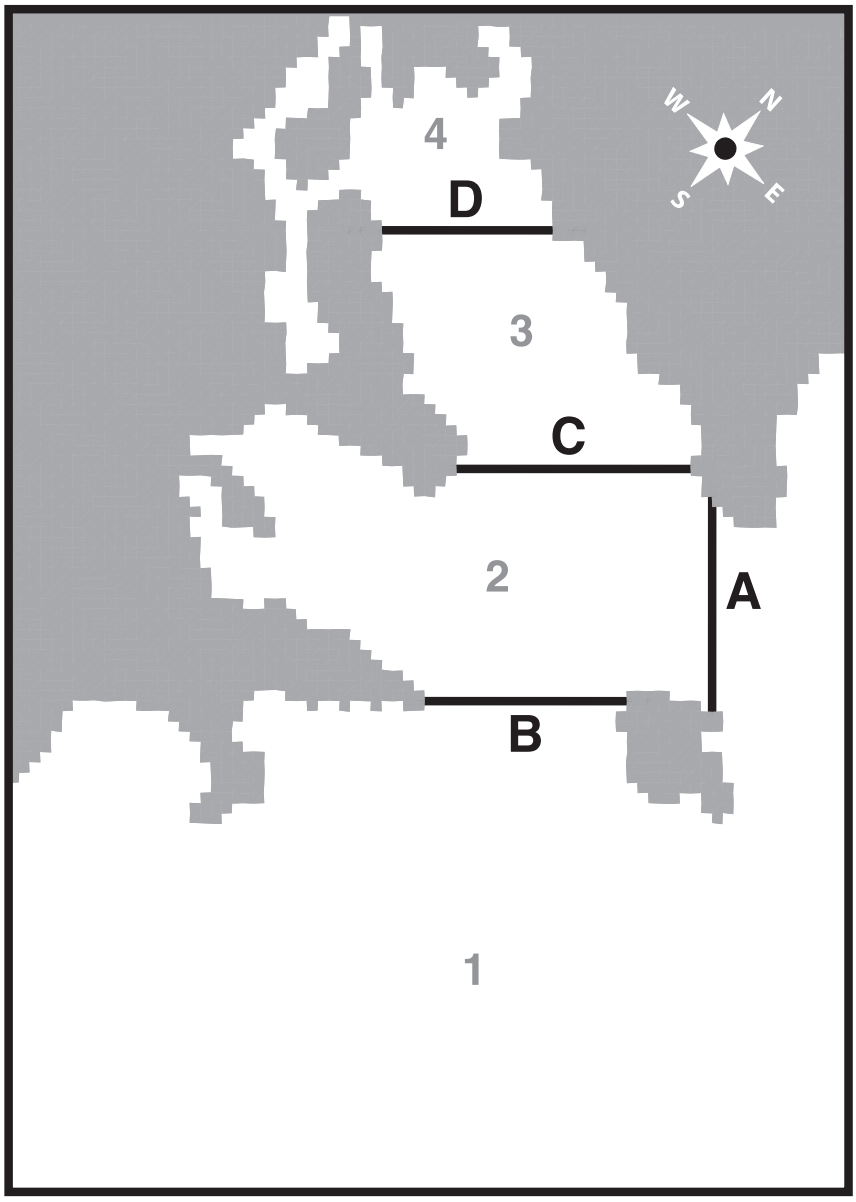

Figure 4.5: Map of the ISS-LB.3 grid showing the areas (1–4) and boundary lines (A, B, C and D) used during the analysis to calculate transport and spatial averages of nutrient and phytoplankton. Each boundary line corresponds to the interface between two areas.

study the biological transport and to compute spatial averages (Figure 4.5). Zones 1, 2, 3 and 4 represent respectively the areas characteristic of the outside, the deep-end side, the mid-bay, and the inshore of the Lunenburg Bay. The boundaries A, B, C and D represent the limits between these areas (Figure 4.5).

4.2.3.2 Sensitivity Runs

Two additional model runs (S^+ and S^-) are carried out to investigate the role of nitracline depth (i.e., depth at which there is a sharp vertical gradient in nitrate concentration) on the Scotian Shelf on the biological response to the upwelling. The two runs are carried out with the same physical and biogeochemical settings as the standard run (S^0), except for the nitrate field. In the standard run, the nitrate initial and boundary conditions are prescribed from density using the standard nitrate-density relationship (Figure 4.3B). In the first sensitivity run (S^+) a shallower nitracline is simulated by lowering the cut-off value of the nutrient-density relationship to 1025 kg m^{-3} (Figure 4.3A). Below and above this value, the same relationships as in the standard run are used (see Eq. 4.1). In the second sensitivity run (S^-) a deeper nitracline is simulated by increasing the cut-off value of the nutrient-density relationship to 1026 kg m^{-3} (Figure 4.3C). Sensitivity results are presented as anomalies (%) from the control run such that the sensitivity of a variable X is $sens(X^+) = (X^+ - X^0)/X^0 \times 100$ and $sens(X^-) = (X^- - X^0)/X^0 \times 100$ for S^+ and S^- respectively.

4.2.4 Post-Processing and Analysis

4.2.4.1 Upwelling Response

A relative phytoplankton biomass response to the upwelling event (upwelling response) is calculated at the various locations of the model grid ISS-LB.2 (MB, SMB and OS, see Figure 4.1) and ISS-LB.3 (SB2, N3, T5 and X6), and also over the whole grid domains. With the exception of OS on the inner shelf, all the stations are located inshore. In Lunenburg Bay, the stations are characterized by their position along the inshore-offshore axis, which represents a change in bathymetry, whereas Mahone Bay and SMB stations represent two other systems, but with distinct bathymetry (shallow for Mahone Bay and

deep for Saint Margarets Bay). The upwelling response is the ratio between the average phytoplankton biomass per unit area (mmolN m^{-2}) at a specific location during the relaxation phase (days 194–203) and the pre-upwelling time period (days 175–178). Similarly, the effect of pulse 1 on the phytoplankton biomass (mmolN m^{-2}) is the ratio between the phytoplankton biomass at the peak of pulse 1 (day 183) and the average pre-events phytoplankton biomass. A low value (< 1) represents a decrease in phytoplankton biomass associated with the event (negative effect).

4.2.4.2 Transport Across Boundary Lines

The model velocity and transport time series are presented as subtidal data series with the dominant tidal component of the signal removed. The subtidal series are computed using a low-pass filter with a cut-off frequency at 0.5 d^{-1}.

The transport of nitrate (TNO3; mmol s^{-1}), DIN (TDIN; mmol s^{-1}) and phytoplankton (TP; mmolN s^{-1}) across boundary lines A, B, C and D (see Figure 4.5) is calculated as follow:

$$\mathrm{TNO3}(t) = \sum_{j=1}^{m} \sum_{k=1}^{n} \frac{u(j,k,t) \cdot NO3(j,k,t)}{\mathrm{A}(j,k)}, \tag{4.2}$$

$$\mathrm{TDIN}(t) = \sum_{j=1}^{m} \sum_{k=1}^{n} \frac{u(j,k,t) \cdot (NH4(j,k,t) + NO3(j,k,t))}{\mathrm{A}(j,k)}, \tag{4.3}$$

$$\mathrm{TP}(t) = \sum_{j=1}^{m} \sum_{k=1}^{n} \frac{u(j,k,t) \cdot Phy(j,k,t)}{\mathrm{A}(j,k)}, \tag{4.4}$$

where $NO3$ (mmol m^{-3}) is the nitrate concentration, $NH4$ (mmol m^{-3}) is the ammonium concentration, Phy (mmolN m^{-3}) is the phytoplankton biomass, u (m s^{-1}) is horizontal advection in the i-direction and A (m^2) is the vertical area of a grid cell. j corresponds to the j-direction index (horizontal) and k to the z-direction index (vertical) on the model grid. m and n are the total number of grid cell in each direction. The transport across boundary C is further divided into transport in ($TNO3_{in}$, TP_{in}) and out ($TNO3_{out}$, TP_{out}) of the mid-bay area. It represents the total transports into and from areas 3 and 4 (see Figure 4.5).

4.2.4.3 Nitrate Trapping

Nitrate transport across areas 3 and 4 ($TNO3_{in}$, $TNO3_{out}$) is used to estimate the efficiency of Lunenburg Bay as a trap for nitrate ($E_{NO_3^-}$; %) for the whole upwelling simulation using the following relationship:

$$E_{NO_3^-} = \frac{\sum_{t=1}^{n} \left(TNO3_{in}(t) - TNO3_{out}(t) \right)}{\sum_{t=1}^{n} TNO3_{in}(t)} \times 100, \tag{4.5}$$

where t is the time and n the length of the simulation.

4.2.4.4 Production-Transport Contributions

The contributions of production and transport to the phytoplankton biomass and DIN dynamics are computed for the area inside the mid-bay and the inner-bay (area 3 and 4, Figure 4.5) and for the whole bay (areas 2, 3 and 4) in order to examine which of production (primary production or DIN regeneration) or transport dominates the dynamics of phytoplankton and DIN during the simulation. Total daily primary production (PP; mmolN s^{-1}) is calculated for each area such that:

$$PP(t) = \sum_{i=1}^{l} \sum_{j=1}^{m} \sum_{k=1}^{n} \frac{\mu(i, j, k, t) \cdot Phy(i, j, k, t)}{V(i, j, k)}, \tag{4.6}$$

where μ is the temperature, light and nutrient limited phytoplankton growth rate (d^{-1}) and V (m^3) is the volume of a grid cell. i corresponds to the i-direction index, j to the j-direction index and k to the z-direction index on the model grid. l, m and n are the total number of grid cell in each direction.

Similarly, the production of DIN (PDIN; mmol s^{-1}) is the addition of the rate of ammonia production in the water column ($PDIN_{wc}$; mmol s^{-1}) and in the sediment ($PDIN_{sed}$;

mmol s^{-1}), such that:

$$\mathrm{PDIN}_{wc} = l_{BM}Zoo + l_E\frac{Phy^2}{k_P + Phy^2}\beta Zoo^2 + r_{SD}SDet + r_{LD}LDet \tag{4.7}$$

$$\mathrm{PDIN}_{sed} = \frac{4}{16\Delta z}\left(w_{Phy}\,Phy|_{z=H} + w_{SDet}SDet|_{z=H} + w_{LDet}LDet|_{z=H}\right) \tag{4.8}$$

The model equations, variables and parameters names are detailed in Appendix D and in Eq. D.5 and D.16.

The contribution of primary production to phytoplankton dynamics is calculated as PP/(PP+TP), whereas the contribution of transport is TP/(PP+TP). Similarly, the contribution of local regeneration to DIN dynamics is calculated as PDIN/(PDIN+TDIN), whereas the contribution of transport is TDIN/(PDIN+TDIN). When the contribution of primary production (regeneration) is greater than 0.5, primary production (regeneration) is larger than transport, whereas for values less than 0.5, phytoplankton (DIN) transport dominates primary production (regeneration).

4.3 Results

4.3.1 Simulated Hydrography

4.3.1.1 Inner Shelf

Sea surface temperatures (Figure 4.6) and a cross-shelf transect across the three model domains (Figure 4.7A) illustrate the hydrographic response to the upwelling simulated by the circulation model. The model simulates coastal bands of cold surface water nearshore on day 184 (July 3) during pulse 1 (Figure 4.6D,G) and on day 193 (July 12) at the end of pulse 2 when upwelling conditions starts to relax (Figure 4.6E,H). During the two upwelling events (pulse 1 and 2), the model simulates a northeastward surface alongshore flow near the coast (Figure 4.6D,G). This alongshore geostrophic current is characteristic of coastal upwelling events (e.g., *Allen*, 1980) and results from the onshore pressure gradient associated with the tilting of the isopycnals (see Appendix A). A week after the end

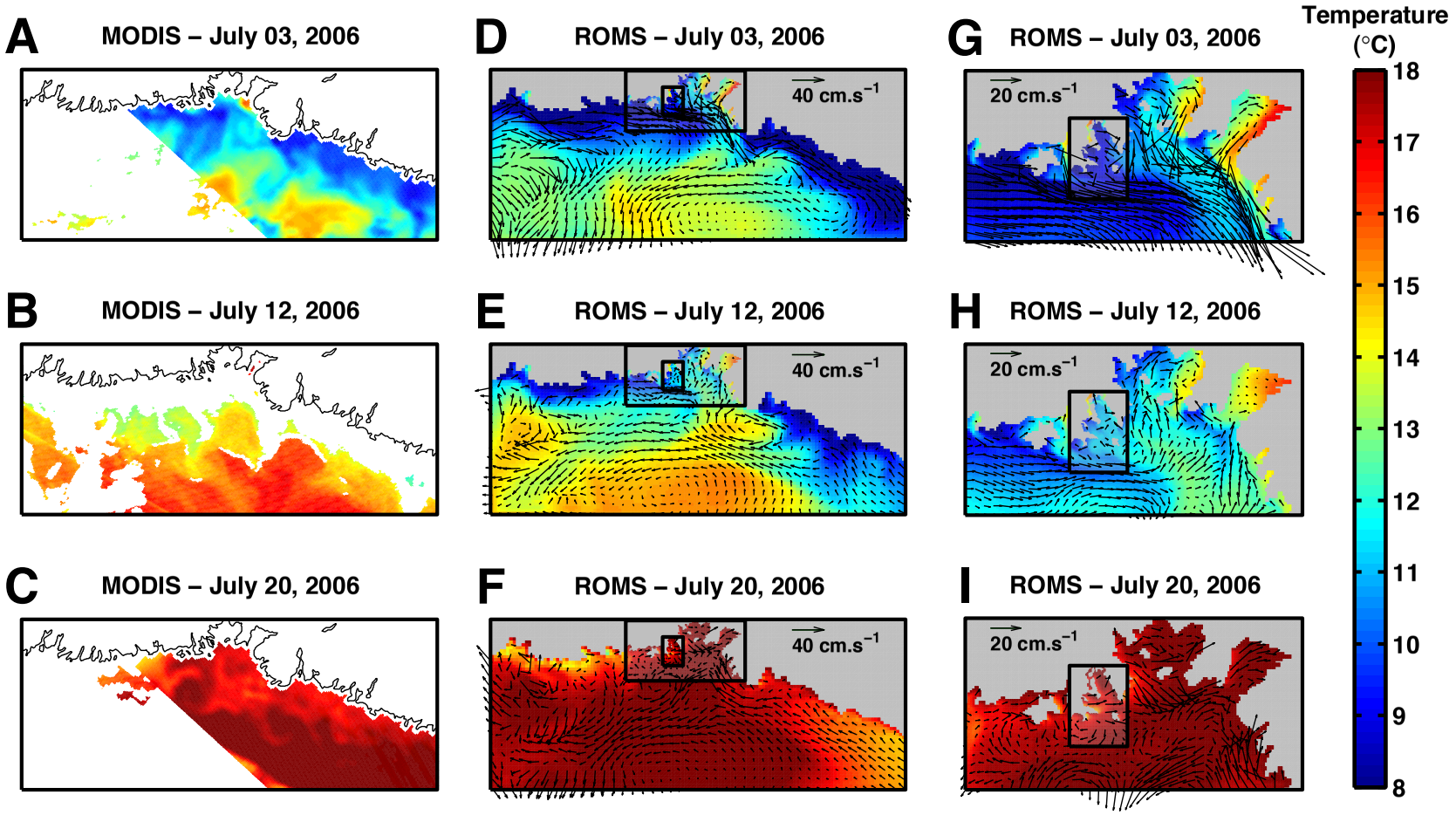

Figure 4.6: Observed (A-C) and modelled (D-I) sea surface temperature (color) and surface velocities (arrows, model only) on the inner Scotian Shelf during pulse 1 (upper panels), at the end of pulse 2 (middle panels) and after the upwelling event (bottom panels). Mid panels (vertical) show the entire model grid domains whereas the right panels show only ISS-LB.2 & 3. The black boxes represent the limit of each nested grid. The arrows are scaled relative to the surface current speed. The scale varies between the entire model grid domains (D-F, 40 cm s^{-1}) and the inner grid domains (G-I, 20 cm s^{-1}).

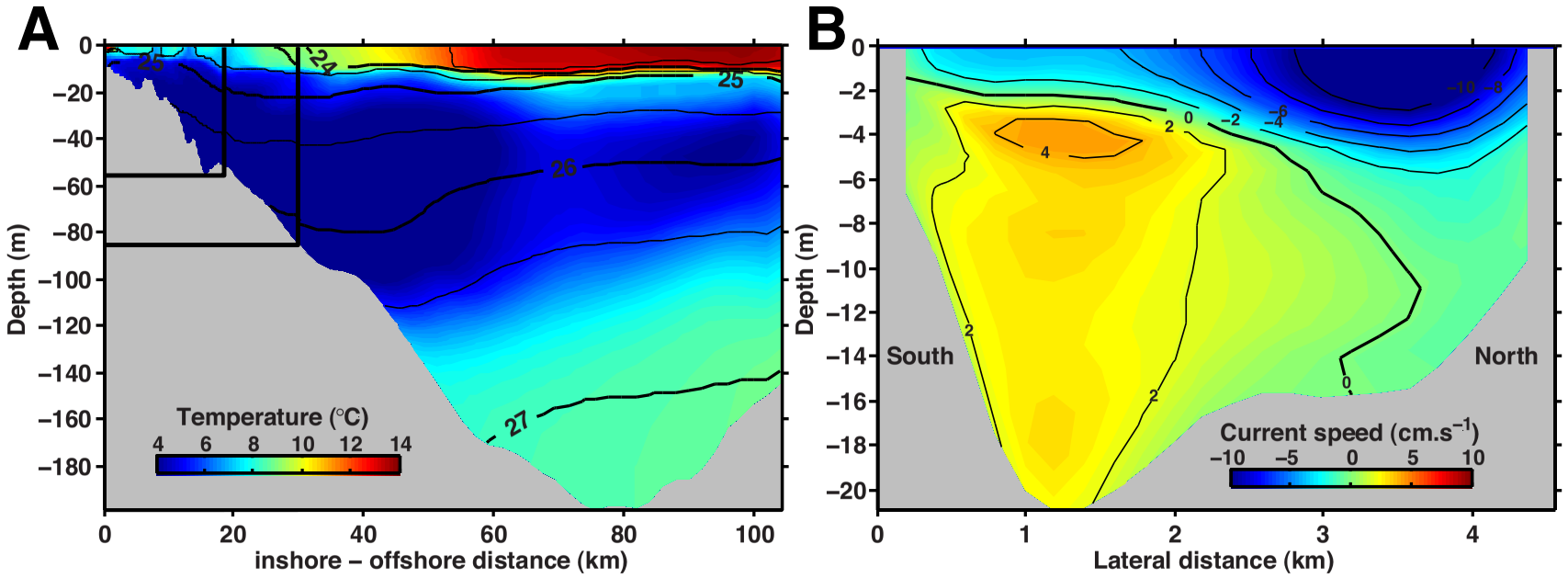

Figure 4.7: Modelled hydrography of Lunenburg Bay and the Scotian Shelf on July 2, 2006 (day 183) at the peak of pulse 1. A. Cross-shore transect of temperature (color) and density (sigma-*t*; kg m^{-3}, contour lines) through the three nested grids. The location of the transect is indicated in Figure 4.1. The black boxes represent the limit of each nested grid. B. Subtidal velocity field through a cross section in the mid-bay area of Lunenburg Bay (boundary C, Figure 4.5). The figure corresponds to a view into Lunenburg Bay, with positive current values representing velocities into the bay.

of pulse 2 on day 201 (July 20), the model simulates warm surface water throughout the three model domains. The coastal bands of cold water have disappeared, indicating the relaxation of upwelling conditions (Figure 4.6F,I).

Limited observations are available on the inner Scotian Shelf during the simulation. Nevertheless, sea surface temperature observations are available on the three dates discussed above (Figure 4.6A–C). The comparison between observed and simulated sea surface temperatures shows three general patterns: (1) the large scale temperature patterns in the model agree qualitatively with the features observed on the satellite images; the observed and simulated location of the bands of cold surface water during pulse 1 and 2 is similar, (2) the simulated spatial patterns are smoother than the observation; the model tends to smooth out the high spatial variability associated with the upwelling event, and (3) surface temperatures are underestimated by the model in comparison to the observations.

The cross-shelf transect across the model domains at the peak of pulse 1 (day 183) indicates a 10 m shoaling of shallow subsurface isopycnals about 20 km offshore of Lunenburg Bay (Figure 4.7A). At this location, the pycnocline reaches the surface, which induces the 20 km-wide coastal band of cold surface water revealed in the simulated sea surface temperatures (Figure 4.6 D,G). Within this area, subsurface isopycnals propagate shoreward, including inside Lunenburg Bay. At station X6, located outside Lunenburg Bay (ISS-LB.3 model grid), the vertical movement of the isopycnals results from the development of an upward flow during each upwelling pulse (i.e., vertical velocities w, Figure 4.8A). In contrast, during the relaxation following pulse 2, the model simulates a downward flux of water that results in the deepening of subsurface isopycnals (Figure 4.8 and Figure 4.9). Simulated vertical velocities are highest at this station at the peak of pulse 1 (day 183) and during the relaxation following pulse 2 (w of ±4–6 m d^{-1}).

4.3.1.2 Lunenburg Bay

The model simulates the development of the upwelling at the entrance of Lunenburg Bay as a characteristic subtidal circulation: a deep flow entering the bay coupled with a surface outflow (Figure 4.7B). The topography at the entrance of the bay and the surface pressure gradient across the bay due to the local wind forcing result in a subsurface inflow along

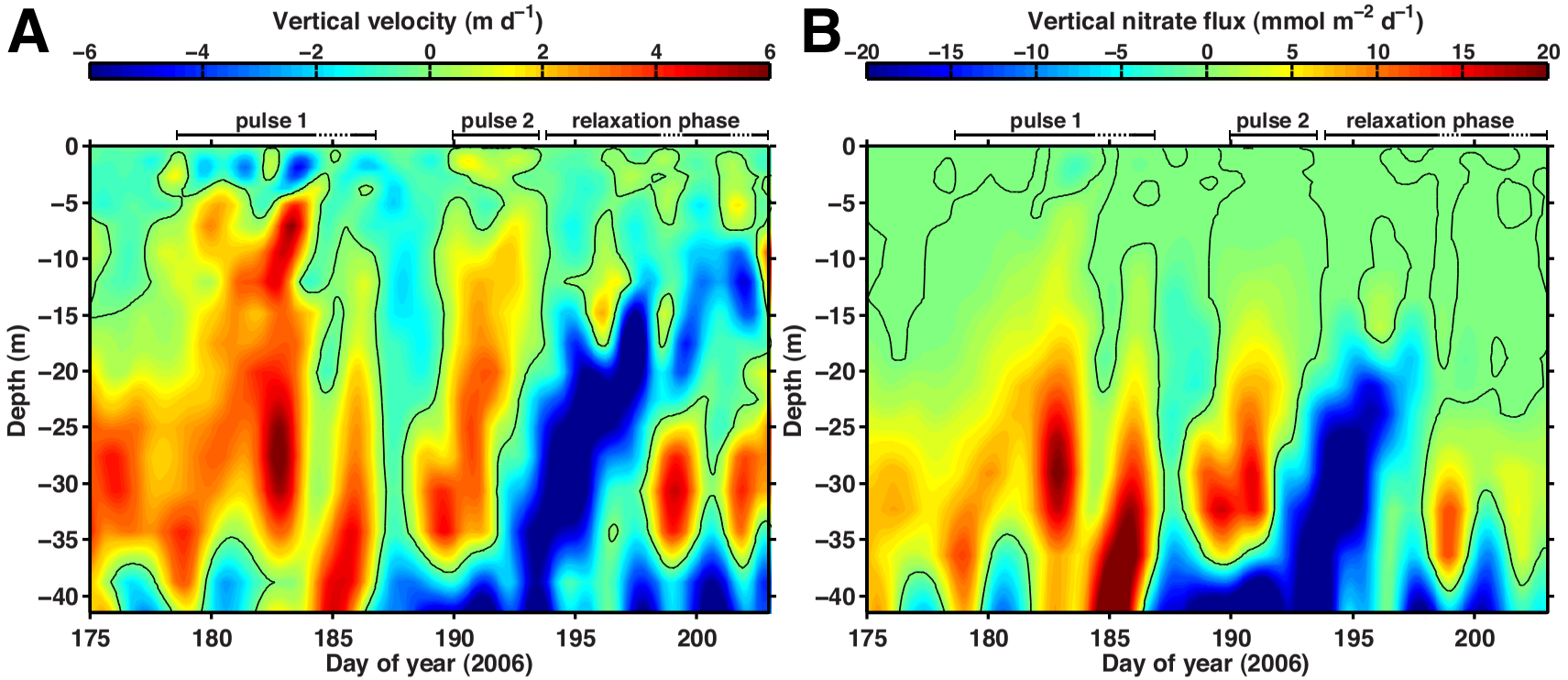

Figure 4.8: Vertically resolved time series of A. subtidal vertical velocity (w; m d^{-1}) and B. subtidal vertical nitrate fluxes simulated at station X6. Positive values indicate an upward velocity or nitrate flux. The black contours indicate the zero values. The upwelling events (main phases) are indicated at the top of each figure.

the deep southern side (i.e., from X6) and a surface outflow on the northern side of the bay (i.e., toward Mahone Bay), as observed in Chapter 3. Similar circulation patterns were previously described in Lunenburg Bay by *Zhai et al*. (2008b) in association with upwelling conditions. Such patterns, which were simulated in Chapter 3, are important in the biological coupling between the inner shelf and the bay (see Section 4.3.4).

Temperature variations are simulated inside Lunenburg Bay in relation to the different phases of the wind forcing (Figure 4.4). At the mid-bay mooring location SB3, the sequence of simulated water temperature indicates the hydrographic response of the bay to the upwelling event. Water temperature decreases throughout the water column during pulse 1 (day 179–186) to reach a minimum of 5°C near the bottom on day 183. Upwelling conditions shortly relax on day 185 due to the moderate northward wind conditions. The decrease in water column temperature during pulse 1 corresponds to the intrusion and shoaling of deep isopycnals from the inner shelf into the bay through its southeastern side (Figure 4.7). Upwelling conditions relax between pulse 1 and 2 (day 187–189) during the period of low wind forcing (Figure 4.4). Lower water temperatures are simulated during pulse 2, but this pattern is not as pronounced as during pulse 1. The model simulates the increase of water temperature after pulse 2 when wind forcing is low (day 194–203), indicating the relaxation of upwelling conditions in Lunenburg Bay (Figure 4.4). A transient decrease in water temperature is simulated on day 199 when strong wind forcing occurs.

4.3.1.3 Comparison with Observed Temperature at the SB3 Mooring

The comparison between observed and simulated water temperature at the mooring station SB3 (mid-bay) demonstrates the ability of the model to simulate the overall hydrographic response of the bay to the upwelling event (Figure 4.4). Nonetheless, some discrepancy appears, that can be related in part to the frequency of the NCEP meteorological dataset (1 d^{-1}) used to force the model. First, the variability is higher in the observations. The daily-averaged NCEP wind forcing does not reproduce the high-frequency variability in the wind and therefore has a smoothing effect on the model results. Also, in comparison to the simulation the observed hydrographic response is faster and shorter, which results in discrepancies in the timing and duration of the onset of upwelling conditions; it occurs earlier and for a longer period in the model. As a consequence, the model does not

resolve the short-term variations in the temperature field associated with the upwelling. Finally, the hydrographic response to short wind events (i.e., days 194–195 and 199–200) is misrepresented in the model due to a mismatch between NCEP and observed wind forcing (timing and direction).

Surface stratification is weak in the model, which can also induce the discrepancy between the modelled and the observed hydrographic response to upwelling conditions (Figure 4.4). The lack of freshwater flux from the local watershed in the model may be the source of the weak stratification. There is no river input inside Lunenburg Bay, but lower salinity is observed at the surface inside the bay, indicating the presence of sources of freshwater in the nearshore area that are not considered in the model. Weak stratification may also originate from the shelf where simulated sea surface temperature is underestimated (Section 4.3.1.1).

These discrepancies will influence the biological response to the upwelling events because the ecosystem model does not experience the high-frequency variability occurring in the real ecosystem. Therefore, the model will not capture the phytoplankton response at a short time scale ($\sim$ 1 day) but will resolve longer time scales associated with each upwelling event ($\sim$ 5 day) and the overall period of upwelling forcing (weeks). Hereafter, the simulated biological response to the upwelling is discussed with respect to time scales resolved by the model.

4.3.2 Simulated Biological Response to the Upwelling

4.3.2.1 Nitrate Concentration Along the Transect Line

The model simulates the vertical displacement of the nitracline outside (Figure 4.9D) and inside (Figure 4.9A-C) Lunenburg Bay during the different periods of wind forcing (see periods in Section 4.2.2.5). However, only low nitrate concentrations reach the shallow inshore area (Figure 4.9A). Substantial variations in nitrate concentrations during the upwelling (0–4 mmol m^{-3}) are therefore restricted to the middle and outer part of the bay, whereas low nitrate concentration is characteristic of the inshore area (0–1 mmol m^{-3}). After the relaxation of upwelling conditions, only background nitrate concentrations remain throughout most of the bay until the end of the simulation.

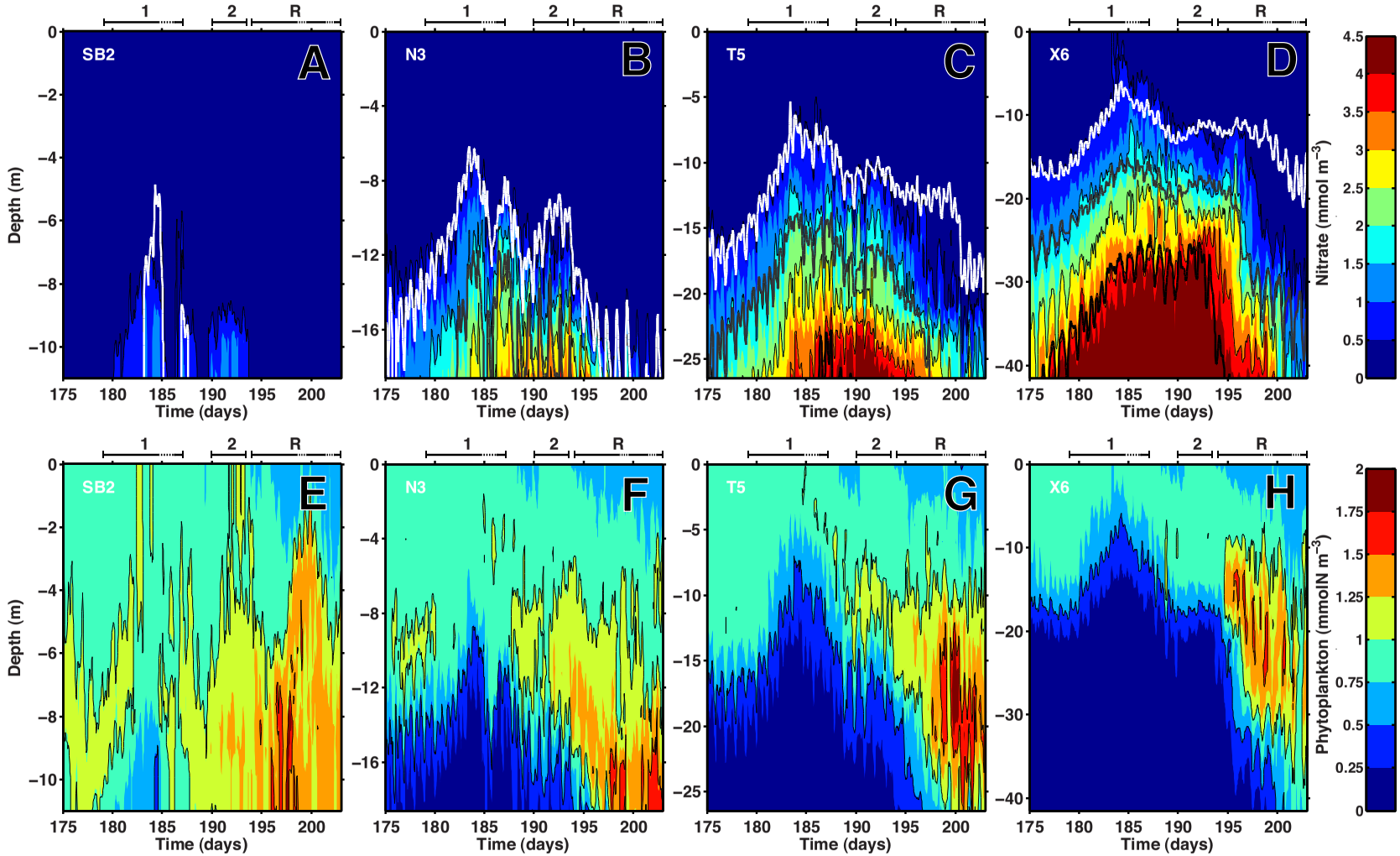

Figure 4.9: Simulated nitrate concentration (A-D) and phytoplankton biomass (E-H) at the five stations along the transect line in Lunenburg Bay (see position in Figure 4.1), from inshore to offshore (left-right). On the upper panels the thick lines represent three isopycnals: sigma-*t* equal to 25.0, 25.25 and 25.5 kg.m^{-3}. The upwelling events (main phases) are indicated at the top of each plot (1: pulse 1, 2: pulse 2, R: relaxation following pulse 2).

The simulated upward movement of the nitracline during pulses 1 and 2 is associated with the intensification of the vertical nitrate flux resulting from the shoaling of subsurface isopycnals (Figure 4.8B and Figure 4.9D). The flux is maximum on day 183 at the peak of pulse 1 (e.g., 9.2 mmol m^{-2} d^{-1} at 20 m) and overall more substantial during pulse 1 than during pulse 2 (e.g., 4.2 and 3.3 mmol m^{-2} d^{-1} respectively at 20 m). The upward variation of the nitracline is therefore more important during pulse 1. It sums up to a total displacement of about 10 m (17 → 7 m). During the long period of upwelling relaxation following pulse 2, the deepening of the isopycnals induces a downward nitrate flux (Figure 4.8B) that results in the rapid deepening of the nitracline (Figure 4.9D). Similar temporal patterns are simulated inside Lunenburg Bay at station T5 (deep end side), N3 (mid-bay) and SB2 (inshore)(Figure 4.9).

4.3.2.2 Phytoplankton Biomass Along the Transect Line

The model simulates a well defined phytoplankton biomass response to the upwelling event (Figure 4.9E-H). The response can be separated into distinct periods associated with the wind forcing: pulse 1 (day 179–186), pulse 2 (day 190–193), and the relaxation period following pulse 2 (day 194–203).

Pulse 1. The intrusion of nutrient-rich, but phytoplankton-poor, subsurface waters from the Scotian Shelf during pulse 1 results in the decrease of phytoplankton biomass outside the bay at X6 (Figure 4.9H) and throughout the bay in the deep-end side (T5, Figure 4.9G), the mid-bay (N3, Figure 4.9F) and inshore (SB2, Figure 4.9E). This effect is contrasted to the variation in nitrate concentration simulated during the same period (Figure 4.9A-D). Inshore (SB2), where nitrate variations are small, this effect is less pronounced. The upwelling conditions simulated during pulse 1 have therefore a substantial negative effect on the phytoplankton biomass in Lunenburg Bay.

Pulse 2. At station X6 outside Lunenburg Bay, phytoplankton biomass increases to the pre-upwelling level during pulse 2 (1 mmolN m^3, Figure 4.9H). Inside Lunenburg Bay, the model simulates a moderate increase of phytoplankton biomass in the subsurface layer (5–12 m, Figure 4.9E-G), which starts during the relaxation of pulse 1. The response to pulse 1 is therefore different from the response to pulse 2.

Upwelling relaxation. At station X6, the model simulates a subsurface peak in phytoplankton biomass near the nitracline during the relaxation phase following pulse 2. This phytoplankton maximum subsequently deepens with the nitracline, to reach a maximum of 1.75 mmolN m^{-3} at 25 m. This is about twice the pre-upwelling biomass (Figure 4.9 H). Inside Lunenburg Bay, subsurface phytoplankton biomass accumulates until the end of the simulation (Figure 4.9E-G). Following the patterns simulated at X6, the subsurface phytoplankton maximum deepens with the relaxation of upwelling conditions. The main phytoplankton response to the upwelling is therefore simulated during the main relaxation phase of upwelling conditions (i.e., following pulse 2). This phase has therefore a substantial role in the accumulation of phytoplankton biomass inside Lunenburg Bay.

4.3.2.3 Transport Across the Boundary Lines

The variation in nitrate concentration simulated at the three locations inside Lunenburg Bay (SB2, N3 and T5, Figure 4.9A-C) is explained by the transport of nitrate across the four boundaries delimiting the different areas of Lunenburg Bay (see locations in Figure 4.5). An inflow of nitrate from the Scotian Shelf occurs through the southeastern side (boundary B) during most of pulse 1 and during pulse 2 (Figure 4.10A), with in average 1.5 and 0.4 mol s^{-1} for each pulse (Table 4.1). The transport of nitrate is maximum at the peak of pulse 1 (day 183) with a maximum nitrate input of 4.2 mol s^{-1} into the deep-end side. A fraction of the nitrate exits directly through the northeastern side of the bay (boundary A, Table 4.1). This outflow is also maximal at the peak of pulse 1 (1.2 mol s^{-1}). Another fraction is transmitted to the mid-bay area (boundary C, Table 4.1). This input to the mid-bay area reaches a maximum of 1.1 mol s^{-1} at the end pulse 1 (day 186)(Figure 4.10C). Only a small fraction of this nitrate is transmitted to the inshore area (boundary D, Table 4.1), with a maximum input of 0.2 mol s^{-1} at the end of pulse 1 (Figure 4.10C). Overall, nitrate transport is more important during pulse 1. The direction of the transport reverts at the outer boundaries during the relaxation phase after pulse 1 and during the main relaxation phase following pulse 2 (Figure 4.10A,C). An outflow of nitrate occurs during these periods (Table 4.1).

Phytoplankton transport at the interface between Lunenburg Bay and the inner shelf is significant during the simulation (Figure 4.10B and Table 4.1). The transport is characteristic of upwelling conditions (i.e., pulse 1, pulse 2 and the upwelling relaxation periods).

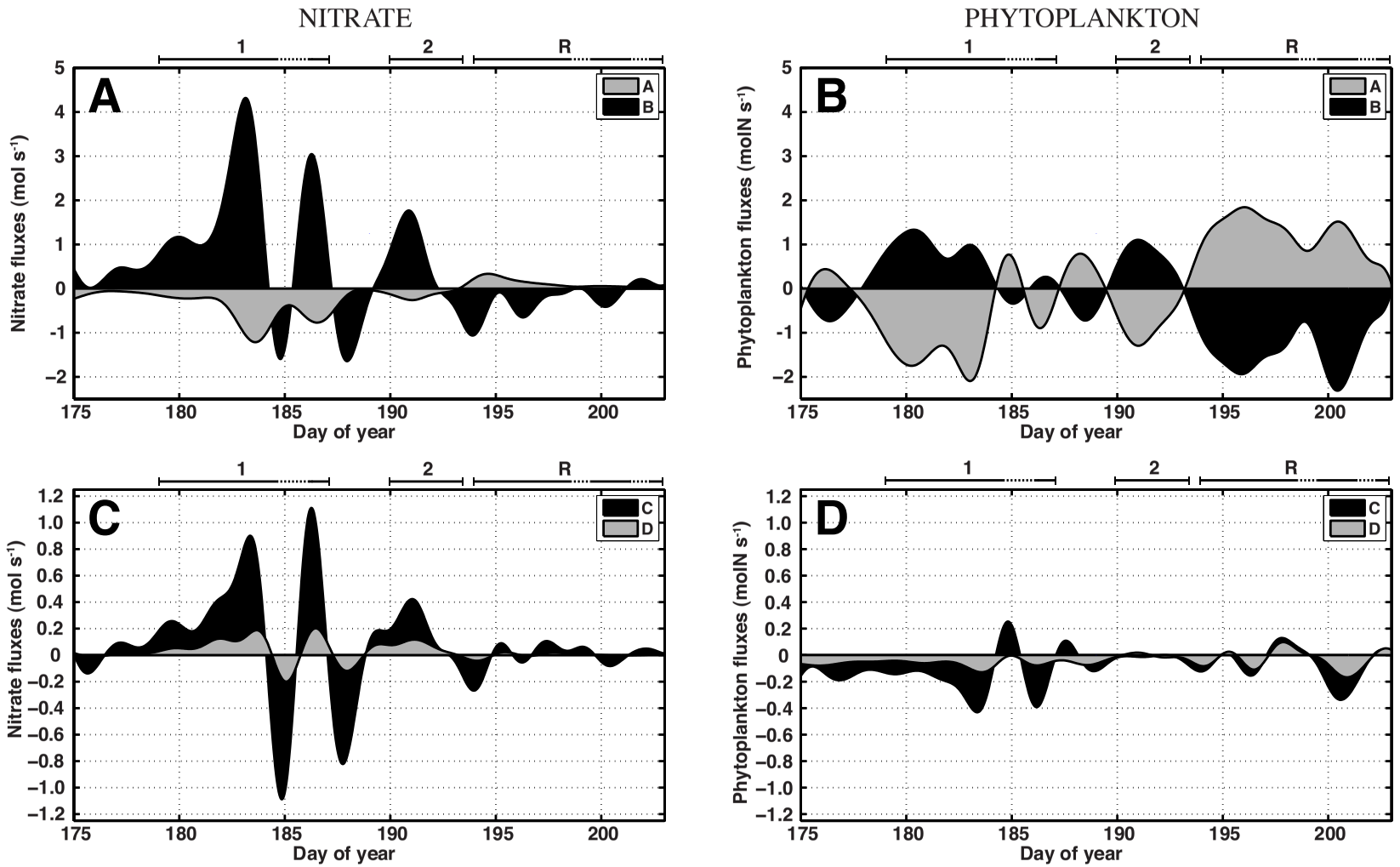

Figure 4.10: Subtidal advective fluxes of nitrate and phytoplankton computed at the four boundary lines in Lunenburg Bay (Figure 4.5). A. Nitrate transport across boundary A (northeast) and B (southeast) at the interface between Lunenburg Bay and the inner shelf. B. Phytoplankton transport across boundary A and B. C. Nitrate transport across boundary C (mid-bay) and D (inshore). D. Phytoplankton transport across boundary C and D. Positive (negative) transport is directed into (out of) Lunenburg Bay. The upwelling events (main phases) are indicated at the top of each plot (1: pulse 1, 2: pulse 2, R: relaxation following pulse 2).

Table 4.1: Average nitrate and phytoplankton transport across the four boundary lines in Lunenburg Bay during the simulation (see boundary locations in Figure 4.5). Average transport is the mean value of TNO3 (nitrate) or TP (phytoplankton)(see calculation in Section 4.3.2.3) during the main periods of upwelling: pulse 1, pulse 2 and the relaxation phase following pulse 2. A positive (negative) transport is oriented into (out of) the bay. Transport values are in molN s^{-1}.

Boundary	Pulse 1	Pulse 2	Relaxation
	NO_3^- transport (mol s^{-1})		
A	-0.53	-0.11	0.11
B	1.53	0.42	-0.22
C	0.27	0.13	0.00
D	0.06	0.05	0.00
	Phytoplankton transport (molN s^{-1})		
A	-1.03	-0.60	1.26
B	0.60	0.49	-1.43
C	-0.17	-0.03	0.07
D	-0.06	-0.01	0.03

During pulse 1 and pulse 2, phytoplankton is transported into Lunenburg Bay through the southeastern side (boundary B) and out of the bay through the northeastern side (boundary A, Table 4.1). Within that period, the maximum inflow is 1.3 mol s^{-1} at the beginning of pulse 1 and the maximum outflow is 2.0 mol s^{-1} at the peak of pulse 1 (Figure 4.10B). Over this phase, the average outflow exceeds the inflow (Table 4.1) and therefore phytoplankton is exported northward from the bay, toward Mahone Bay and the inner shelf. Over pulse 2, the inflow and outflow are of similar magnitude (Table 4.1) and therefore the export of phytoplankton is small. The model simulates a similar pattern, with a lower intensity, across the mid-bay and the inshore boundaries (boundary C and D, Figure 4.10D): an outflow of phytoplankton is simulated during pulse 1 (maximum of 0.4 and 0.1 mol s^{-1} respectively) and negligible transport during pulse 2 (Table 4.1). These patterns are important to explain phytoplankton variability in the model (see Section 4.3.4.2). During the

periods of upwelling relaxation, in particular following pulse 2 (day 194–203), the pattern of phytoplankton transport is reversed at the interface between the bay and the inner shelf (Figure 4.10B): phytoplankton is transported into Lunenburg Bay on the northeastern side (boundary A) with a peak at 1.9 mol s^{-1} at the beginning of the relaxation of pulse 2 (day 196), and out of the bay on the southeastern side (boundary B) with a peak at 2.2 mol s^{-1} at the end of the simulation (day 200). The magnitude of phytoplankton transport in and out of the bay is similar during the relaxation following pulse 2, except at the end of the simulation when phytoplankton is exported. Overall, a small export of phytoplankton occurs during the main relaxation (Table 4.1). Inside the bay, the model simulates a small export of phytoplankton biomass from the mid-bay (boundary C) and the inshore (boundary D) areas during most of the relaxation phase following pulse 2 (day 194–203) (Figure 4.10D). The maximum export from these areas (0.4 and 0.2 mol s^{-1} respectively) occurs at the end of the simulation (day 200).

4.3.2.4 Comparison with Observations at the Moorings

The comparison of nitrate concentration simulated at the mid-bay mooring station SB3 with the nitrate proxy time series developed in Chapter 2 (see Section 2.2.4.1) indicates that the model simulates the observed range of variability in bottom nitrate concentration during pulse 1 and 2 (0–3 mmol m^{-3}, Figure 4.4C). A large discrepancy occurs during the onset of pulse 1 when nitrate concentration is overestimated in the model. This discrepancy is associated with a mismatch in the timing of the onset of the upwelling inside Lunenburg Bay (Section 4.3.1.3).

The comparison between the simulated and the observed phytoplankton response to the upwelling event highlight several key characteristics of phytoplankton dynamics in the simulation. First, the model reproduces the background chlorophyll concentration inside Lunenburg Bay at the inshore mooring station SB2, and also at the mid-bay mooring station SB3 (Figure 4.11B). This result is important because the ecosystem model was initialized only with the nitrate-density relationship on the Scotian Shelf and the output from the NENA domain. The conditions on the shelf therefore explain the background level of phytoplankton observed inside Lunenburg Bay. Also, the time scale of the variation in chlorophyll biomass differs between the simulation and the observations. At

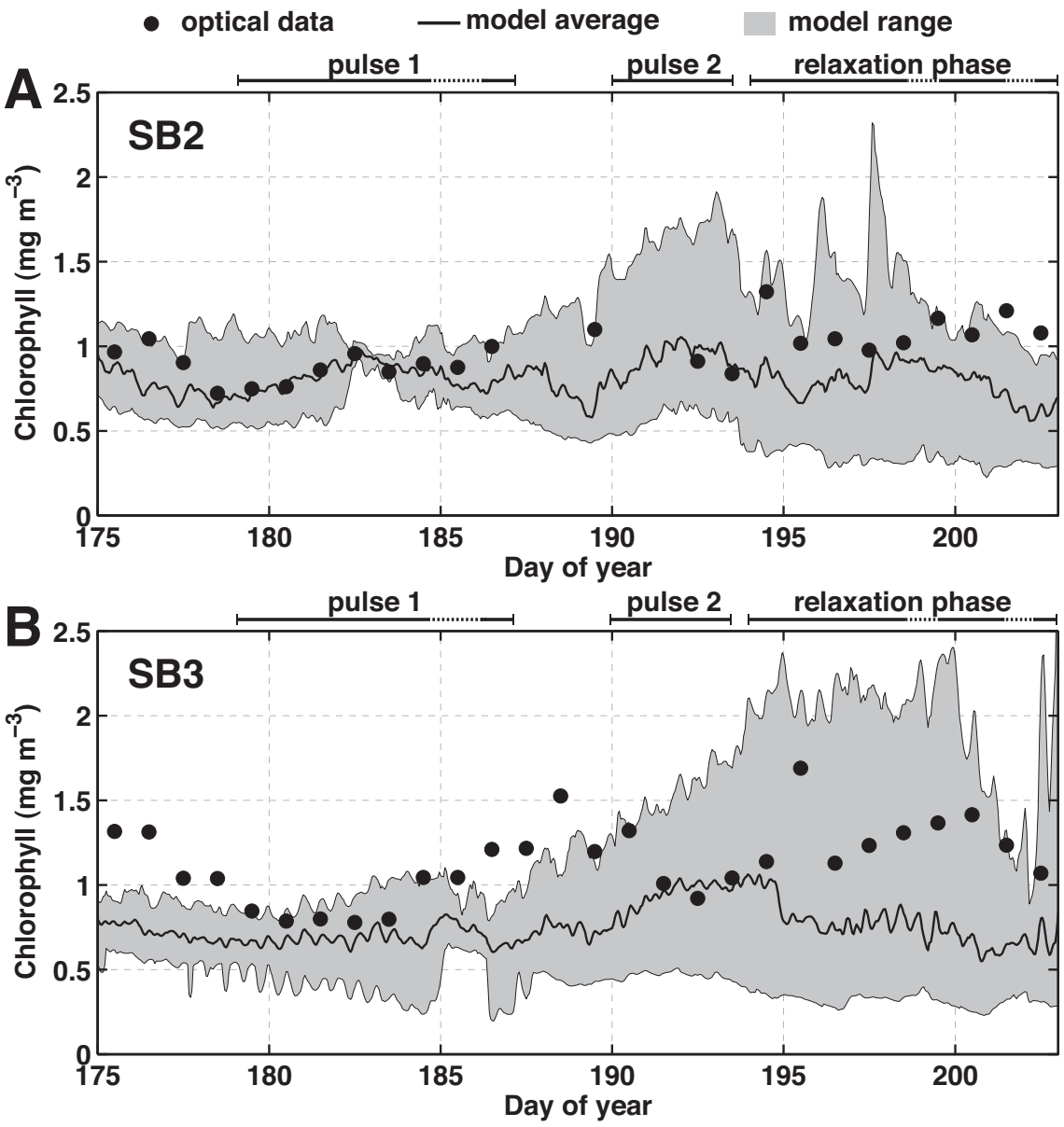

Figure 4.11: Comparison between modelled and observed (optical data) chlorophyll time series inshore at SB2 (A) and in the mid-bay at SB3 (B). The black dots are the observations (see Chapter 2), the black line indicates the water column average of modelled chlorophyll biomass and the grey area represents the range of modelled chlorophyll biomass in the water column (i.e., the upper (lower) bound is the maximum (minimum) value of chlorophyll biomass in the water column). The upwelling events (main phases) are indicated at the top of each plot.

the inshore mooring station (SB2) the observed response to the upwelling event is small and therefore modelled and observed chlorophyll concentrations are similar. However, at the mid-bay mooring station (SB3), the model does not simulate the increase in phytoplankton biomass following pulse 1 (Figure 4.11B). Rather, the model simulates a slow increase in maximum biomass during and following pulse 2, whereas a peak of chlorophyll concentrations is observed during the relaxation of pulse 1 and pulse 2. At this station, the model does not reproduce the magnitude of chlorophyll variability (water column average), which is much higher in the observations. This discrepancy indicates that the dynamics of chlorophyll biomass are dampened in the model. However, phytoplankton biomass does show a characteristic response to the upwelling event (Figure 4.9E-H and Figure 4.12A). A mismatch in the carbon to chlorophyll ratio (C:Chl) may result in the underestimated chlorophyll biomass by the model. A better agreement with the observation is found when chlorophyll biomass is directly estimated from phytoplankton biomass using a fixed value of C:Chl (see Appendix E). In this configuration, the overall chlorophyll response to the upwelling event is simulated correctly at SB3 but the short-term component of the response is still unresolved by the model. Given the uncertainties in simulated chlorophyll biomass, further analysis of the simulation is carried out using phytoplankton biomass as nitrogen rather than as chlorophyll.

4.3.3 'Bathymetry Effect' on the Phytoplankton Response to Upwelling

The phytoplankton response to the upwelling pulses is described in Figure 4.12A and summarized in Table 4.2 and Figure 4.13A-C. The comparison between phytoplankton biomass time series (per unit area, mmolN m^{-2}) inside Lunenburg Bay (stations SB2, N3, T5 and X6) and in the neighbouring areas (stations MB, SMB and OS, see Figure 4.1) reveals that the magnitude of the simulated response to the upwelling events is strongly dampened in the inshore, shallow areas (Figure 4.12A and Figure 4.13A-C). The negative phytoplankton response to pulse 1 (day 179–186) is significant at N3, T5 and X6, the mid and outer stations of Lunenburg Bay (0.7, 0.6 and 0.6 respectively, see Table 4.2 and Figure 4.13A-C) and at OS, the station offshore (0.6), but weak at the shallow station inside Mahone Bay (MB)—the inlet adjacent to Lunenburg Bay—and at the inshore station SB2 inside Lunenburg Bay (0.9, see Table 4.2). The effect is also weak inside Saint Margarets Bay (SMB)—the foremost northeastern inlet of the area (Figure 4.13B).

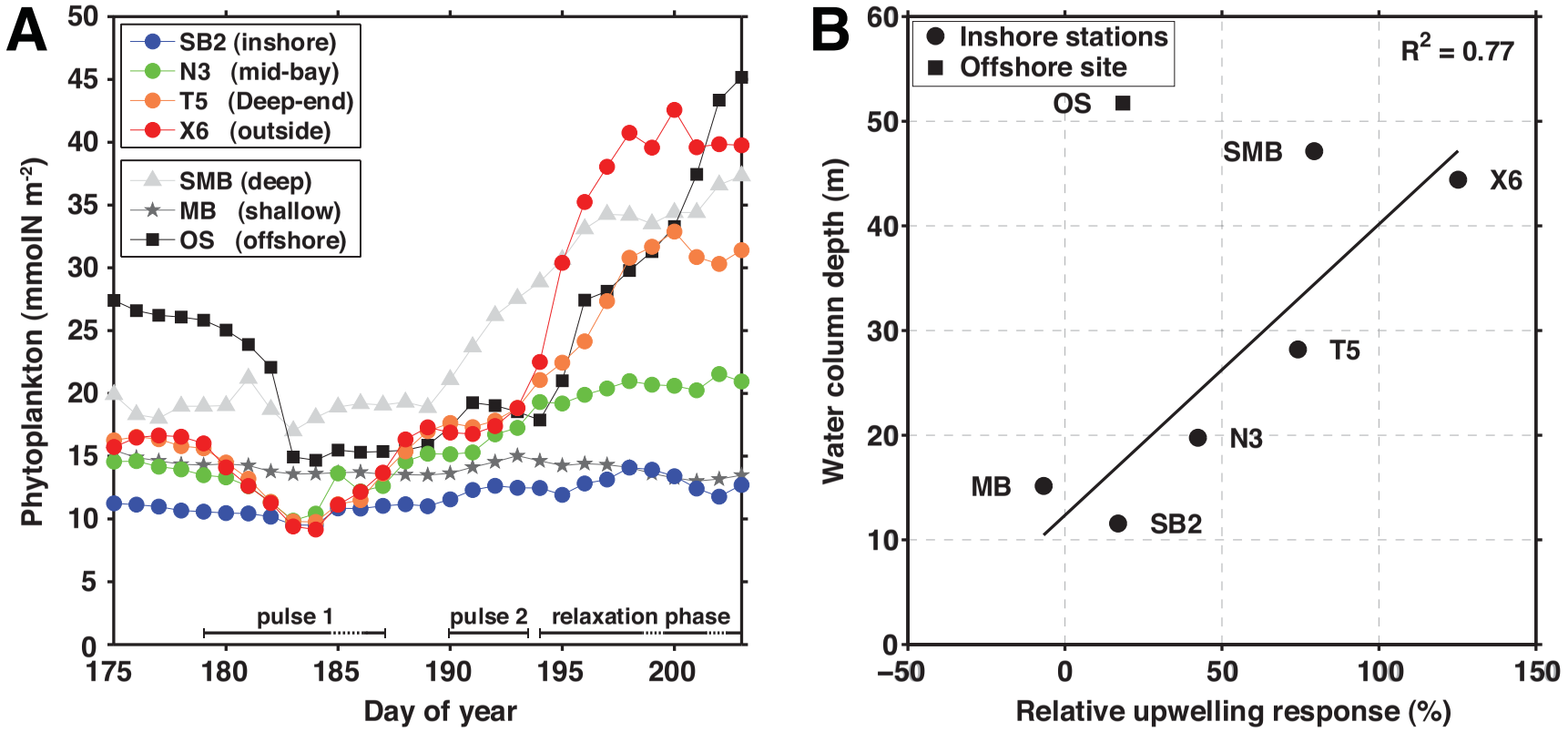

Figure 4.12: Phytoplankton biomass response to the upwelling inside Lunenburg Bay (SB2, N3, T5 and X6), Mahone Bay (MB), Saint Margarets Bay (SMB) and at an offshore station (OS)(see locations in Figure 4.1). A. Time series of depth-integrated phytoplankton biomass during the simulation (daily-averaged). The upwelling events (main periods) are indicated along the x-axis. B. Relationship between the relative phytoplankton biomass response to the upwelling and depth. The upwelling response is calculated from the values presented in Figure 4.12A as the relative change in average phytoplankton biomass per unit area between the pre-upwelling events time period (day 175–178) and the upwelling relaxation phase following pulse 2 (day 194–203). The black line is the linear fit between the upwelling response and depth for all the inshore stations (i.e., excluding OS). The R-square of the fit is $R^2 = 0.77$ ($F = 13.3$, $n = 6$, $p < 0.05$).

The moderate increase in phytoplankton biomass simulated in Lunenburg Bay during pulse 2 (day 190–193) and the accumulation of phytoplankton during the relaxation phase of the upwelling (day 194–203)(see Section 4.3.2.2) also occur offshore (OS station). During the relaxation phase, the magnitude of the phytoplankton response in Lunenburg Bay (i.e., biomass accumulation, see Section 4.2.4.1) increases along the transect line from the inshore to the outside of the bay (Figure 4.12A and Table 4.2). At the deep station inside Saint Margarets Bay (SMB), the accumulation of phytoplankton biomass occurs throughout pulse 2 and the relaxation phase (Figure 4.12A), denoting a particular response, but a similar overall effect at this location. The model does not simulate a phytoplankton response at the shallow station inside Mahone Bay (MB) however. The dynamics simulated at this station are therefore significantly different than at the other locations, except for the shallow inshore station in Lunenburg Bay (SB2) where the overall response to the upwelling is small (Figure 4.12A and Figure 4.13A-C).

The patterns emerging from the spatial comparison of phytoplankton response to the upwelling are then: (1) the response follows a similar temporal pattern at most locations, (2) the magnitude of the response during the relaxation phase is spatially-dependent; it decreases shoreward inside Lunenburg Bay, and (3) no response occurs in Mahone Bay.

The spatial variability observed in the simulated phytoplankton response to the whole upwelling event (i.e., upwelling response, see definition in Section 4.2.4.1) suggests a relationship between water column depth and the overall phytoplankton response to the upwelling. This relationship is well established for the stations along the transect line in Lunenburg Bay (Figure 4.12B). The response increases linearly as the stations get deeper toward the outside of the bay. A similar relationship occurs between the shallow station MB and at the deep station SMB (Figure 4.12B). Overall, the relationship is significant at these stations ($R^2 = 0.77, F = 13.3, n = 6, p < 0.05$). However, the relationship does not hold at the offshore station (OS). The delayed response at this station (Figure 4.12A) and the higher phytoplankton biomass before the upwelling event explains the lower relative upwelling response at this station, and therefore the lack of relationship with water depth. The upwelling response at this location is therefore stronger than indicated in Figure 4.12B, but the metrics does not capture this response.

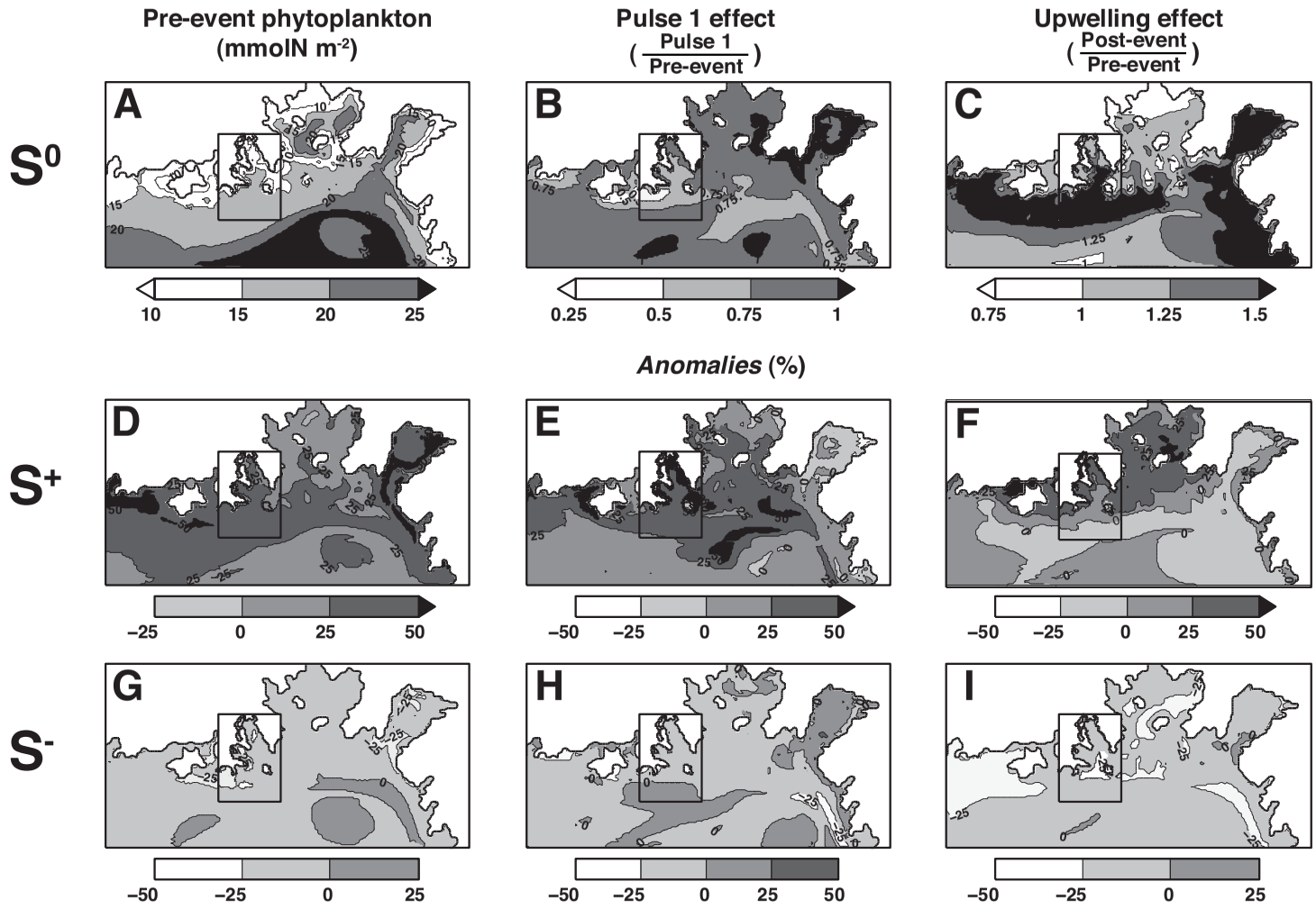

Figure 4.13: Maps of phytoplankton sensitivity to the variation of the nitracline depth in the medium (outer) and high (inner box) resolution grids. S^0 is the control run (A-C), S^+ is the simulation with a shallower nitracline (D-F) and S^- the simulation with a deeper nitracline (G-I)(see Figure 4.3). S^+ and S^- are expressed in percentage, as anomalies from the S^0 values. Details on the calculation of pre-event phytoplankton (A, D, G), pulse 1 effect (B, E, H) and upwelling effect (C, F, I) can be found in Section 4.2.3.2.

Table 4.2: Sensitivity of phytoplankton biomass to the variation of the nitracline depth on the Scotian Shelf during the simulations. Pre-events phytoplankton corresponds to the average phytoplankton biomass per unit area during the pre-upwelling events period (days 175–178). The pulse 1 effect is the ratio of phytoplankton biomass at the peak of pulse 1 (day 183) and pre-event phytoplankton. The upwelling effect is the ratio between the phytoplankton biomass per unit area during the relaxation phase following pulse 2 (days 194–203) and the pre-events phytoplankton biomass (days 175–178). S^0 is the control run, and S^+ and S^- respectively the shallower and deeper nitracline simulations (see Figure 4.3). S^+ and S^- are expressed in percentage, as anomalies from the S^0 values (see Section 4.2.3.2).

	Sensitivity of phytoplankton																				
	Pre-events phytoplankton (mmolN m^{-2})							Pulse 1 effect							Upwelling effect						
Run	SB2	N3	T5	X6	MB	SMB	OS	SB2	N3	T5	X6	MB	SMB	OS	SB2	N3	T5	X6	MB	SMB	OS
S^0	11.0	14.3	16.3	16.4	14.8	18.8	26.6	0.9	0.7	0.6	0.6	0.9	0.9	0.6	1.2	1.4	1.7	2.3	0.9	1.8	1.2
												Anomalies (%)									
S^+	+29	+28	+39	+42	+9	+35	+16	+65	+39	+32	+36	+18	0	+52	+40	+22	+6	+5	+30	−5	0
S^-	−22	−23	−15	−20	−14	−22	−4	−9	−14	−20	−15	+1	+13	−7	−22	−23	−15	−20	−14	−22	−4

The water column depth used in this relationship is not necessarily the explanatory variable for the phytoplankton response to the upwelling. The position of the stations in Lunenburg Bay along a gradient of increasing depth, the deep entrance and average depth of Saint Margarets Bay and the shallow average depth at the entrance and inside Mahone Bay suggest that the shape of the inlet (i.e., the slope of the bathymetry gradient) and the depth at the entrance of the inlet might be better predictors for the phytoplankton response to the upwelling. However, this was not tested since it would require the comparison between more inlets with different shape and slope characteristics.

4.3.4 Effect of Transport on the Response to the Upwelling

4.3.4.1 Nitrate Retention

Large variations in the magnitude and direction of nitrate transport are associated with the upwelling phases in Lunenburg Bay (Section 4.3.2.3). Transport between the deep-end and the mid-bay areas (boundary C) controls the amount of nitrate delivered to the mid-bay and the inshore areas, which is essential for the phytoplankton response to the upwelling in this region. The characteristics of nitrate transport across boundary C are the short duration of the nitrate pulses and the similar magnitude of the nitrate inflow and outflow.

The periods of nitrate inputs associated with upwelling conditions (pulse 1 and 2) are short (1–4 days) and directly followed by short periods (1–2 days) of outflow during relaxation periods. The overall duration of nitrate pulses is therefore limited. The similar magnitude of the inflow and the outflow also suggests that a significant part of the nitrate remains unused in Lunenburg Bay because it is not taken up quickly enough by phytoplankton. This is confirmed by the efficiency of the bay to trap nitrate during the simulation ($E_{NO_3^-}$, Eq. 4.5), through either the uptake by phytoplankton or a local accumulation. During the simulation, the efficiency is only 23% in Lunenburg Bay. This low value is a lower limit, since the misrepresentation of the short-term phytoplankton response to the upwelling event (i.e., mid-bay mooring station SB3, Section 4.3.2.4) may be a source of underestimation.

4.3.4.2 Transport vs. Local Production

The production-transport index (i.e., which of production (biological process) or transport (physical process) has a dominant role in the model, see Section 4.2.4.4), varies with time during the simulation. These variations are associated with the main periods of upwelling (Figure 4.14).

For phytoplankton (Figure 4.14A,B, x-axis), transport dominates the dynamics throughout Lunenburg Bay during pulse 1. This is related to the flushing of the bay with phytoplankton-poor inner shelf waters during this phase, resulting in a low phytoplankton biomass (see Figure 4.9E-G) and an outflow of pre-upwelling phytoplankton from the bay (see Section 4.3.2.3). During pulse 2, primary production equals or dominates phytoplankton transport and therefore the accumulation of biomass simulated during this phase (Figure 4.12A) is dominated by local production (Figure 4.14A,B, x-axis).

During the relaxation phase following pulse 2, the production-transport index for phytoplankton varies spatially. Considering the whole bay (areas 2, 3 and 4, see Figure 4.5), the index indicates that primary production dominates local phytoplankton dynamics during most of the relaxation phase (Figure 4.14B, x-axis). The accumulation of phytoplankton biomass in the bay during the relaxation period (see Figure 4.12A) is therefore dominated by local primary production. Considering only the inshore and the mid-bay (areas 3 and 4), the index reveals that phytoplankton transport equals or dominates primary production (Figure 4.14A, x-axis). The accumulation of phytoplankton biomass decreases shoreward in this area during the upwelling relaxation (Figure 4.12A). Although limited, export (see Figure 4.10D and Table 4.1) rather than primary production is therefore the dominant process in this area during the relaxation phase following pulse 2.

The production-transport index for DIN (Figure 4.14A,B, y-axis) indicates that DIN dynamics are dominated by transport during pulse 1 and most of pulse 2, when nitrate input from the Scotian Shelf occurs in the bay. The comparison of the index for the whole bay (Figure 4.14B) and the mid and inner bay (Figure 4.14A) during these time periods shows that transport has a stronger effect on DIN dynamics in the outer bay. This agrees with the inshore-offshore patterns of nitrate concentration during pulse 1 and 2 (Figure 4.9A-C). During the relaxation phase following pulse 2, internal production (recycling) equals

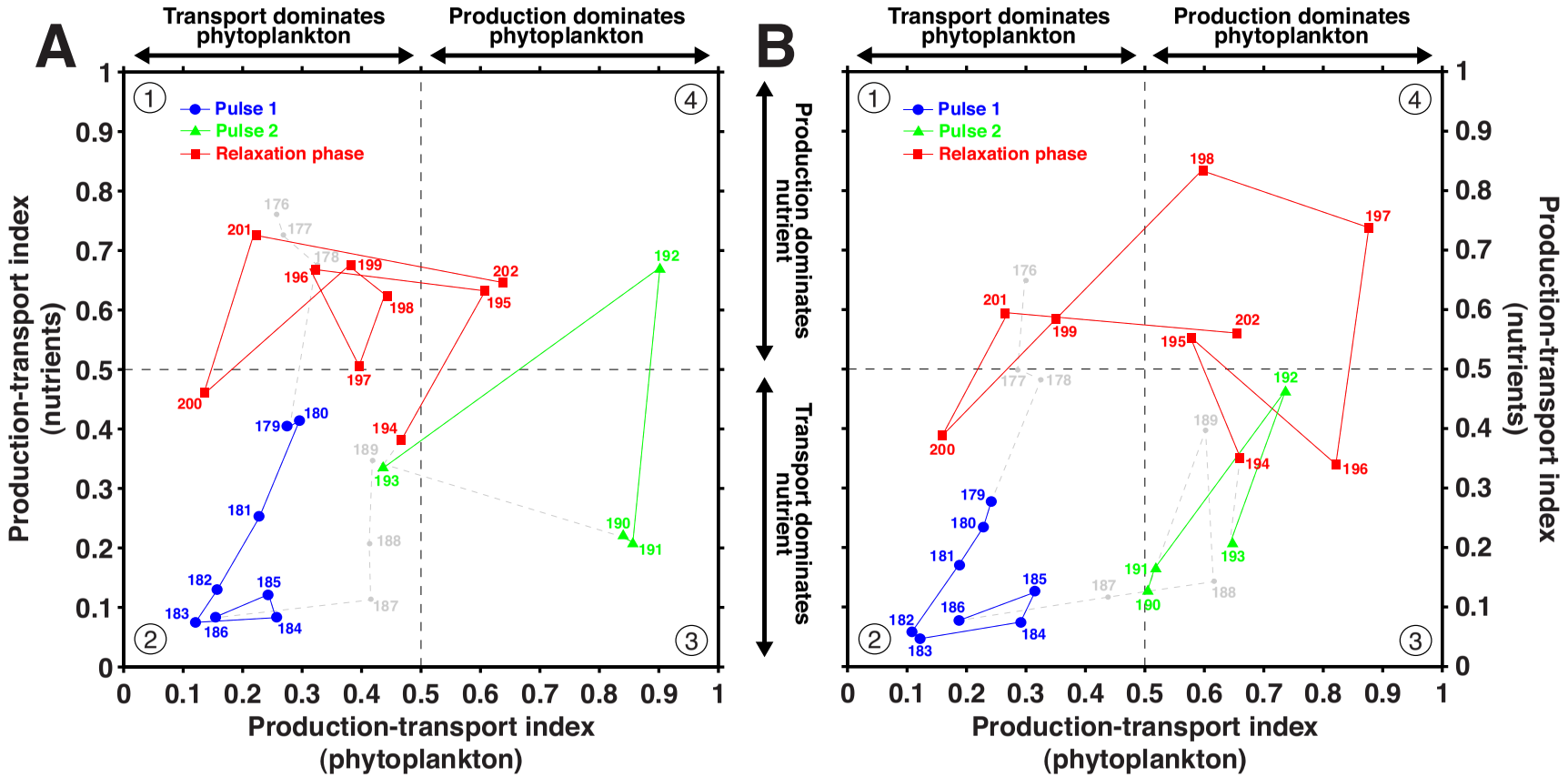

Figure 4.14: Daily-averaged contributions of production and transport to phytoplankton (x-axis) and nutrient (DIN, y-axis) dynamics in Lunenburg Bay for A. the inshore and mid-bay (area 3 and 4, see Figure 4.5) and B. the entire bay (area 2, 3 and 4). The contributions are represented by a production-transport index. The calculation of the index is detailed in Section 4.2.4.4. The contributions are plotted as day number and grouped into pulse 1 (blue), pulse 2 (green), the relaxation phase following pulse 2 (red) and the remaining periods (grey). The black dashed lines indicate an equal contribution of production and transport and delineate four zones: (1) Transport dominates phytoplankton and recycling dominates nutrient dynamics; (2) Transport dominates both phytoplankton and nutrient dynamics; (3) Local production dominates phytoplankton and transport dominates nutrient; (4) local production dominates both phytoplankton and nutrient dynamics.

or dominates DIN transport in the bay, which also corresponds to pre-upwelling conditions. The dynamics are more pronounced in the inshore areas (Figure 4.14A). Overall in the simulation, DIN dynamics are controlled by transport during each upwelling event (pulse 1 and 2) and by recycling during the pre-upwelling and the relaxation phase following pulse 2.

Two general patterns also emerge from the production-transport diagram. The model simulates a month-long response of Lunenburg Bay to the upwelling perturbation with different phases rather than a series of pulsed responses in the phytoplankton during each upwelling event and the outer bay has a more classical response to the upwelling perturbation (i.e., cycle of production) than the inner bay.

4.3.5 Sensitivity of Results to Nitrate Concentration on the Shelf

The variation of the nitracline depth on the Scotian Shelf (S^- and S^+ sensitivity runs, see Section 4.2.3.2) influences the simulated response to the upwelling events in Lunenburg Bay and the surrounding areas (Figure 4.13D-I, Table 4.2 and Table 4.3). Overall, a shallower nitracline (S^+) has a positive effect (increased response) whereas a deeper nitracline (S^-) has a negative effect (lower response) on biological transport and phytoplankton biomass during the simulation.

With a deeper nitracline (S^-), phytoplankton biomass is lower than in the control run before the upwelling events (Figure 4.13G and Table 4.2). The negative effect of pulse 1 is increased (negative value) in Lunenburg Bay (SB2, N3, T5 and X6) and offshore (OS) due to the lower phytoplankton biomass in upwelling source waters (Figure 4.13H and Table 4.2). The effect in Saint Margarets Bay (SMB), which was small in the control run is even smaller in this configuration. Nitrate and phytoplankton transport are also lower (Table 4.3) and the phytoplankton response to the upwelling event decreases accordingly, with a similar magnitude at all the stations inside and outside Lunenburg Bay except offshore (OS). At this location and in the surrounding area, the upwelling response is not sensitive to the variation in nitracline depth (Table 4.2 and Figure 4.13F,I).

A shallower nitracline (S^+) results in opposite effects. Pre-events phytoplankton biomass increases, indicating a higher background phytoplankton biomass simulated by the model

Table 4.3: Sensitivity of biological transport and nitrate trapping efficiency in Lunenburg Bay to the variation of the nitracline depth on the Scotian Shelf during the simulations. Horizontal transport corresponds to the average advective transport into (in) and outside (out) of Lunenburg Bay through boundary C (see Figure 4.5). $Q^{N}_{z=20}$ is the average vertical advective transport of nitrate at 20 m at X6 during the simulation. $E_{NO_3^-}$ is the efficiency of the bay to trap nitrate calculated from $NO^-_{3\,in}$ and $NO^-_{3\,out}$ (see Section 4.2.4.3). S^0 is the control run, and S^+ and S^- respectively the shallower and deeper nitracline simulations (see Figure 4.3). S^+ and S^- are expressed in percentage, as anomalies from the S^0 values (see Section 4.2.3.2).

Sensitivity of transport processes						
	Horizontal transport (molN s^{-1})				Vertical flux at X6 (mmol m^{-2} d^{-1})	Efficiency (%)
Run	$NO^-_{3\,in}$	$NO^-_{3\,out}$	P_{in}	P_{out}	$Q^{N}_{z=20}$	$E_{NO_3^-}$
S^0	0.32	0.25	0.56	0.65	1.9	23
				Anomalies (%)		
S^+	+224	+219	+63	+61	+243	+5
S^-	−46	−43	−31	−29	−47	−16

(Table 4.2), although this increase is small in the shallow Mahone Bay (MB) and the deep offshore (OS) stations (Figure 4.13D). In this configuration, the negative effect of pulse 1 on phytoplankton biomass is attenuated (positive anomalies) due to higher phytoplankton biomass in the upwelling source waters (Figure 4.13E and Table 4.2). As for the S^- run, the change is small in Saint Margarets Bay (SMB), indicating the particular dynamics at this location. Subsurface vertical transport of nitrate ($Q^{N}_{z=20}$) is much larger at station X6 outside Lunenburg Bay (Table 4.3). Horizontal transport of nitrate ($TNO3_{in}$, $TNO3_{out}$) between the deep-end and the mid Lunenburg Bay areas (boundary C) increases similarly. However, the efficiency of the bay to trap nitrate ($E_{NO_3^-}$) remains the same as in the control run (Table 4.3), which denotes a controlling effect of transport (see Section 4.3.2.3). Higher nitrate transport results in an enhanced upwelling effect at the shallow locations in Mahone Bay (MB) and Lunenburg Bay (SB2, N3), whereas the relative effect remains the same at the other locations (Figure 4.13F and Table 4.3). This result agrees with

the interpretation of a limited response to the upwelling at shallow inshore locations due to a 'bathymetry effect' (i.e., Section 4.3.3), which restricts the delivery of upwelled nitrate to the shallow inshore areas. Phytoplankton transport (P_{in}, P_{out}) increases as well in this configuration, with a net export of phytoplankton from the bay during the simulation (Table 4.3).

The effects of the upwellling (pulse 1 and overall event) in the two configurations (S^+, S^-) reveal an asymmetry between the response to the variations of the nitracline: model results are more sensitive to the shoaling of the nitracline (S^+). This asymmetry indicates that the conditions simulated in the control run (S^0) are closer to the deep nitracline case (S^-). This result suggests a nonlinear response to nitracline depth and a threshold beyond which rises in nitracline depth will have an effect. In the simulation of the 2006 upwelling events (standard run), the conditions were below this threshold.

Overall, the sensitivity experiment reveals the importance of the far-field distribution of nitrate in the phytoplankton biomass response to periods of upwelling conditions inside Lunenburg Bay and neighbouring inlets, especially in shallow areas where the input of upwelled nitrate is limited. This denotes a bathymetry-related constraint to the delivery of nitrate in shallow inshore areas.

4.4 Discussion

The simulation of two episodes of northeastward wind conditions over the Scotian Shelf in early summer 2006 and the development of upwelling conditions on the inner shelf and in Lunenburg Bay revealed a limited response in the phytoplankton, which supports the findings from the previous chapters (Chapter 2 and Chapter 3). This response has, however, notable spatial differences between inshore and offshore areas. The spatially-varying response in the model is associated with transport patterns and nitrate concentration in upwelling source waters, which are dominant factors controlling phytoplankton dynamics in a tidal inlet (i.e., nitrate availability in source waters vs. specific transport, S^* vs. F^*, see Figure 3.12). The analyses of the model results indicate that during the upwelling

events in 2006, the underlying processes for this control were: (1) the spatial and temporal characteristics of transport associated with upwelling conditions; (2) the bathymetry gradient in inshore areas; and (3) the vertical distribution of nitrate on the Scotian Shelf. The role of each process is developed in the discussion, after considering the validity of the results from the simulation.

4.4.1 Validity of Simulation Results

The simulation reveals the control of hydrographic properties in Lunenburg Bay by wind-induced upwelling events in July 2006. This control is characterized by an input of upwelled waters through a northward flow at the entrance of the bay, the development of a two-layer upwelling circulation, and a large scale development of upwelling conditions along the coast suggesting the occurrence of similar nearshore processes across the region under investigation. This wind-induced upwelling control was previously established for its effect on the high-frequency variation in salinity and temperature in Lunenburg Bay (*Zhai et al*., 2007) and on the hydrography of inlets along the Atlantic coast of Nova Scotia (*Heath*, 1973).

However, the inability of the model to simulate the high-frequency variations in hydrographic conditions resulted in a discrepancy in the timing, magnitude and duration of upwelling conditions in Lunenburg Bay. Short-term variations in phytoplankton during the upwelling (i.e., pulsed response) are therefore not represented in the model. Rather, a low frequency response controlled by transport is simulated. Hence, the role of transport might be overestimated in the model. The consequence of lower transport is more retention of nitrate and phytoplankton and therefore a larger influence of upwelling events on the productivity of Lunenburg Bay. Despite this inconsistency, over the whole simulation the model is able to simulate characteristic patterns associated with the upwelling that were observed in Chapter 2, such as (1) the flushing of the bay with nitrate-enriched—but phytoplankton-poor—Scotian Shelf waters during the development of upwelling conditions, (2) the limitation of the phytoplankton response by nitrate concentration in upwelling source waters, (3) the inshore-offshore spatial variation in nitrate concentration and phytoplankton response to the upwelling, and (4) the accumulation of phytoplankton biomass during the relaxation phase following pulse 2.

The model is therefore able to reproduce the general patterns of phytoplankton response during a period of upwelling events in Lunenburg Bay. It is a valid tool to study the general processes underlying the phytoplankton dynamics observed during an upwelling event. Further development of the model is necessary to better represent the short-term variations associated with upwelling events. This will enable the assessment of short-term contributions on the phytoplankton response to the upwelling events.

4.4.2 Role of Transport on DIN and Phytoplankton Dynamics

The time-scale of transport relative to the time-scale for growth is essential to the regulation of phytoplankton dynamics in aquatic systems (*Lucas et al.*, 2009). A pulse of upwelling typically lasts no more than a few days in Lunenburg Bay and the ocean transport moves the water (including nutrients and phytoplankton) through the system on a time scale of about 1–4 days (Figure 4.10). This event time-scale is short relative to the time scale for the primary producers to consume the nitrate and accumulate (i.e. Figure 3.12), considering their low biomass in upwelled waters (e.g., *Álvarez-Salgado et al.*, 1996b). This time scale is within the same range as the time lag between nitrate input and the accumulation of phytoplankton biomass determined in Chapter 2 (2.7 days). Given this short time scale, Lunenburg Bay has a limited ability to convert the nutrients into biomass during a coastal upwelling event and therefore its efficiency to trap nitrate is low ($E_{NO_3^-} = 23\%$). This efficiency estimated from the model corresponds to the low end of the values reported for the NW Iberian Upwelling System (i.e., $25\% \leqslant E_{NO_3^-} \leqslant 81\%$, *Álvarez-Salgado et al.*, 1996b; *Piedracoba et al.*, 2008a; *Villegas-Ríos et al.*, 2010). Weak stratification and the washing-out effect typically induced by the flushing of inlets are usually associated with low efficiencies (*Álvarez-Salgado et al.*, 1996a; *Pérez et al.*, 2000). The two factors occur during the simulation, but the overall weak stratification in the model, and the misrepresentation of the short-term response of the phytoplankton to upwelling pulses, is likely a source of underestimation for the efficiency of Lunenburg Bay to trap nitrate.

Overall, this limitation from the short time scale associated with an upwelling event confirms that the short duration of an upwelling event limits the development of phytoplankton biomass in Lunenburg Bay. It is an important characteristic of the coupling

between Lunenburg Bay and the coastal ocean and an important result of this analysis. This limitation is complementary to the findings of Chapter 3 (S^* vs. F^*, Figure 3.12) that classified Lunenburg Bay as a system dominated by transport (i.e., high F^*) under a steady state upwelling forcing.

Transport is also directly involved in the overall dynamics of DIN and phytoplankton during the upwelling event. In the simulation, it regulates phytoplankton biomass, which accumulates from local primary production only during pulse 2 (small) and the subsequent relaxation phase (main accumulation) when transport rate decreases (Figure 4.14). This indicates that the accumulation of phytoplankton during the relaxation phase is the result of local primary production rather than transport. Similarly, transport dominates DIN production during the upwelling pulses whereas local production of DIN prevails when nutrient transport is low during the relaxation phase. This cycle (i.e., Figure 4.14B) is rather typical of upwelling systems (e.g., *Pérez et al*., 2000; *Piedracoba et al*., 2008a) and depends on upwelling intensity as well as on pre-upwelling water-column stratification (*Álvarez-Salgado et al*., 1996b). The importance of transport during the upwelling simulation agrees with the general dynamics described by the S^* vs. F^* framework (Figure 3.12): phytoplankton biomass develops at moderate transport rate and ecosystem processes (i.e., local recycling of particulate organic matter) develop at low transport rate. However, the simulation also indicates that this cycle of production is more defined in the deep end side of Lunenburg Bay, where upwelled nitrate originates (Figure 4.14). The variation in transport rate during the upwelling controls the accumulation of phytoplankton in the outer part of the bay, whereas inshore, the limitation is more associated with the availability of nutrients in source waters.

Taken together, the results from the upwelling simulation and from Chapter 3 demonstrate that transport is a key process in the control of phytoplankton variability during periods of upwelling events in Lunenburg Bay.

4.4.3 The 'Bathymetry Effect'

An inshore-offshore gradient of phytoplankton response is simulated during the relaxation of the upwelling events in Lunenburg Bay; biomass accumulates toward the outer part of

the bay during this phase (Figure 4.12A). This spatial pattern was observed in the phytoplankton abundance and biomass data collected along the transect line (see Chapter 2). The factors contributing to this gradient were not investigated in Chapter 2, although several controlling processes were suggested, namely the inshore circulation patterns (e.g., *Álvarez-Salgado et al*., 1996b), the upwelling intensity (e.g., *Tilstone et al*., 1994), or the variations in residence time along the transect line (i.e., Chapter 3). While each of these processes will influence the spatial variability in phytoplankton biomass during the upwelling, the simulation suggests a more general controlling factor related to bathymetry; simply, if the water depth is shallow, it is not in contact with nutrient-rich water offshore, even during upwelling.

Several processes simulated in Lunenburg Bay during the upwelling have demonstrated a spatial variability between the inshore (shallow) and the outer (deep) areas of the bay: (1) the relationship between primary production and transport follows a well defined cycle of production in the outer bay but not in the inner bay (Figure 4.14); (2) the negative effect of pulse 1 is larger in the outer bay than in the shallow inner bay (Table 4.2); and (3) the relative phytoplankton response to the upwelling is small in the inner bay in comparison to the deep outer side of the bay (Table 4.2). This spatial variability does not necessarily imply an effect of bathymetry in these areas. However, a consistent pattern is found for the phytoplankton response in Lunenburg Bay, Mahone Bay and Saint Margarets Bay: the phytoplankton response is systematically larger at the deep sites (T5, X6, SMB) in comparison to the shallow sites (SB2, MB)(Figure 4.12B). This confirms the role of inshore bathymetry patterns in limiting the development of phytoplankton biomass during an upwelling event in Lunenburg Bay.

Although water column depth is the common factor that discriminates phytoplankton response at the different locations, it is not the main predictor for this response. The stations in Lunenburg Bay are located along a gradient of increasing depth. It is suggested that the main factors controlling the phytoplankton response are the depth at the entrance of the inlet and the slope of the bathymetry gradient inside the inlet. However, more work is required to test the effect of these two factors. The sensitivity of phytoplankton biomass to a shallower nitracline at the shallow sites (i.e., increased phytoplankton response) reveals that for Lunenburg Bay and Mahone Bay, the bathymetry effect limits the delivery

of upwelled nitrate to the shallow inshore areas during the upwelling event. Therefore, both the offshore nitrate concentration and the bathymetry of the inlet limit the development of nearshore phytoplankton biomass during periods of upwelling event. Data from the outside of Lunenburg Bay were not available during this study and therefore the collection of additional data in Mahone Bay and Saint Margarets Bay is required to support this interpretation.

4.4.4 Limitation from Nitrate Concentration in Upwelling Source Waters

The vertical position of the nitracline on the Scotian Shelf influences the effect of the upwelling event because it limits the transport of nitrate between Lunenburg Bay and the coastal ocean, and constrains the delivery of nitrate to the shallow inshore areas, limiting the phytoplankton response inshore.

The nitrate input simulated at the peak of the upwelling event in Lunenburg Bay is more than an order of magnitude lower than the values reported for an eastern boundary system such as the Rìa de Arousa (NW Iberian upwelling system, *Álvarez-Salgado et al*., 1996b). Although Lunenburg Bay is a smaller inlet, it results in a limited transport of nitrate through the bay during the simulation despite the occurrence of upwelling conditions. This limitation is relieved when a shallower nitracline is simulated on the Scotian Shelf. In this configuration, nitrate transport (horizontal and vertical) increases significantly in the bay (+224% and +243% respectively, see Table 4.3). This relationship between the depth of the nitracline on the shelf and nitrate transport in the bay is an important result because it indicates a general limitation to the effect of an upwelling due to the nitrate concentration available in upwelling source waters. This was established for steady state conditions in Chapter 3 (S^* vs. F^*, Figure 3.12). However, this steady state analysis lacks the temporal variability typical of an upwelling event (see Section 3.4.3). The upwelling simulation supports the findings from the steady state analysis and therefore extends these findings to the dynamical conditions characteristic of an upwelling event in Lunenburg Bay.

The ‘bathymetry effect’ revealed in the upwelling simulation and in the observations from Chapter 2 indicates that a spatial gradient in the phytoplankton response to upwelling

events is inherent to the upwelling dynamics of Lunenburg Bay. The positive of a shallower nitracline (S^+) on the phytoplankton response in the shallow inshore areas denote that the gradient is generated by the nitrate concentration available in upwelling source waters (in association with bathymetry). The low nitrate concentration available in the upwelling source waters therefore constrains the development of phytoplankton biomass during the upwelling event, in particular in the shallow inshore areas of Lunenburg Bay.

4.4.5 Generalization

4.4.5.1 Processes Relevant to Nova Scotian and Other Inlets

The upwelling-induced flushing of inlets along the Atlantic coast of Nova Scotia is a large scale process occurring throughout the Scotian Shelf (*Heath*, 1973). Nova Scotian inlets are then under the same forcing as Lunenburg Bay, which has implications for the dynamics of their biological systems. Therefore, which are the findings from the present work specific to Lunenburg Bay and that can be generalized at the regional scale (i.e., to the inlets along the Atlantic coast of Nova Scotia) or at larger scale?

(1) *Transport*. Upwelling-induced transport results in flushing (*Heath*, 1973) and nitrate input (*Platt et al*., 1972) at a regional scale in Nova Scotian inlets. However, the short upwelling event duration—that result in low nitrate retention efficiency—limits the effects of this transport. The spatial patterns of transport are however site-specific; they depend on the details of the local bathymetry (*Zhai et al*., 2008b) and are influenced by the local component of the wind (e.g., *Yang and Sheng*, 2008). The effect of transport on nitrate retention will therefore be modulated locally. The simulation indicates that the effect of transport vary spatially in Lunenburg Bay, with a more pronounced cycle of transport and production in the deep end side near the interface with the inner shelf (Figure 4.14). In other systems, this spatial variability will be modulated by the local bathymetry.

(2) *'Bathymetry effect'*. The 'bathymetry effect' revealed in the simulation is a general process that can be used to infer or to relate the upwelling response of Nova Scotian inlets to the local properties of the inlet (i.e., bathymetry patterns). This effect is associated with the vertical distribution of the nitracline on the Scotian Shelf, which depends on its biogeochemistry. The simulation indicates a nonlinear response to nitracline depth.

For inlets adjacent to slope-dominated continental margins where surface nitrate concentration is high during the upwelling season, bathymetry is therefore unlikely to have a limiting effect in inshore areas (e.g., *Brown and Ozretich*, 2009). However, for the inlets adjacent to shelf-dominated continental margins (i.e., with a deep nitracline), the limitation will depend on the depth of the nitracline, hence on the local biogeochemistry. It was suggested that bathymetry is a proxy for the mean depth at the entrance of the inlet and the slope of the bathymetry gradient. Their influence was not tested in this study and will need to be validated in future work. They will be useful criterias to assess the effects of coastal upwelling on nearshore coastal areas.

(3) *Limited nitrate in source waters*. The limitation due to nitrate concentration in source waters depends on the characteristics of the continental margin. On the Scotian Shelf, a relatively uniform distribution of nitrate is found at mid-depth in summer (2–4 mmol m^{-3} at 50 m, *Petrie and Yeats*, 2000). The present simulation and previous observations (*Platt et al*., 1972; *Petrie et al*., 1987) indicate that the development of upwelling conditions is a coast-wide phenomenon in the region. Nitrate concentration in upwelling source waters will therefore have a similar limiting effect on the other inlets of the region. In other western boundary inlets the limitation due to nitrate in upwelling source waters will depend on the shelf biogeochemistry, but aslo on the intensity of the upwelling events.

4.4.5.2 Implications of Longer Time Scales

The difference between the biogeochemistry of the Scotian Shelf (shelf-dominated margin, see definition in Section 1.1.2) and the biogeochemistry of eastern boundary margins (slope-dominated margins) was used in Chapter 3 to explain the biological dynamics in Lunenburg Bay in comparison to the dynamics observed in the west coast inlets. However, nitrate concentration also varies temporally in relation to multi-annual transport processes. Long-term variations in nitrate concentration have been observed on the central Scotian Shelf (offshore Lunenburg Bay) in relation to changes in water mass structure (*Petrie and Yeats*, 2000). Decadal variations in temperature and salinity are related to the transport of Labrador Slope Water onto the shelf (*Petrie and Drinkwater*, 1993). This transport is associated with an enhanced Arctic outflow during periods of low North Atlantic

Oscillation (NAO)(*Visbeck et al*., 2003). A lower nitrate concentration is associated to these events (*Petrie and Yeats*, 2000), resulting from the young age of the Labrador Sea waters. Therefore on the Scotian Shelf, the nitrate-density relationship will vary at a decadal time scale associated with the NAO. It is not known how these variations interact with nitrate concentration in upwelling source waters (i.e., change in the nitracline depth and/or in the slope of the nitrate-density relationship). If the nitrate variations occur within these waters, the anticipated effect on phytoplankton biomass in Lunenburg Bay should be similar to the anomalies observed in the sensitivity experiment. Since the transport of Labrador Slope Water onto the shelf has a negative effect on deep nitrate concentration, the subsequent change in the nitrate-density relationship should result in an enhanced limitation to the effect of upwelling events in Lunenburg Bay and other Nova Scotian inlets due to the low nitrate concentration in upwelling source waters (i.e., S^- case, Table 4.2).

Similar to the NAO effect, changes in water mass characteristics due to increased transport of Labrador Sea Water in the Scotian Shelf and Gulf of Maine area have been recently associated with global warming (*Townsend et al*., 2010). Such changes alter the nutrient regime on the shelf (ibid) and therefore may interact with upwelling source water (same effect as negative NAO). Furthermore, upwelling intensity is expected to vary under the influence of global warming (*Bakun*, 1990). Future upwelling intensity cannot be forecast presently and therefore its biological effect is not well known (e.g., *Varela et al*., 2008). Nonetheless, recent studies indicate the weakening of coastal upwelling conditions in the northeastern Atlantic due to the decrease in upwelling wind intensity (*Álvarez-Salgado et al*., 2008; *Pérez et al*., 2010). Such a change on the Scotian Shelf would result in the weakening of Ekman transport and therefore lower upwelled nitrate concentration during summer upwelling events. This would lower the effect of these events on inshore phytoplankton.

4.5 Conclusions

The simulation of an upwelling event in Lunenburg Bay revealed a limitation to the effect of upwelling on inshore phytoplankton biomass. This limitation results from the

four factors that were hypothesized: (1) the short duration of an upwelling event; (2) the upwelling-induced circulation; (3) the low nitrate concentration in upwelling source waters; and (4) the inlet bathymetry patterns (i.e., shallow inshore areas). The hypotheses were therefore verified by the results of the simulations. In complement to the general dynamics described by the S^* vs. F^* framework (nitrate availability in source waters vs. specific transport), this knowledge provides a relevant framework to better understand the constraints and implications of the development of upwelling events on inshore phytoplankton dynamics along the Atlantic coast of Nova Scotia. This is important to the management of local inlets and, furthermore, to evaluate the implications of global warming on the biological dynamics of Nova Scotian inlets.

Chapter 5

The MEPS-Bay Observatory: Experience from the Study

The MEPS-Bay interdisciplinary coastal observatory has provided real-time observations of meteorological and oceanographic conditions inside and outside Lunenburg Bay for the period 2002–2007 (dataset available at http://www.cmep.ca). The observatory was the core of the Lunenburg Bay project, which made a significant contribution to the understanding of coastal ocean dynamics in the region and generated the development of an interdisciplinary forecast capability of nearshore marine conditions. The main results and achievements of the project are discussed in *Cullen et al*. (2008). In this chapter, the coastal observatory is discussed with respect to the use and needs of data during the present investigations.

5.1 Use of the Dataset Available at the Observatory

The dominant control of wind-driven events on biological processes in Lunenburg Bay results in the requirement for high-frequency data collection in order to resolve the variability of the dominant biological processes. This time-scale can be achieved only through automated measurements, hence the importance of a coastal observatory to monitor and study the biological dynamics in this coastal systems. In addition to temperature and salinity, the collection of high temporal frequency bio-optical data at the moorings (frequency of 1 h^{-1}, reduced to 1 d^{-1}) and the development of an inverse bio-optical model to retrieve phytoplankton biomass (*Huot et al*., 2007) were important achievements of the MEPS-Bay project (*Cullen et al*., 2008). High-frequency measurements of temperature,

salinity and bio-optical properties have been essential to detect, characterize and measure the magnitude of the variability in phytoplankton biomass and nitrate concentration using simple tools (Figure 2.7) and enabled the inference of general patterns of variability in phytoplankton biomass in the bay at a multi-annual time scale (i.e., regression model, EOF). This variability was more difficult to characterize with the water samples (e.g., Figure 2.7).

Some of the analysis ($\widehat{\text{Chl}}$ analysis, Figure 2.8; NMDS, Figure 2.11–2.13) relied, however, on discrete ship-based measurements collected at the observatory (Chapter 2). There were three reasons for choosing to carry out these ship-based measurements:

(1) to collect the data which were not directly available from the buoys (nutrients, plankton species composition);

(2) to increase the spatial domain and the vertical resolution of the dataset; and

(3) to collect data outside Lunenburg Bay, which appeared to be essential to characterize the boundary conditions and to compute the nutrient-density relationship necessary to infer nitrate concentration inside the bay during upwelling events.

Buoy data on plankton species composition were not available during the investigations neither from proxies at the observatory, nor from the model output. The ship-based collection of discrete measurements of phytoplankton and zooplankton species composition was therefore essential to characterize phytoplankton and zooplankton assemblages. Nonetheless, if this analysis revealed important patterns, their interpretation was limited due to the low temporal frequency of the sampling. The inability to resolve the temporal variability associated with meteorological events was therefore a limitation to the ship-based measurements, due to the weekly sampling frequency during the routine sampling campaigns. This frequency is not sufficient to resolve the processes associated with phytoplankton variability nearshore. These measurements were also carried out outside periods of bad weather, which are characteristic of meteorological events. Even after a wind-driven event (e.g., Storm Event adaptive sampling), high sea state prevented sampling at the exposed X6 station outside of the bay. Ship-based measurements alone were thus inadequate to infer the processes regulating plankton dynamics in Lunenburg Bay. The coupling between buoy and ship-based measurements such as the development of

a nitrate-density relationship to infer nitrate concentrations from high-frequency density data measured at the buoys, was the only mean to describe the variability in nitrate concentration inside the bay during the investigations using a proxy derived from observations and modelling. Altogether, the combination of high-frequency (hourly) biophysical measurements at the buoys, spatially-resolved weekly ship-based sampling of biophysical and chemical data, and the development of spatially/temporally resolved biophysical models was therefore essential to the present investigations.

5.2 Need for Enhanced Measurements

Several limitations of the dataset from the observatory were revealed during the study. High-frequency measurements from the outside of Lunenburg Bay were not available in 2006 or during most of the MEPS-Bay operational time-period. Such measurements were only available from the SeaHorse moored profiler (*Fowler et al*., 1997) for a short period of time in early summer 2005. Given the dynamic coupling between inlets and the coastal ocean and the importance of the Scotian Shelf as a nitrate source to the Nova Scotian inlets, such a dataset, including high-frequency nitrate measurements, should be made available in the implementation of future inshore coastal observatories in the area to characterize the forcing from the coastal ocean (as illustrated by the S^* vs F^* framework, Figure 3.12), and to parameterize the coastal biophysical models used in these inlets. Inshore high-frequency nitrate measurements should also be collected to get an accurate representation of nitrate variability, including inshore sources. Such observations are important to understand phytoplankton dynamics (*Pitcher et al*., 2008). Sensors are now available for their continuous measurement at moorings (e.g. *Babin et al*., 2005; *Chang and Dickey*, 2008) and are included in the new generation of monitoring systems in Nova Scotian inlets, such as in the Bedford Basin (http://bbomb.ceotr.ca) or in the Northwest Arm (http://lobo.satlantic.com/loboviz).

The MEPS-Bay coastal observatory has provided a highly temporally resolved dataset of biophysical properties in Lunenburg Bay. The horizontal and vertical resolution were limited, however. Their importance was revealed during the sampling transects carried out weekly in 2006 that showed a spatial response in the response to the upwelling events,

with enhanced phytoplankton biomass in the deep end side of the bay where high frequency data were not collected (Figure 2.5). In fact, the position of the moorings in Lunenburg Bay did not match the inshore-offshore axis represented by the sampling transect (Figure 2.1). The results from the present study indicate however, that this inshore-offshore axis of increasing coupling and increasing depth toward the inner Scotian Shelf has a dominant role for the biology of Lunenburg Bay. The appropriate location of the moorings in future implementations of coastal observatories should be carefully investigated (e.g., from modelling studies) to account for the dominant factors controlling the biological dynamics of the system. The factors controlling plankton variability revealed in this study (e.g., upwelling events, bathymetry characteristics, accelerated flushing) can help in the design of future coastal observatories in similar, ocean-dominated inlets.

The 2006 transects and the SeaHorse measurements from 2005 also revealed the importance of vertically resolved biological data to detect the variability in phytoplankton biomass that can be located in a very restricted depth range. Fixed depth measurements have a limited ability to capture this variability (e.g., *Cullen*, 2008). The time series of estimated chlorophyll absorption from the moorings (*Huot et al*., 2007) or the vertically integrated samples of phytoplankton and zooplankton composition did not allow for the representation of vertical patterns in the plankton. For the plankton taxonomy dataset, the temporal resolution was also limited. This should be overcome in the near future with the development of new technology for coastal observatories, including metrics to infer phytoplankton at the group or species level and techniques for in situ identification of phytoplankton and zooplankton species (*Wiebe and Benfield*, 2003; *Babin et al*., 2005, 2008; *Sosik et al*., 2010). In association with spatially resolved sampling tools such as the SeaHorse profiler, it will improve the ability to observe the spatial response of the biological system to meteorological events at shorter time scales (< 7 days).

Finally, the adaptive sampling campaign carried out in August 2006 (Chapter 2) demonstrated the difficulty in implementing a ship-based adaptive sampling in an open system like Lunenburg Bay during the occurrence of a meteorological event and the impossibility to sample the full event (i.e. including the onset phase). This type of sampling is not sufficient to determine the effects of wind-induced events on marine ecosystems (*Schofield*

et al., 2008). Moreover, the high variability in meteorological conditions and the high-frequency response of the bay to wind events limit the possibility to forecast the timing of such a sampling campaign. The use of vertically profiling moorings such as the SeaHorse will reduce the need for adaptive sampling although the horizontal scale is limited with this type of mooring. The use of an autonomous underwater vehicle (AUV), which is particularly adapted to carry out adaptive sampling (*Chang and Dickey*, 2008; *Griffiths*, 2008), combined with the observing system, is therefore a more appropriate method to sample during this type of meteorological event.

Chapter 6

Conclusions

This thesis has investigated several processes that regulate summer plankton dynamics in a temperate coastal inlet. The starting point of the research was the observation of recurrent wind-induced upwelling and downwelling events in summer that control the local hydrography at a subtidal time scale (*Zhai et al*., 2007). However simultaneously, only low nitrate and chlorophyll concentrations were measured in the water samples collected at the MEPS-Bay observatory. This apparent discrepancy between the dynamic physical environment, in particular the occurrence of upwelling events, and the small variations in chlorophyll biomass suggested the existence of factors limiting the development of phytoplankton in Lunenburg Bay. Because of the deployment of the MEPS-Bay observatory, this bay was an appropriate site for the study of inlet-ocean coupling and its implications for the biological system of an inlet. Thence to improve our understanding of the factors regulating plankton variability in this inlet during the summer, this research aimed to:

(1) ***assess the drivers of variability in phytoplankton biomass and plankton community structure; and***

(2) ***reveal the main factors limiting the development of phytoplankton biomass inside Lunenburg Bay.***

To reach these objectives, a series of field sampling experiments were conducted in Lunenburg Bay (Chapter 2) and two types of physical-biological coupled model were constructed: a low resolution box model of Lunenburg Bay with steady state wind forcing (Chapter 3) and a high resolution nested model of Lunenburg Bay and the inner shelf (Chapter 4). The importance of upwelling events in driving the variability in phytoplankton biomass and the effects on plankton community structure were diagnosed

from the MEPS-Bay coastal observatory dataset in Chapter 2. It confirmed the recurrent upwelling events in summer, as well as the discrepancy—i.e., no strong response in chlorophyll concentration—and laid out several factors explaining the underlying causes of this discrepancy. The role of these factors, including transport that was not examined in Chapter 2, were investigated in the modelling studies of Chapter 3 and Chapter 4.

6.1 Factors Controlling Plankton Dynamics in Lunenburg Bay

Throughout the thesis, four factors appeared to regulate phytoplankton dynamics inside Lunenburg Bay: (1) the duration of an upwelling event, (2) the nitrate concentration in source waters, (3) the flushing rate of the inlet (hence transport), and (4) the bathymetry along the inshore-offshore axis of the bay. Regarding plankton communities, (1) the occurrence of upwelling and (2) the inshore-offshore gradient of increasing depth appeared to regulate the structure of respectively phytoplankton and zooplankton communities. Each regulating factor was developed into a hypothesis in Chapter 1. A summary of the hypotheses examined in this thesis and their validation from each chapter is presented in Table 6.1.

6.1.1 Dominant Drivers of Variability in Phytoplankton Biomass

The first step of this work was to examine if the variability in phytoplankton biomass is determined by the occurrence of meteorological events during the summer in Lunenburg Bay. The analysis in Chapter 2 revealed a direct relationship between:

(1) the variation in water column density (i.e., promoted by meteorological events) and chlorophyll biomass for the period 2003–2006;

(2) the variability in nitrate concentration and the occurrence of upwelling events; and

(3) upwelled nitrate and chlorophyll biomass.

These findings, that were also supported by the modelling studies of Chapter 3 (for both upwelling and downwelling wind regimes) and Chapter 4, corroborate earlier observations from Nova Scotian inlets (*Platt et al*., 1972; *Mitchell*, 1991). They demonstrate a

Table 6.1: Summary of support for the hypotheses from results presented in Chapter 2–4. A tick mark indicates a hypothesis supported by results from the chapter whereas a cross indicates a hypothesis not supported by the results from the chapter. The Results column indicates if the hypothesis is ✓ verified or × falsified. Refer to Section 1.5 for the full hypotheses.

		Chapters			
Description	Hypothesis	2	3	4	Results
	Drivers of variability in phytoplankton biomass				
Phytoplankton variability is independent of wind events	1.0	×		×	×
Phytoplankton variability is determined by wind events	1.1	✓		✓	✓
	Influence and limitations of upwelling events				
Significant effect of upwelling on phytoplankton biomass (i.e., ΔChl > 5 mg m^{-3})	2.0	×	×	×	×
No detectable upwelling effect on phytoplankton biomass	2.1	×	×	×	×
Low NO_3^- in source waters limits upwelling effect	2.2	✓	✓	✓	✓
Short upwelling events limits nitrate availability	2.3	✓		✓	✓
Bathymetry limits nitrate input from the shelf	2.4			✓	✓
	Physical constraint to phytoplankton accumulation				
Rapid flushing rate limits phytoplankton accumulation	3.0		✓	✓	✓
	Phytoplankton community structure				
Phytoplankton groups are determined by upwelling events	4.0	✓			✓
	Zooplankton community structure				
Zooplankton communities are determined by upwelling events	5.0	×			×
Zooplankton communities are structured spatially	5.1	✓			✓

consistent multiannual pattern in Lunenburg Bay that agrees with the concept of inshore biological systems dominated by remote processes in the region (i.e., occurring on the shelf, *Lewis and Platt*, 1982) and hence by inlet-ocean coupling.

The time series from the observatory (Chapter 2) and the modelling study of the 2006 upwelling event (Chapter 4) revealed that upwelling conditions in Lunenburg Bay have successively opposite effects on the local phytoplankton biomass due to the flushing of the bay with nitrate-enriched—but phytoplankton-poor—deep water from the shelf. This effect is typical of upwelling environments (e.g., *Brown and Field*, 1986; *Zimmerman et al*., 1987) and is an important driver of phytoplankton variability in Lunenburg Bay on the time scale of days to weeks.

6.1.2 Influence and Limitations of Upwelling Events

Despite the role of upwelling events in controlling the variability of nitrate concentration and phytoplankton biomass, the limited range of variability in chlorophyll biomass observed in the preliminary dataset was confirmed by the sampling experiments in 2006 as well as by the optical measurements from the observatory for the period 2003–2006. Therefore, the question is: which factor limits the development of a phytoplankton bloom during an upwelling event in Lunenburg Bay?

Low nitrate concentration in upwelling source waters

The limitation due to low nitrate concentration in upwelling source waters was demonstrated from the observatory dataset that indicates a modest variation in nitrate concentration during an upwelling event in Lunenburg Bay (0–3 mmol m^{-3}) and a corresponding change in chlorophyll biomass ($\widehat{\text{Chl}}$ analysis, Section 2.3.2). The limitation to the development of phytoplankton biomass was attributed to the depth of the nitracline on the Scotian Shelf (sensitivity analysis, Section 4.3.5). The limitation of phytoplankton biomass by low nitrate concentration in the inlet source waters was generalized on the S^* vs. F^* framework (nitrate availability in source waters vs. specific transport, Section 3.3.4.2).

The cause for low nitrate concentration in upwelling source waters was attributed to the shelf-dominated continental margin (*Jahnke*, 2010) that characterizes western boundary

margins such as the Scotian Shelf. The consequence of long term variation in nitracline depth, resulting from changes in water mass associated to decadal oscillations or global warming, was suggested to be a stronger limitation to the effect of upwelling events in Lunenburg Bay due to a deepening of the nitracline on the Scotian Shelf.

Short duration of an upwelling event

The short duration of an upwelling event was found to limit the development of phytoplankton biomass inside Lunenburg Bay for two reasons:

(1) the sustained upwelling events (time scale $\geqslant$ 4 days) were associated with the development of upwelling conditions in Lunenburg Bay and the shoaling of the nitracline, but not the storm-induced upwelling event with a shorter time scale ($\sim$ 1 days); and

(2) the characteristic time scale of a sustained upwelling event ($\sim$ 4 days) is short, especially compared to the time lag for the phytoplankton response to the upwelling (2.7 days, Section 2.3.4). The availability of upwelled nitrate to primary producers is thus limited in time, and as a consequence nitrate retention during an upwelling event is low in Lunenburg Bay.

Bathymetry characteristics of Lunenburg Bay

The observations from Chapter 2 and the modelling experiment of Chapter 4 have demonstrated a limited response and an inshore-offshore pattern of increasing phytoplankton biomass during the upwelling relaxation due to the lack of upwelled nitrate reaching the shallow inshore area. This effect was correlated with depth (Figure 4.12B): a small response in the shallow inshore areas, and a significant response in the deep outer areas. This relationship was supported by the modelled results from the neighbouring inlets. However, given the characteristics of the inlets used in the relationship (gradual change in depth from inshore to offshore or similar depth inside and at the mouth of the inlet), it is suggested that depth is a proxy but not the real explanatory variable for this effect. Two other explanatory variables have been proposed—but not tested—that are the depth at the entrance of the inlet and the slope of the bathymetry gradient inside the inlet. Future work will be necessary to test their effect.

Wind-induced accelerated transport

A direct relationship between upwelling conditions and accelerated transport of nitrate and phytoplankton was demonstrated in the upwelling simulation (Chapter 4). The accelerated transport of phytoplankton from the bay was a limiting factor to the development of a self-supporting bloom inside Lunenburg Bay during each pulse of the upwelling, but not during the relaxation phase when transport rate was reduced. In Lunenburg Bay, phytoplankton export dominates during the active phase of the upwelling, whereas local primary production is dominant during the relaxation phase of the upwelling (Figure 4.14); the other sources of limitation prevail during this phase. The limitation associated with accelerated transport during the active phase of the upwelling was also demonstrated by the steady state box model experiment (Chapter 3) that revealed an accelerated flushing of Lunenburg Bay induced by upwelling wind forcing controlling the accumulation of phytoplankton biomass in the bay (Section 3.3.2.3).

6.1.3 Seasonal Variability in Plankton Communities

The dataset collected during 2006 (Chapter 2) has revealed that inside Lunenburg Bay, the patterns of variability in phytoplankton and zooplankton species composition (spatial and temporal) differ and are controlled by different processes: phytoplankton community structure tends to be spatially homogeneous and to vary temporally with the occurrence of upwelling events, whereas the zooplankton community is structured spatially along a depth gradient but not substantially influenced by upwelling events.

Phytoplankton groups are determined by the occurrence of upwelling events

Phytoplankton community structure oscillated between periods dominated by dinoflagellates species in pre-upwelling conditions during a sustained period without nitrate input from the Scotian Shelf, and mixed assemblages dominated by diatoms following the occurrence of an upwelling event. The event favoured the development of diatoms and therefore determined which of the diatoms or dinoflagellates group prevailed during the period of study. Pre-existing conditions, such as previous upwelling or time without nitrate supply to the bay, determine if the dinoflagellates group prevails prior to the upwelling. Overall, although some gaps in the dataset prevent this observation to be conclusive, the patterns of variability in phytoplankton community structure seem to occur bay-wide.

Zooplankton communities are structured along an inshore-offshore gradient

The dominant species of zooplankton vary in time during the summer, but space is the main structuring factor among the zooplankton assemblages. The community changes gradually along an inshore-offshore gradient of increasing depth. The underlying causes of this spatial pattern were not investigated in the thesis. It was suggested that inshore, a selective predation and the restricted vertical habitat due to the shallow depth may control the occurrence of zooplankton species (*Kimmerer*, 1991, 1993; *Ueda*, 1991) and select for species with restricted migratory behaviour, such as *Acartia* spp. (*Tiselius*, 1998). This pressure on vertically migrating species is relieved in the deeper waters outside Lunenburg Bay.

The occurrence of upwelling events did not change significantly this dominant spatial structure. This was interpreted in three different ways, not mutually exclusive: (1) the limited increase in phytoplankton biomass imposes a constraint on the grazers; (2) the duration of an upwelling is short considering the typical turnover timescale of nearshore copepods (*Kimmerer*, 1993 and references therein); and (3) vertical migration can induce a spatial discontinuity between phytoplankton and zooplankton during an upwelling event (*Walsh*, 1976), which results in a decoupling between primary and secondary production. The sampling frequency and the vertically integrated measurements did not allow for sorting out the underlying factors.

6.2 Significance of the Results

The thesis was focused on Lunenburg Bay, a small inlet of the Atlantic coast of Nova Scotia. Then, how are the findings regarding the processes regulating plankton variability in Lunenburg Bay relevant to other systems of the region? Moreover, how does this work contribute to the general knowledge of plankton dynamics in coastal systems?

6.2.1 Applicability of Key Findings at Larger Scale

The dominant source of variability in summer in Lunenburg Bay arises from the development of upwelling conditions at the coast. This phenomenon controls the flushing of

Nova Scotian inlets (*Heath*, 1973) and influences their nutrient variability (*Platt et al.*, 1972). Phytoplankton variability in these systems is therefore under a similar control to Lunenburg Bay: the synoptic wind forcing and its characteristics (northeastward direction, short event duration); the low nitrate concentration in upwelling source waters; the effect of bathymetry; as well as rapid transport associated with accelerated flushing. Transport patterns are however induced by the combination of local and remote wind (e.g., *Yang and Sheng*, 2008) and the interaction with local bathymetry (*Zhai et al.*, 2008b). This aspect is therefore inherent to the inlet. Overall, most of the processes that were found to control phytoplankton dynamics in Lunenburg Bay then apply to the other inlets of the region. This generalization is important because the current findings can then be used to:

(1) define the current state of phytoplankton dynamics in Nova Scotian inlets;

(2) assess their main drivers of variability; and

(3) determine potential impacts, including the effects of climate change.

This knowledge will be useful in the future development of integrated management initiatives for coastal and inshore areas of Atlantic Nova Scotia (*DFO*, 2007).

The tools that were developed during this thesis to investigate the dynamics of phytoplankton in Lunenburg Bay are transferable to other inlets. The regression model for phytoplankton biomass developed in Chapter 2 (Section 2.3.4) is a simple tool but has demonstrated some predictability based on simple measurements (temperature, salinity). Given the large-scale processes controlling phytoplankton variability in Nova Scotian inlets (i.e., *Platt et al.*, 1972; *Lewis and Platt*, 1982), this tool can be used to diagnose and potentially forecast—in combination with other tools—phytoplankton variability in other inlets of the region. Similarly, the nutrient source - flushing rate framework (S^* vs. F^*) developed in Chapter 3 to assess the role of nutrient source and flushing rate in controlling plankton dynamics in Lunenburg Bay (Section 3.3.4.2), can be used to describe the dynamics of other systems (see Section 6.2.2 below).

6.2.2 The Nutrient Source - Flushing Rate Framework (S^* vs. F^*)

The dimensionless framework (S^* vs. F^*) was developed in Chapter 3 to support the hypotheses of a limitation to the effect of an upwelling event due to the nitrate concentration

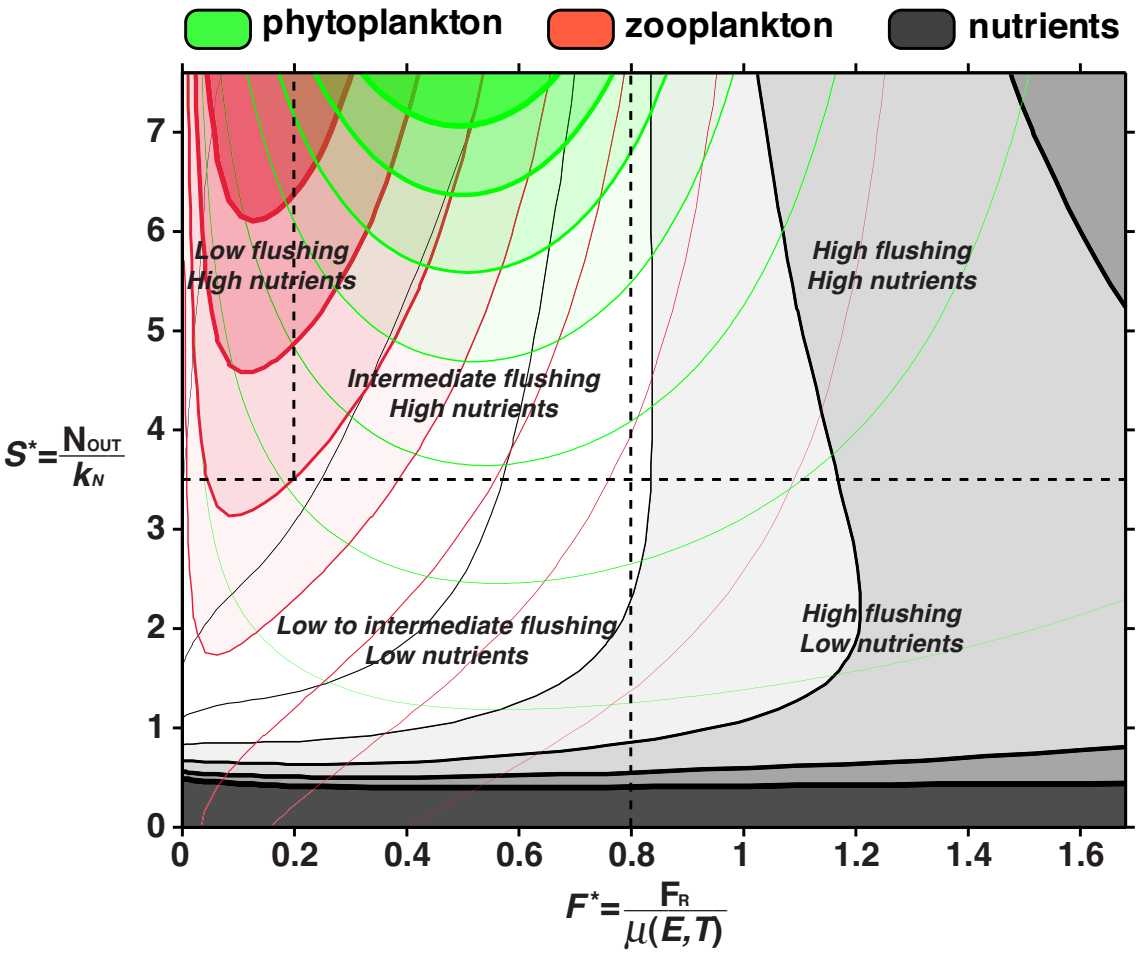

Figure 6.1: Effect of flushing (F^*) and nutrient availability in source waters (S^*) on the relative concentration of phytoplankton (green), zooplankton (red) and nutrients (grey) inside an inlet (i.e., X^*_P, X^*_Z and X^*_N, see Section 3.2.5.2). The relative concentration (X^*) is the ratio between the concentration inside and at the boundary of the inlet. Flushing (F^*) is the ratio between the flushing rate (F_R; d^{-1}) and the light (E; W m^{-2}) and temperature (T; °C) limited growth rate of phytoplankton ($\mu(E,T)$; d^{-1}). Nutrient availability in source waters (S^*) is the ratio between nitrate concentration at the boundary (N_{OUT}; mmol m^{-3}) and the half-saturation constant for nutrient uptake by phytoplankton (k_N; mmol m^{-3}). The colour scale for X^* is indicative only (darker colours represent higher values of X^*). A more detailed and quantitative figure is presented in Chapter 3 (Figure 3.12).

in upwelling source waters and the accelerated flushing associated with the upwelling. Although this framework is simple with regards to the complexity of coastal processes (steady state conditions, pelagic ecosystem only), it conceptualizes the influence of rapid transport and low nutrient available in source waters on the dynamics of the biological system in Lunenburg Bay (see Figure 6.1). Because of the scaled variables, this framework is not specific to Lunenburg Bay but rather represents a general model of plankton dynamics in coastal inlets and other aquatic systems for which chemostat dynamics is a reasonable approximation. It has enabled to extend the limiting factors revealed in Lunenburg Bay (i.e., flushing and nutrients) to other Nova Scotian inlets under the same forcing conditions. Moreover, it is a useful tool to compare the dynamics revealed in Lunenburg Bay with other systems and therefore to formalize general controls over plankton dynamics in inshore systems.

Overall, the framework indicates (Figure 6.1):

(1) a general limitation in Nova Scotian inlets due to the low nutrient concentration in source waters; this is opposed to the dynamics of eastern boundary inlets where upwelling events have an important effect on inshore phytoplankton (i.e., through transport or local production);

(2) an optimum 'window' for the accumulation of phytoplankton biomass at intermediate flushing and high nutrient in source waters; and

(3) the development of secondary producers (and internal recycling processes) at low flushing.

A framework-data comparison will be necessary in the future to evaluate the exactitude of the dynamics indicated in the framework and to assess its limitations. Flushing is calculated from the volumetric flow rate and therefore this variable must be known. It can be calculated with data from moored current sensors or derived from CTD measurements (e.g., *Rosón et al*., 1997). Nitrate in source waters can be derived from moored nitrate sensors or water samples on the inner shelf and the knowledge of circulation patterns at the inlet-coastal ocean interface—as demonstrated with the wind regimes in Chapter 3. Further development of the framework is also suggested to include benthic grazing that

can influence or control phytoplankton biomass in an inlet (e.g., *Cloern*, 1982; *Lucas et al*., 1999a).

6.3 Future Work and Perspectives

This thesis has investigated the processes controlling plankton dynamics in Lunenburg Bay, with respect to the inlet-ocean coupling. This source of variability is dominant in this system in summer, and in similar inlets of the region. Nonetheless, the role of land-inlet and benthic-pelagic coupling should be investigated in the future. The hydrodynamic control on nitrate input has been well established in the study; its importance is described in the S^* vs. F^* framework. However, during periods of slow flushing local biological processes dominate and recycling becomes more important (Figure 4.14). Nutrient recycling in the sediment may alter nutrient retention during these periods and therefore influence local phytoplankton dynamics. Further development of the S^* vs. F^* framework should also include this process or at least assess its contribution to plankton dynamics in the low F^* range (i.e., long flushing time scale).

Using weekly measurements, the thesis has revealed a temporal variability in phytoplankton groups (diatoms/dinoflagellates) and a spatial structure in the zooplankton community of Lunenburg Bay, suggesting the presence of a spatial component in the foodweb structure. Higher resolution time series (i.e., increased sampling frequency) of phytoplankton species composition should be collected, using simple automated in-situ platforms and new metrics to characterize phytoplankton communities (e.g., *Babin et al*., 2008), in order to assess the high-frequency response to upwelling events. Specific work should also be conducted to elucidate the underlying cause for the spatial structure in the zooplankton community (e.g., vertical migration, selective grazing, food source). It is also suggested to investigate the role of the spatial component in the foodweb and to assess its effect on the results of biogeochemical models of the nearshore environments.

Lower nitrate concentration in upwelling source water was suggested as a potential effect of global warming on Nova Scotian inlets. This is a hypothetical effect, considering the present findings and the current knowledge of the impacts of global warming on the

western Atlantic margin. With regards to coastal management, future work should be developed to address the specific effects of global warming on Nova Scotian inlets. The development of a regional forecasting capability using nested models, such as the ones used in this study, will be useful to assess these effects. The expertise gathered in the present work can be used for the development of these models. Improvements from the present model will be necessary to better represent the short time scale response of the phytoplankton to the meteorological events.

Appendix A

Coastal Upwelling

A.1 Ekman Layer

The Ekman layer is the frictional boundary layer developing on a geostrophic flow. It occurs both at the surface and the bottom of the ocean resulting from frictional stress prescribed by the surface wind and the bottom boundary respectively. Wind-driven surface currents in the ocean are the result of this process: the balance between frictional forces and the Coriolis effect in the surface boundary layer. The solution to this balance can be calculated for idealistic conditions, i.e. no temporal variation or horizontal gradient, an homogeneous fluid, and an infinite ocean. In the northern hemisphere, for a geostrophic flow ($\bar{u}$, $\bar{v}$; m s^{-1}) under a surface wind stress (τ^x, τ^y; N m^{-2}), the velocity field (u, v; m s^{-1}) in the surface Ekman layer of depth D_E (m) is as follow:

$$u = \bar{u} + \frac{1}{\rho\sqrt{A_\nu f}}\, e^{z/D_E}\left[\tau^x \cos\left(\frac{z}{D_E} - \frac{\pi}{4}\right) - \tau^y \sin\left(\frac{z}{D_E} - \frac{\pi}{4}\right)\right] \tag{A.1}$$

$$v = \bar{v} + \frac{1}{\rho\sqrt{A_\nu f}}\, e^{z/D_E}\left[\tau^x \sin\left(\frac{z}{D_E} - \frac{\pi}{4}\right) + \tau^y \cos\left(\frac{z}{D_E} - \frac{\pi}{4}\right)\right] \tag{A.2}$$

where ρ (kg m^{-3}) is the water density, A_ν (m^2 s^{-1}) is the vertical eddy viscosity coefficient (constant), f (s^{-1}) is the Coriolis parameter, z is depth. The solution for periodic wind forcing can be found in *Cushman-Roisin and Beckers* (2011).

The depth of the Ekman layer is expressed as follow:

$$D_E = \sqrt{\frac{2A_\nu}{f}} \tag{A.3}$$

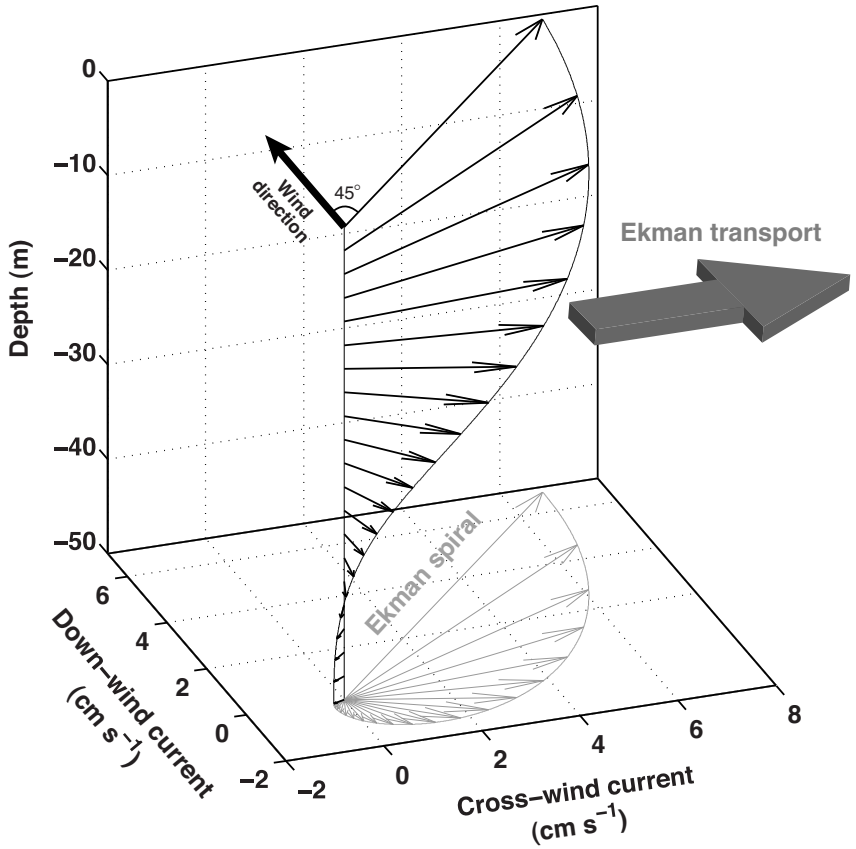

Figure A.1: Velocity field in the surface Ekman layer (black) and representation of the Ekman spiral (grey) at 45° latitude for a wind stress along the y-axis $\tau^y = 0.1$ N m^{-2}, a water density $\rho = 1025$ kg m^{-3} and an eddy viscosity coefficient $A_\nu = 10^{-2}$ m^2 s^{-1}. The depth-integrated Ekman transport perpendicular to the wind direction is represented by the grey arrow.

The resulting depth-integrated zonal and meridional mass transport (M_x, M_y; kg m^{-1} s^{-1}) in the Ekman layer is:

$$M_x = \int_{-\infty}^{0} \rho\,(u - \bar{u})\,dz = \frac{\tau^y}{f}, \tag{A.4}$$

$$M_y = \int_{-\infty}^{0} \rho\,(v - \bar{v})\,dz = -\frac{\tau^x}{f}, \tag{A.5}$$

which indicates that Ekman transport is perpendicular to the surface wind stress. The velocity field in the Ekman layer for $\bar{u} = \bar{v} = 0$ is represented in Figure A.1.

Deviation from these idealized conditions often occur. Strong surface stratification

induces a two layer system where Ekman transport is restricted to the mixed layer. At mid latitude the diurnal heat flux cycle reduces the Ekman layer further, which is surface trapped with an accelerated flow and enhanced deflection of velocity with depth (*Price and Sundermeyer*, 1999).

A.2 Coastal Upwelling

When the wind is oriented alongshore, with the coast on the left (right) in the Northern (Southern) Hemisphere, offshore Ekman transport induces low pressure at the coast, compensated by an onshore and upward movement of deep water at the coast. Under sustained wind forcing, the pycnocline reaches the surface at the coast, which creates a front that moves offshore to a distance dependent on the wind speed (*Csanady*, 1982). The cross-shore distance over which the pycnocline rises to the surface is the Rossby radius of deformation (R), in the order of 10 km, at which rotational and inertial forces are equal. For Nova Scotia Atlantic coast, *Petrie et al*. (1987) reported a value $R = 6.8$ km.

The onshore pressure gradient resulting from the tilting of the isopycnals is compensated by an alongshore geostrophic current oriented with the wind. The average velocity field from the ROMS model (Chapter 4) for the period June 29–July 2, 2006 during the upwelling event (pulse 1) provides an example of upwelling-induced cross-shore and alongshore currents during the period investigated (Figure A.2).

Alongshore variability in bathymetry results in spatial variability in upwelling conditions that can be restricted to specific areas (upwelling centers) and the development of offshore jets of upwelled water (*Flament et al*., 1985). The interaction with a slopping bathymetry (*Smith*, 1981), buoyancy intrusions (*Tilburg and Garvine*, 2003) or fluctuating winds (*Cushman-Roisin and Beckers*, 2011) are also a source of deviation from the simple coastal upwelling case and therefore generate variability in the upwelling. Localized upwelling can generate internal Kelvin waves that propagate alongshore.

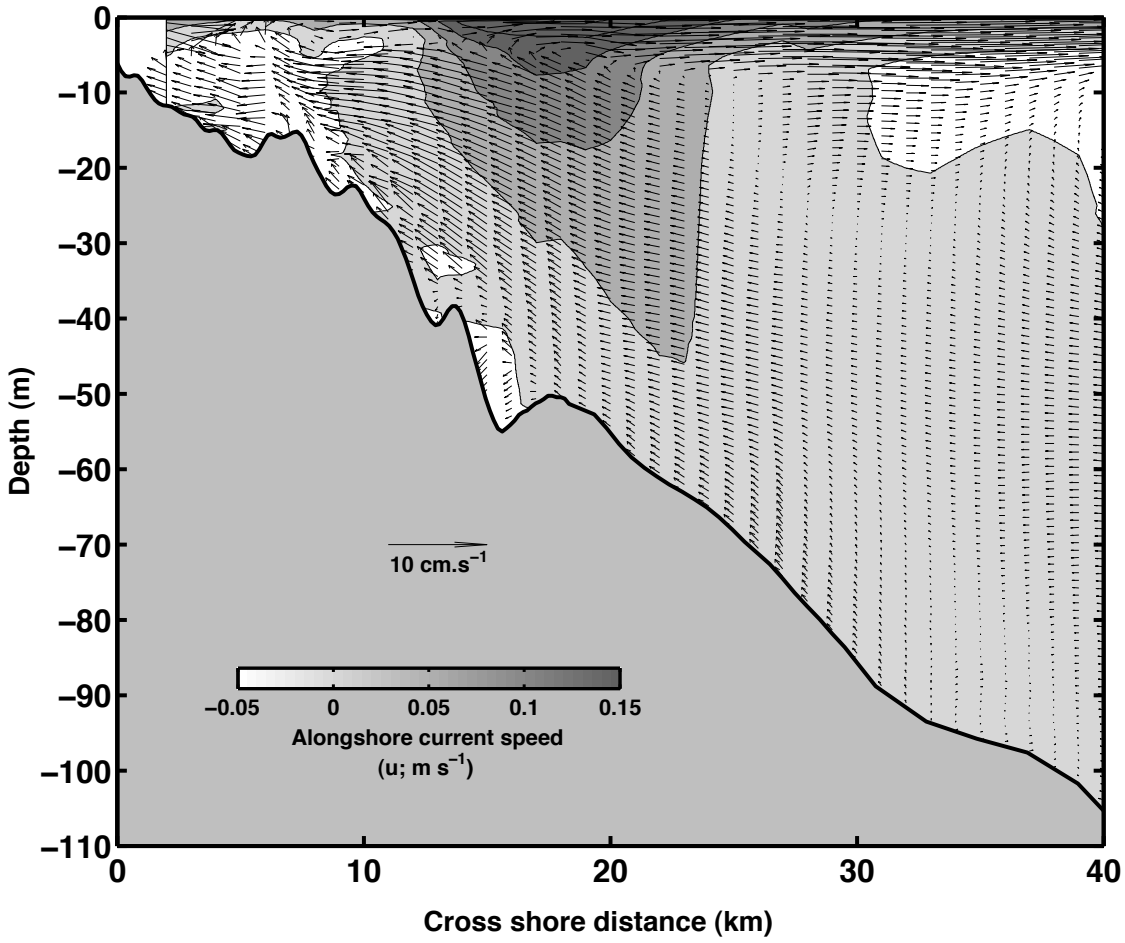

Figure A.2: Average velocity field from the ROMS model (Chapter 4) for the period June 29–July 2, 2006 (day 180–183) during the upwelling event (pulse 1). The arrows represent the cross-shore velocity field, which indicates an offshore transport at the surface and an onshore transport underneath near the coast. The contour plot represents the along-shore velocity field and indicate the position of the coastal jet. The along-shore current is positive northeastward (into the page).

Appendix B

Empirical Orthogonal Functions

In addition to the regression analysis carried out in Chapter 2, the patterns of variability in the high frequency time series were analyzed statistically at the mooring stations SB2 and SB3 (Figure 2.1) by calculating empirical orthogonal functions (EOF). The dataset is the same as in Chapter 2, including years 2003 to 2006 (see Section 2.2.4.3), complemented by cross-shore and alongshore wind stress (τ_c, τ_a; N m^{-2}) for Battery Point meteorological station and bottom cross-shore current (u_c; m s^{-1}, 330° inshore-offshore direction and positive toward inshore) calculated from current velocities recorded at the moorings (7.5 m at SB2, 9 m at SB3). The variables are described in Table B.1.

B.1 Method for Calculating the EOF

The time series were low pass filtered, using a zero-phase forward and reverse digital filtering, with a cut-off at 26 h to remove the tidal signal. The series were detrended, their mean removed and then normalized by their standard deviations.

The EOF analysis was carried out on the normalized time series matrix (M) at each mooring using singular value decomposition (SVD, *Emery and Thomson*, 1998). The SVD technique decomposes the $m \times n$ data matrix into a factorial form such that:

$$M = U \cdot D \cdot V^T \tag{B.1}$$

where U and V are respectively $m \times m$ and $n \times n$ orthonormal matrices and D is a $m \times n$ diagonal matrix. The principal components (EC, expansion coefficients) and the eigenvalues

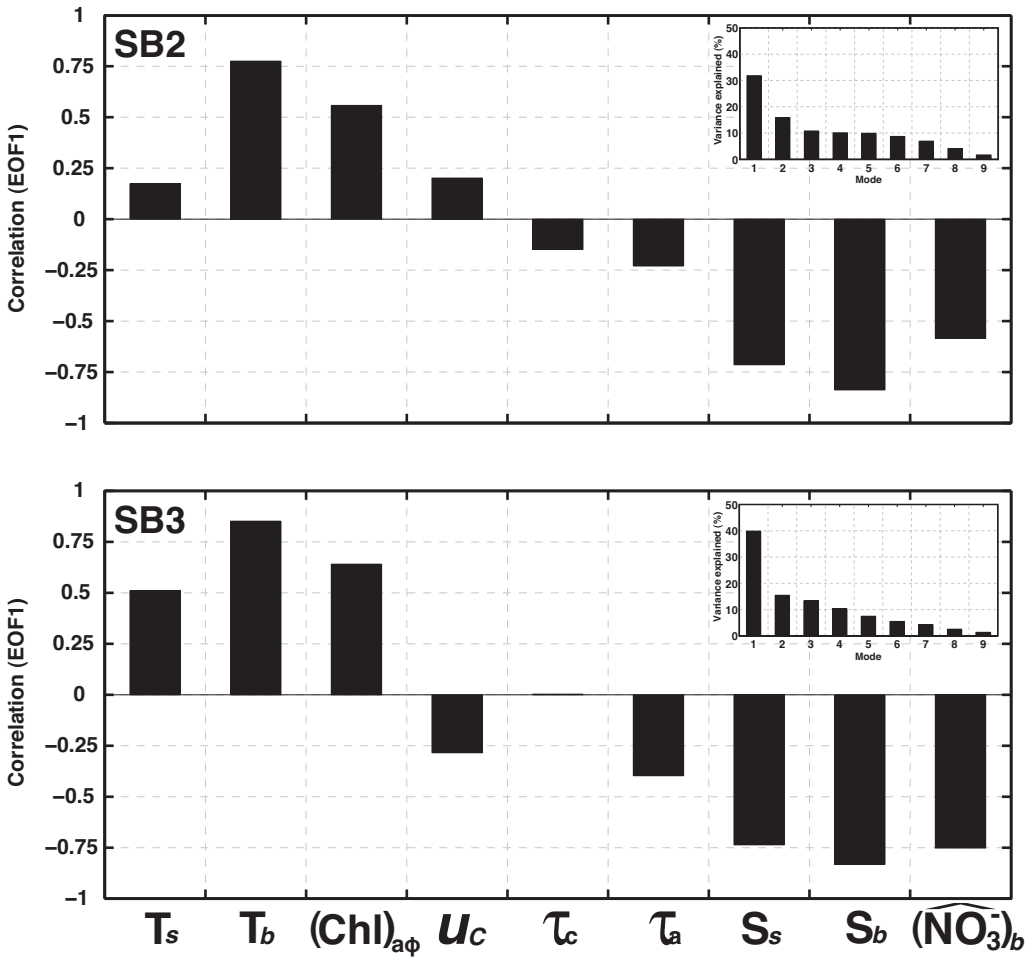

Figure B.1: Correlations between the explanatory variables and the first mode of the EOF analysis (EOF1) for SB2 and SB3 locations. The top right corner of each figure indicates the percentage of variance explained by each mode, 32% and 40% of the variance for EOF1 at SB2 and SB3 respectively. The variables are described in Table B.1.

(L) are obtained from the following relationships:

$$EC = U \cdot D \tag{B.2}$$

$$L = \frac{diag\,(D)^2}{n-1} \tag{B.3}$$

The amount of variance VAR (%) explained by each principal component is then given by:

$$VAR = \frac{L}{n} \times 100 \tag{B.4}$$

The first two modes of the EOF are plotted in Figure B.1.

B.2 Results

The dominant part of the variance in the dataset is explained by the first mode of the analysis (EOF1, Figure B.1). The variance explained by the other modes is less significant (Figure B.1) and therefore the patterns emerging from these modes are not interpreted. The first mode (EOF1) explains more variance at SB3 (40%) than at SB2 (32%) and is associated with the change in salinity and temperature (especially bottom temperature). The nitrate anomalies are positively correlated to salinity anomalies along EOF1, but inversely correlated to chlorophyll and temperature anomalies. The patterns are stronger at SB3 than at SB2. Water velocity and wind stress did not show a strong relationship with the other variables along EOF1. The lag between the wind forcing and the hydrodynamic response of the bay (e.g. upwelling conditions) can explain the lack of a strong relationship with the alongshore wind stress. The lack of relationship with bottom current speed is more surprising but indicates that other processes control its variability.

Overall, this analysis supports the results of the phytoplankton biomass prediction model in Chapter 2 and suggests a spatial variability in the effect of upwelling events and changes in hydrography on nitrate and chlorophyll concentration, which is more important at the mid-bay mooring station SB3 compare to the inshore mooring SB2.

Table B.1: Variables used for the EOF analysis.

Variable	Symbol	Units	Location	Depth (m)
Surface temperature	T_s	°C	SB2/SB3	1*
Bottom temperature	T_b	°C	SB2/SB3	8/9
Surface salinity	S_s	°C	SB2/SB3	1*
Bottom salinity	S_b	°C	SB2/SB3	8/9
Cross-shore current	U_C	m s^{-1}	SB2/SB3	7.5/9
Nitrate	$\widehat{(NO_3^-)}_b$	mmol m^{-3}	SB2/SB3	8/9
Chlorophyll	$(Chl)_{a_\phi}$	mg m^{-3}	SB2/SB3	depth integrated
Alongshore wind stress	τ_a	N m^{-2}	BatPt	-
Cross-shore wind stress	τ_c	N m^{-2}	BatPt	-

*The surface sensor was located at 3 m in 2003

Appendix C

Box Model Fluxes

C.1 Advective Fluxes

C.1.1 Horizontal Advective Fluxes

For each circulation regime, advective fluxes are computed every $\Delta t = 10$ minutes during the last tidal cycle of the circulation model run. Horizontal advective fluxes are computed for every vertical layer at each grid cell located on a boundary (Figure C.1). The resulting horizontal advective flux (Q^h_{adv}; $m^3\ s^{-1}$) through each boundary is calculated such as:

$$Q^h_{adv}(i,l,t) = \sum_{j=1}^{n}\sum_{k=1}^{m}(\upsilon_{j,k,t} \cdot \Delta L_i \cdot \Delta z_{l,k}) \tag{C.1}$$

where $\upsilon_{j,k}$ is the horizontal advection normal to the boundary ($m\ s^{-1}$), ΔL_i is the cell fraction of the boundary length and $\Delta z_{l,k}$ is the height of the vertical level. Also, i represents the horizontal boundary (1–11), l the layer (upper or lower), t time, n the number of grid cells in the boundary and m the number of vertical levels in the layer. The height of the z-levels in the circulation model are as follow: $\Delta z = 3$ m at the surface, $\Delta z = 1$ m down to 20 m and $\Delta z = 4.5$ m for the remaining layers inside the domain of interest. Therefore, $m = 3$ for the upper layer and $2 \leq m \leq 18$ for the lower layer depending on the maximum depth of the boundary. A schematic of the bay with the various parameters is presented in Figure C.1.

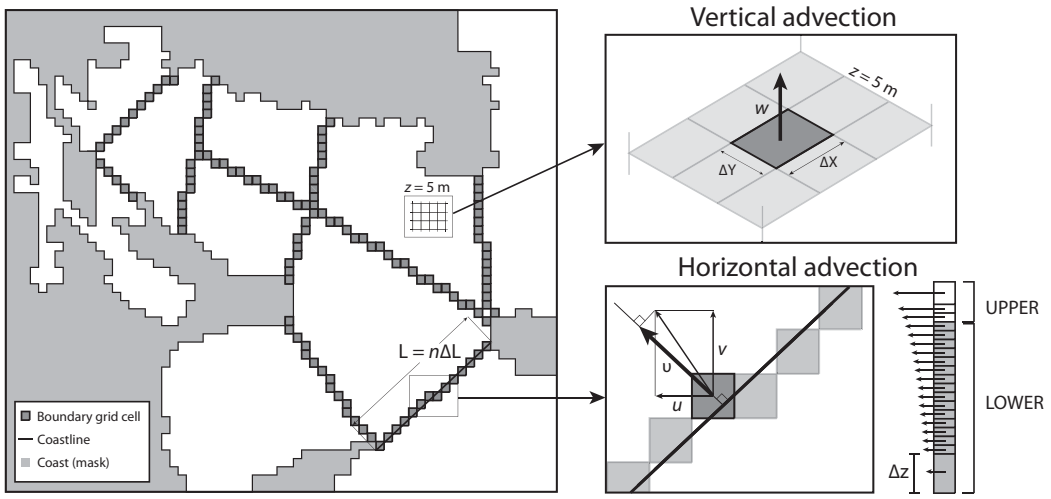

Figure C.1: Schematic of the computation of horizontal and vertical advective fluxes in the box model used in Chapter 3. Δx, Δy, Δz (m) are, respectively, the width, height and thickness of a model grid cell. Horizontal advective fluxes are calculated at each grid cell on a boundary. L (m) and n are respectively the length and number of grid cell in a boundary. $\Delta \mathrm{L}_i$ is the cell fraction of the boundary length. $\upsilon_{j,k}$ (m s^{-1}) is the horizontal advection normal to the boundary calculated from the eastward (U, m s^{-1}) and northward (V, m s^{-1}) components of horizontal advection in the circulation model. Vertical advective fluxes are calculated at z = 5 m for each grid cell from the vertical velocity (W, m s^{-1}).

C.1.2 Vertical Advective Fluxes

The vertical advective fluxes are computed from the vertical velocity values (w) of the circulation model at the boundary between the upper and the lower layer of the box model (z = 5 m) and for every cell within a box (see Figure C.1, upper right panel). The resulting vertical advective flux (Q^v_{adv}; m^3 s^{-1}) through each vertical boundary is calculated such as:

$$Q^v_{adv}(i,t) = \sum_{j=1}^{n} (w_{j,t} \cdot \Delta x \cdot \Delta y) \tag{C.2}$$

where $w_{i,t}$ is the vertical advection at 5 m (m s^{-1}), Δx is the width of the grid cell and Δy is the length of the grid cell. Also, i represents the vertical boundary (1–8), t time and n the number of grid cells within each box. If $z_j \leq 5$ m, then $w_j = 0$.

C.1.3 Corrections

The sea surface height varies in the circulation model. The volume of the upper boxes is therefore adjusted at every time step to take into account the variation in sea surface height. The sum of all advective fluxes in each box is computed at every time step and the variation in box volume between t and $t + \Delta t$ is compared with the variation in volume due to the change of advective fluxes over the same period. This procedure is necessary to make sure the flows are balanced. Small errors induced by the computation of advective fluxes are removed by correcting each box boundary flows proportionally to their values. The corrections are carried out stepwise, from the inner to the outer boxes. Once corrected the values are fixed for that box and the procedure continue in the next box. All fluxes were balanced prior to their use in the box model (see the tidally average fluxes in Figure 3.3).

The advective fluxes Q^h_{adv} and Q^v_{adv}, across each boundary, are subsequently divided by the volume of the boxes to retrieve the exchange rates (r_{adv}; d^{-1}) used for the box model simulations.

C.2 Diffusion

Horizontal diffusion coefficients from individual grid cells of the circulation model were used to calculate the horizontal diffusive flux (Q^{h}_{diff}; $m^3 s^{-1}$) at every time step on each layer of each boundary such as:

$$Q_{diff,h}(i,l,t) = \sum_{j=1}^{n} \sum_{k=1}^{m} \left(kh_{j,k,t} \cdot \frac{\Delta L_i \cdot \Delta z_{l,k}}{\Delta l} \right) \tag{C.3}$$

where $kh_{j,k,t}$ ($m^2\ s^{-1}$) is the horizontal diffusion coefficient in the circulation model and Δl (m) is the length between the centre of two boxes. The other variables are the same as for the horizontal advection.

The diffusive flux at vertical boundaries is calculated similarly such as:

$$Q^{v}_{diff}(i,t) = \sum_{j=1}^{n} \left(kv_{j,t} \cdot \frac{\Delta x_j \cdot \Delta y_j}{\Delta l} \right) \tag{C.4}$$

where $kv_{j,t}$ ($m^2\ s^{-1}$) is the vertical diffusion coefficient between the upper and the lower layer of the box model (z = 5 m). The other variables are the same as for the vertical advection. As for the advection, the diffusive fluxes were divided by the volume of the boxes to retrieve the exchange rates (r_{diff}; d^{-1}).

Appendix D

Equations and Parameters for the Biogeochemical Model in ROMS

The biogeochemical model coupled with the circulation model in ROMS has been developed by *Fennel et al*. (2006). This appendix provides the equations of the biogeochemical model and the parameter values used in Chapter 4. The reader in referred to *Fennel et al*. (2006) for a detailed explanation on the equations and parameters choice.

The time rates of change of ecosystem state variables due to biological processes are modelled as follow:

$$\frac{\partial Phy}{\partial t} = \mu Phy - gZoo - m_P Phy - \tau(SDet + Phy)Phy - w_{Phy}\frac{\partial Phy}{\partial z} \tag{D.1}$$

$$\frac{\partial Chl}{\partial t} = \rho_{Chl}\mu Chl - gZoo - m_P Chl - \tau(SDet + Phy)Chl \tag{D.2}$$

$$\frac{\partial Zoo}{\partial t} = g\beta Zoo - l_{BM}Zoo - l_E\frac{Phy^2}{k_P + Phy^2}\beta Zoo^2 - m_Z Zoo^2 \tag{D.3}$$

$$\frac{\partial NO3}{\partial t} = -\mu_{max}(T)f(E)L_{NO3}Phy + nNH4 \tag{D.4}$$

$$\begin{aligned}\frac{\partial NH4}{\partial t} = {} & -\mu_{max}f(E)L_{NH4}Phy - nNH4 + l_{BM}Zoo + l_E\frac{Phy^2}{k_P + Phy^2}\beta Zoo^2 \\ & + r_{SD}SDet + r_{LD}LDet\end{aligned} \tag{D.5}$$

$$\frac{\partial SDet}{\partial t} = g(1-\beta)Zoo + m_Z Zoo^2 + m_P Phy - \tau(SDet + Phy)SDet - r_{SD}SDet - w_{SDet}\frac{\partial SDet}{\partial z} \quad \text{(D.6)}$$

$$\frac{\partial LDet}{\partial t} = \tau(SDet + Phy)^2 - r_{LD}LDet - w_{LDet}\frac{\partial LDet}{\partial z} \quad \text{(D.7)}$$

were the states variables are phytoplankton (*Phy*), chlorophyll (*Chl*), zooplankton (*Zoo*), nitrate (*NO3*), ammonium (*NH4*), small detritus (*SDet*) and large detritus (*LDet*). Parameter names and values are presented in Table D.1. The specific biological processes are described below.

Phytoplankton growth (μ; d^{-1}) is limited by temperature (T; °C), the photosynthetically available radiation (E; W m^{-2}), nitrate and ammonia such as:

$$\mu = \mu_{max}(T) \cdot f(E) \cdot (L_{NO3} + L_{NH4}) \quad \text{(D.8)}$$

The maximum growth rate (μ_{max}; d^{-1}) is limited by temperature following the formulation of *Eppley* (1972):

$$\mu_{max} = \mu_0 \cdot 1.066^T \quad \text{(D.9)}$$

where μ_0 is the phytoplankton growth rate at 0°C.

Light limitation $f(E)$ is modelled with an instantaneous growth rate vs. light function (*Evans and Parslow*, 1985):

$$f(E) = \frac{\alpha E}{\sqrt{\mu_{max}^2 + \alpha^2 E^2}}, \quad \text{(D.10)}$$

where α ((W m^{-2})$^{-1}$$d^{-1}$) is the initial slope of the instantaneous growth rate vs. light curve.

Nitrate uptake limitation (L_{NO3}) is modelled with a Michaelis-Menten function and a function representing the inhibition of nitrate uptake in the presence of ammonia (*Parker*, 1993):

$$L_{NO3} = \frac{NO3}{k_{NO3} + NO3} \cdot \frac{1}{1 + NH4/k_{NH4}}, \tag{D.11}$$

where k_{NO3} and k_{NH4} are the half saturation concentrations for respectively nitrate and ammonia uptake.

Ammonia uptake limitation (L_{NH4}) is modelled with a Michaelis-Menten function:

$$L_{NH4} = \frac{NH4}{k_{NH4} + NH4} \tag{D.12}$$

The chlorophyll content in a phytoplankton cell varies with time as the cell acclimates to the changes in light and nutrient conditions, following the model from *Geider et al.* (1996, 1997). Only a fraction of phytoplankton growth (ρ_{chl}) is dedicated to chlorophyll synthesis such as:

$$\rho_{chl} = \frac{\theta_{max}\mu Phy}{\alpha EChl}, \tag{D.13}$$

where θ_{max} (mgChl mgC^{-1}) is the maximum chlorophyll to carbon ratio in a phytoplankton cell. The ratio ρ_{chl} represents the ratio between actual and maximum photosynthesis.

Phytoplankton grazing by zooplankton (g; d^{-1}) is modelled with a sigmoidal functional form (Holling Type III):

$$g = g_{max}\frac{Phy^2}{k_P + Phy^2}, \tag{D.14}$$

where g_{max} (d^{-1}) is the maximum grazing rate and k_P ((mmol N m^{-3})^2) is the half-saturation concentration for phytoplankton ingestion. This formulation allows a saturating response at high prey concentration and a refuge from grazing at low concentration, which is important to prevent large oscillations due to limit cycles.

The rate of nitrification (n; d^{-1}) is inhibited by light using the relationship:

$$n = n_{max}\left(1 - max\left[0, \frac{E - E_0}{k_E + E - E_0}\right]\right), \tag{D.15}$$

where n_{max} (d^{-1}) is the maximum rate of nitrification and k_E (W m^{-2}) is the light intensity for half-saturated inhibition of nitrification.

Finally, organic matter that reach the bottom boundary layer of depth H and thickness Δz is remineralized in the sediment into ammonia. A fraction of this ammonia is nitrified into nitrate which is then used for denitrification and lost from the nutrient pool. The remainder is returned to the overlying water. The bottom boundary condition is therefore:

$$\left.\frac{\partial NH4}{\partial t}\right|_{z=H} = \frac{4}{16\Delta z}\left(w_{Phy}\, Phy|_{z=H} + w_{SDet} SDet|_{z=H} + w_{LDet} LDet|_{z=H}\right) \tag{D.16}$$

Table D.1: Values and description of ROMS ecosystem parameters from *Fennel et al*. (2006) used for the simulations of Chapter 3.

Symbol	Description	Value	Unit
μ_0	Phytoplankton growth rate at 0°C	0.59	d^{-1}
T	Water temperature	-	°C
α	Initial slope of the instantaneous growth rate vs light curve	0.025	$(W\ m^{-2})^{-1}d^{-1}$
k_{NO3}	Nitrate half saturation concentration	0.5	mmol N m^{-3}
k_{NH4}	Ammonium half saturation concentration	0.5	mmol N m^{-3}
k_P	Phytoplankton ingestion half-saturation concentration	2	$(mmol\ N\ m^{-3})^2$
g_{max}	Maximum grazing rate	0.6	$(mmol\ N\ m^{-3})^{-1}d^{-1}$
m_P	Phytoplankton mortality	0.15	d^{-1}
τ	Phytoplankton and suspended detritus aggregation rate	0.02	d^{-1}
θ_{max}	Maximum chlorophyll to phytoplankton ratio	0.053	mgChl mgC^{-1}
β	Zooplankton assimilation efficiency	0.75	Dimensionless
l_{BM}	Excretion rate due to basal metabolism	0.1	d^{-1}
l_E	Maximum rate of assimilation related excretion	0.1	d^{-1}
m_Z	Zooplankton mortality	0.025	d^{-1}
r_{SD}	Remineralization rate of suspended detritus	0.4	d^{-1}
r_{LD}	Remineralization rate of large detritus	0.01	d^{-1}
n_{max}	Maximum nitrification rate	0.2	d^{-1}
k_E	Light intensity for half-saturated inhibition of nitrification	0.1	W m^{-2}
E_0	Threshold for light-inhibition of nitrification	0.0095	W m^{-2}
w_{Phy}	Sinking velocity of phytoplankton	0.1	m d^{-1}
w_{SDet}	Sinking velocity of suspended detritus	0.1	m d^{-1}
w_{LDet}	Sinking velocity of larger particles	5	m d^{-1}
E	Photosynthetically available radiation	-	W m^{-2}
k_w	Light attenuation coefficient for water	0.04	m^{-1}
k_{chl}	Light attenuation coefficient for chlorophyll	0.025	$(mgChl)^{-1}m^{-2}$

Appendix E

Discrepancy in Modelled vs. Observed Chlorophyll

The comparison between observed and simulated chlorophyll biomass at the mooring stations indicates that the simulated temporal patterns in chlorophyll biomass do not match the observations (Figure E.1A,B and Figure 4.11 in Chapter 4). However, simulated phytoplankton biomass varies in response to the upwelling event in Lunenburg Bay, and its spatial patterns agree with the observations from Chapter 2 (Figure 4.9E-H). A mismatch between real and simulated carbon to chlorophyll ratio ($70 < \text{C:Chl} < 130$ gC gChl^{-1} during the simulation, Figure E.1C,D) is a possible explanation for the disagreement between observed and simulated chlorophyll time series at the SB3 mooring ($p > 0.05$, $F = 0.1$, $n = 43$). There is a significant relationship at this mooring between modelled carbon to chlorophyll ratio and the observed chlorophyll biomass ($p < 0.01$, $F = 7.6$, $n = 43$), which increase simultaneously during the simulation (Figure E.1C). The variations in modelled phytoplankton biomass during the periods of upwelling are therefore dampened in the chlorophyll signal (Figure E.1A). An estimate of chlorophyll biomass using a fixed carbon to chlorophyll ratio (C:Chl = 60 gC gChl^{-1}) yields a better agreement between the model and the observations at the SB3 mooring station ($R^2 = 0.27$, $p < 0.01$, $F = 9.8$, $n = 43$)(Figure E.1E). In this configuration, the variations in simulated chlorophyll biomass reproduce the overall observed response to the upwelling event at SB3, although the short-term response to the upwelling is still missing from the simulation (Figure E.1A). However, this estimate results in the overestimation of chlorophyll biomass at SB2, the inshore mooring station (Figure E.1F).

Since the dataset collected at the coastal observatory does not include phytoplankton biomass, it is not known if the variations in modelled C:Chl are accurate or not. The range of C:Chl simulated corresponds to the range observed inshore in the region (*Harrison and Platt*, 1980; *Côté and Platt*, 1983). Moreover, the model uses a standard formulation of the carbon to chlorophyll ratio (*Geider et al*., 1996, 1997). Nonetheless, this model does not account for the variations in the value of C:Chl that result from changes in phytoplankton species composition (e.g., *Harrison and Platt*, 1980; *Côté and Platt*, 1983). Such changes were observed during the period of investigation (see Chapter 2).

The uncertainties on the time variation of the carbon to chlorophyll ratio may thus explain some of the discrepancy between modelled and observed chlorophyll biomass.

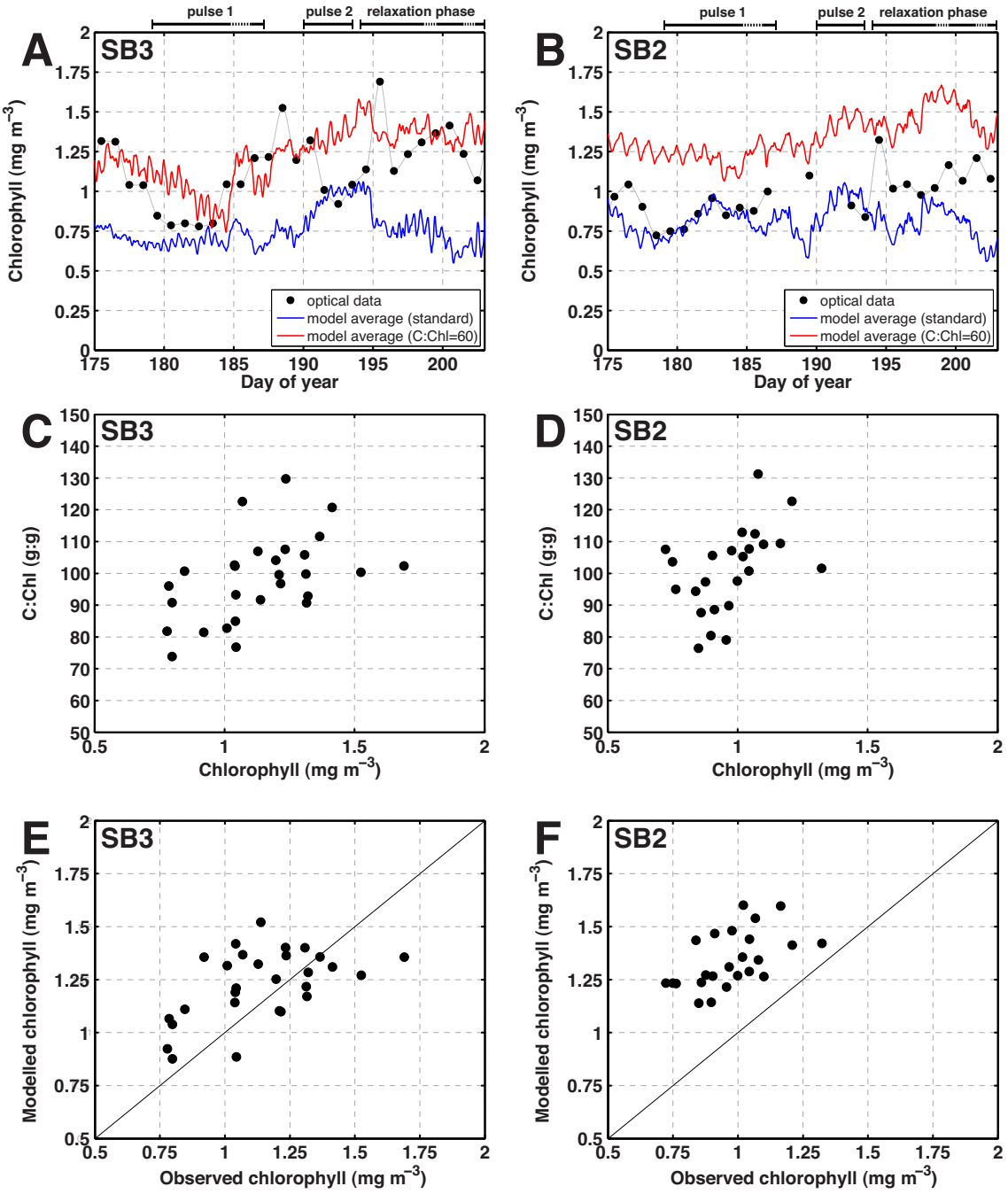

Figure E.1: Comparison between observed and modelled chlorophyll biomass and modelled carbon to chlorophyll ratio (C:Chl; g g^{-1}) at the mooring station SB3 (mid-bay, left panels) and SB2 (inshore, right panels). A,B. Comparison between the time series of chlorophyll biomass from the optical model (filled circles), from modelled chlorophyll (blue) and from chlorophyll calculated with modelled phytoplankton biomass using a constant carbon to chlorophyll ratio (C:Chl = 60). The main time periods of the upwelling event are indicated at the top. C,D. Comparison between chlorophyll biomass from the optical model (x-axis) and the carbon to chlorophyll ratio in the model (y-axis). E-F. Comparison between chlorophyll biomass from the optical model (x-axis) and modelled chlorophyll calculated with the fixed C:Chl ratio.

Bibliography

Allen, J. S., Models of wind-driven currents on the continental shelf, *Annu Rev Fluid Mech*, *12*, 389–433, 1980.

Alpine, E. A., and J. E. Cloern, Trophic interactions and direct physical effects control phytoplankton biomass and production in an estuary, *Limnol Oceanogr*, *37*, 946–955, 1992.

Álvarez-Salgado, X. A., G. Róson, F. F. Pérez, F. G. Figueiras, and Y. Pazos, Nitrogen cycling in an estuarine upwelling system, the Rìa de Arousa (NW Spain). I. Short-time-scale patterns of hydrodynamic and biogeochemical circulation, *Mar Ecol Prog Ser*, *135*, 259–273, 1996a.

Álvarez-Salgado, X. A., G. Róson, F. F. Pérez, F. G. Figueiras, and A. F. Ríos, Nitrogen cycling in an estuarine upwelling system, the Ria de Arousa (NW Spain). II. Spatial differences in the short-time-scale evolution of fluxes and net budgets, *Mar Ecol Prog Ser*, *135*, 275–288, 1996b.

Álvarez-Salgado, X. A., J. Gago, B. M. Miguéz, M. Gilcoto, and F. F. Peréz, Surface waters of the NW iberian margin: upwelling on the shelf versus outwelling of upwelled waters, *Est Coast Shelf Sci*, *51*, 821–837, 2000.

Álvarez-Salgado, X. A., U. Labarta, M. J. Fernández-Reiriz, F. G. Figueiras, G. Rosón, S. Piedracoba, R. Filgueira, and J. M. Cabanas, Renewal time and the impact of harmful algal blooms on the extensive mussel raft culture of the Iberian coastal upwelling system (SW Europe), *Harmful Algae*, *7*, 849–855, 2008.

Álvarez-Salgado, X. A., A. V. Borges, F. G. Figueiras, and C. L, *Carbon and Nutrient Fluxes in Continental Margins: A Global Synthesis*, chap. 2.6. Iberian Margin: The Rías, pp. 103–120, IGBP Book Series, Springer, Berlin, 2010.

Andrade, Y., Upwelling on the Scotian Shelf inferred from satellite and coastal measurements, Ph.D. thesis, Dalhousie University, 1991.

Andrews, W. R. H., and L. Hutchings, Upwelling in the southern benguela current, *Prog Oceanogr*, *9*, 1–81, 1980.

Arrigo, K. R., Marine microorganisms and global nutrient cycles, *Nature*, *437*, 349–355, 2005.

Babin, M., J. J. Cullen, and C. S. Roesler (Eds.), *Real-time coastal observing systems for marine ecosystem dynamics and harmful algal blooms: Theory, instrumentation and modelling*, Oceanographic Methodology series, UNESCO Publishing, 2008.

Babin, M., et al., New approaches and technologies for observing harmful algal blooms, *Oceanography*, *18*, 210–227, 2005.

Bakun, A., Global climate change and intensification of coastal ocean upwelling, *Science*, *247*, 198–201, 1990.

Bakun, A., D. B. Field, A. Redondo-Rodriguez, and S. J. Weeks, Greenhouse gas, upwelling-favorable winds, and the future of coastal ocean upwelling ecosystems, *Global Change Biol*, *16*, 1213–1228, 2010.

Banas, N. S., B. M. Hickey, J. A. Newton, and J. L. Ruesink, Tidal exchange, bivalve grazing, and patterns of primary production in Willapa Bay, Washington, USA, *Mar Ecol Prog Ser*, *341*, 123–139, 2007.

Banse, K., Net zooplankton and total zooplankton, *Rapp Proc Verb, Cons Int Explor Mer*, *153*, 211–215, 1962.

Barth, J. A., et al., Delayed upwelling alters nearshore coastal ocean ecosystems in the northern California Current, *Proc Natl Acad Sci*, *104*, 3719, 2007.

Beckmann, A., and D. B. Haidvogel, Numerical simulation of flow around a tall isolated seamount. Part I: Problem formulation and model accuracy, *J Phys Oceanogr*, *23*, 1736–1753, 1993.

Behrenfeld, M. J., and P. G. Falkowski, Photosynthetic rates derived from satellite-based chlorophyll concentration, *Limnol Oceanogr*, pp. 1–20, 1997.

Beres, D. L., and D. M. Hawkins, Plackett-Burman technique for sensitivity analysis of many-parametered models, *Ecol Model*, *141*, 171–183, 2001.

Bienfang, P. K., Phytoplankton sinking rates in oligotrophic waters off Hawaii, USA, *Mar Biol*, *61*, 69–77, 1980.

Bienfang, P. K., Sinking rates of heterogeneous, temperate phytoplankton populations, *J Plankton Res*, *3*, 235–253, 1981.

Bienfang, P. K., and P. J. Harrison, Sinking-rate response of natural assemblages of temperate and subtropical phytoplankton to nutrient depletion, *Mar Biol*, *38*, 293–300, 1984.

Blanton, J. O., K. R. Tenore, F. Castillejo, L. P. Atkinson, F. B. Schwing, and A. Lavin, The relationship of upwelling to mussel production in the rias on the western coast of Spain, *J Mar Res*, *45*, 497–511, 1987.

Bode, A., and M. Varela, Primary production and phytoplankton in three Galician Rias Altas (NW Spain): seasonal and spatial variability, *Sci Mar*, *62*, 319–330, 1998.

Boje, R., and M. Tomczak (Eds.), *Upwelling ecosystems*, Springer-Verlag, Berlin, 1978.

Bollens, S. M., and B. W. Frost, Zooplanktivorous fish and variable diel vertical migration in the marine planktonic copepod *calanus pacificus*, *Limnol Oceanogr*, *34*, 1072–1083, 1989.

Bray, J. R., and J. T. Curtis, An ordination of the upland forest communities of southern Wisconsin, *Ecol Monogr*, *27*, 325–349, 1957.

Brock, T. D., Calculating solar radiation for ecological studies, *Ecol Model*, *14*, 1–19, 1981.

Brown, C. A., and R. J. Ozretich, Coupling between the coastal ocean and Yaquina Bay, Oregon: Importance of oceanic inputs relative to other nitrogen sources, *Estuaries and Coasts*, *32*, 219–237, 2009.

Brown, P. C., and J. G. Field, Factors limiting phytoplankton production in a nearshore upwelling area, *J Plankton Res*, *8*, 55–68, 1986.

Brown, P. C., and L. Hutchings, Phytoplankton distribution and dynamics in the Southern Benguela Current, in *Simposio Internacional sobre las áreas de afloramiento más importantes del oeste africano (Cabo Blanco y Benguela)*, edited by C. Bas, R. Margalef, and P. Rubies, pp. 319–344, Instituto de investigaciones pesqueras, Barcelona, 1985.

Bujan, S., C. Grenz, R. Fichez, and P. Douillet, Modélisation préliminaire de l'évolution saisonnière du cycle biogéochimique du lagon sud-ouest de Nouvelle-Calédonie, *CR Acad sci, Sér 3, Sci vie*, *323*, 225–233, 2000.

Carter, H. H., T. O. Najarian, D. W. Pritchard, and R. E. Wilson, The dynamics of motion in estuaries and other coastal water bodies, *Rev Geophys*, *17*, 1585–1590, 1979.

Cembella, A., and C. Rafuse, *Microscopic and molecular methods for quantitative phytoplankton analysis*, chap. The filter - transfer - freeze method for quantitative phytoplankton analysis, pp. 41–46, IOC Manuals and Guides, no. 55, Springer, Paris, 2010.

Cermeño, P., E. Marañón, V. Pérez, P. Serret, E. Fernández, and C. G. Castro, Phytoplankton size structure and primary production in a highly dynamic coastal ecosystem (Rìa de Vigo, NW-Spain): Seasonal and short-time scale variability, *Est Coast Shelf Sci*, *67*, 251–266, 2006.

Chang, G. C., and T. D. Dickey, *Real-time coastal observing systems for marine ecosystem dynamics and harmful algal blooms: Theory, instrumentation and modelling*, chap. Interdisciplinary sampling strategies for detection and characterization of harmful algal blooms, pp. 43–84, Oceanographic Methodology series, UNESCO Publishing, 2008.

Chapelle, A., P. Lazure, and A. Ménesguen, Modelling eutrophication events in a coastal ecosystem. sensitivity analysis, *Est Coast Shelf Sci*, *39*, 529–548, 1994.

Chapman, D. C., Numerical treatment of cross-shelf open boundaries in a barotropic coastal ocean model, *J Phys Oceanogr*, *15*, 1060–1075, 1985.

Chen, C. T. A., *Carbon and nutrient fluxes in continental margins*, chap. Cross-boundary exchanges of carbon and nitrogen in continental margins, pp. 561–574, Springer, Berlin, 2010.

Chen, C. T. A., K. K. Liu, and R. Macdonald, *Ocean biogeochemistry*, chap. Continental margin exchanges, pp. 53–97, Springer, 2003.

Chereskin, T. K., Direct evidence for an Ekman balance in the California Current, *J Geophys Res*, *100*, 261–18, 1995.

Clemente-Colón, P., and X. H. Yan, Observations of east coast upwelling conditions in synthetic aperture radar imagery, *IEEE Trans Geosci Remote Sens*, *37*, 2239–2248, 1999.

Cloern, J. E., Does the benthos control phytoplankton biomass in south San Francisco Bay (USA)?, *Mar Ecol Prog Ser*, *9*, 191–202, 1982.

Cloern, J. E., Phytoplankton bloom dynamics in coastal ecosystems: A review with some general lessons from sustained investigation of San Francisco Bay, California, *Rev Geophys*, *34*, 127–168, 1996.

Cloern, J. E., and R. Dufford, Phytoplankton community ecology: principles applied in San Francisco Bay, *Mar Ecol Prog Ser*, *285*, 11–28, 2005.

Conover, R. J., Assimilation of organic matter by zooplankton, *Limnol Oceanogr*, *11*, 338–345, 1966.

Costanza, R., et al., The value of the world's ecosystem services and natural capital, *Nature*, *387*, 253–260, 1997.

Côté, B., and T. Platt, Day-to-day variations in the spring-summer photosynthetic parameters of coastal marine phytoplankton, *Limnol Oceanogr*, *28*, 320–344, 1983.

Crespo, B. G., F. G. Figueiras, P. Porras, and I. G. Teixeira, Downwelling and dominance of autochthonous dinoflagellates in the NW Iberian margin: The example of the Ría de Vigo, *Harmful Algae*, *5*, 770–781, 2006.

Csanady, G. T., *Circulation in the coastal ocean*, Environmental fluid mechanics, Reidel Publishing Company, 1982.

Cullen, J. J., *Real-time coastal observing systems for marine ecosystem dynamics and harmful algal blooms: Theory, instrumentation and modelling*, chap. Observation and prediction of harmful algal blooms, pp. 1–41, Oceanographic Methodology series, UNESCO Publishing, 2008.

Cullen, J. J., P. J. S. Franks, D. M. Karl, and A. Longhurst, Physical influences on marine ecosystem dynamics, in *The Sea*, edited by A. R. Robinson, J. J. McCarthy, and B. J. Rothschild, vol. 12, pp. 297–336, John Wiley & Sons, New York, 2002.

Cullen, J. J., et al., The Lunenburg Bay project, *CMOS Bulletin SCMO*, *36*, 199–205, 2008.

Cushman-Roisin, B., and J.-M. Beckers, *Introduction to geophysical fluid dynamics*, vol. 98 of *International Geophysics Series*, 2nd edition ed., Academic Press, 2011.

Denman, K. L., and M. A. Peña, A coupled 1-d biological/physical model of the north-east subarctic pacific ocean with iron limitation, *Deep-Sea Res Part II*, *46*, 2877–2908, 1999.

Denman, K. L., and T. M. Powell, Effects of physical processes on planktonic ecosystems in the coastal ocean, *Oceanogr Mar Biol Annu Rev*, *22*, 125–168, 1984.

DFO, Eastern scotian shelf integrated ocean management plan : strategic plan, *Tech. rep.*, Canada. Dept. of Fisheries and Oceans. Maritimes Region. Oceans and Habitat Branch, Dartmouth, Nova Scotia, 2007.

Dickey, T. D., The emergence of concurrent high-resolution physical and bio-optical measurements in the upper ocean and their applications, *Rev Geophys*, *29*, 383–414, 1991.

Diffenbaugh, N. S., M. A. Snyder, and L. C. Sloan, Could CO2-induced land-cover feedbacks alter near-shore upwelling regimes?, *Proc Natl Acad Sci*, *101*, 27, 2004.

Dixon, P., VEGAN, a package of R functions for community ecology, *J Veg Sci*, *14*, 927–930, 2003.

Dowd, M., On predicting the growth of cultured bivalves, *Ecol Model*, *104*, 113–131, 1997.

Dowd, M., Seston dynamics in a tidal inlet with shellfish aquaculture: a model study using tracer equations, *Est Coast Shelf Sci*, *57*, 523–537, 2003.

Dowd, M., A bio-physical coastal ecosystem model for assessing environmental effects of marine bivalve aquaculture, *Ecol Model*, *183*, 323–346, 2005.

Ducklow, H. W., and L. McCallister, The biogeochemistry of carbon dioxyde in the coastal oceans, in *The global coastal ocean. Multiscale interdisciplinary processes*, edited by A. R. Robinson and K. H. Brink, vol. 13 of *The Sea*, pp. 269–305, John Wiley & Sons, New York, 2005.

Dugdale, R., and J. Goering, Uptake of new and regenerated forms of nitrogen in primary productivity, *Limnol Oceanogr*, *12*, 196–206, 1967.

Dugdale, R., and F. Wilkerson, New production in the upwelling center at Point Conception, California: temporal and spatial patterns, *Deep-Sea Res Part A*, *36*, 985–1007, 1989.

Duxbury, A. C., Upwelling and estuary flushing, *Limnol Oceanogr*, pp. 627–633, 1979.

Dyer, K. R., *Estuaries: a physical introduction*, John Wiley, London, 1973.

Dyer, K. R., *Estuarine hydrography and sedimentation*, Cambridge University Press, Cambridge, 1979.

Edwards, A., K. Jones, J. M. Graham, C. R. Griffiths, N. MacDougall, J. Patching, J. M. Richard, and R. Raine, Transient coastal upwelling and water circulation in Bantry Bay, a ria on the south-west coast of Ireland, *Est Coast Shelf Sci*, *42*, 213–230, 1996.

Ekman, V. W., On the influence of the earth's rotation on ocean currents, *Ark Mat Astron Fys*, *2*, 1–52, 1905.

Emery, W. J., and R. E. Thomson, *Data analysis methods in physical oceanography*, Pergamon, 1998.

Eppley, R. W., Temperature and phytoplankton growth in the sea, *Fish Bull*, *70*, 1063–1085, 1972.

Eppley, R. W., and B. J. Peterson, Particulate organic matter flux and planktonic new production in the deep ocean, *Nature*, *282*, 677–680, 1979.

Eppley, R. W., E. H. Renger, W. G. Harrison, and J. J. Cullen, Ammonium distribution in southern california coastal waters and its role in the growth of phytoplankton, *Limnol Oceanogr*, *24*, 495–509, 1979.

Estrada, M., and D. Blasco, Phytoplankton assemblages in coastal upwelling areas, in *Simposio internacional sobre las áreas de afloramiento más importantes del oeste africano (Cabo Blanco y Benguela)*, edited by C. Bas, R. Margalef, and P. Rubies, pp. 379–402, Instituto de investigaciones pesqueras, Barcelona, 1985.

Evans, G. T., and J. S. Parslow, A model of annual plankton cycles, *Biol Oceanogr*, *3*, 327–347, 1985.

Falkowski, P. G., R. T. Barber, and V. Smetacek, Biogeochemical controls and feedbacks on ocean primary production, *Science*, *281*, 200–206, 1998.

Falkowski, P. G., et al., The global carbon cycle: A test of our knowledge of earth as a system, *Science*, *290*, 291–296, 2000.

Fasham, M. J. R., H. W. Ducklow, and S. M. McKelvie, A nitrogen-based model of plankton dynamics in the oceanic mixed layer, *J Mar Res*, *48*, 591–639, 1990.

Fenchel, T., Ecology of heterotrophic microflagellates. II. Bioenergetics and growth, *Mar Ecol Prog Ser*, *8*, 225–231, 1982.

Fennel, K., J. Wilkin, J. Levin, J. Moisan, J. O'Reilly, and D. Haidvogel, Nitrogen cycling in the Middle Atlantic Bight: results from a three-dimensional model and implications for the North Atlantic nitrogen budget, *Global Biogeochem Cycles*, *20*, 2006.

Fennel, K., J. Wilkin, M. Previdi, and R. Najjar, Denitrification effects on air-sea CO2 flux in the coastal ocean: Simulations for the northwest North Atlantic, *Geophys Res Lett*, *35*, 2008.

Fennel, W., and T. Neumann, *Introduction to the modelling of marine ecosystems*, Elsevier Science, 2004.

Field, C. B., M. J. Behrenfeld, J. T. Randerson, and P. Falkowski, Primary production of the biosphere: integrating terrestrial and oceanic components, *Science*, *281*, 237, 1998.

Figueiras, F. G., and A. F. Rios, Phytoplankton succession, red tides and the hydrographic regime in the Rías Bajas of Galicia, in *Toxic phytoplankton blooms in the sea*, edited by T. J. Smayda and Y. Shimizu, pp. 239–244, Elsevier Science, New York, 1993.

Figueiras, F. G., U. Labarta, and M. J. Fernández Reiriz, Coastal upwelling, primary production and mussel growth in the Rías Baixas of Galicia, *Hydrobiologia*, *484*, 121–131, 2002.

Figueiras, F. G., G. C. Pitcher, and M. Estrada, *Ecology of Harmful Algae*, vol. 189 of *Ecological studies*, chap. Harmful Algal Bloom Dynamics in Relation to Physical Processes, Springer Berlin Heidelberg, 2006.

Flament, P., L. Armi, and L. Washburn, The evolving structure of an upwelling filament, *J Geophys Res C*, *90*, 765–11, 1985.

Flather, R. A., A tidal model of the northwest European continental shelf, *Mém Soc r Sci Liège*, *6*, 141–164, 1976.

Fournier, R. O., J. Marra, R. Bohrer, and M. Van Det, Plankton dynamics and nutrient enrichment of the Scotian Shelf, *CJFAS*, *34*, 1004–1018, 1977.

Fowler, G. A., J. M. Hamilton, B. D. Beanlands, D. J. Belliveau, and A. R. Furlong, A wave powered profiler for long term monitoring, in *Oceans'97 MTS/IEEE Conference Proc.*, pp. 225–228, 6-9 October, Halifax, 1997.

Fraga, S., D. M. Anderson, I. Bravo, B. Reguera, K. A. Steidinger, and C. M. Yentsch, Influence of upwelling relaxation on dinoflagellates and shellfish toxicity in Ría de Vigo, Spain, *Est Coast Shelf Sci*, *27*, 349–361, 1988.

Franks, P. J. S., Coupled physical-biological models in oceanography, *Rev Geophys*, *33*, 1177–1187, 1995.

Franks, P. J. S., NPZ models of plankton dynamics: their construction, coupling to physics, and application, *J Oceanogr*, *58*, 379–387, 2002.

Franks, P. J. S., and D. M. Anderson, Alongshore transport of a toxic phytoplankton bloom in a buoyancy current: Alexandrium tamarense in the Gulf of Maine, *Mar Biol*, *112*, 153–164, 1992a.

Franks, P. J. S., and D. M. Anderson, Toxic phytoplankton blooms in the southwestern Gulf of Maine: testing hypotheses of physical control using historical data, *Mar Biol*, *112*, 165–174, 1992b.

Franks, P. J. S., J. S. Wroblewski, and G. R. Flierl, Behavior of a simple plankton model with food-level acclimation by herbivores, *Mar Biol*, *91*, 121–129, 1986.

Fulton, E. A., A. D. M. Smith, and C. R. Johnson, Effect of complexity on marine ecosystem models, *Mar Ecol Prog Ser*, *253*, 1–16, 2003.

Galperin, B., L. H. Kantha, S. Hassid, and A. Rosati, A quasi-equilibrium turbulent energy model for geophysical flows, *J Atmos Sci*, *45*, 55–62, 1988.

Gargett, A., and J. Marra, Effects of upper ocean physical processes (turbulence, advection and air-sea interaction) on oceanic primary production, in *The Sea*, edited by A. R. Robinson, J. J. McCarthy, and B. J. Rothschild, vol. 12, pp. 19–49, John Wiley & Sons, New York, 2002.

Garrison, D. L., Monterey Bay phytoplankton I. Seasonal cycles of phytoplankton assemblages, *J Plankton Res*, *1*, 241–265, 1979.

Garvine, R. W., A simple model of estuarine subtidal fluctuations forced by local and remote wind stress, *J Geophys Res C*, *90*, 1985.

Gattuso, J. P., M. Frankignoulle, and R. Wollast, Carbon and carbonate metabolism in coastal aquatic ecosystems, *Annu Rev Ecol Syst*, *29*, 405–434, 1998.

Geider, R. J., and B. A. Osborne, Respiration and microalgal growth: a review of the quantitative relationship between dark respiration and growth., *New Phytol*, *112*, 327–341, 1989.

Geider, R. J., H. L. MacIntyre, and T. M. Kana, A dynamic model of photoadaptation in phytoplankton, *Limnol Oceanogr*, *41*, 1–15, 1996.

Geider, R. J., H. L. MacIntyre, and T. M. Kana, Dynamic model of phytoplankton growth and acclimation: Responses of the balanced growth rate and the chlorophyll a:carbon ratio to light, nutrient-limitation and temperature, *Mar Ecol Prog Ser*, *148*, 187–200, 1997.

Gentleman, W., A. Leising, B. Frost, S. Strom, and J. Murray, Functional responses for zooplankton feeding on multiple resources: a review of assumptions and biological dynamics, *Deep-Sea Res Part II*, *50*, 2847–2875, 2003.

Geyer, R. W., and R. P. Signell, A reassessment of the role of tidal dispersion in estuaries and bays, *Estuaries*, *15*, 97–108, 1992.

Gilcoto, M., X. A. Álvarez-Salgado, and F. F. Pérez, Computing optimum estuarine residual fluxes with a multiparameter inverse method (OERFIM): application to the Ria de Vigo (NW Spain), *J Geophys Res C*, *106*, 31,303–31,318, 2001.

Gilcoto, M., P. C. Pardo, X. A. Álvarez-Salgado, and F. F. Pérez, Exchange fluxes between the ría de vigo and the shelf: A bidirectional flow forced by remote wind, *J Geophys Res C*, *112*, C06001, 2007.

Glenn, S., et al., Biogeochemical impact of summertime coastal upwelling on the new jersey shelf, *J Geophys Res C*, *109*, 2004.

Grant, J., M. Dowd, K. Thompson, C. Emerson, and A. Hatcher, *Bivalve Filter Feeders and Marine Ecosystem Processes*, chap. Perspectives on field studies and related biological models of bivalve growth, pp. 371–420, Springer, New York, 1993.

Grant, J., A. Hatcher, D. B. Scott, P. Pocklington, C. T. Schafer, and G. V. Winters, A multidisciplinary approach to evaluating impacts of shellfish aquaculture on benthic communities, *Estuaries*, *18*, 124–144, 1995.

Grasshoff, K., K. Kremling, and M. Ehrhardt (Eds.), *Methods of Seawater Analysis*, 3rd ed., Wiley-VCH, Weinheim, 1999.

Greenan, B. J. W., B. Petrie, G. Harrison, and N. S. Oakey, Are the spring and fall blooms on the Scotian Shelf related to short-term physical events?, *Cont Shelf Res*, *24*, 603–625, 2004.

Gregory, D., and S. Narayanan, A national archive for marine biology and chemistry data, *AZMP Bulletin*, pp. 11–13, 2003.

Griffies, S. M., *Fundamentals of ocean climate models*, Princeton University Press, Princeton, NJ, 2004.

Griffiths, *Real-time coastal observing systems for marine ecosystem dynamics and harmful algal blooms: Theory, instrumentation and modelling*, chap. Glider and autonomous underwater vehicle observing systems, pp. 495–525, Oceanographic Methodology series, UNESCO Publishing, 2008.

Guillaud, J. F., F. Andrieux, and A. Menesguen, Biogeochemical modelling in the Bay of Seine (France): an improvement by introducing phosphorus in nutrient cycles, *J Mar Syst*, *25*, 369–386, 2000.

Hachey, H. B., Ekman's theory applied to water replacement on the Scotian Shelf, *Proc N S Inst Sci*, *19*, 264–276, 1937.

Haidvogel, D. B., and A. Beckmann, *Numerical ocean circulation modelling*, vol. 2 of *Series on environmental science and management*, Imperial College Press, London, 1999, book from Killam library.

Haidvogel, D. B., et al., Ocean forecasting in terrain-following coordinates: Formulation and skill assessment of the regional ocean modeling system, *J Comput Phys*, *227*, 3595–3624, 2008.

Håkanson, L., Optimal size of predictive models, *Ecol Model*, *78*, 195–204, 1995.

Hales, B., W. J. Cai, B. G. Mitchell, C. L. Sabine, and O. Schofield, North American continental margins: a synthesis and planning workshop., *Tech. rep.*, Carbon Cycle Scientific Steering Group and Interagency Working Group. U.S. Carbon Cycle Science Program, Washington, DC, 2008.

Harley, C. D. G., A. Randall Hughes, K. M. Hultgren, B. G. Miner, C. J. B. Sorte, C. S. Thornber, L. F. Rodriguez, L. Tomanek, and S. L. Williams, The impacts of climate change in coastal marine systems, *Ecol Lett*, *9*, 228, 2006.

Harrison, W. G., and T. Platt, Variations in assimilation number of coastal marine phytophytoplankton: Effects of environmental co-variates, *J Plankton Res*, *2*, 249–260, 1980, printed copy only.

Harrison, W. G., L. R. Harris, and B. D. Irwin, The kinetics of nitrogen utilization in the oceanic mixed layer: Nitrate and ammonium interactions at nanomolar concentrations, *Limnol Oceanogr*, *41*, 16–32, 1996.

Hatcher, A., J. Grant, and B. Schofield, Effects of suspended mussel culture (mytilus spp.) on sedimentation, benthic respiration and sediment nutrient dynamics in a coastal bay, *Mar Ecol Prog Ser*, *115*, 215–235, 1994.

Heath, R. A., Flushing of coastal embayments by changes in atmospheric conditions, *Limnol Oceanogr*, *18*, 849–862, 1973.

Hewes, C. D., and O. Holm-Hansen, A method for recovering nanoplankton from filters for identification with the microscope: The filter-transfer-freeze (ftf) technique, *Limnol Oceanogr*, *28*, 389–394, 1983.

Hickey, B. M., and N. S. Banas, Oceanography of the U.S. Pacific Northwest coastal ocean and estuaries with application to coastal ecology, *Estuaries and Coasts*, *26*, 1010–1031, 2003.

Huot, Y., C. Brown, and J. J. Cullen, Retrieval of phytoplankton biomass from simultaneous inversion of reflectance, the diffuse attenuation coefficient, and sun-induced fluorescence in coastal waters, *J Geophys Res C*, *112*, C06013, 2007.

Hutchings, L., G. C. Pitcher, T. A. Probyn, and G. W. Bailey, The chemical and biological consequences of coastal upwelling, in *Upwelling in the ocean: modern processes and ancient records. Report of the Dahlem Workshop on Upwelling in the Ocean, Modern Processes and Ancient Records, Berlin 1994, September 25-30*, edited by C. P. Summerhayes, K.-C. Emeis, M. V. Angel, R. L. Smith, and B. Zeitzschel, pp. 64–81, John Wiley, Chichester, England, 1995.

Jahnke, R. A., *Carbon and nutrient fluxes in continental margins*, chap. Global synthesis, pp. 597–615, Springer, Berlin, 2010.

Joint, I., M. Inall, M. Torres, F. G. Figueiras, X. A. Álvarez-Salgado, A. P. Rees, and E. M. S. Woodward, Two lagrangian experiments in the Iberian Upwelling System: tracking an upwelling event and an off-shore filament, *Prog Oceanogr*, *51*, 221–248, 2001.

Jørgensen, S. E., and G. Bendoricchio, *Fundamentals of Ecological Modelling*, vol. 21 of *Developments in environmental modelling*, 3rd ed., Elsevier Science, Amsterdam, 2001.

Jouffre, D., T. Lam-Hoai, B. Millet, and M. Amanieu, Structuration spatiale des peuplements zooplanctoniques et fonctionnement hydrodynamique en milieu lagunaire, *Oceanol Acta*, *14*, 489–504, 1991.

Kalnay, E., et al., The NCEP/NCAR 40-year reanalysis project, *B Am Meteorol Soc*, *77*, 437–471, 1996.

Kantha, L. H., and C. A. Clayson, An improved mixed layer model for geophysical applications, *J Geophys Res C*, *99*, 25235–25266, 1994.

Kimmerer, W. J., Predatory influences on copepod distributions in coastal waters., *Bull Plankton Soc Japan, Spec Vol*, pp. 161–174, 1991.

Kimmerer, W. J., Distribution patterns of zooplankton in Tomales Bay, California, *Estuaries and Coasts*, *16*, 264–272, 1993.

Kiørboe, T., Pelagic fisheries and spatio-temporal variability in zooplankton productivity, *Bull Plankton Soc Japan, Spec Vol*, pp. 229–249, 1991.

Kiørboe, T., Formation and fate of marine snow: small-scale processes with large-scale implications, *Sci Mar*, *65*, 57–71, 2001.

Kiørboe, T., and T. G. Nielsen, Effects of wind stress on vertical water column structure, phytoplankton growth, and productivity of planktonic copepods, in *Trophic relationships in the marine environment, Proc 24th Europ Mar Biol Symp*, pp. 28–40, Aberdeen University Press, 1990.

Kjerfve, B., J. E. Greer, and R. L. Crout, Low-frequency response of estuarine sea level to non-local forcing, *Estuarine interactions*, pp. 497–513, 1978.

Kremer, H. H., M. D. A. Le Tissier, P. R. Burbridge, L. Talaue-McManus, N. N. Rabalais, J. Parslow, C. J. Crossland, and B. Young, LOICZ science plan and implementation strategy. IGBP Report No. 51, *Tech. rep.*, IGBP Secretariat, Stockholm, 2004.

Large, W. G., and S. Pond, Open ocean momentum flux measurements in moderate to strong winds, *J Phys Oceanogr*, *11*, 324–336, 1981.

Le Pape, O., F. Jean, and A. Ménesguen, Pelagic and benthic trophic chain coupling in a semi-enclosed coastal system, the Bay of Brest (France): a modelling approach, *Mar Ecol Prog Ser*, *189*, 135–147, 1999.

Legendre, L., and S. Demers, Towards dynamic biological oceanography and limnology, *Can J Fish Aquat Sci*, *41*, 2–19, 1984.

Legendre, L., and J. Le Fèvre, Hydrodynamical singularities as controls of recycled versus export production in oceans, in *Productivity of the ocean: present and past*, edited by W. H. Berger, V. S. Smetacek, and G. Wefer, pp. 49–63, John Wiley & Sons, New York, 1989.

Legendre, P., and L. Legendre, *Numerical Ecology*, chap. Ordination in reduced space, pp. 387–480, 2nd ed., Elsevier Science, Amsterdam, 1998.

Lewis, M. R., and T. Platt, Scales of variability in estuarine ecosystems, in *Estuarine Comparisons: proceedings of the Sixth Biennial International Estuarine Research Conference, Gleneden Beach, Oregon, November 1-6, 1981*, edited by V. S. Kennedy, pp. 3–19, Academic Press, New York, 1982.

Lewis, M. R., J. J. Cullen, and T. Platt, Relationships between vertical mixing and photoadaptation of phytoplankton: similarity criteria, *Mar Ecol Prog Ser*, *15*, 141–149, 1984.

Liu, K.-K., L. Atkinson, R. A. Quiñones, and L. Talaue-McManus, *Carbon and nutrient fluxes in continental margins*, chap. Biogeochemistry of continental margins in a global context, p. 757, Global change : the IGBP series, Springer, Berlin, 2010.

Longhurst, A., S. Sathyendranath, T. Platt, and C. Caverhill, An estimate of global primary production in the ocean from satellite radiometer data, *J Plankton Res*, *17*, 1245–1271, 1995.

Longhurst, A. R., *Ecological geography of the sea*, 1st ed., Academic Press, 1998.

Lu, Y., D. G. Wright, and D. Brickman, Internal tide generation over topography: Experiments with a free-surface z-level ocean model, *J Atmos Ocean Technol*, *18*, 1076–1091, 2001.

Lucas, L. V., J. R. Koseff, J. E. Cloern, S. G. Monismith, and J. K. Thompson, Processes governing phytoplankton blooms in estuaries. I: The local production-loss balance, *Mar Ecol Prog Ser*, *187*, 1–15, 1999a.

Lucas, L. V., J. R. Koseff, S. G. Monismith, J. E. Cloern, and J. K. Thompson, Processes governing phytoplankton blooms in estuaries. II: The role of horizontal transport, *Mar Ecol Prog Ser*, *187*, 17–30, 1999b.

Lucas, L. V., J. K. Thompson, and L. R. Brown, Why are diverse relationships observed between phytoplankton biomass and transport time?, *Limnol Oceanogr*, *54*, 381–390, 2009.

Maclsaac, J. J., R. C. Dugdale, R. T. Barber, D. Blasco, and T. T. Packard, Primary production cycle in an upwelling center, *Deep-Sea Res*, *32*, 503–529, 1985.

Mann, K. H., and J. R. N. Lazier, *Dynamics of marine ecosystems: biological-physical interactions in the oceans*, Blackwell, 1992.

Marañon, E., and E. Fernández, Changes in phytoplankton ecophysiology across a coastal upwelling front, *J Plankton Res*, *17*, 1999–2008, 1995.

Margalef, R., Life-forms of phytoplankton as survival alternatives in an unstable environment, *Oceanol Acta*, *1*, 493–509, 1978a.

Margalef, R., Phytoplankton communities in upwelling areas. the example of NW Africa, *Oecol Aquat*, *3*, 97–132, 1978b.

Margalef, R., *Our biosphere*, vol. 10 of *Excellence in Ecology*, chap. Engineering a forest, Ecology Institute, Oldendorf/Luhe, Germany, 1997.

Marra, J., R. R. Bidigare, and T. D. Dickey, Nutrients and mixing, chlorophyll and phytoplankton growth, *Deep-Sea Res Part A*, *37*, 127–143, 1990.

McBride, G. B., Simple calculation of daily photosynthesis by means of five photosynthesis-light equations, *Limnol Oceanogr*, *37*, 1796–1808, 1992.

Mellor, G. L., and T. Yamada, Development of a turbulence closure model for geophysical fluid problems, *Rev Geophys Space Phys*, *20*, 851–875, 1982.

Ménesguen, A., P. Cugier, S. Loyer, A. Vanhoutte-Brunier, T. Hoch, J. F. Guillaud, and F. Gohin, Two-or three-layered box-models versus fine 3D models for coastal ecological modelling? a comparative study in the English Channel (Western Europe), *J Mar Syst*, *64*, 47–65, 2007.

Miller, B. A., and R. B. Emlet, Influence of nearshore hydrodynamics on larval abundance and settlement of sea urchins Strongylocentrotus franciscanus and S. purpuratus in the Oregon upwelling zone, *Mar Ecol Prog Ser*, *148*, 83–94, 1997.

Minas, H. J., M. Minas, and T. T. Packard, Productivity in upwelling areas deduced from hydrographic and chemical fields, *Limnol Oceanogr*, pp. 1182–1206, 1986.

Mitchell, M. R., The influence of local wind forcing on the low-frequency variations of chlorophyll a in a small marine basin, *Cont Shelf Res*, *11*, 53–66, 1991.

Mitchell, M. R., G. Harrison, K. Pauley, A. Gagné, G. Maillet, and P. Strain, Atlantic zonal monitoring program sampling protocol, *Can Tech Rep Hydrogr Ocean Sci*, *223*, 2002.

Moline, M. A., S. M. Blackwell, R. Chant, M. J. Oliver, T. Bergmann, S. Glenn, and O. M. E. Schofield, Episodic physical forcing and the structure of phytoplankton communities in the coastal waters of New Jersey, *J Geophys Res C*, *109*, C12S05, 2004.

Monsen, N. E., J. E. Cloern, L. V. Lucas, and S. G. Monismith, A comment on the use of flushing time, residence time, and age as transport time scales, *Limnol Oceanogr*, *47*, 1545–1553, 2002.

Morozov, A. Y., Emergence of Holling type III zooplankton functional response: Bringing together field evidence and mathematical modelling, *J Theor Biol*, *265*, 45–54, 2010.

Morozov, A. Y., and E. G. Arashkevich, Patterns of zooplankton functional response in communities with vertical heterogeneity: a model study, *Math Model Nat Phenom*, *3*, 131–148, 2008.

Morozov, A. Y., and E. G. Arashkevich, Towards a correct description of zooplankton feeding in models: Taking into account food-mediated unsynchronized vertical migration, *J Theor Biol*, *262*, 346–360, 2010.

Muller-Karger, F. E., R. Varela, R. Thunell, R. Luerssen, C. Hu, and J. J. Walsh, The importance of continental margins in the global carbon cycle, *Geophys Res Lett*, *32*, 2005.

Mulligan, R. P., A. E. Hay, and A. J. Bowen, Wave-driven circulation in a coastal bay during the landfall of a hurricane, *J Geophys Res*, *113*, 2008.

Murray, A. G., The use of simple models in the design and calibration of a dynamic 2D model of a semi-enclosed Australian bay, *Ecol Model*, *136*, 15–30, 2001.

Murray, A. G., and J. S. Parslow, Modelling of nutrient impacts in Port Phillip Bay - a semi-enclosed marine Australian ecosystem, *Mar Freshw Res*, *50*, 597–612, 1999.

O'Brien, J. J., and J. S. Wroblewski, On advection in phytoplankton models, *J Theor Biol*, *38*, 197, 1973.

Ohman, M. D., The demographic benefits of diel vertical migration by zooplankton, *Ecol Monogr*, *60*, 257–281, 1990.

Oschlies, A., *Ocean weather forecasting. An integrated view of oceanography*, chap. On the use of data assimilation in biogeochemical modelling, pp. 525–547, Springer, 2006.

Oschlies, A., and V. Garçon, An eddy-permitting coupled physical-biological model of the North Atlantic 1. Sensitivity to advection numerics and mixed layer physics, *Global Biogeochem Cycles*, *13*, 135–160, 1999.

Paffenhöfer, G. A., and R. P. Harris, Feeding, growth and reproduction of the marine planktonic copepod *Pseudocalanus elongatus*, *J Mar Biol Ass U K*, *56*, 327–344, 1976.

Paranjape, M. A., and R. J. Conover, Zooplankton of St. Margaret's Bay: 1968 to 1971, *Tech. Rep. 401*, Marine Ecology Laboratory, Canada Fisheries Research Board, Dartmouth, Nova Scotia, 1973.

Pardo, P. C., M. Gilcoto, and F. F. Pérez, Short-time scale coupling between thermohaline and meteorological forcing in the Ría de Pontevedra, *Sci Mar*, *65*, 229–240, 2001.

Parker, R. A., Dynamic models for ammonium inhibition of nitrate uptake by phytoplankton, *Ecol Model*, *66*, 113–120, 1993.

Parsons, T. R., M. Takahashi, and B. Hargrave (Eds.), *Biological Oceanographic Processes*, 3rd ed., Pergamon Press, Oxford, 1984.

Pearre, S. J., Eat and run? The hunger/satiation hypothesis in vertical migration: history, evidence and consequences, *Biol Rev Camb Philos Soc*, *78*, 1–79, 2003.

Penven, P., P. Marchesiello, L. Debreu, and J. Lefèvre, Software tools for pre-and post-processing of oceanic regional simulations, *Environ Modell Softw*, *23*, 660–662, 2008.

Pérez, F. F., X. A. Álvarez-Salgado, and G. Rosón, Stoichiometry of the net ecosystem metabolism in a coastal inlet affected by upwelling. The Ría de Arousa (NW Spain), *Mar Chem*, *69*, 217–236, 2000.

Pérez, F. F., X. A. Padín, Y. Pazos, M. Gilcoto, M. Cabanas, P. C. Pardo, M. D. Doval, and L. Farina-Busto, Plankton response to weakening of the Iberian coastal upwelling, *Global Change Biol*, *16*, 1258–1267, 2010.

Peterson, W. T., D. F. Arcos, G. B. McManus, H. Dam, D. Bellantoni, T. Johnson, and P. Tiselius, The nearshore zone during coastal upwelling: Daily variability and coupling between primary and secondary production off central chile, *Prog Oceanogr*, *20*, 1–40, 1988.

Petrie, B., The Halifax section: A brief history, *AZMP Bulletin*, pp. 26–29, 2004.

Petrie, B., and K. Drinkwater, Temperature and salinity variability on the Scotian Shelf and in the Gulf of Maine 1945–1990, *J Geophys Res C*, *98*, 20079, 1993.

Petrie, B., and P. Yeats, Annual and interannual variability of nutrients and their estimated fluxes in the Scotian Shelf - Gulf of Maine region, *Can J Fish Aquat Sci*, *57*, 2536–2546, 2000.

Petrie, B., P. Yeats, and P. Strain, Nitrate, silicate and phosphate atlas for the Scotian shelf and the Gulf of Maine, *Can Tech Rep Hydrogr Ocean Sci*, *203*, 96 pp, 1999.

Petrie, B. D., B. J. Topliss, and D. G. Wright, Coastal upwelling and eddy development off Nova Scotia, *J Geophys Res C*, *29*, 979–991, 1987.

Piedracoba, S., M. Nieto-Cid, C. Souto, M. Gilcoto, G. Roson, X. A. Alvarez-Salgado, R. Varela, and F. G. Figueiras, Physical-biological coupling in the coastal upwelling system of the Ria de Vigo (NW Spain). I: In situ approach, *Mar Ecol Prog Ser*, *353*, 27, 2008a.

Piedracoba, S., M. Nieto-Cid, I. G. Teixeira, J. L. Garrido, X. A. Alvarez-Salgado, G. Roson, C. G. Castro, and F. F. Perez, Physical-biological coupling in the coastal upwelling system of the Ria de Vigo (NW Spain). II: In vitro approach, *Mar Ecol Prog Ser*, *353*, 41, 2008b.

Pinel-Alloul, P., Spatial heterogeneity as a multiscale characteristic of zooplankton community, *Hydrobiologia*, *300*, 17–42, 1995.

Pitcher, G. C., S. Bernard, and A. Fawcett, *Real-time coastal observing systems for marine ecosystem dynamics and harmful algal blooms: Theory, instrumentation and modelling*, chap. Real-time coastal observing systems for ecosystem dynamics and harmful algal blooms: needs and expectations of users, pp. 765–797, Oceanographic Methodology series, UNESCO Publishing, 2008.

Plackett, R. L., and J. P. Burman, The design of optimum multifactorial experiments, *Biometrika*, *33*, 305–325, 1946.

Platt, T., A. Prakash, and B. Irwin, Phytoplankton, nutrients and flushing of inlets on the coast of Nova Scotia, *Le Naturaliste Canadien*, *99*, 253–261, 1972.

Pond, S., and G. L. Pickard, *Introductory dynamical oceanography*, Pergamon Press, Oxford, 1983.

Prego, R., D. Guzman-Zuniga, M. Varela, M. deCastro, and M. Gomez-Gesteira, Consequences of winter upwelling events on biogeochemical and phytoplankton patterns in a western Galician ria (NW Iberian peninsula), *Est Coast Shelf Sci*, *73*, 409–422, 2007.

Price, J. F., and M. A. Sundermeyer, Stratified Ekman layers, *J Geophys Res*, *104*, 20,467–20,494, 1999.

Price, J. F., R. A. Weller, and R. R. Schudlich, Wind-driven ocean currents and Ekman transport, *Science*, *238*, 1534–1538, 1987.

Raillard, O., and A. Ménesguen, An ecosystem box model for estimating the carrying capacity of a macrotidal shellfish system, *Mar Ecol Prog Ser*, *115*, 117–130, 1994.

Richards, F. A. (Ed.), *Coastal upwelling*, Coastal and Estuarine Sciences, American Geophysical Union, Washington, DC, 1981.

Roegner, G. C., and A. L. Shanks, Import of coastally-derived chlorophyll a to South Slough, Oregon, *Estuaries and Coasts*, *24*, 244–256, 2001.

Roegner, G. C., B. M. Hickey, J. A. Newton, A. L. Shanks, and D. A. Armstrong, Wind-induced plume and bloom intrusions into Willapa Bay, Washington, *Limnol Oceanogr*, *47*, 1033–1042, 2002.

Rosón, G., X. A. Álvarez-Salgado, and F. F. Pérez, A non-stationary box model to determine residual fluxes in a partially mixed estuary, based on both thermohaline properties: Application to the ria de arousa (nw spain), *Est Coast Shelf Sci*, *44*, 249–262, 1997.

Rothschild, B. J., Population dynamics and physical forcing, in *Biological-physical interactions in the sea*, edited by A. R. Robinson, J. J. McCarthy, and B. J. Rothschild, vol. 12 of *The Sea*, pp. 245–296, John Wiley & Sons, New York, 2005.

Ryther, J. H., and W. M. Dunstan, Nitrogen, phosphorus, and eutrophication in the coastal marine environment, *Science*, *171*, 1008–1013, 1971.

Sarmiento, J. L., and N. Gruber, *Ocean Biogeochemical Dynamics*, chap. Oceanic carbon cycle, atmospheric CO2 , and climate, pp. 392–458, Princeton University Press, 2006.

Schofield, O., J. Bosch, S. Glenn, G. Kirkpatrick, J. Kerfoot, S. Lohrenz, M. Moline, M. Oliver, and P. Bissett, *Real-time coastal observing systems for marine ecosystem dynamics and harmful algal blooms: Theory, instrumentation and modelling*, chap. Bio-optics in integrated ocean observing networks: potential for studying harmful algal blooms, pp. 85–107, Oceanographic Methodology series, UNESCO Publishing, 2008.

Shanks, A. L., and L. Brink, Upwelling, downwelling, and cross-shelf transport of bivalve larvae: Test of a hypothesis, *Mar Ecol Prog Ser*, *302*, 1–12, 2005.

Shchepetkin, A. F., and J. C. McWilliams, Quasi-monotone advection schemes based on explicit locally adaptive dissipation, *Mon Weather Rev*, *126*, 1998.

Shchepetkin, A. F., and J. C. McWilliams, A method for computing horizontal pressure-gradient force in an oceanic model with a nonaligned vertical coordinate, *J Geophys Res*, *108*, 3090, 2003.

Shchepetkin, A. F., and J. C. McWilliams, The regional oceanic modeling system (ROMS): a split-explicit, free-surface, topography-following-coordinate oceanic model, *Ocean Modelling*, *9*, 347–404, 2005.

Sheng, J., and L. Wang, Numerical study of tidal circulation and nonlinear dynamics in Lunenburg Bay, Nova Scotia, *J Geophys Res C*, *109*, C10018, 2004.

Sheng, J., J. Zhao, and L. Zhai, Examination of circulation, dispersion, and connectivity in Lunenburg Bay of Nova Scotia using a nested-grid circulation model, *J Mar Syst*, *77*, 350–365, 2009.

Siefert, R., and G. K. Plattner, The role of coastal zones in global biogeochemical cycles, *EOS Trans Am Geophys Union*, *85*, 469–469, 2004.

Smagorinsky, J., General circulation experiments with the primitive equations, *Mon Weather Rev*, *91*, 99–164, 1963.

Small, L. F., and D. W. Menzies, Patterns of primary productivity and biomass in a coastal upwelling region, *Deep-Sea Res Part A*, *28*, 123–149, 1981.

Smith, P. C., and F. B. Schwing, Mean circulation and variability on the eastern canadian continental shelf, *Cont Shelf Res*, *11*, 977–1012, 1991.

Smith, R. L., A comparison of the structure and variability of the flow field in three coastal upwelling regions: Oregon, northwest africa, and peru, in *Coastal Upwelling*, edited by F. A. Richards, vol. 1 of *Coastal and Estuarine Sciences*, pp. 107–118, American Geophysical Union, Washington, DC, 1981.

Smolarkiewicz, P. K., and L. G. Margolin, MPDATA: a finite-difference solver for geophysical flows, *J Comput Phys*, *140*, 459–480, 1998.

Snyder, M. A., L. C. Sloan, N. S. Diffenbaugh, and J. L. Bell, Future climate change and upwelling in the California Current, *Geophys Res Lett*, *30*, 1823, 2003.

Song, Y., and D. Haidvogel, A semi-implicit ocean circulation model using a generalized topography-following coordinate system, *J Comput Phys*, *115*, 228–244, 1994.

Sosik, H. M., R. J. Olson, and E. V. Armbrust, Flow cytometry in phytoplankton research, in *Chlorophyll a fluorescence in aquatic sciences: Methods and applications*, edited by D. J. Suggett, O. Prášil, and M. A. Borowitzka, vol. 4 of *Developments in Applied Phycology*, pp. 171–185, Springer, Berlin, 2010.

Steele, J. H., and E. W. Henderson, A simple plankton model, *Am Nat*, *117*, 676–691, 1981.

Strain, P. M., and P. A. Yeats, The relationships between chemical measures and potential predictors of the eutrophication status of inlets, *Marine Pollution Bulletin*, *38*, 1163–1170, 1999.

Sullivan, B. K., and L. T. McManus, Factors controlling seasonal succession of the copepods *Acartia hudsonica* and *A. tonsa* in Narragansett Bay, Rhode Island: Temperature and resting egg production, *Mar Ecol Prog Ser*, *28*, 121–128, 1986.

Talaue-McManus, L., *Carbon and nutrient fluxes in continental margins*, chap. Examining human impacts on global biogeochemical cycling via the coastal zone and ocean margins, pp. 497–514, Springer, Berlin, 2010.

Therriault, J. C., et al., Proposal for a northwest Atlantic zonal monitoring program, *Can Tech Rep Hydrogr Ocean Sci*, *194*, 1–57, 1998.

Tilburg, C. E., and R. W. Garvine, Three-dimensional flow in a shallow coastal upwelling zone: Alongshore convergence and divergence on the New Jersey shelf, *J Phys Oceanogr*, *33*, 2113–2125, 2003.

Tilstone, G. H., F. G. Figueiras, and F. Fraga, Upwelling-downwelling sequences in the generation of red tides in a coastal upwelling system, *Mar Ecol Prog Ser*, *112*, 241–253, 1994.

Tilstone, G. H., B. M. Miguez, F. G. Figueiras, and E. G. Fermin, Diatom dynamics in a coastal ecosystem affected by upwelling: Coupling between species succession, circulation and biogeochemical processes, *Mar Ecol Prog Ser*, *205*, 23–41, 2000.

Tiselius, P., Short term feeding responses to starvation in three species of small calanoid copepods, *Mar Ecol Prog Ser*, *168*, 119–126, 1998.

Townsend, D. W., N. D. Rebuck, M. A. Thomas, L. Karp-Boss, and R. M. Gettings, A changing nutrient regime in the gulf of maine, *Cont Shelf Res*, *30*, 820–832, 2010.

Ueda, H., Horizontal distribution of planktonic copepods in inlet waters, *Bull Plankton Soc Japan, Spec Vol*, pp. 143–160, 1991.

Varela, M., R. Prego, and Y. Pazos, Spatial and temporal variability of phytoplankton biomass, primary production and community structure in the Pontevedra Ria (NW Iberian Peninsula): oceanographic periods and possible response to environmental changes, *Mar Biol*, *154*, 483–499, 2008.

Villegas-Ríos, D., X. A. Álvarez-Salgado, S. Piedracoba, G. Rosón, U. Labarta, and M. J. Fernández-Reiriz, Net ecosystem metabolism of a coastal embayment fertilised by upwelling and continental runoff, *Cont Shelf Res*, *In Press, Corrected Proof*, 2010.

Visbeck, M., E. P. Chassignet, R. Curry, T. Delworth, B. Dickson, and G. Krahmann, *The North Atlantic oscillation : climatic significance and environmental impact*, vol. 134 of *Geophysical monograph*, chap. The Ocean's Response to North Atlantic Oscillation Variability, American Geophysical Union, Washington, DC, 2003.

Walsh, J. J., Herbivory as a factor in patterns of nutrient utilization in the sea, *Limnol Oceanogr*, *21*, 1–13, 1976.

Walsh, J. J., *On the nature of continental shelves*, Academic Press, 1988.

Walsh, J. J., Importance of continental margins in the marine biogeochemical cycling of carbon and nitrogen, *Nature*, *350*, 53–55, 1991.

Wang, L., J. Sheng, A. E. Hay, and D. J. Schillinger, Storm-induced circulation in Lunenburg Bay of Nova Scotia: Observations and numerical simulations, *J Phys Oceanogr*, *37*, 873–895, 2007.

Wang, M., J. E. Overland, and N. A. Bond, Climate projections for selected large marine ecosystems, *J Mar Syst*, *79*, 258–266, 2010.

Webb, W. L., M. Newton, and D. Starr, Carbon dioxide exchange of Alnus rubra, *Oecologia*, *17*, 281–291, 1974.

Webster, I., S. Smith, and J. Parslow, Implications of spatial and temporal variation for biogeochemical budgets of estuaries, *23*, 341–350, 2000.

Weisberg, R. H., The nontidal flow in the Providence River of Narragansett Bay: A stochastic approach to estuarine circulation, *J Phys Oceanogr*, *6*, 721–734, 1976.

Welschmeyer, N. A., Fluorometric analysis of chlorophyll a in the presence of chlorophyll b and pheopigments, *Limnol Oceanogr*, *39*, 1985–1992, 1994.

Wiebe, P. H., and M. C. Benfield, From the Hensen net toward four-dimensional biological oceanography, *Prog Oceanogr*, *56*, 7–136, 2003.

Wijffels, S. E., E. Firing, and H. Bryden, Direct observations of the Ekman balance at 10°N in the Pacific, *J Phys Oceanogr*, *24*, 1666–1679, 1994.

Wong, K.-C., and A. Valle-Levinson, On the relative importance of the remote and local wind effects on the subtidal exchange at the entrance to the Chesapeake Bay, *J Mar Res*, *60*, 477–498, 2002.

Wooster, W. S., A. Bakun, and D. R. McLain, The seasonal upwelling cycle along the eastern boundary of the north atlantic, *J Mar Res*, *34*, 1–14, 1976.

Wroblewski, J. S., J. J. O'Brien, and T. Platt, On the physical and biological scales of phytoplankton patchiness in the ocean, *Mém Soc r Sci Liège*, *7*, 43–57, 1975.

Yamamoto, T., and M. Okai, Effects of diffusion and upwelling on the formation of red tides, *J Plankton Res*, *22*, 363–380, 2000.

Yamamoto, T., T. Seike, T. Hashimoto, and K. Tarutani, Modelling the population dynamics of the toxic dinoflagellate *Alexandrium tamarense* in Hiroshima Bay, Japan, *J Plankton Res*, *24*, 33–47, 2002.

Yang, B., and J. Sheng, Process study of coastal circulation over the inner Scotian Shelf using a nested-grid ocean circulation model, with a special emphasis on the storm-induced circulation during tropical storm Alberto in 2006, *Ocean Dynamics*, *58*, 375–396, 2008.

Yentsch, C. S., The influence of geostrophy on primary production, *Tethys*, *6*, 111–118, 1974.

Yentsch, C. S., Vertical mixing, a constraint to primary production: an extension of the concept of an optimal mixing zone, in *Ecohydrodynamics, Proceedings of the 12th International Liège Colloquium on Ocean Hydrodynamics, 1980*, edited by J. C. J. Nihoul, pp. 67–77, 1981.

Zaret, T. M., and J. S. Suffern, Vertical migration in zooplankton as a predator avoidance mechanism, *Limnol Oceanogr*, *21*, 804–813, 1976.

Zentara, S. J., and D. Kamykowski, Latitudinal relationships among temperature and selected plant nutrients along the west coast of North and South America, *J Mar Res*, *35*, 321–337, 1977.

Zhai, L., J. Sheng, and R. J. Greatbatch, Observations of the dynamical response of a coastal embayment to wind, tide and buoyancy forcing, *Cont Shelf Res*, *27*, 2534–2555, 2007.

Zhai, L., J. Sheng, and R. J. Greatbatch, Application of a nested-grid ocean circulation model to Lunenburg Bay of Nova Scotia: Verification against observations, *J Geophys Res C*, *113*, C02024, 2008a.

Zhai, L., J. Sheng, and R. J. Greatbatch, Baroclinic dynamics of wind-driven circulation in a stratified bay: A numerical study using models of varying complexity, *Cont Shelf Res*, pp. 2357–2370, 2008b.

Zimmerman, R. C., J. N. Kremer, and R. C. Dugdale, Acceleration of nutrient uptake by phytoplankton in a coastal upwelling ecosystem: A modeling analysis, *Limnol Oceanogr*, *32*, 359–367, 1987.